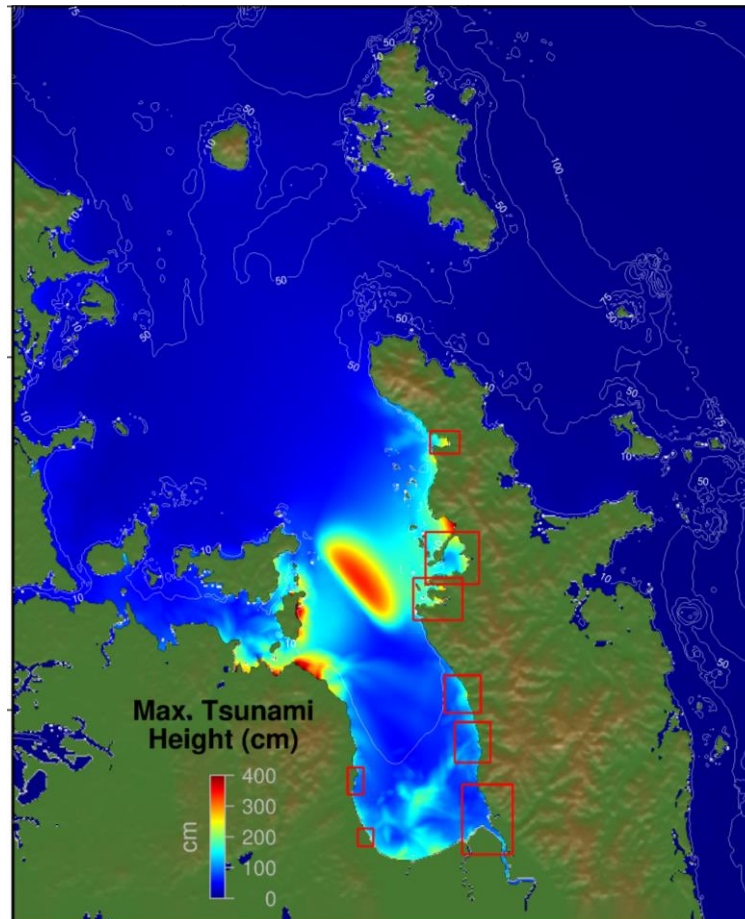


Numerical Modelling of Tsunami Inundation in the Firth of Thames



eCoast Limited
Marine Consulting and Research
P.O. Box 151
Raglan, New Zealand

jose@ecoast.co.nz

<BLANK PAGE>

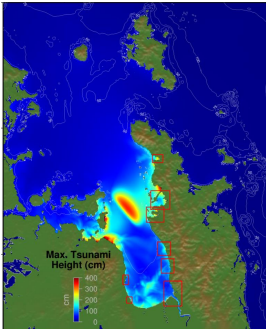
Numerical Modelling of Tsunami Inundation in Firth of Thames

Report Status

Version	Date	Status	Approved By:
2.0	19 December 2018	Pre-Final	JCB
2.1	19 February 2019	Final	JCB
2.2	21 March 2019	Final	JCB

It is the responsibility of the reader to verify the currency of the version number of this report.

Jose C. Borrero Ph.D.



Cover Picture: Maximum computed tsunami height from a rupture on an offshore segment of the Kerepehi Fault.

The information, including the intellectual property, contained in this report is confidential and proprietary to eCoast Limited. It may be used by the persons to whom it is provided for the stated purpose for which it is provided and must not be imparted to any third person without the prior written approval of eCoast. eCoast Limited reserves all legal rights and remedies in relation to any infringement of its rights in respect of its confidential information.

© eCoast Limited 2018

<BLANK PAGE>

EXECUTIVE SUMMARY

This report describes the assessment of tsunami effects resulting from local, near and distant source earthquakes along the coast of the Firth of Thames, New Zealand. This report focuses on the effects in and around the Firth including detailed assessments for Colville, Coromandel, Manaia, Te Mata/Tapu, Te Puru, Thames, Miranda, Kaiaua, and Whakatiwai. Results presented here include the quantification of maximum and minimum tsunami wave heights, the extents of tsunami inundation and tsunami induced flood depths and the strength of tsunami induced currents. The results from this study are intended to guide emergency management and evacuation planning activities. As such, this study focuses primarily on extreme tsunami scenarios in an effort to define likely maximum credible events for the purposes of planning evacuation routes and increasing public awareness.

For the local faulting we consider ruptures on the offshore segments of the Kerepehi Fault as described by Chick (1999) and Chick et al, (2001). These studies propose earthquakes with magnitudes (M_w) between 6.5 and 7.1 occurring on one of 5 offshore segments of the Kerepehi Fault with fault displacement on the four southern segments (A-D1) of 2.4 m and displacement on the northernmost segment (D2) of 8.5 m.

For the regional source tsunami, we assumed a tsunami source on the southern segments of the Tonga Kermadec Trench. For this scenario we used the 'TK8' rupture scenario developed in recent years as a 'maximum credible event' (MCE) for defining tsunami hazards in the Waikato region. This source is based on rupture models for the 2011 Tohoku Japan earthquake that were used to accurately simulate the nearfield inundation extents and tsunami waveforms.

The effect from distant source tsunamis was assessed by simulating the propagation and local inundation from three extreme tsunami events originating in South America. These were the 1868 event from northern Chile, the 1960 event from southern Chile and a hypothetical event based on the 1960 source model positioned offshore of central Peru.

Numerical modelling of the tsunami inundation was conducted using the ComMIT tsunami modelling system. Detailed numerical modelling grids were constructed from high-resolution LiDAR topography and best available bathymetry. The model was validated against tide gauge measurements of tsunami wave heights from the 2010 Chile, 2011 Japan and the 2016 East Cape tsunamis. The model showed a good fit to the measured data for each of the cases suggesting its applicability for local, regional and distant source events.

The model results suggested that the distant source scenarios produced insignificant levels of inundation, but that they would cause potentially strong and long-lasting tsunami induced currents which would be particularly hazardous for maritime activities in the area including but not limited to recreational boating and commercial fishing or aquaculture.

While the regional source scenario produced more inundation than the distant source events, it was still relatively minor compared to sites on the eastern shores of the Coromandel Peninsula. As with the distant source scenarios the tsunami induced currents were shown to be potentially hazardous with maximum modelled speeds in excess of 10 knots in the Colville area.

The greatest degree of inundation was produced by the largest of the local source scenarios. This was the 'D2' scenario represented by a rupture on the northern extent of

the Kerepehi fault with 8.5 m of co-seismic slip on a 16 km long fault plane extending south-eastward from the eastern end of Waiheke Island.

The tsunamis modelled from this source caused appreciable and potentially damaging inundation at all the sites considered. We note however that the degree of inundation was strongly influenced by the tide level assumed during the simulation. For cases run at mean sea level (MSL) the tsunami inundation generally did not rise above the high-water shoreline. This is because at mean sea levels, there are extensive intertidal areas exposed and the inundation from the tsunami just covered these intertidal zones. At mean high water spring (MHWS) water levels the results were markedly different with inundation extending across public reserves and through some near shore settlements and neighbourhoods. Modelled flow depths from these scenarios however were generally less than 1.5 m.

In general, the model results suggest that the overall tsunami hazard at sites in the Firth of Thames is relatively low. This is in line with the conclusions of Chick et al. (2001) who highlight the long recurrence interval for maximum credible events of 2,500 – 9,000 years on the local source scenarios. Persaud et al. (2015) however state that major earthquakes could occur on the Kerepehi Fault (including the offshore segments) once every 1000 years, equivalent to a 1% probability of occurrence in 10 years.

CONTENTS

TABLE OF FIGURES	II
TABLE OF TABLES	VII
1 INTRODUCTION.....	8
1.1 TSUNAMI HISTORY IN THE FIRTH OF THAMES.....	9
1.2 MODELLING APPROACH.....	10
1.3 NUMERICAL MODELLING GRIDS.....	11
1.4 VALIDATION OF THE COMMIT TSUNAMI MODEL	17
1.4.1 Case 1: The February 27, 2010 Maule, Chile Earthquake and Tsunami	17
1.4.2 Case 2: The March 11, 2011 Tohoku Earthquake and Tsunami	18
1.4.3 Case 3: The September 2, 2016 East Cape Earthquake and Tsunami..	20
2 TSUNAMI SOURCE MODELS	24
2.1 LOCAL TSUNAMI SOURCES	24
2.2 REGIONAL TSUNAMI SOURCE MODEL	28
2.3 DISTANT TSUNAMI SOURCE MODELS.....	29
3 MODEL RESULTS LOCAL FAULTS	33
3.1 DISCUSSION OF INUNDATION AT MIRANDA.....	40
4 MODEL RESULTS: TONGA-KERMADEC TRENCH SOURCES	41
4.1 ARRIVAL TIMES, MAXIMUM AMPLITUDES AND TSUNAMI INDUCED CURRENTS.....	41
5 MODEL RESULTS: DISTANT SOURCE TSUNAMIS	49
5.1 PROPAGATION MODELS.....	49
5.2 ARRIVAL TIMES.....	52
5.3 TSUNAMI HEIGHTS, INUNDATION EXTENTS AND CURRENT SPEEDS.....	53
6 RESULTS SUMMARY	59
6.1 DIRECT COMPARISON OF INUNDATION EXTENTS	59
6.2 COMPARISON TO MODELLING OF CHICK (1999).....	62
7 SUMMARY AND CONCLUSIONS.....	63
8 REFERENCES.....	65
9 APPENDIX 1 – TIME SERIES FOR LOCAL SOURCE SCENARIOS	68
10 APPENDIX 2 – TIME SERIES FOR TK TRENCH SCENARIO	85
11 APPENDIX 3 – TIME SERIES FOR DISTANT SOURCE SCENARIOS.....	87
12 APPENDIX 4 – INUNDATION PLOTS FOR DISTANT SOURCE SCENARIOS	92
13 APPENDIX 5 – MAX TSUNAMI HEIGHT AND CURRENT SPEED FOR	104
DISTANT SOURCE SCENARIOS	104
14 APPENDIX 6 – MAX TSUNAMI HEIGHTS AND CURRENT SPEEDS TK8	114
SCENARIO.	114

TABLE OF FIGURES

Figure 1.1 Location map for the study sites in and around the Firth of Thames. Red box denoted the extent of the B level modelling grid while yellow boxes indicate the extents of the various C level grids..... 8

Figure 1.2 The ComMIT propagation model database for tsunamis in the world's oceans. Insets show the details of the source zone discretization in to rectangular sub-faults..... 12

Figure 1.3 Definition sketch for tsunami height, flow depth, runup and inundation distance..... 12

Figure 1.4 The A-level modelling grid for the distant and regional source scenarios. 13

Figure 1.5 The B-level modelling grid for the distant and regional source scenarios. This same grid was used as the propagation grid for the local source scenarios. 13

Figure 1.6 The final C level numerical modelling grids for Colville, Coromandel, Manaia and Te Mata/Tapu. 14

Figure 1.7 The final C level numerical modelling grids for Te Puru, Thames, Miranda and Whakatiwai/Kaiaua. The red line is the 0.0 m MSL contour. 15

Figure 1.8 Grid set up for the local source modelling. The outer yellow rectangle is the propagation model grid, then the green and red rectangles denote the A and B level grids. The smaller yellow rectangles are the extents of the C-level grids. 16

Figure 1.9 Tsunami source model (left) and the trans-pacific propagation pattern (right) for the 2010 Maule, Chile tsunami. Slip amounts (in meters) for the individual fault segments are indicated in white. 17

Figure 1.10 Modelled water level time series compared to measured data at the Port Gisborne tide gauge for the 2010 Maule, Chile tsunami..... 17

Figure 1.11 Tsunami source model (left) and the trans-pacific propagation pattern (right) for the 2011 Tohoku, Japan tsunami. Slip amounts (in meters) for the individual fault segments are indicated in white. 18

Figure 1.12 Modelled water level time series compared to measured data at Auckland (top) and Great Barrier Island (bottom) for the 2011 Tohoku, Japan tsunami..... 19

Figure 1.13 Source location of the September 2nd East Cape Earthquake (USGS, 2017). 21

Figure 1.14 (following page) Top panel: Earthquake source model for the September 2, 2017 East Cape earthquake (reproduced from USGS, 2017). The top panel shows the location of the fault plane (white region). Epicentre of the mains shock is indicated by a star with aftershocks indicated by black circles. Coloured patches indicate coseismic slip amounts according to the colour scale. The thin red line is the top of the fault plane. The white line is the axis of the Tonga-Kermadec Trench. The purple rectangle shows the location of a 100x50 km fault plane source available in the ComMIT tsunami modelling database. Bottom panel: A detail of the slip distribution along the fault plane with the amount of slip indicated by the colour scale. The location of the earthquake hypocentre is

indicated by the star with the arrows indicating the direction of the rupture displacement. The contour lines are the timing (in seconds) of the rupture. The red arrow at the top of the fault plane corresponds to the red arrow in the upper panel. The purple box shows the dimensions of a 100x50 km fault plane..... 21

Figure 1.15 Modelled (blue and black traces) versus measured (red trace) water levels at Lottin Point (top) and Tauranga (bottom) for the 1 September 2016 tsunami..... 23

Figure 2.1 Yellow lines indicate the locations of the surface traces of the offshore fault segments associated with the Kerepehi Fault. Coloured rectangles are the A, B and C level grids used for the local source modelling. Inset shows the locations of the fault traces as described in Chick (1999). 25

Figure 2.2 Initial sea-floor deformation for sources A and B..... 26

Figure 2.3 Initial sea-floor deformation for source C and D1 27

Figure 2.4 Initial sea-floor deformation for source D2, note the different colour scale. 27

Figure 2.5 Source model used for the 2011 Tohoku tsunami, The amount of slip on each segment is indicated in the left panel, while the vertical deformation of the sea floor is shown on the right (image reproduced from Wei et al., 2013)..... 28

Figure 2.6 Case TK 8, the Japan 2011 tsunami source positioned at the southern end of the Tonga-Kermadec Trench..... 28

Figure 2.7 (left) Unit source segments used to define the 1960 Chilean Earthquake suite of events. (right) initial sea floor deformation at the source region..... 30

Figure 2.8 Seafloor deformation for cases, FF 7 uses the the southern concentrated slip distribution. 31

Figure 2.9 Source segments used to model the 1868 Arica tsunami. A uniform slip amount of 39.6 m was applied to each segment. 32

Figure 3.1 Modelled maximum tsunami heights across the 200 m resolution local propagation grid for sources A-D1. 34

Figure 3.2 Modelled maximum tsunami heights across the 200 m resolution local propagation grid for sources D2. Note the increased colour scale relative to Figure 3.1. 35

Figure 3.3 Time series of modelled water levels at MSL for Source A. 36

Figure 3.4 Time series of modelled water levels at MHWS for Source A. Note the similarity between the MSL and MHWS time series at Whakatiwai. 36

Figure 3.5 Inundation at Colville from Source D2 at MSL (left) MHWS (right)..... 37

Figure 3.6 Inundation at Coromandel from Source D2 at MSL (left) MHWS (right).. 37

Figure 3.7 Inundation at Manaia from Source D2 at MSL (left) MHWS (right)..... 37

Figure 3.8 Inundation at Tapu and Te Puru from Source D2 at MSL (left panels) MHWS (right panels)..... 38

Figure 3.9 Inundation at Thames from Source D2 at MSL (left) MHWS (right). 38

Figure 3.10 Inundation at Miranda from Source D2 at MSL (left) MHWS (right). 39

Figure 3.11 Inundation at Whakatiwai from Source D2 at MSL (left) MHWS (right). 39

Figure 3.12 Time series of tsunami water level at Miranda for the A1 (top) and D2 sources (bottom). 40

Figure 4.1 Water level time series plots for the TK 8 sources affecting the 8 study sites..... 42

Figure 4.2 Maximum predicted tsunami amplitudes in the A grid for the TK 8 source. 43

Figure 4.3 Maximum predicted tsunami amplitudes in the B grid for the TK 8 source 43

Figure 4.4 TK 8 scenario maximum overland inundation at Colville for MSL (left) and MHWS (right). 44

Figure 4.5 TK 8 scenario maximum overland inundation at Coromandel for MSL (left) and MHWS (right)..... 44

Figure 4.6 TK 8 scenario maximum overland inundation at Manaia for MSL (left) and MHWS (right). 44

Figure 4.7 TK 8 scenario maximum overland inundation at Tapu for MSL (left) and MHWS (right). 45

Figure 4.8 TK 8 scenario maximum overland inundation at Te Puru for MSL (left) and MHWS (right). 45

Figure 4.9 TK 8 scenario maximum overland inundation at Thames for MSL (left) and MHWS (right). 46

Figure 4.10 TK 8 scenario maximum overland inundation at Miranda for MSL (left) and MHWS (right)..... 46

Figure 4.11 TK 8 scenario maximum overland inundation at Whakatiwai for MSL (left) and MHWS (right). 47

Figure 4.12 Modelled current speeds at select sites (Colville, Coromandel, Thames and Whakatiwai) caused by the TK8 scenario at MSL. 48

Figure 5.1 (following page) Comparison between trans-Pacific propagation patterns for the 1868 Arica (top left) 1960 Valdivia (top mid) and the FF 7 scenarios (top right). (bottom row) Close up on New Zealand for the trans-Pacific propagation. 49

Figure 5.2 Maximum tsunami height in the A and B grids for the 1868 (left) 1960 (mid) and FF 7 scenarios. 51

Figure 5.3 Modelled tsunami water levels at Colville (top) and Thames (bottom) for the 1868 scenario at MSL. 52

Figure 5.4 Modelled tsunami water levels at Colville (top) and Thames (bottom) for the 1960 scenario at MSL. 52

Figure 5.5 Modelled tsunami water levels at Colville (top) and Thames (bottom) for the FF 7 scenario at MSL. 52

Figure 5.6 Predicted inundation extents at Colville for the 1868 (top) FF 7 (mid) and 1960 (bottom) scenarios. MSL on the left and MHWS on the right. 54

Figure 5.7 Predicted inundation extents at Thames for the 1868 (top) FF 7 (mid) and 1960 (bottom) scenarios. MSL on the left and MHWS on the right. 55

Figure 5.8 Maximum current speeds at Colville, Coromandel, Manaia and Thames for the 1868 scenario at MSL. 56

Figure 5.9 Maximum current speeds at Colville, Coromandel, Manaia and Thames for the FF 7 scenario at MSL. 57

Figure 5.10 Maximum current speeds at Colville, Coromandel, Manaia and Thames for the 1960 scenario at MSL. 58

Figure 6.1 Direct comparison between the D2 local, TK8 regional and 1868 distant source scenarios at Colville..... 60

Figure 6.2 Direct comparison between the D2 local, TK8 regional and 1868 distant source scenarios at Thames. Note the different colour scale for the 1868 scenario..... 61

Figure 9.1 Time series of modelled tsunami water levels at Colville (MHWS). Note the varying y-scale-for each scenario..... 69

Figure 9.2 Time series of modelled tsunami water levels at Colville (MSL). Note the varying y-scale-for each scenario..... 70

Figure 9.3 Time series of modelled tsunami water levels at Coromandel (MHWS). Note the varying y-scale for each scenario. 71

Figure 9.4 Time series of modelled tsunami water levels at Coromandel (MSL). Note the varying y-scale for each scenario. 72

Figure 9.5 Time series of modelled tsunami water levels at Manaia (MHWS). Note the varying y-scale for each scenario. 73

Figure 9.6 Time series of modelled tsunami water levels at Manaia (MSL). Note the varying y-scale for each scenario. 74

Figure 9.7 Time series of modelled tsunami water levels at Tapu (MHWS). Note the varying y-scale for each scenario. 75

Figure 9.8 Time series of modelled tsunami water levels at Tapu (MSL). Note the varying y-scale for each scenario. 76

Figure 9.9 Time series of modelled tsunami water levels at Te Puru (MHWS). Note the varying y-scale for each scenario. 77

Figure 9.10 Time series of modelled tsunami water levels at Te Puru (MSL). Note the varying y-scale for each scenario. 78

Figure 9.11 Time series of modelled tsunami water levels at Thames (MHWS). Note the varying y-scale for each scenario. 79

Figure 9.12 Time series of modelled tsunami water levels at Thames (MSL). Note the varying y-scale for each scenario. 80

Figure 9.13 Time series of modelled tsunami water levels at Miranda (MHWS). Note the varying y-scale for each scenario. 81

Figure 9.14 Time series of modelled tsunami water levels at Miranda (MSL). Note the varying y-scale for each scenario. 82

Figure 9.15 Time series of modelled tsunami water levels at Whakatiwai (MHWS). Note the varying y-scale. For each scenario. 83

Figure 9.16 Time series of modelled tsunami water levels at Whakatiwai (MSL). Note the varying y-scale. For each scenario..... 84

Figure 10.1 Water level time series plots for the TK 8 at MSL sources affecting the 8 study sites. 85

Figure 10.2 Water level time series plots for the TK 8 at MHWS sources affecting the 8 study sites. 86

Figure 11.1 FF7 MHWS 87

Figure 11.2 FF7 MSL 88

Figure 11.3 FF 1868 MHWS 89

Figure 11.4 FF 1868 MSL 90

Figure 11.5 FF 1960 MSL 91

Figure 12.1 Inundation extents for the 1868 scenario at MSL (left column) and MHWS (right column)..... 95

Figure 12.2 Inundation extents for the FF 7 scenario at MSL (left column) and MHWS (right column)..... 99

Figure 12.3 Inundation extents for the 1960 scenario at MSL (left column) and MHWS (right column)..... 103

Figure 13.1 Maximum modelled tsunami heights and current speeds for the 1868 scenario at MSL. 106

Figure 13.2 Maximum modelled tsunami heights and current speeds for the FF 7 scenario at MSL. 109

Figure 13.3 Maximum modelled tsunami heights and current speeds for the 1960 scenario at MSL. 113

Figure 14.1 Maximum modelled tsunami heights and current speeds for the TK8 scenario at MSL (upper panels) and MHWS (lower panels)..... 121

TABLE OF TABLES

Table 1.1 Tide offset levels	12
Table 2.1 Fault parameters for the 'most credible earthquake' scenarios described in Chick (1999), Table 4.2.	26
Table 2.2 Description of the distant source tsunami scenarios. The 'FF 1' (1960), 'FF 3' (1868) and 'FF 7' sources were modelled in this study.....	29
Table 2.3 Faults segment slip amounts for the 1960 Chilean tsunami. Segments with slip >20 m are highlighted in pink.	30
Table 2.4 The rearranged slip distribution for the southern concentrated slip case. Segments with slip >20 m are highlighted in pink.....	31
Table 5.1 Modelled tsunami arrival times (in hours after the earthquake) at Coromandel and Thames for the three distant source scenarios.	53
Table 9.1 Locations where time series data in the following plots were extracted. ..	68

1 INTRODUCTION

This report describes the assessment of tsunami effects resulting from local, regional and distant source earthquakes along the coast of the Firth of Thames, New Zealand. This report focuses on the effects in and around the Firth including detailed assessments for Colville, Coromandel, Manaia, Ta Mata/Tapu, Te Puru, Thames, Miranda, Kaiaua, and Whakatiwai (Figure 1.1). Results presented here include the quantification of maximum and minimum tsunami wave heights, the extents of tsunami inundation and tsunami induced flood depths and the strength of tsunami induced currents. The results from this study are intended to guide emergency management and evacuation planning activities. As such, this study focuses primarily on extreme tsunami scenarios in an effort to define likely maximum credible events for the purposes of planning evacuation routes and increasing public awareness.

We use the current state-of-the art tsunami modelling tools (ComMIT: Titov et al. 2011) and the most recent scientific literature on the relevant tsunami source mechanisms. Model results are compared quantitatively and qualitatively to available historical information.



Figure 1.1 Location map for the study sites in and around the Firth of Thames. Red box denoted the extent of the B level modelling grid while yellow boxes indicate the extents of the various C level grids.

1.1 Tsunami History in the Firth of Thames

There are several accounts of tsunami activity in the Firth of Thames (FoT) available in the historical record. Historical records are discussed in De Lange and Healy (1986) while additional information can be found in the GNS on-line historical tsunami database (<http://data.gns.cri.nz/tsunami/> and described in Downes et al. 2017). Additionally, De Lange and Healy (2001) conducted a thorough overview of tsunami hazards in the Hauraki Gulf, including the Firth of Thames. In their report they consider distant, regional and far-field events. Their report however focuses only on existing data for their qualitative assessment and discussion of other potential events is only qualitative in nature.

Below we summarise some of the more important and relevant events for the Firth of Thames.

13 August 1868: A very large ($M > 9$) earthquake near the Peru/Chile border created a transpacific tsunami. Effects were noted throughout New Zealand but were generally stronger on the South Island, particularly at Lyttleton which experienced a water level fall/rise of ~7.6 m.

In the region of the Firth of Thames, a 2 m rise in water level was observed on Great Barrier Island and there was flooding reported in Port Charles. There was also a report of bores reaching the upper Tamaki Estuary followed by water level fluctuations of 1.2 to 1.5 m. [De Lange and Healy, 1986].

At Port Charles on August 15, water rushed into houses on the flat near the sawmill without warning. [The water reached a level] about 3 ft vertically above spring tides, and [flooded] mill buildings built on blocks 2 ft high. Water was over two feet high in houses, and considerable difficulty experienced in removing people to safety. Some swam to high ground. "During the same day", water receded below LW mark at ebb tide, and then returned suddenly as a big wave of several feet in height. The flow and recession occurred several times during low water. It drove logs up creeks, carried away all stacked timber, and depositing it on the flat. Boats and a tramway were washed away. Some logs floated to Pakiri and also a boat. No damage to the sawmill machinery. One schooner at mouth of creek held fast and was not wrecked. (Daily Southern Cross 2 September 1868). [GNS Database]

10 May 1877: Another very large ($M \sim 9$) earthquake in Northern Chile caused a significant trans Pacific tsunami.

At the Piako River, a bore of about 2 ft (0.6 m) was observed creating strong current. The water level fell in a few minutes by the same extent. (Thames Advertiser 14 May 1877). In Thames a boat at wharf moved by "immense" wave passing round boat, resulting in damaged rail and broken rope. (Thames Advertiser 14 May 1877); Report at 09:00 May 12: 2 ft tide rushed in and out again at 16:00 on May 11 at Y flood. On May 12, 2 hrs after HW water rushed in to nearly HW and stayed there a short time. (Evening Post 12 May 1877). [GNS Database].

Clevedon, Wairoa River: At 06:00 remarkably high flood tide. 2 hrs later it was low tide at the bar of the river. [GNS Database]

Warkworth: At 7 a.m. on 11 May the water level rose 1.8 m in a few minutes before receding. There were three more waves. Two, 1.5 m high waves, occurred at 9 a.m. and 10 a.m., with a 1.2 m wave at 12.45 p.m. Between the peaks, the water receded

sufficiently to ground the steamer Kina as it was navigating the Mahurangi Estuary just below the Warkworth Wharf. [De Lange and Healy, 1986].

Port Charles: There is some doubt about the actual place referred to for this account, but only Port Charles appears to fit the description. The actual location referred to was Port Charters, near Auckland. The wave of 11 May washed 200-300 logs away from the sawmill. The tide rushed in and out every 20 min all day long with an average range of 2.5 m and a maximum of 3.0- 3.6 m. A punt anchored in Reef Bay broke its moorings and was swept ashore, and the wharf was damaged. [De Lange and Healy, 1986].

22 May 1960: A great earthquake of $M \sim 9.4$ occurred in southern Chile and created a significant trans-Pacific tsunami.

Leigh: The water level dropped 2.4 m in a few minutes and then returned as a 1.2 m surge washing away bridge supports. [De Lange and Healy, 1986]

Auckland: The tide was irregular starting late on the evening of the 23rd. Fluctuations exceeding 0.6 m were recorded in the Waitemata Harbour during the 24th and 25th. [De Lange and Healy, 1986]

Coromandel: Phenomenal tides experienced as a result of the tidal wave. "The tide was seen to go out at 4ft 6in and then came in and out again several times." No damage reported. (Coromandel and Mercury Bay Gazette (Whitianga) Wednesday 1 June 1960). [GNS Database]

Thames: On May 24, fluctuations of water levels occurred at Shortland Wharf, and in the Waihou River. No serious effects recorded. Fluctuations occurred later than at Whitianga. At 0600 May 24 tide was dropping, then turned and came in. Tide was three quarters of the way out at 0745 May 24, and at an exceptionally high tide mark an hour later. In the river [Waihou?] boat in 8 ft of water grounded, then water returned as quickly as it had receded. (Thames Star (Thames) 24 May 1960); Tidal disturbances still evident on the Thames Coast on May 25. Four tides at Thames on May 24, another freak tide rising at 1400. On May 25 at 1030, ebbing tide reversed and came in again to rise about two feet, but then went straight out again. Thames fisherman have been undisturbed by the phenomena, and this morning every boat of the fleet was out fishing as usual, except one confined to port with engine trouble. Most serious result damage was the loss of two net anchors when a surging rise lifted the nets and broke the anchor bridles. Only other problems were tangled nets. (Thames Star (Thames) 24 May 1960). [GNS Database]

Other Events: In addition, the 1964 Alaska tsunami was recorded in Auckland with a total height of 0.45 m. Also, the tsunamis of 2010 (Maule, Chile) and 2011 (Tohoku Japan) were recorded on tide gauges throughout New Zealand (Borrero and Greer 2012) with the 2011 event causing significant flooding in Port Charles (Borrero et al., 2014).

1.2 Modelling Approach

The numerical modelling presented in this study was carried out using the Community Model Interface for Tsunamis (ComMIT) numerical modelling tool. The ComMIT model interface was developed by the United States Government National Oceanic and Atmospheric Administration's (NOAA) Centre for Tsunami Research (NCTR) at the Pacific Marine Environmental Laboratory (PMEL) following the December 26, 2004 Indian Ocean tsunami as a way to efficiently distribute assessment capabilities amongst tsunami prone countries.

The backbone of the ComMIT system is a database of pre-computed deep-water propagation results for tsunamis generated by unit displacements on fault plane segments (100 x 50 km) positioned along the world's subduction zones. Currently, there are 1,691 pre-computed unit source propagation model runs covering the world's oceans included in the propagation database. Using linear superposition, the deep ocean tsunami propagation results from more complex faulting scenarios can be created by scaling and/or combining the pre-computed propagation results from several unit sources (Titov et al., 2011). The resulting trans-oceanic tsunami propagation results are then used as boundary inputs for a series of nested near shore grids covering a coastline of interest. The nested model propagates the tsunami to shore computing wave height, velocity and overland inundation. The hydrodynamic calculations contained within ComMIT are based on the MOST (Method Of Splitting Tsunami) algorithm described in Titov and Synolakis (1995, 1997, 1998) and Titov and Gonzalez (1997). This technique is used for the distant and regional source tsunami scenarios.

For the local source scenarios, a modified version of the ComMIT model is set up in a manner that allows for the implementation of a fully custom tsunami source based on co-seismic seafloor deformation predicted by standard elastic earthquake deformation models (i.e. Okada, 1985). For these scenarios the earthquake source parameters are input directly, and the model is run using that source as an initial condition. The results from the local propagation model are then fed in to a 3-level nest of near-shore grids.

1.3 Numerical Modelling Grids

The Waikato Regional Council provided raw bathymetry and LiDAR topography data for construction of the numerical modelling grids. The data were provided with a reference datum of MSL and a WGS84 projection. The data were combined with additional data sets covering the regional offshore bathymetry and on land topography. This included the Shuttle Radar Topography Mission (SRTM) 90 m resolution topography, 200 m resolution bathymetry from NIWA, as well as nautical chart data from Land Information New Zealand (LINZ). The data were combined in to a master set of (x, y, z) triplets and then gridded in to different resolutions and coverage areas as shown in Figure 1.6 and Figure 1.7. Model grids were set up at mean sea level (MSL) and at mean high water spring (MHWS). The MHWS grids were created by shifting the 'zero' value from MSL to MHWS based on data from the Waikato Regional Council Website (WRC, 2018) and reproduced in Table 1.1 below.

For the local source modelling, we used the 'B' level grid from the distant/regional source model as our propagation level grid, then developed additional A and B level grids surrounding each of the study sites. The gridding arrangement for this set up is shown in Figure 1.4 through Figure 1.7.

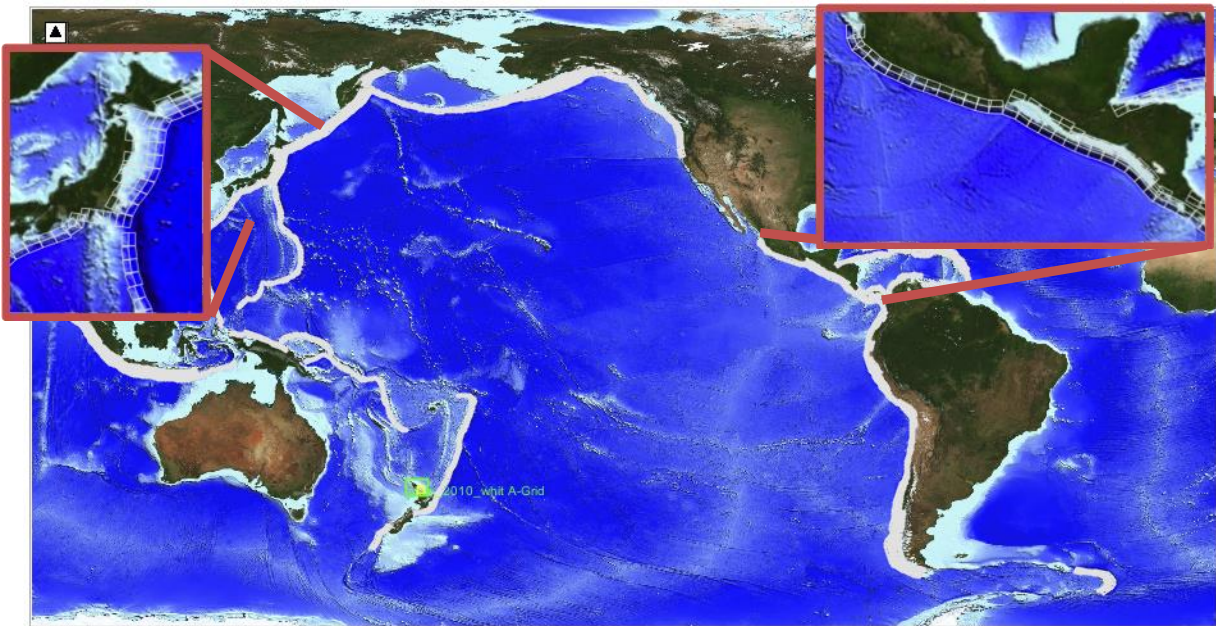


Figure 1.2 The ComMIT propagation model database for tsunamis in the world’s oceans. Insets show the details of the source zone discretization in to rectangular sub-faults.

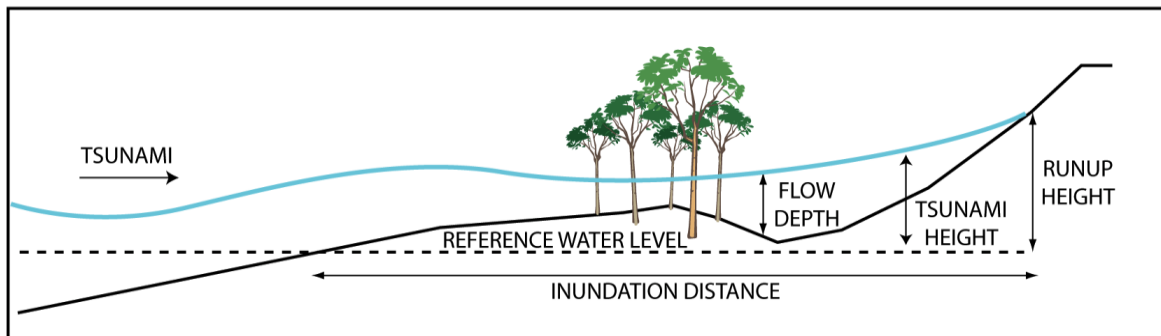


Figure 1.3 Definition sketch for tsunami height, flow depth, runup and inundation distance.

Table 1.1 Tide offset levels

Site	Offset to MHWS (m)
Colville	1.51
Coromandel	1.58
Manaia	1.60
Te Mata/Tapu	1.71
Te Puru	1.75
Thames	1.79
Miranda	1.80
Kaioua/Whakatiwai	1.77

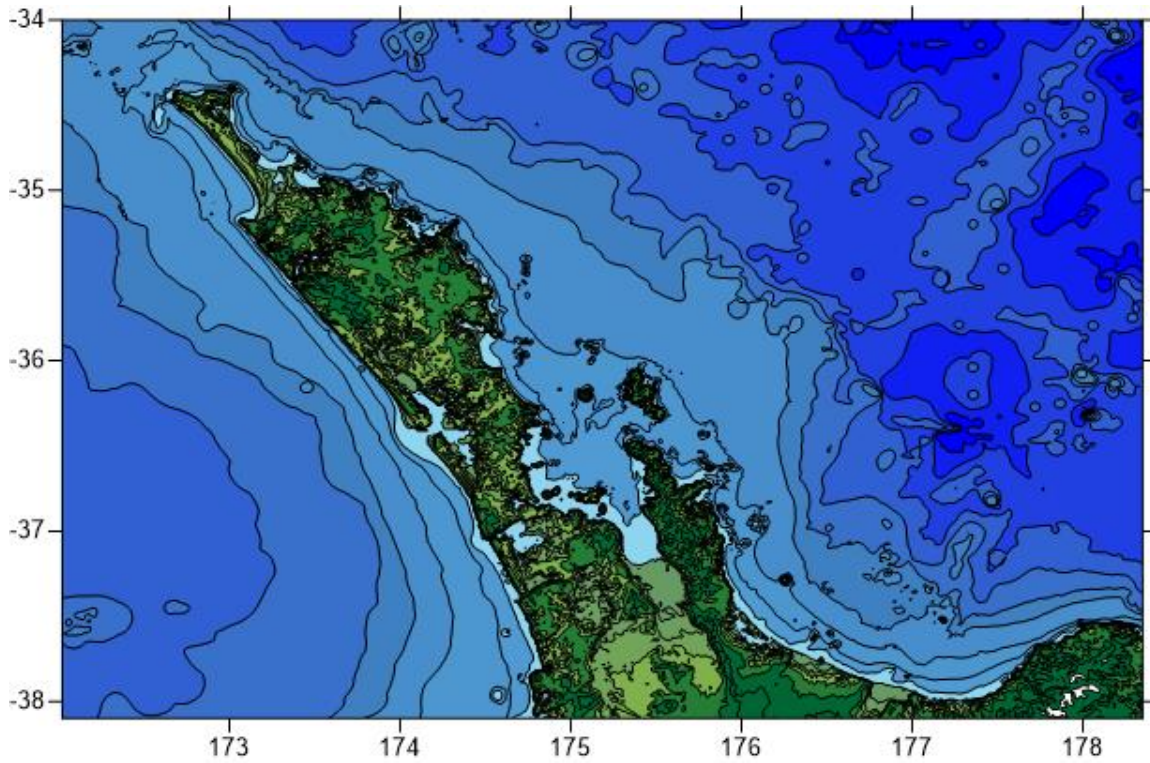


Figure 1.4 The A-level modelling grid for the distant and regional source scenarios.

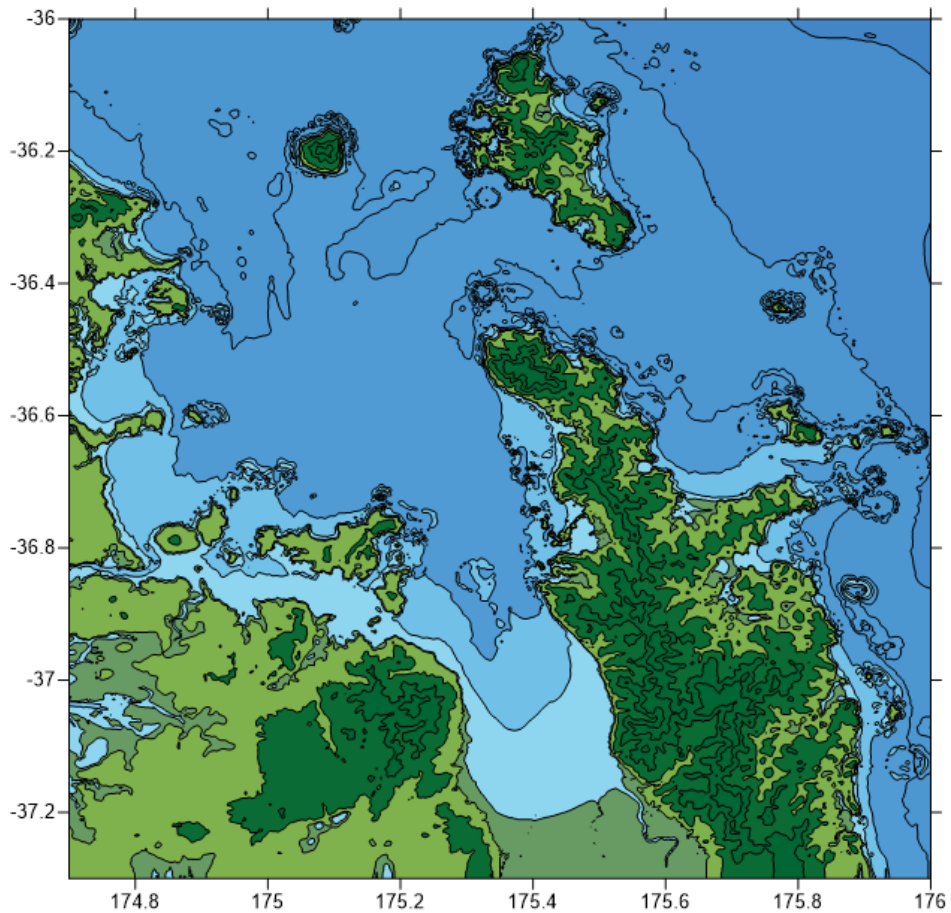


Figure 1.5 The B-level modelling grid for the distant and regional source scenarios. This same grid was used as the propagation grid for the local source scenarios.

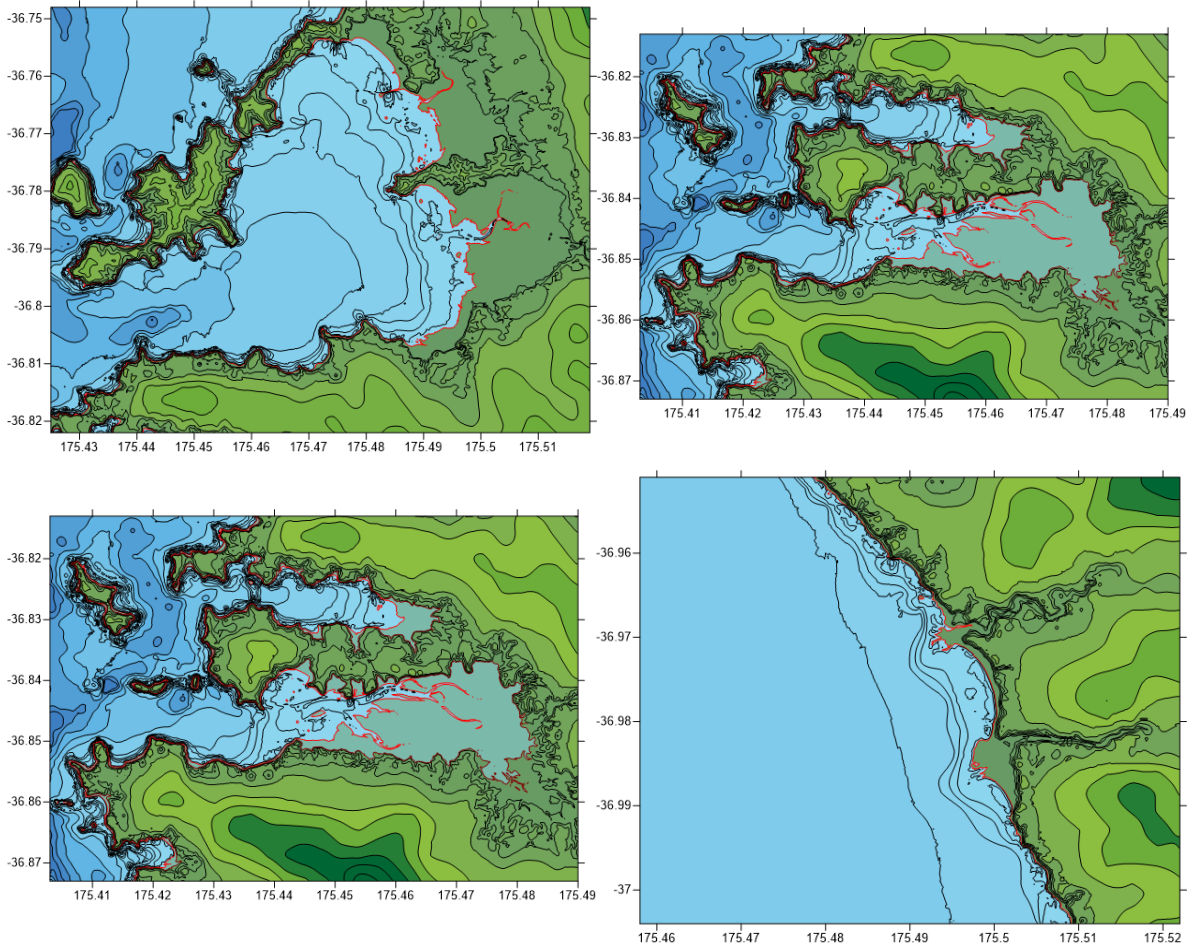


Figure 1.6 The final C level numerical modelling grids for Colville, Coromandel, Manaia and Te Mata/Tapu.

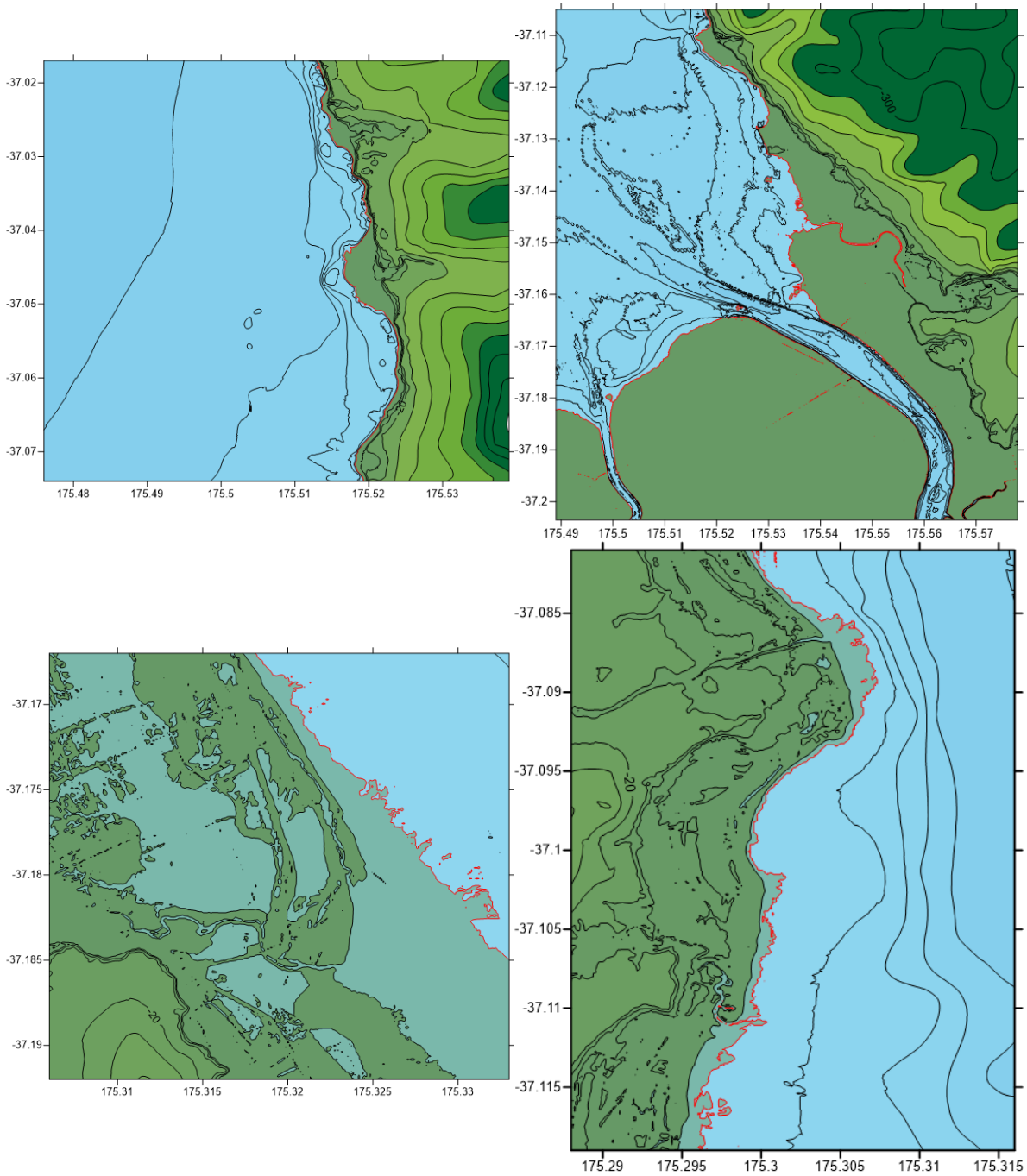


Figure 1.7 The final C level numerical modelling grids for Te Puru, Thames, Miranda and Whakatiwai/Kaiaua. The red line is the 0.0 m MSL contour.

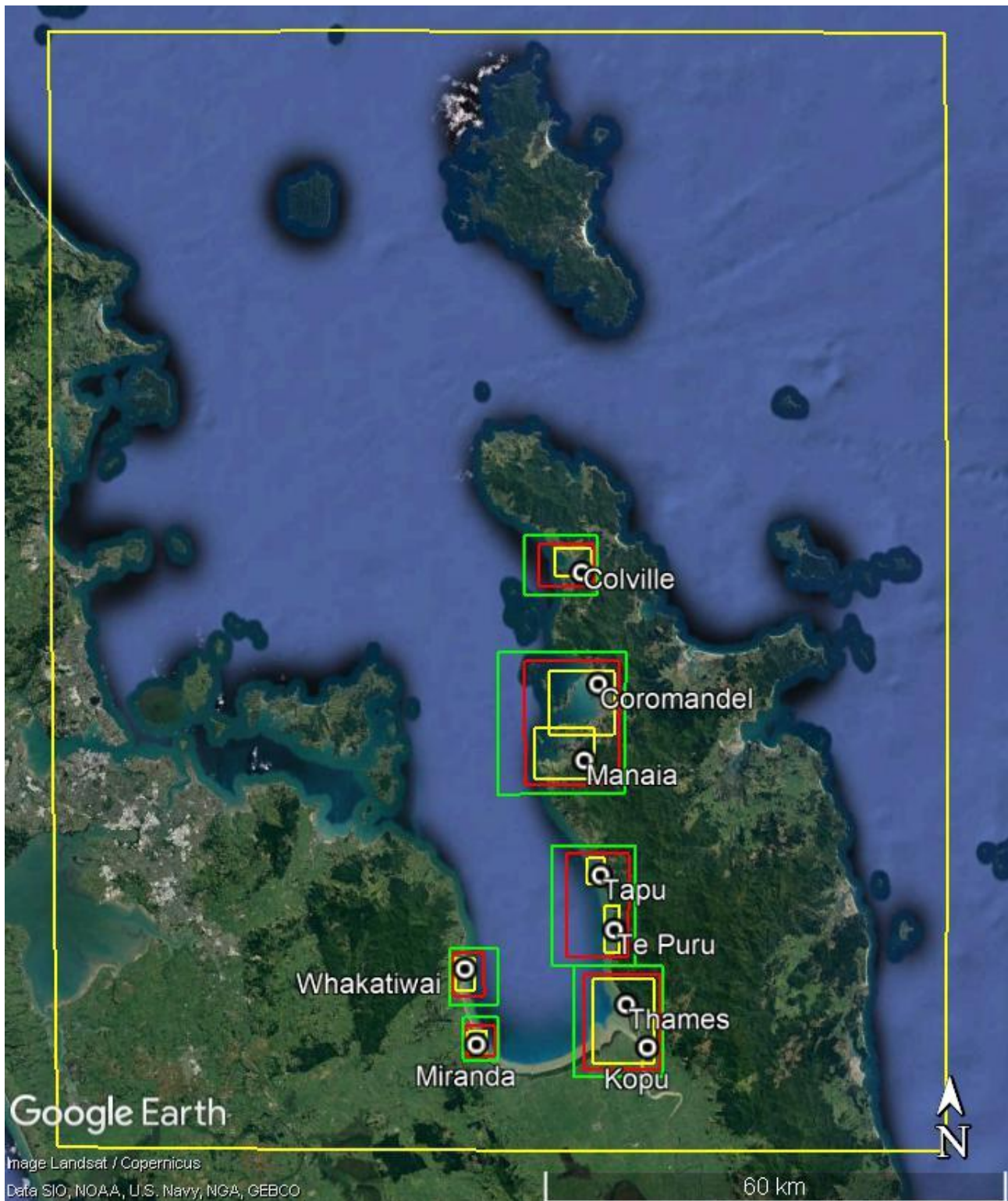


Figure 1.8 Grid set up for the local source modelling. The outer yellow rectangle is the propagation model grid, then the green and red rectangles denote the A and B level grids. The smaller yellow rectangles are the extents of the C-level grids.

1.4 Validation of the ComMIT Tsunami Model

The ComMIT model has been validated for both distant source and near source events. In the following sections we present results showing the performance.

1.4.1 Case 1: The February 27, 2010 Maule, Chile Earthquake and Tsunami

For the 2010 Maule Chile event we used the tsunami source model developed by NOAA for use within the ComMIT system. This source is shown in Figure 1.9 below along with the resultant trans Pacific propagation pattern of the maximum tsunami amplitude. We compared the model output to water level recorded at Auckland because this is the nearest site to the study area with available tide gauge data from a tsunami event. The model to measured comparison is presented in Figure 1.10 and shows a good fit in terms of arrival time, wave shape and amplitude between the measured and model result.

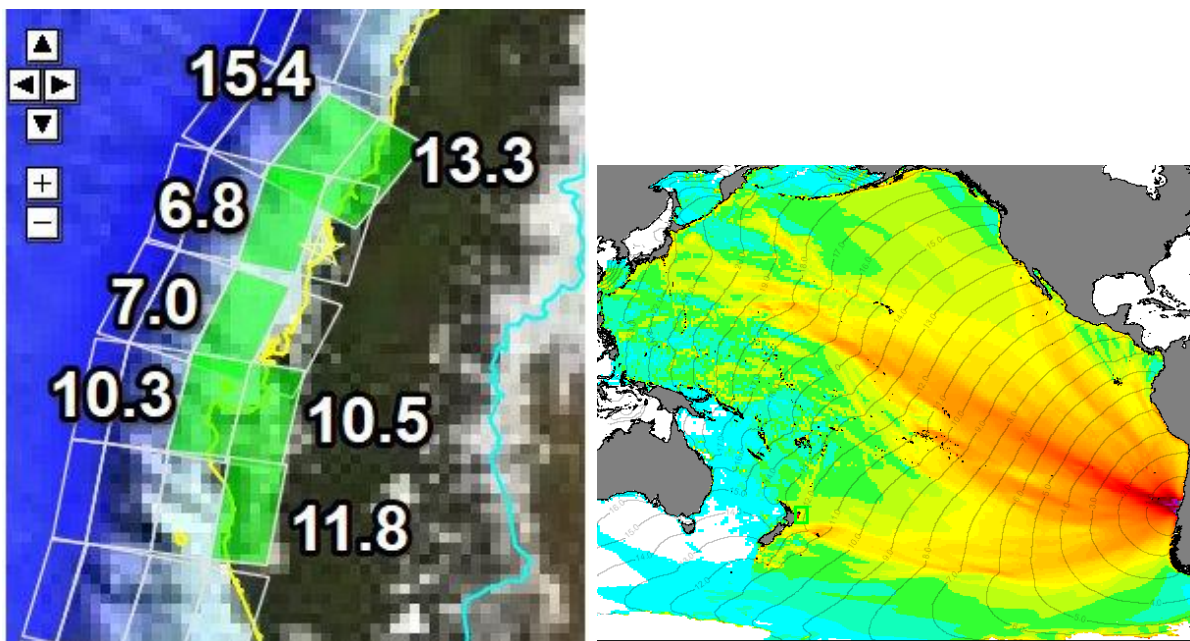


Figure 1.9 Tsunami source model (left) and the trans-Pacific propagation pattern (right) for the 2010 Maule, Chile tsunami. Slip amounts (in meters) for the individual fault segments are indicated in white.

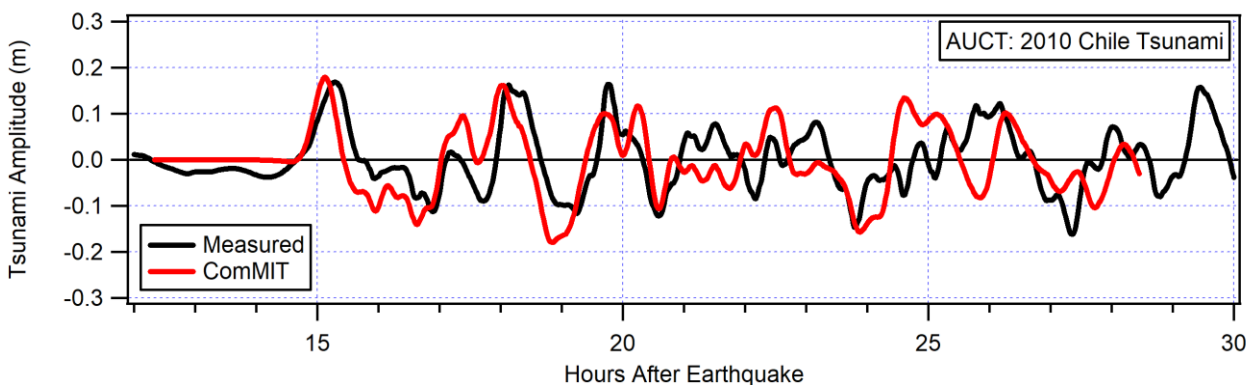


Figure 1.10 Modelled water level time series compared to measured data at the Port Gisborne tide gauge for the 2010 Maule, Chile tsunami.

1.4.2 Case 2: The March 11, 2011 Tohoku Earthquake and Tsunami

The March 11, 2011 Tohoku earthquake and tsunami also presents an excellent case study for the validation of the ComMIT model. The tsunami event was recorded on tide gauges throughout New Zealand with a wealth of data recorded on 5 water level gauges and one current meter in Tauranga Harbour (Lynett et al., 2012, Borrero et al., 2012, Borrero and Greer 2013). As with the 2010 event, here we compare the model results to the nearest available sites with recorded tide gauge data from the event, namely Great Barrier Island and Auckland. Also, as with the Chile event, the model was initialised using the tsunami source developed by NOAA for use within the ComMIT modelling system (see Figure 1.11).

The model results (Figure 1.12) show a good fit to the measured data. In terms of arrival time, wave form and amplitude as compared to the Auckland tide gauge data. At Great Barrier, the model also does a very good job at matching the arrival time and amplitudes over the first five hours of tsunami activity. One exception being the large wave cycle occurring between 15 and 16 hours after the earthquake. After 17 hours, the model tends to under-predict the measured amplitudes at Great Barrier.

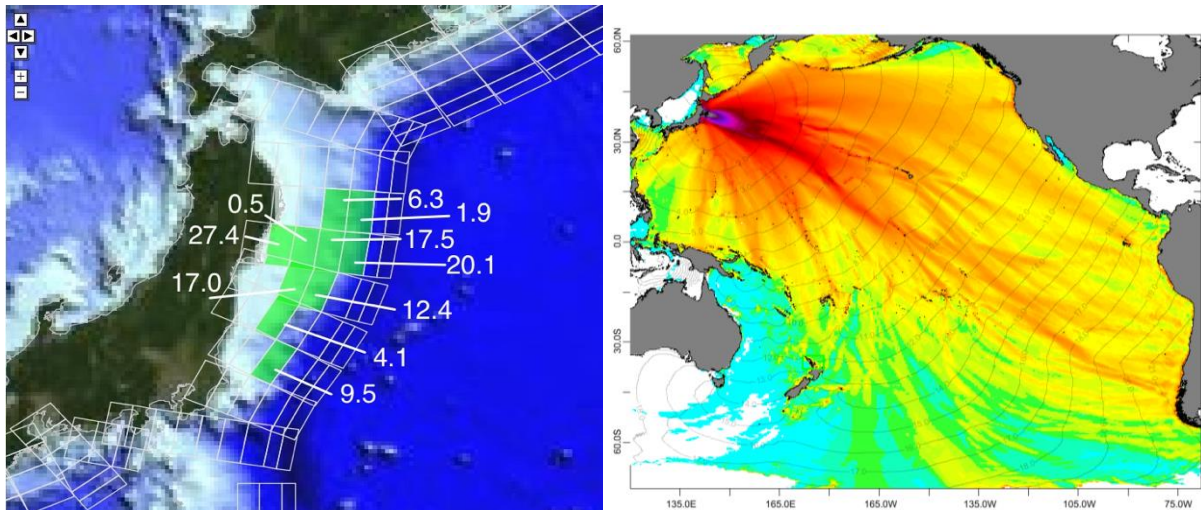


Figure 1.11 Tsunami source model (left) and the trans-Pacific propagation pattern (right) for the 2011 Tohoku, Japan tsunami. Slip amounts (in meters) for the individual fault segments are indicated in white.

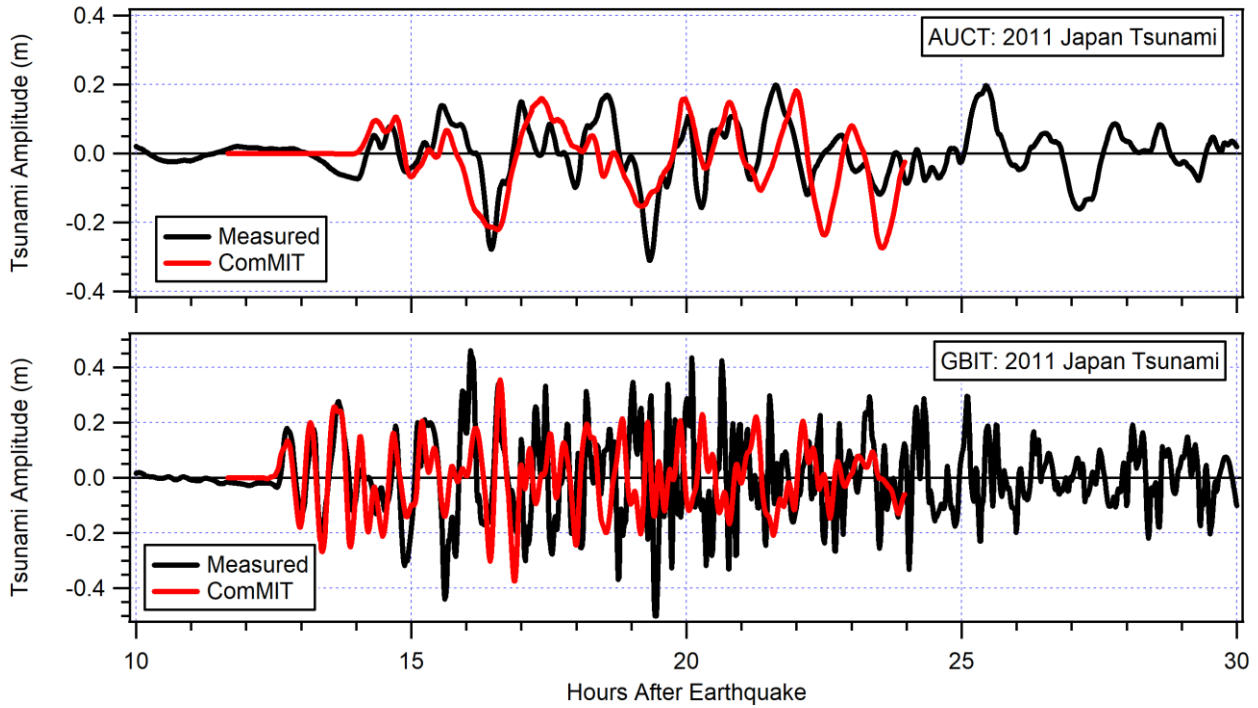


Figure 1.12 Modelled water level time series compared to measured data at Auckland (top) and Great Barrier Island (bottom) for the 2011 Tohoku, Japan tsunami.

1.4.3 Case 3: The September 2, 2016 East Cape Earthquake and Tsunami

On 2 September 2016 at 4:37 am NZST (1 September 16:37 UTC), a Magnitude 7.1 (GeoNet) earthquake struck just north-east of the East Cape of New Zealand (Figure 3.10). The event was felt throughout the North Island. More than 4,000 people filed felt earthquake reports on the GeoNet community reporting system, with reports coming in from as far away as Chatham Island and Christchurch (GeoNet, 2017). The event created a small non-damaging tsunami that was recorded on tide gauges in Gisborne and across the Bay of Plenty.

This event is important in that it was relatively strong and occurred along the Tonga-Kermadec subduction zone, and in an area considered as the 'worst-case' source region for generating tsunamis affecting the East Cape, Bay of Plenty, Coromandel and Northland coasts – this due to its proximity and associated short travel times to these regions.

The source mechanism for this event was not, however, a straightforward subduction zone event. The strike of the fault plane was oblique, and the source region was displaced west of the trench axis, suggesting a seismic rupture within the overriding Australian plate (Figure 1.14, top panel). Additionally, the sense of the rupture was that of a 'normal' fault rather than a thrust or 'reverse' fault commonly associated with ruptures on a subduction zone interface. This means that the seafloor displacement above the source area was downward (i.e. negative) rather than upward (uplift). This is indicated by the direction of the slip vector arrows in the bottom panel of Figure 1.14.

To model this event using the pre-computed sources in the ComMIT database, some assumptions and approximations were necessary. Firstly, it was necessary to use a fault segment located to the east of the actual source region. Next, a negative average displacement was applied to the fault plane to produce a negative initial seafloor displacement. Two slip amounts were trialled, -0.4 m and -0.6 m.

The model results are compared to measured tide gauge data at Lottin Point and Tauranga Harbour in Figure 1.15. The comparison of the waveform at Lottin Point is remarkably good - given the approximations - with the results from the two source models neatly bracketing the measured data. Note that the modelled time series had to be shifted 7 minutes earlier to match the timing of the measured data. This accounts for the fact that the source region used in the model is located further away to the west of the actual source region, thus requiring more time for the wave to reach the tide gauge.

The results for Tauranga are not as good with the model over predicting the measured wave heights and requiring a 14-minute time shift to match the timing of the peaks and troughs. However, this is understandable given the very small size of the tsunami and the degree of attenuation that likely occurred as this small signal passed through the narrow entrance of Tauranga Harbour.

Given the limitations of the ComMIT model, the results are good and show that it can be used to accurately predict tsunami heights along the New Zealand coast from near-field tsunami sources.

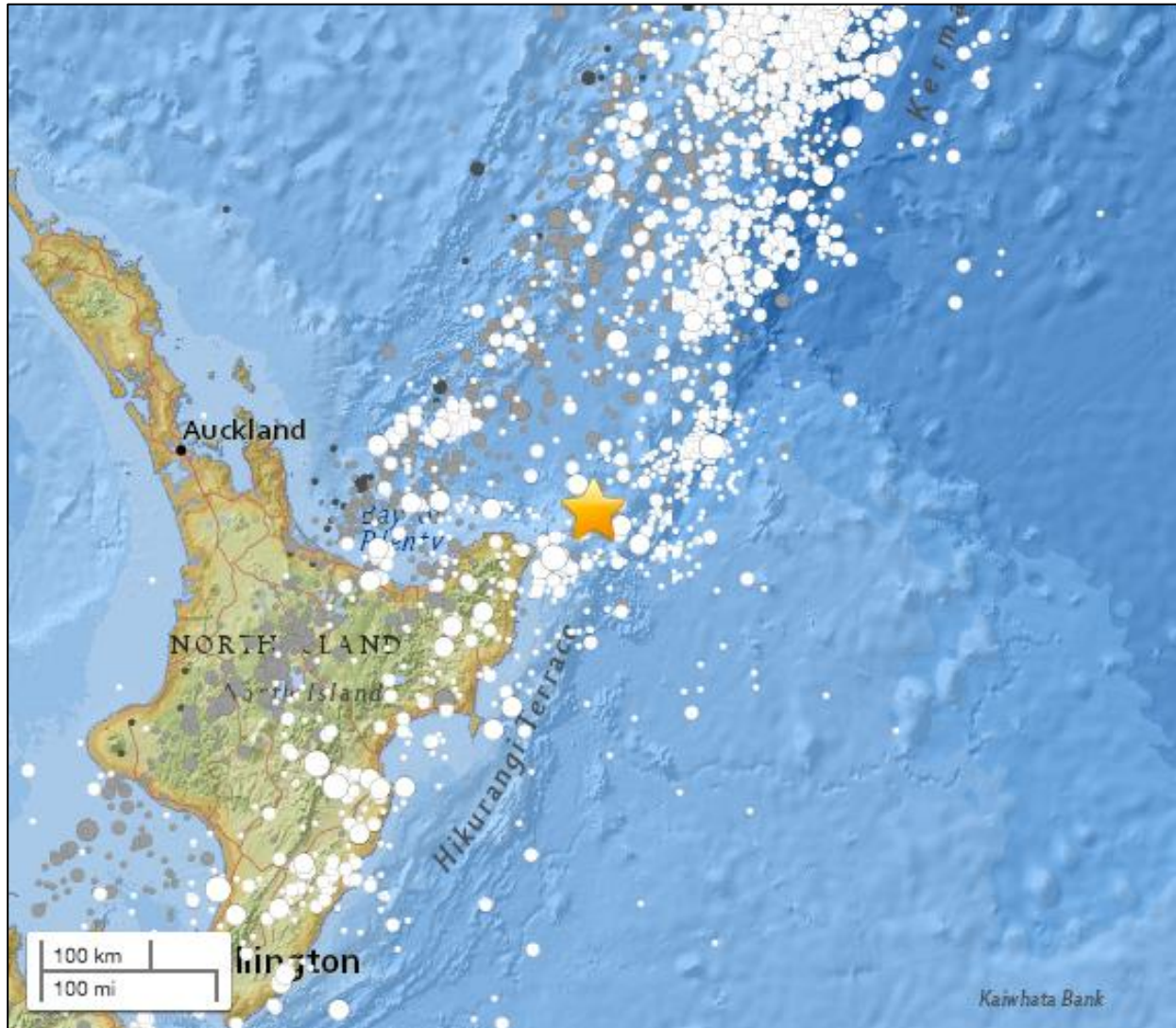
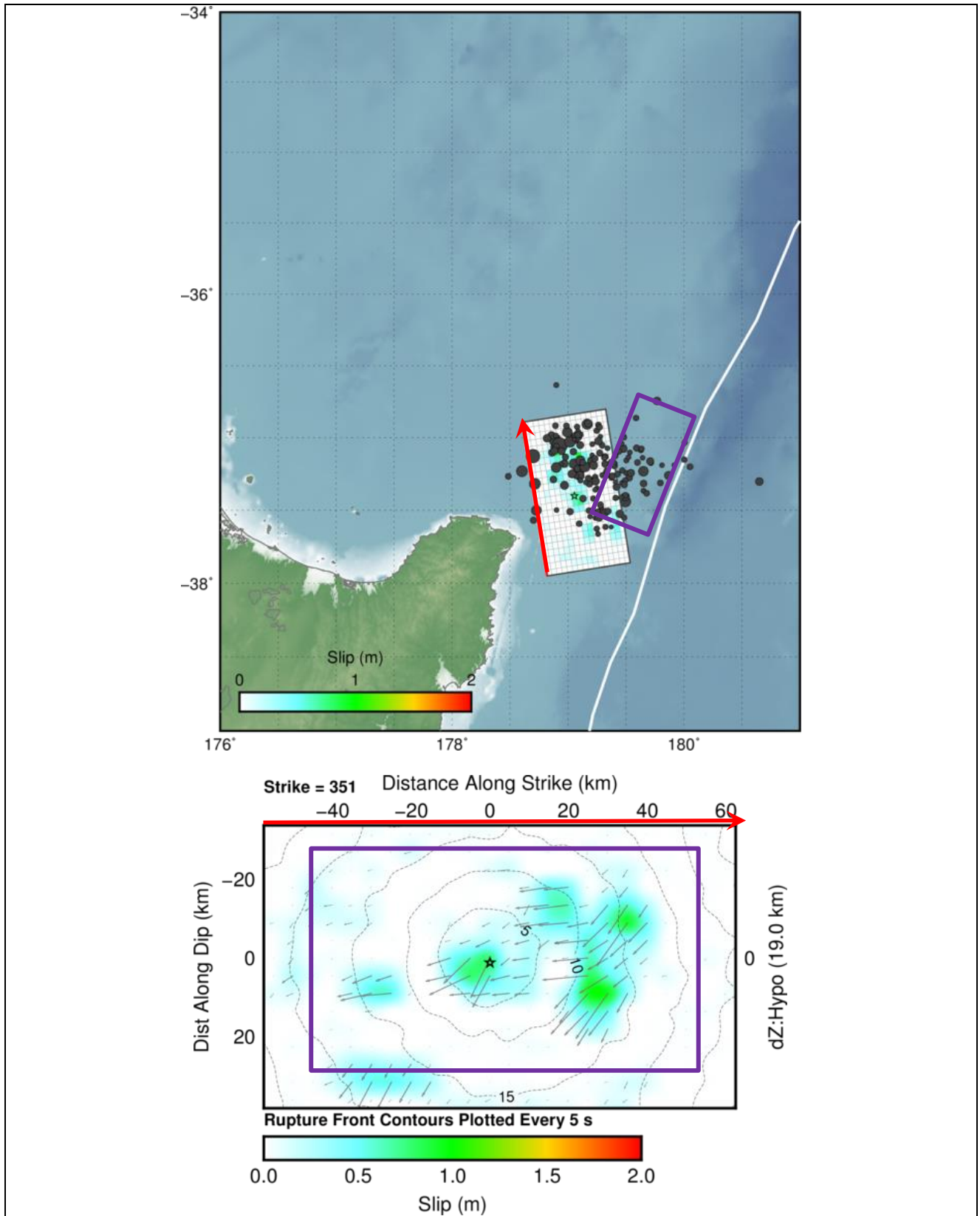


Figure 1.13 Source location of the September 2nd East Cape Earthquake (USGS, 2017).

Figure 1.14 (following page) Top panel: Earthquake source model for the September 2, 2017 East Cape earthquake (reproduced from USGS, 2017). The top panel shows the location of the fault plane (white region). Epicentre of the mains shock is indicated by a star with aftershocks indicated by black circles. Coloured patches indicate coseismic slip amounts according to the colour scale. The thin red line is the top of the fault plane. The white line is the axis of the Tonga-Kermadec Trench. The purple rectangle shows the location of a 100x50 km fault plane source available in the ComMIT tsunami modelling database. Bottom panel: A detail of the slip distribution along the fault plane with the amount of slip indicated by the colour scale. The location of the earthquake hypocentre is indicated by the star with the arrows indicating the direction of the rupture displacement. The contour lines are the timing (in seconds) of the rupture. The red arrow at the top of the fault plane corresponds to the red arrow in the upper panel. The purple box shows the dimensions of a 100x50 km fault plane.



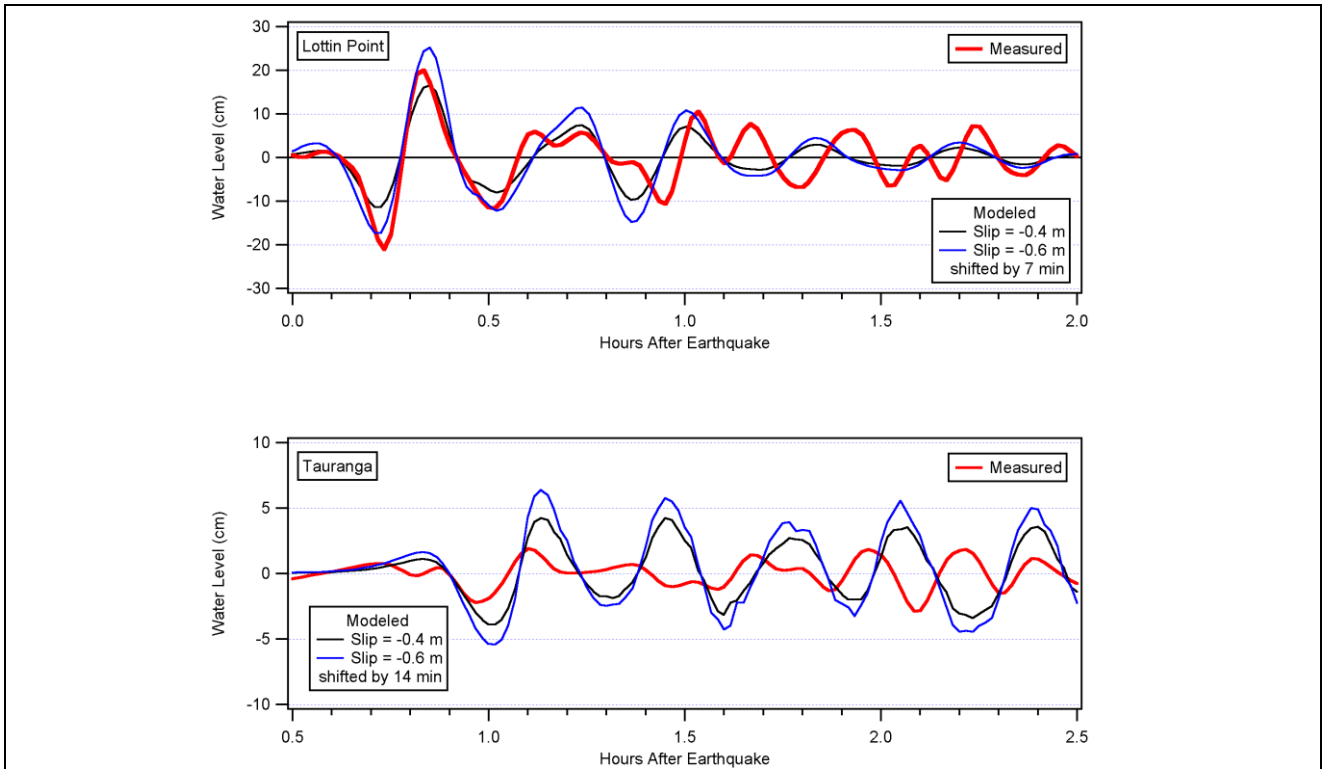


Figure 1.15 Modelled (blue and black traces) versus measured (red trace) water levels at Lottin Point (top) and Tauranga (bottom) for the 1 September 2016 tsunami.

2 TSUNAMI SOURCE MODELS

eCoast has conducted numerous previous studies focussed on tsunami hazards in the Waikato Region. These studies have investigated in detail several potential local, regional and distant source tsunamis to determine a Maximum Credible Event (MCE) for each type of event. It is important to understand that the classification of a tsunami source is dependent on the travel time to the site of interest. These are defined in Power (2013) as follows:

- Distant source – more than 3 hours travel time from New Zealand
- Regional source – 1–3 hours travel time from New Zealand
- Local source – 0–60 minutes travel time to the nearest New Zealand coast.

For the distant source scenarios, we focus on sources from the West Coast of South America while the regional source is a rupture on the southern section of the Tonga-Kermadec (TK) trench just north of East Cape and the local tsunami sources are faults located within the Firth of Thames.

This nomenclature differs somewhat from previous reports which considered the tsunami hazard on the east coast of the Coromandel Peninsula. For these sites, the travel time for the TK trench source to the coast is approximately 1 hour and hence they were considered 'local'. However, for the Firth of Thames (FoT), waves from the TK source arrive at the study sites some 2-3 hours after the causative earthquake and hence the TK source is now considered 'regional' while tsunami generated by faults inside the Firth are the 'local' sources.

2.1 Local Tsunami Sources

For the local tsunami sources, we focussed on ruptures of the offshore extension of the Kerepehi Fault as described primarily by Chick (1999) and to a lesser degree by Persaud et al. (2015). In her study, Chick (1999) identified five separate segments for the offshore extension of the Kerepehi Fault as indicated in Figure 2.1.

Chick's (1999) study also proposed sizes and magnitudes for Most Credible Earthquake scenarios on these segments. These fault parameters are reproduced in Table 2.1 (taken from Table 4.2 in Chick 1999). For the fault parameters given by Chick (1999) we used the moment magnitude, slip amount and fault length to constrain the fault width using the relationship:

$$M_o = \mu u A;$$

where μ is the rigidity of the rock material, A is the fault place area ($L \times W$ in meters) and u is the fault displacement (in meters). Moment magnitude (M_w) is converted to seismic moment (M_o) through the relationship:

$$M_w = 2/3(\log_{10}M_o - 6.05)$$

For this study, in order to be conservative, we assumed a rigidity of 2.5×10^{10} Nm as opposed to a more typical value of 3×10^{10} Nm. The net result of this is to slightly increase the fault width for given values of length, slip amount and seismic moment.

To calculate the sea floor deformation, we use the fault parameters in Table 2.1 with the elastic dislocation model of Okada (1985). This sea floor deformation is then translated

directly to the water surface as the initial condition for the tsunami hydrodynamic model. The initial surface deformation for the five fault scenarios are shown in Figure 2.2 through Figure 2.4.

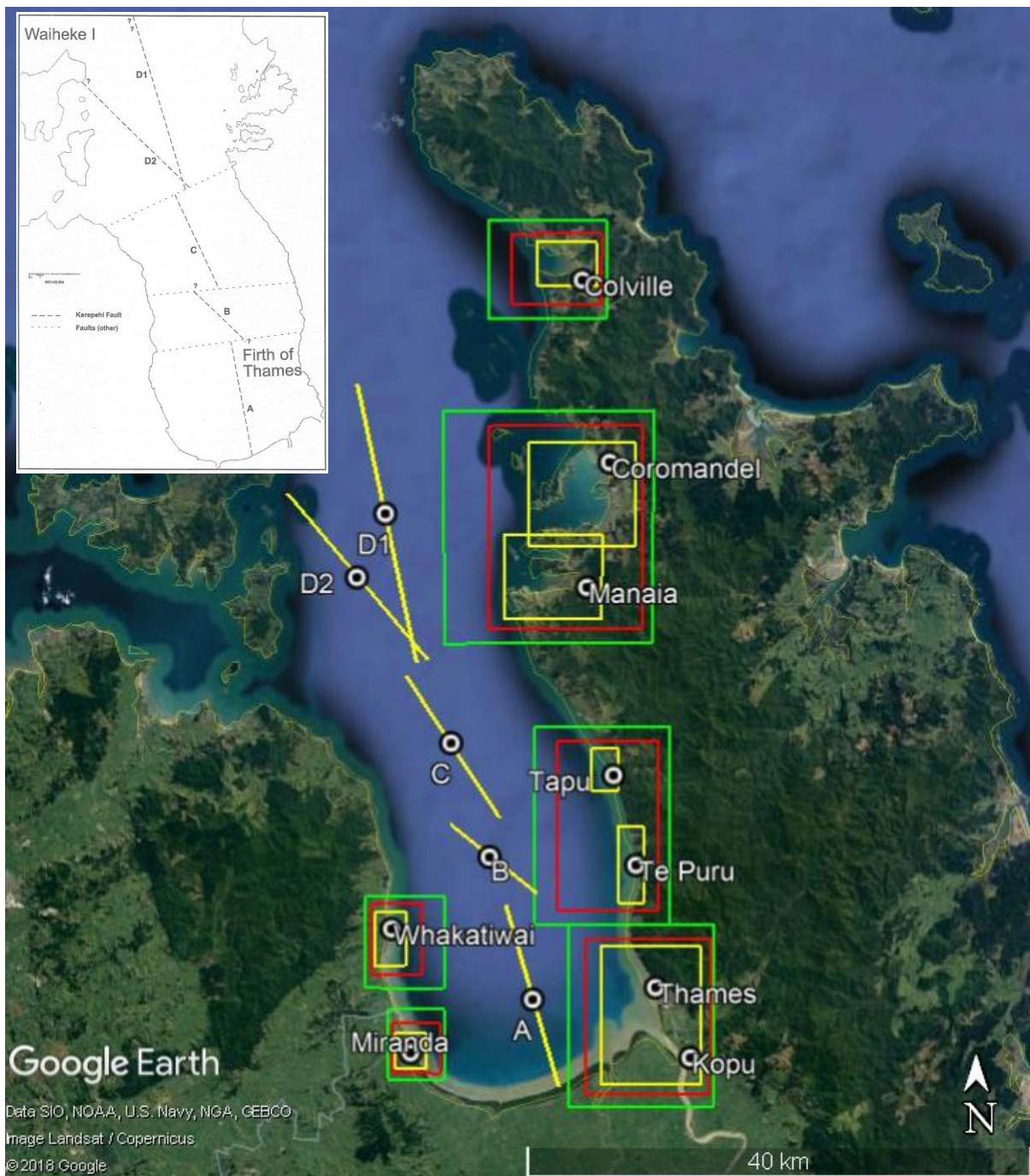


Figure 2.1 Yellow lines indicate the locations of the surface traces of the offshore fault segments associated with the Kerepehi Fault. Coloured rectangles are the A, B and C level grids used for the local source modelling. Inset shows the locations of the fault traces as described in Chick (1999).

Table 2.1 Fault parameters for the 'most credible earthquake' scenarios described in Chick (1999), Table 4.2.

Segment	Mw	L	W	Dip	Rake	Slip
A	6.7	15.0	14.8	60	90	2.4
B	6.5	8.8	12.5	60	90	2.4
C	6.7	13.5	16.5	60	90	2.4
D1	6.8	22.5	14.0	60	90	2.4
D2	7.1	16.0	15.6	60	90	8.5 ¹

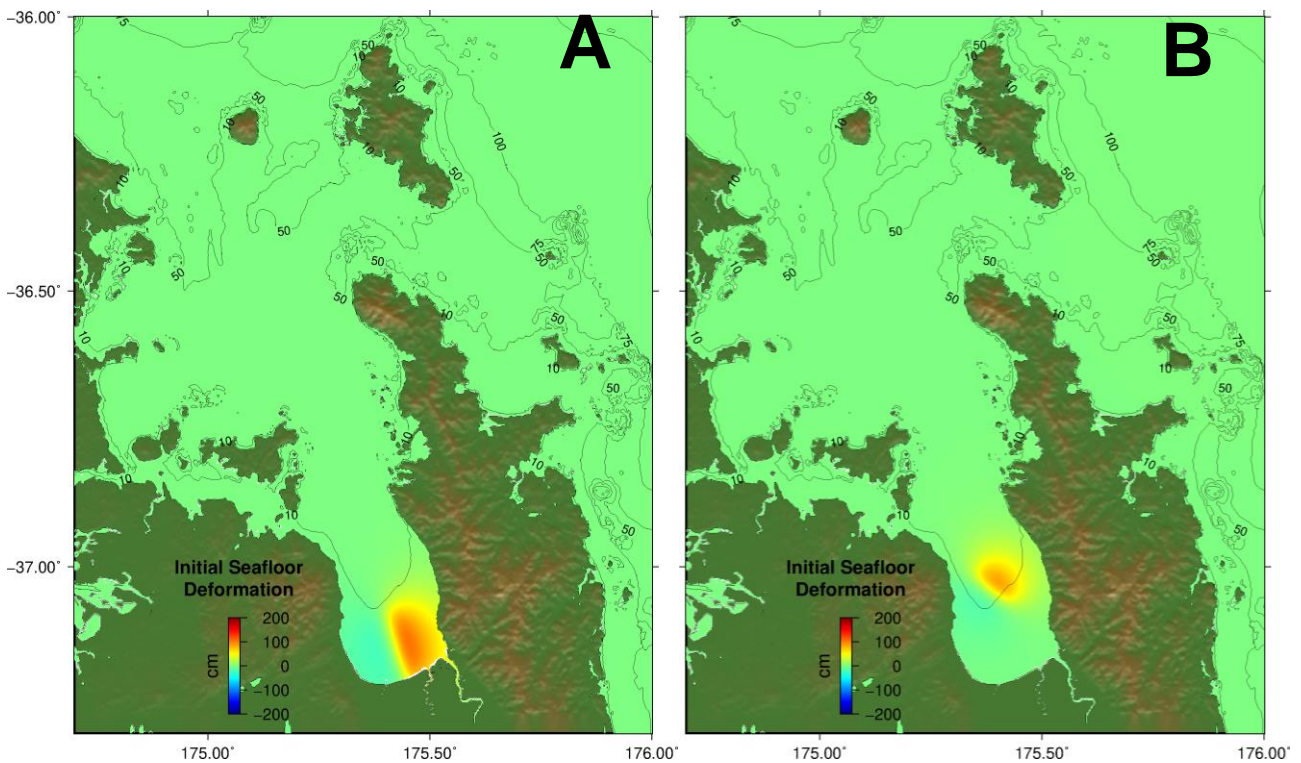


Figure 2.2 Initial sea-floor deformation for sources A and B

¹ Note: these slip amounts are taken from Chick (1999) Table 4.2, Page 74 and are somewhat greater than the values presented later in the thesis in Table 5.1, Page 84 (and also in Chick et al. (2001) Table 1). Hence, they are somewhat conservative.

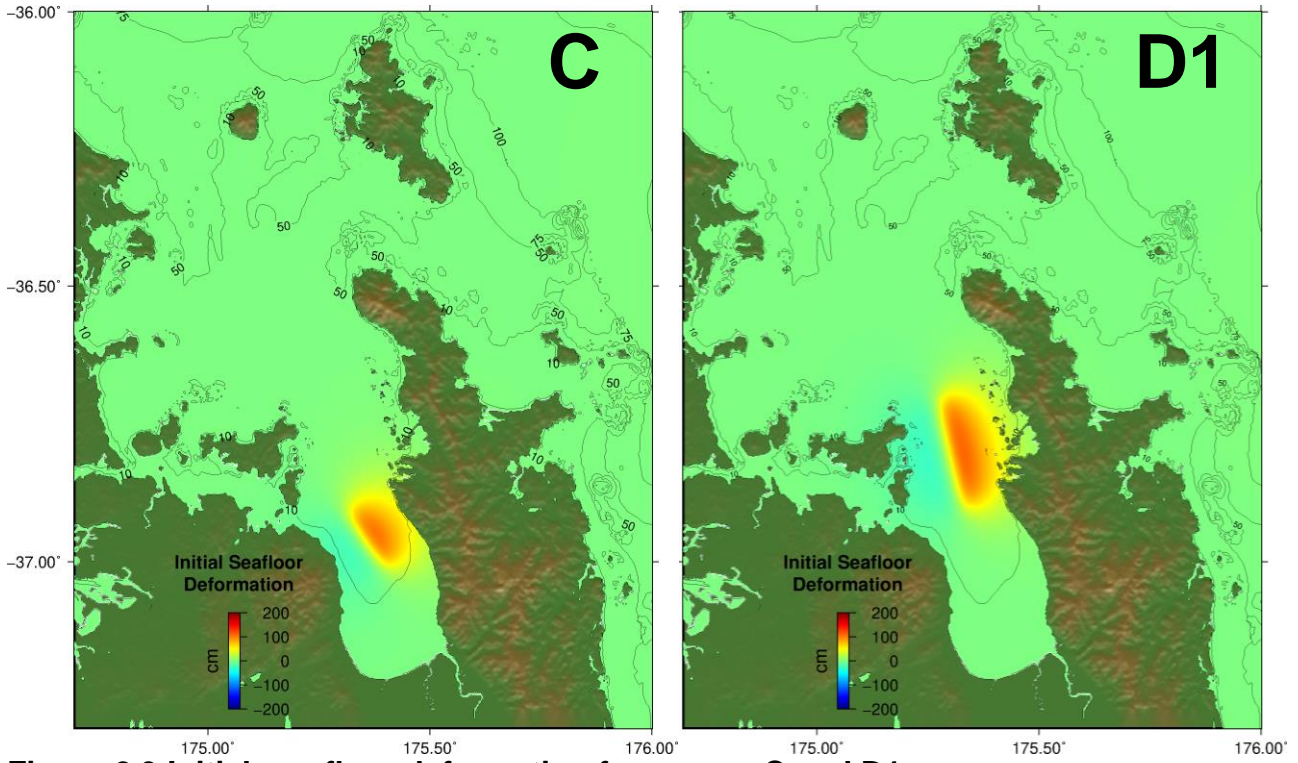


Figure 2.3 Initial sea-floor deformation for source C and D1

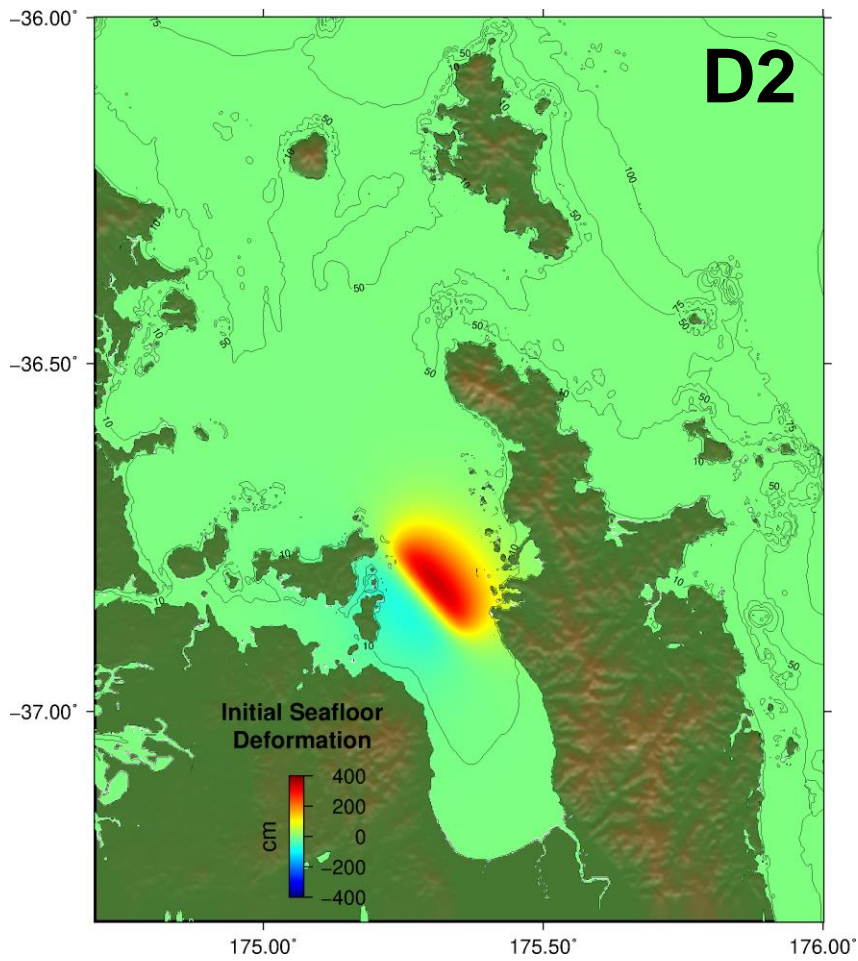


Figure 2.4 Initial sea-floor deformation for source D2, note the different colour scale.

2.2 Regional Tsunami Source Model

Based on previous tsunami hazard studies conducted by eCoast for the WRC, it has been determined that the largest near source hazard comes from a large-scale rupture of the southern sections of the Tonga Kermadec trench situated to the north of East Cape. Specifically, the Waikato Regional Council has adopted a source model designated ‘TK8’ as the Maximum Credible Event for evaluating near source tsunami hazards in the region. This source model is based on the tsunami source used to simulate the effects of the 2011 Tohoku Japan earthquake and tsunami in both the near and far field. The details of this source model are explained in Wei et al. (2013 2014) and shown in Figure 2.5 below. For use in the Waikato region, we simply translated this slip distribution to fault segments located along the southern end of the Tonga Kermadec Trench and used the resulting seafloor deformation to initialise the tsunami hydrodynamic model (Figure 2.6).

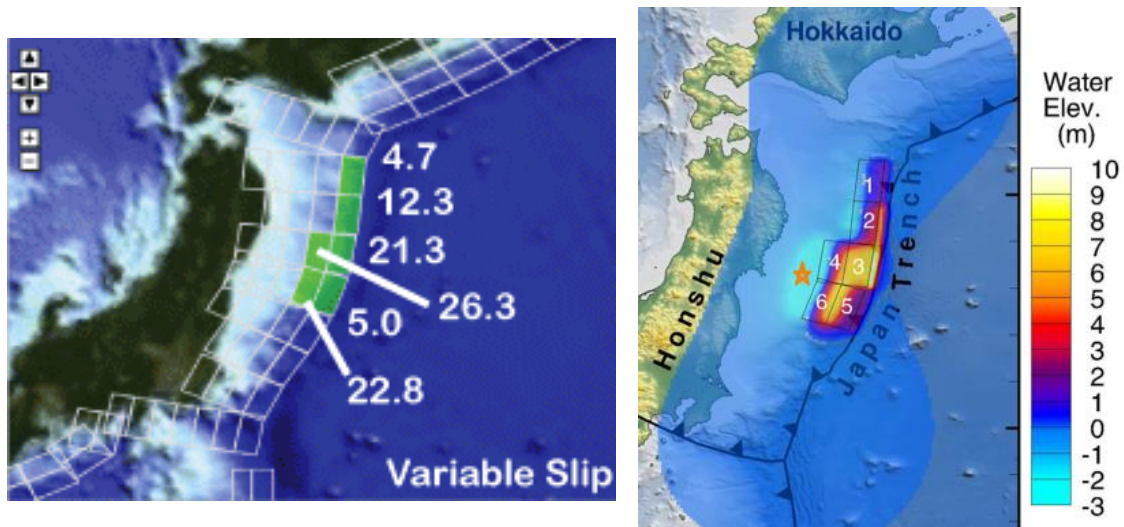


Figure 2.5 Source model used for the 2011 Tohoku tsunami, The amount of slip on each segment is indicated in the left panel, while the vertical deformation of the sea floor is shown on the right (image reproduced from Wei et al., 2013).

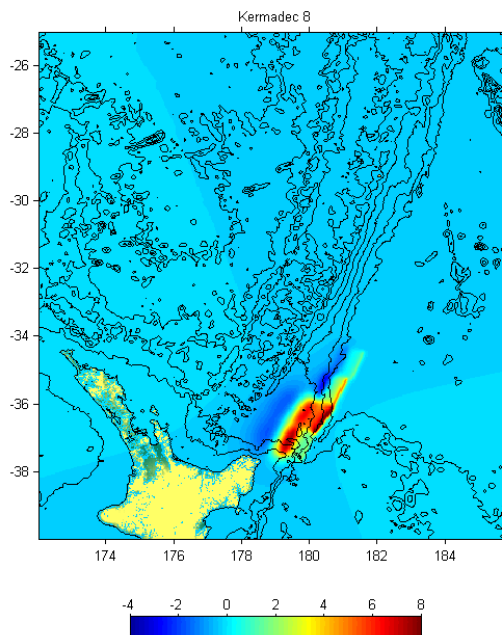


Figure 2.6 Case TK 8, the Japan 2011 tsunami source positioned at the southern end of the Tonga-Kermadec Trench.

2.3 Distant Tsunami Source Models

In the previous tsunami hazard studies mentioned above, a total of eight distant source events were considered (Table 2.2). These are based on three historical events from Chile (1868 Arica, 1960 Valdivia, 2010 Maule) and one historical event from Japan (2011 Tohoku). An additional four sources are derived from the source model for the 1960 Valdivia earthquake but are positioned at different locations and with different slip distributions. Of these, the case 'FF 7' scenario was shown to give the strongest response at Whitianga has been adopted as the MCE for distant source event affecting the Waikato Region. However, because historical information for both the 1868 and 1960 events exists for sites in the Firth of Thames and because the 1868 event was so big, we also modelled these events for this assessment.

Table 2.2 Description of the distant source tsunami scenarios. The 'FF 1' (1960), 'FF 3' (1868) and 'FF 7' sources were modelled in this study.

Number	Source
FF 1 'Chile 1960'	The 1960 Valdivia, Chile earthquake. Source model based on Fujii and Satake (2012) (M ~9.2)
FF 2 'Chile 2010'	The 2010 Maule, Chile earthquake, source derived from NOAA real-time tsunameter inversion. (M ~8.8)
FF 3 'Arica 1868'	1868 Arica – A very large magnitude event (M ~9.4) extending from Arica, Chile 600 km northward into southern Peru. Source uses uniform slip of 39.6 m over the fault plane.
FF 4 'Chile North 1'	Chile North 1 – A variant of the Fuji and Satake (2012) source for the 1960 tsunami modified to concentrate largest amounts of slip towards the north of the fault rupture and positioned such that the deformation region runs from northern Chile towards the south. (M ~9.1)
FF 5 'Chile North 2'	Chile North 2– A variant of the Fuji and Satake (2012) source for the 1960 tsunami modified to concentrate largest amounts of slip towards the north of the fault rupture and positioned such that the deformation region straddles the Peru/Chile border with the largest deformation occurring offshore of southern Peru. (M ~9.2)
FF 6 'Chile North 3'	Chile North 3– A variant of the Fuji and Satake (2012) source for the 1960 tsunami modified to concentrate largest amounts of slip towards the south of the fault rupture and positioned such that the deformation region straddles the Peru/Chile border with the largest deformation occurring offshore of northern Chile. (M ~9.2)
FF 7 'Central Peru'	Peru – A variant of the Fuji and Satake (2012) source for the 1960 tsunami modified to concentrate largest amounts of slip towards the south of the fault rupture and positioned along the coast of Central Peru. (M ~9.2)
FF 8 'Japan 2011'	The 2011 Tohoku, Japan event. (M ~8.8)

The source model for the 1960 Valdivia, Chile earthquake used here was developed in Borrero (2013) and based on Fujii and Satake (2013). Borrero (2013) conducted a detailed analysis of the effects of the 1960 tsunami at Whitianga. In that study the numerical model results from 6 different versions of the 1960 tsunami source were compared with eyewitness accounts and observations of inundation at Whitianga. The results suggested that the earthquake slip distribution proposed by Fujii and Satake (2013) provided the best overall fit to the observed effects. However, it was necessary to increase the slip amounts by 20% to most accurately reproduce the observed inundation. The fault segments, initial seafloor deformation and slip amounts used for the 1960 source are shown in Figure 2.7 and Table 2.3.

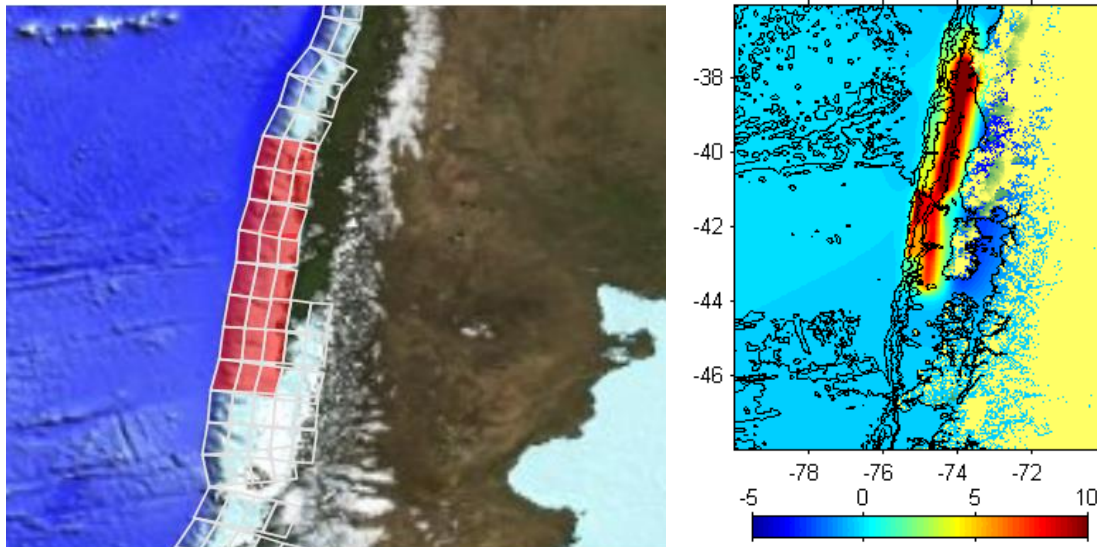


Figure 2.7 (left) Unit source segments used to define the 1960 Chilean Earthquake suite of events. (right) initial sea floor deformation at the source region.

Table 2.3 Faults segment slip amounts for the 1960 Chilean tsunami. Segments with slip >20 m are highlighted in pink.

		Fault Segment Slip Amounts			
North		5.0	12.9	1.2	
		6.6	36.1	21.0	
		2.8	31.1	11.3	
		4.9	29.6	11.5	
		7.8	32.9	6.6	
		25.7	17.8	6.2	
South		15.3	21.7	5.5	
		3.7	20.5	2.7	
		East	←	→	West
		Shallow	←	→	Deep

Using the slip distribution of the 1960 Valdivia earthquake as a starting point, we rearranged the slip values on individual fault segments to concentrate the segments with largest slip together either in the northern or southern ends of the fault plane. This was done to constrain the overall magnitude while possibly generating a stronger tsunami due to the concentration of the high slip areas. The resulting slip distribution is then positioned at the desired location along the South American Subduction Zone. For this study we used the southern concentrated slip case positioned off the coast of central Peru (case FF 7).

Table 2.4 The rearranged slip distribution for the southern concentrated slip case. Segments with slip >20 m are highlighted in pink.

2.8	17.8	1.2
4.9	20.5	5.5
5.0	21.7	6.2
6.6	31.1	6.6
15.3	32.9	11.5
25.7	36.1	21.0
7.8	29.6	11.3
3.7	12.9	2.7

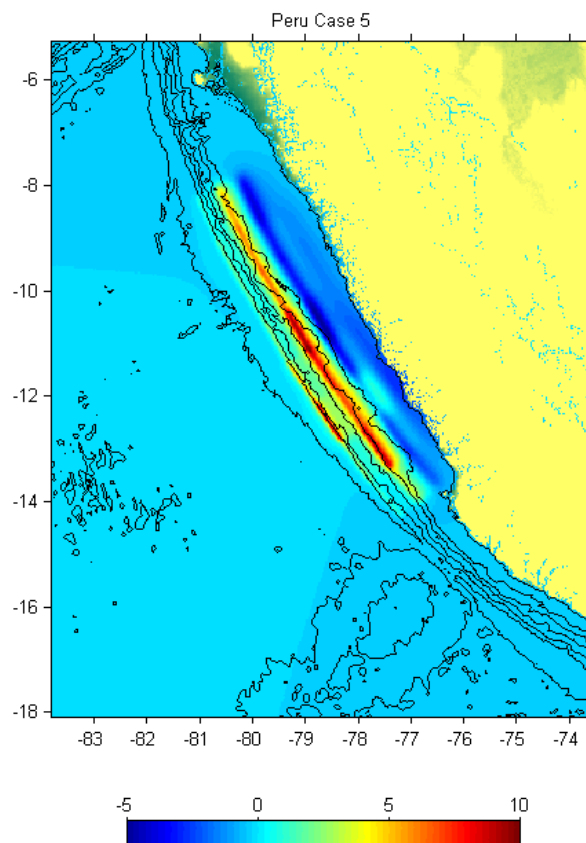


Figure 2.8 Seafloor deformation for cases, FF 7 uses the the southern concentrated slip distribution.

To model the tsunami of 13 August 1868, we based our tsunami source on the rupture length estimate of 600 km presented in Dorbath et al., (1990). Using fault segments extending from Arica northward (Figure 2.9), the model is initialized with a uniform slip amount of 39.6 m. Borrero and Goring (2015) showed that this amount of slip was necessary to replicate the observed 7 m water level change observed in Lyttleton Harbour as described by Gibson (1868).

While there were no instrumental recordings of this tsunami, there are detailed accounts of the wave effects in New Zealand (de Lange and Healey, 1986). It is interesting to note that the effects on the North Island seem to be less severe than those on the South Island, with reported tsunami heights of 1-2 m at Mount Maunganui, Great Barrier Island and in the Tamaki Estuary. Even at Port Charles, the tsunami was only described as ‘a high tide’. This contrasts with the effects at Lyttleton Harbour near Christchurch, where the observations of Gibson (1868) suggested a peak to trough tsunami height of ~7.6 m (25 feet) for the first tsunami wave.

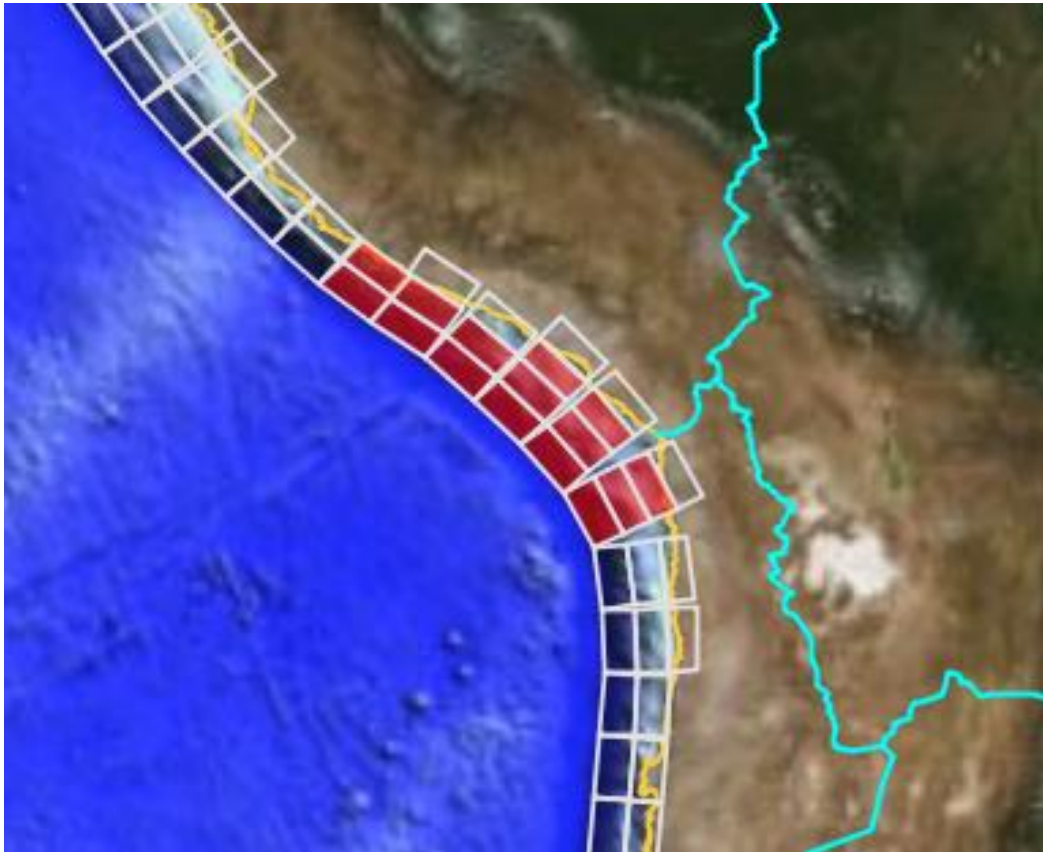


Figure 2.9 Source segments used to model the 1868 Arica tsunami. A uniform slip amount of 39.6 m was applied to each segment.

3 MODEL RESULTS LOCAL FAULTS

In Figure 3.1 and Figure 3.2 we present the maximum computed tsunami amplitude for the five local source scenarios. As expected, the effects are highly localised and largely confined to the Firth of Thames. For each source, the strongest effects and greatest tsunami heights are generally seen on the coastline immediately adjacent to the deformation area or on the opposite shore of the Firth.

One example of this is for source A where we see that the larger tsunami heights are confined to the southern end of the Firth of Thames. In Figure 3.3 we present time series of tsunami water levels from the three sites in the southern portion of the Firth: Thames, Miranda and Whakatiwai. On the Thames grid, we see that the earthquake source itself results in an uplift of the coast on the order of 60 cm. The tsunami itself is then manifest as a withdrawal of the sea surface followed by relatively small oscillations. Due to the uplift of the coast, no inundation is predicted for Thames. On the other side of the Firth at Miranda and Whakatiwai, we see that the model begins with localised subsidence of the order of 10-20 cm. This is followed by a positive surge of approximately 50 cm at both Miranda and Whakatiwai. However, this also does not result in any appreciable inundation at either site.

Time series of tsunami water levels at each study site for the different sources are presented in Appendix 1 (Figure 9.2 through Figure 9.16). Inspection of the plots shows that for all of the cases, tsunami heights from the D2 Source exceed those of the other cases.

In general, for all but source D2, the tsunami heights at the shoreline are small and relatively insignificant. However, for source D2, significant inundation is predicted, particularly for the study sites located nearest to the source region, i.e. Colville, Coromandel and Manaia.

Hence the D2 source is used for the assessment of the inundation extents. These inundation extents are presented for the MSL and MHWS scenarios in Figure 3.5 through Figure 3.11.

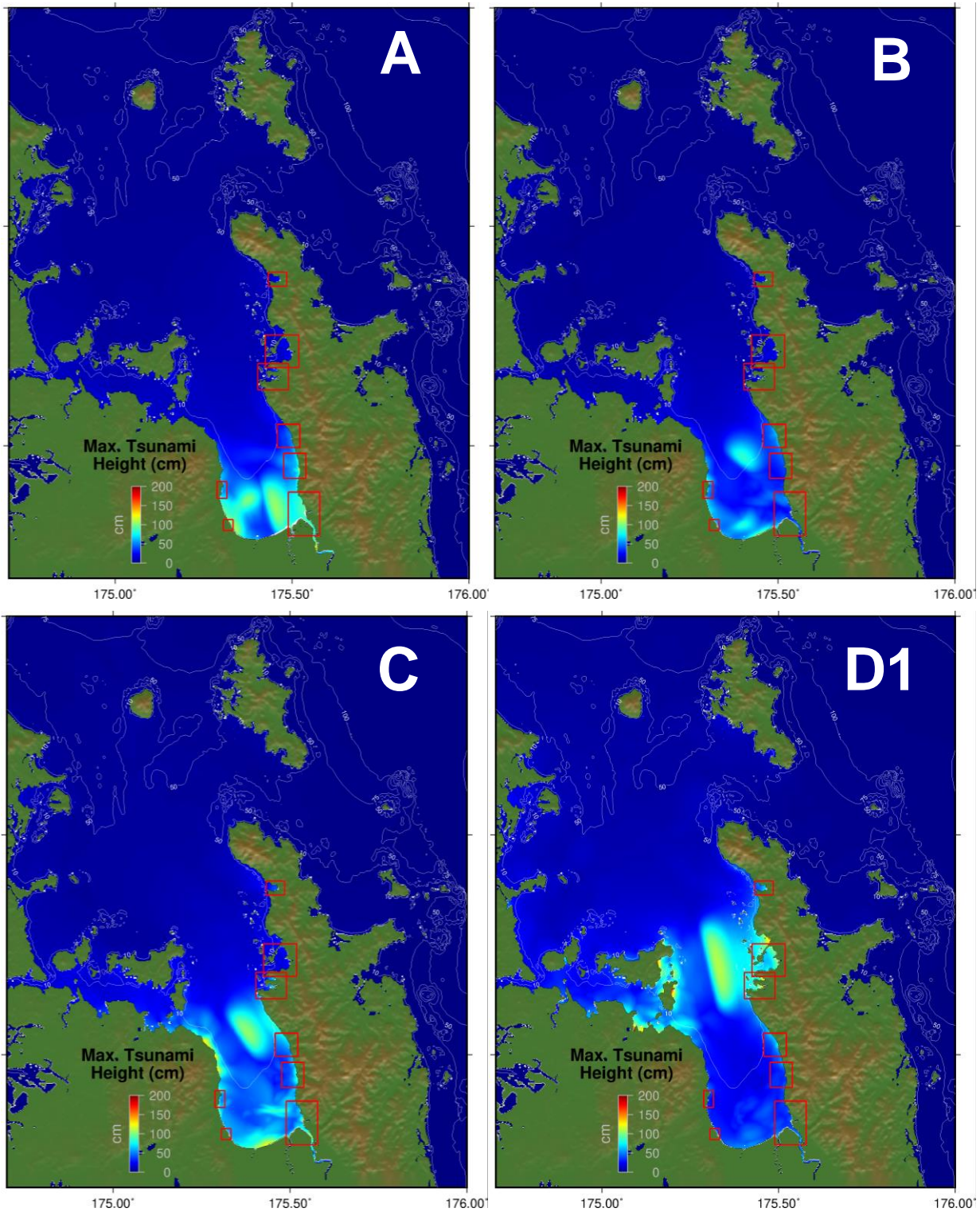


Figure 3.1 Modelled maximum tsunami heights across the 200 m resolution local propagation grid for sources A-D1.

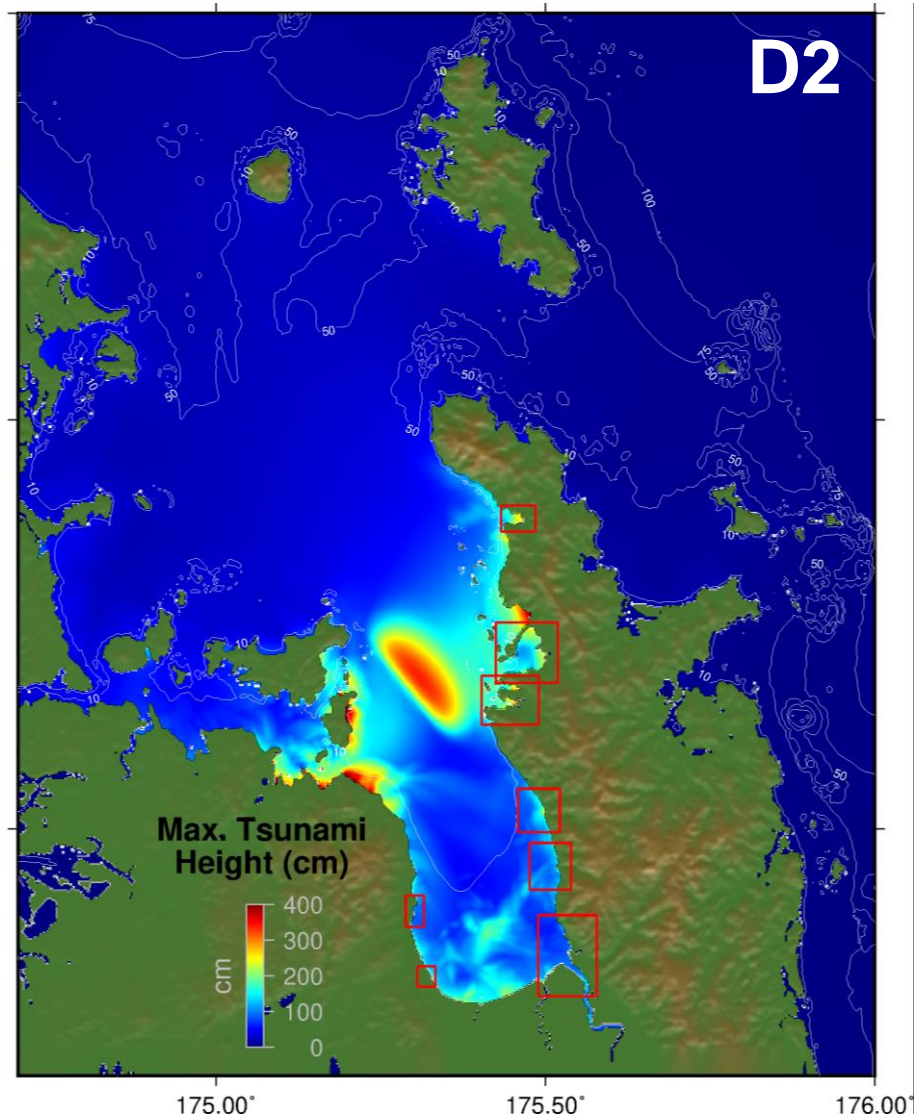


Figure 3.2 Modelled maximum tsunami heights across the 200 m resolution local propagation grid for sources D2. Note the increased colour scale relative to Figure 3.1.

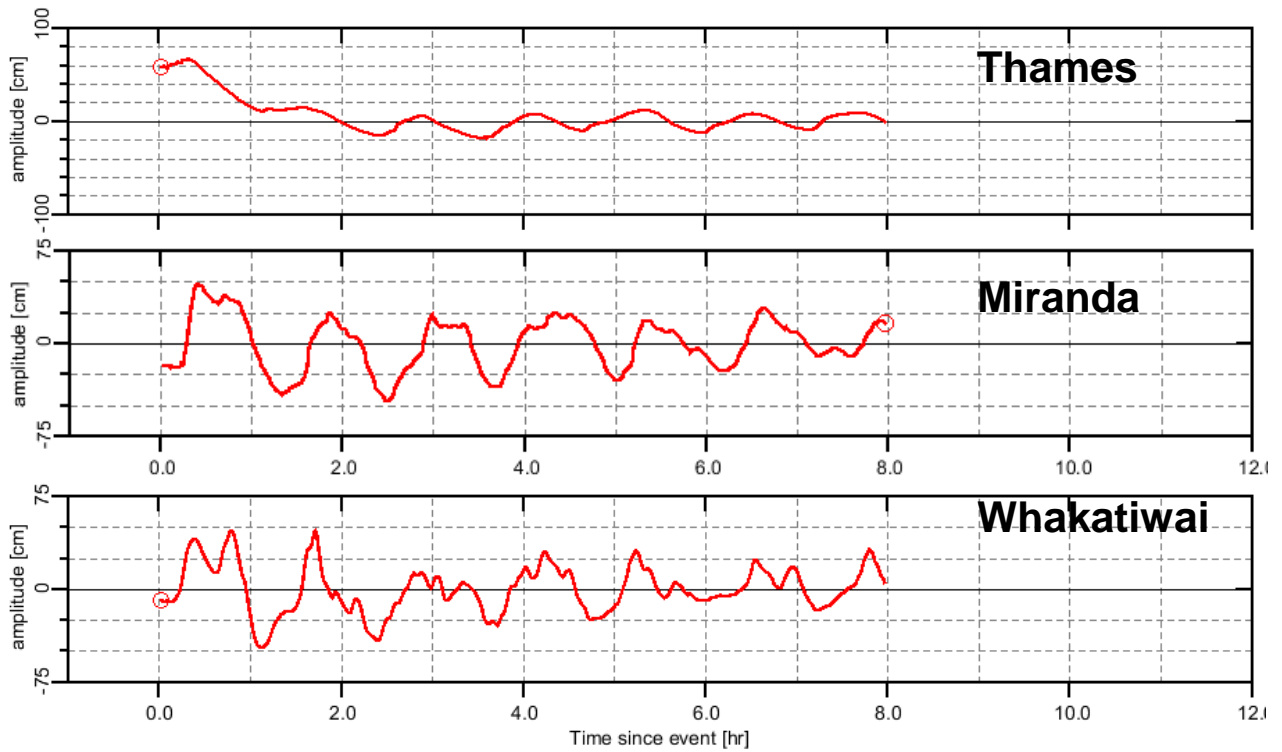


Figure 3.3 Time series of modelled water levels at MSL for Source A.

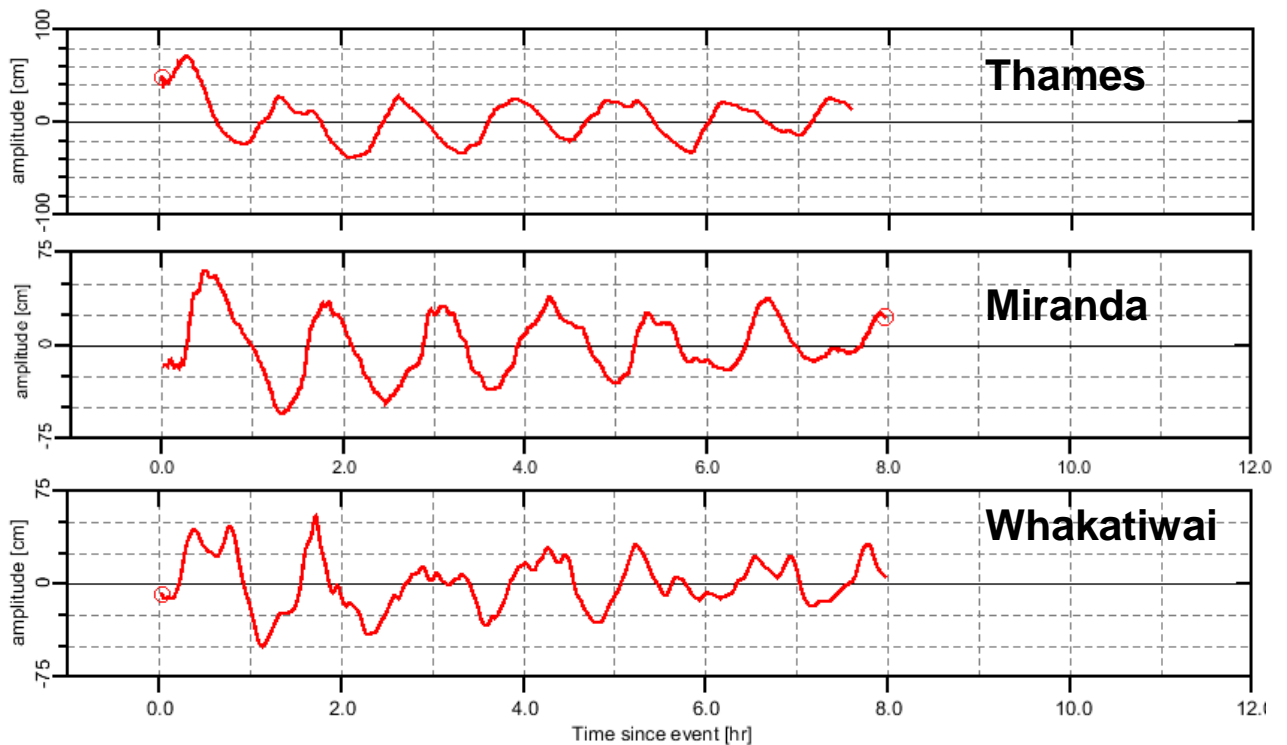


Figure 3.4 Time series of modelled water levels at MHWS for Source A. Note the similarity between the MSL and MHWS time series at Whakatiwai.

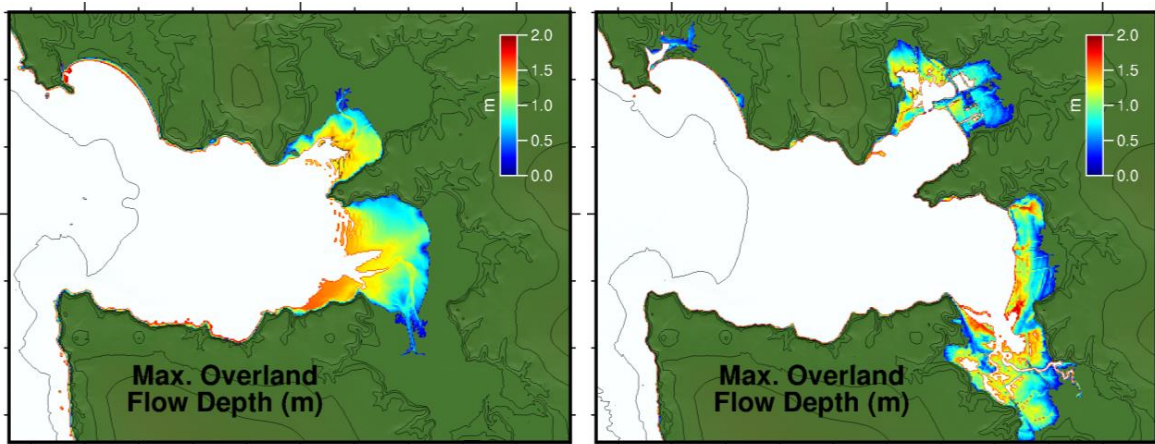


Figure 3.5 Inundation at Colville from Source D2 at MSL (left) MHWS (right).

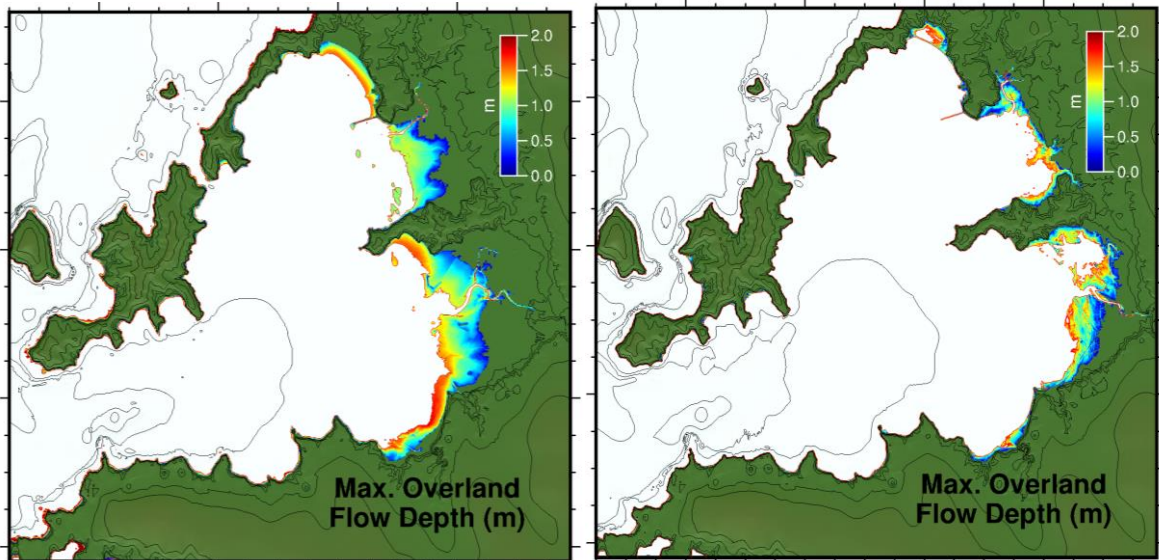


Figure 3.6 Inundation at Coromandel from Source D2 at MSL (left) MHWS (right).

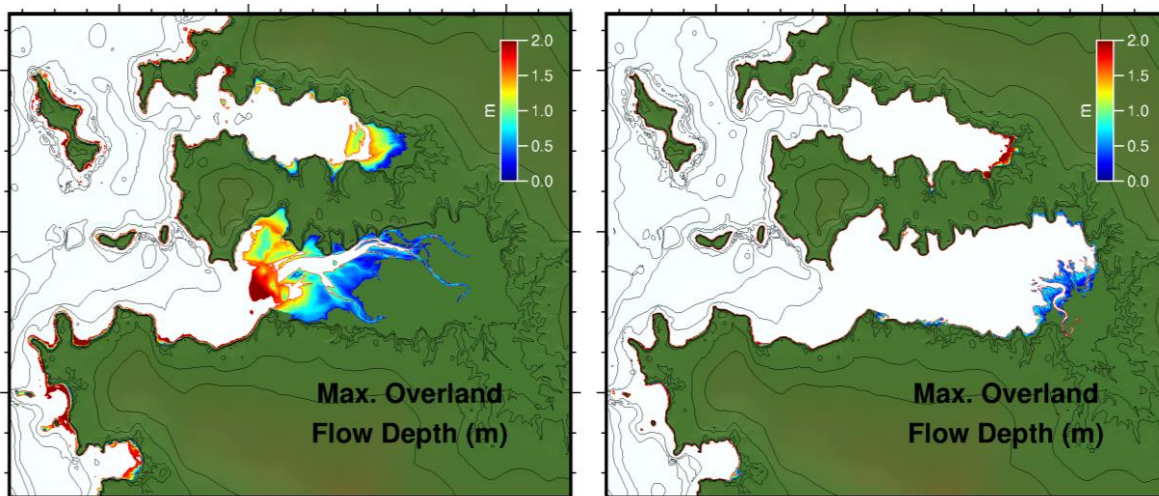


Figure 3.7 Inundation at Manaia from Source D2 at MSL (left) MHWS (right).

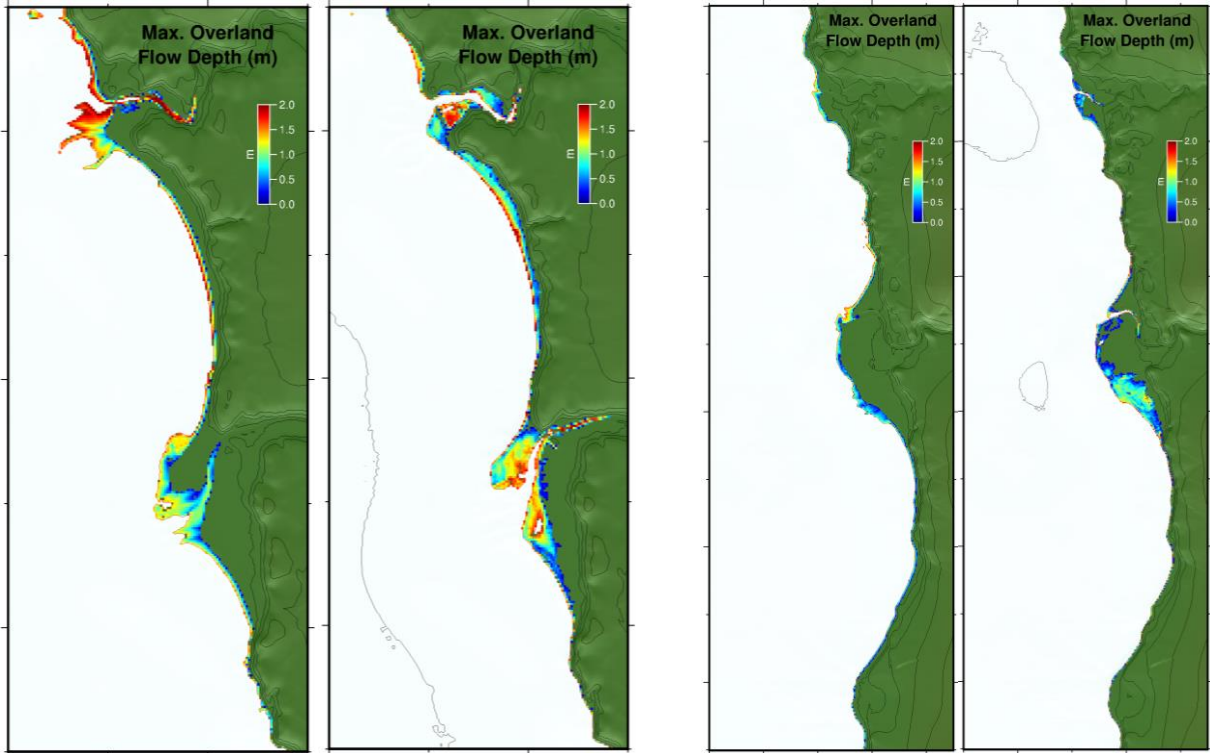


Figure 3.8 Inundation at Tapu and Te Puru from Source D2 at MSL (left panels) MHWS (right panels).

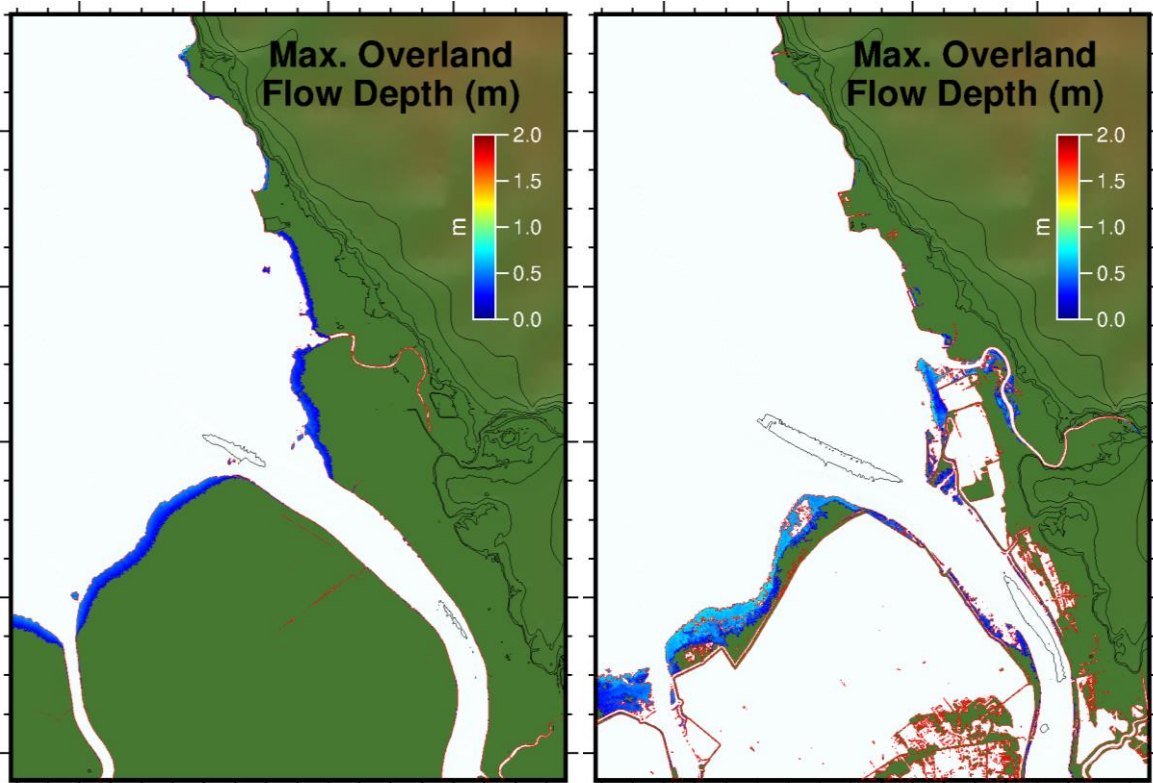


Figure 3.9 Inundation at Thames from Source D2 at MSL (left) MHWS (right).

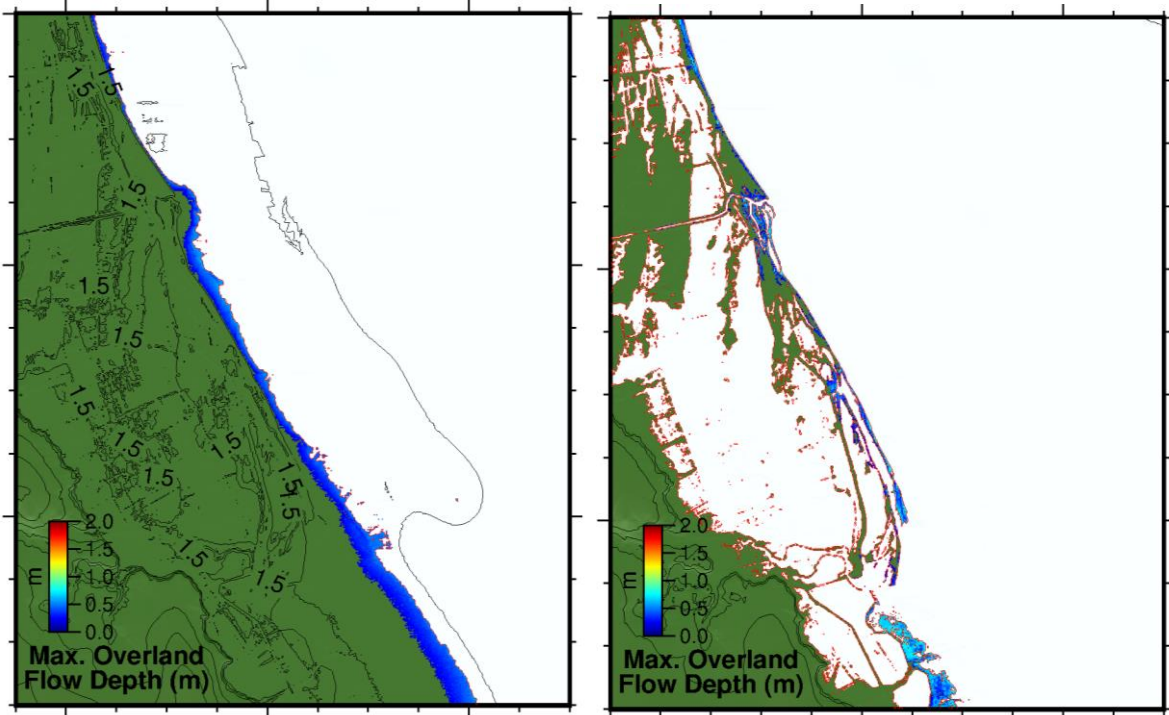


Figure 3.10 Inundation at Miranda from Source D2 at MSL (left) MHWS (right).

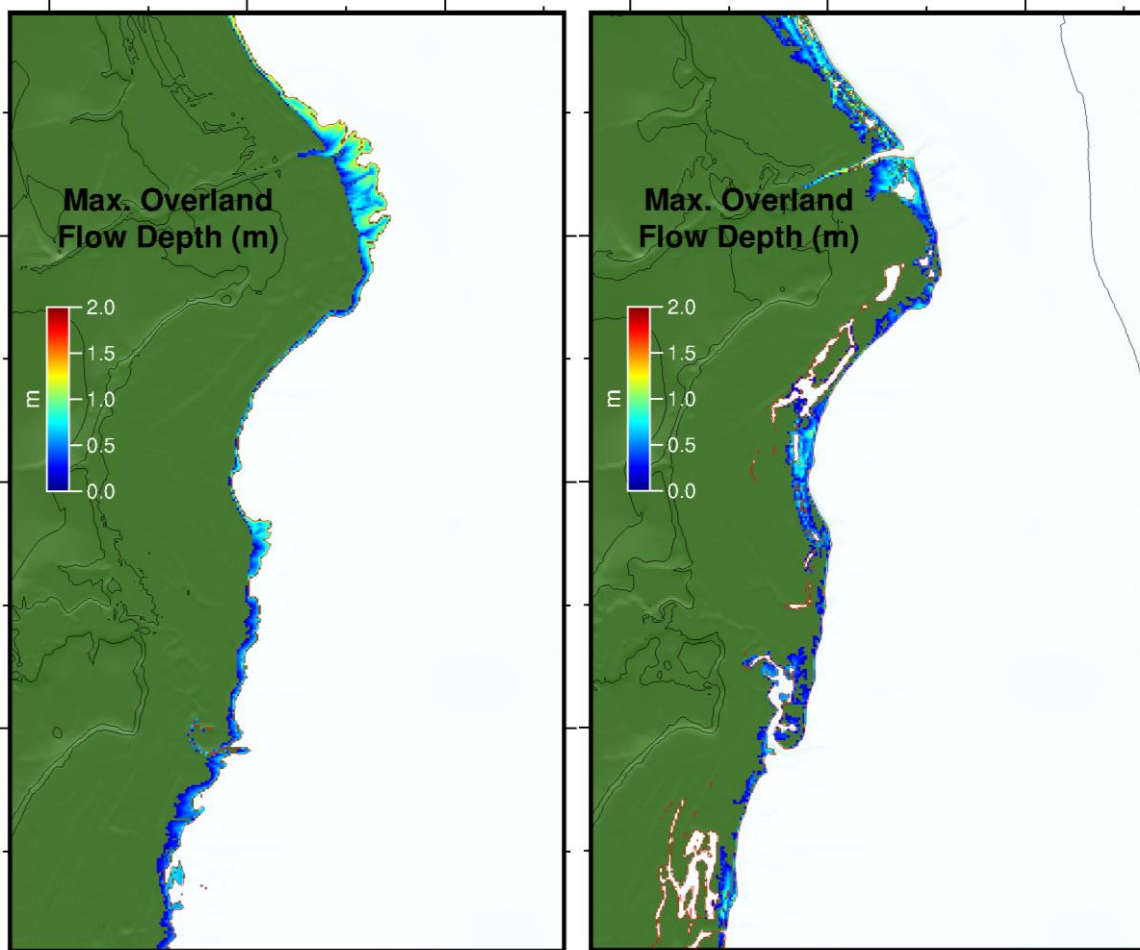


Figure 3.11 Inundation at Whakatiwai from Source D2 at MSL (left) MHWS (right).

3.1 Discussion of Inundation at Miranda

In January 2018 the area around Miranda was flooded as a result of the combined effect of a high astronomical tide, low barometric pressure and high waves caused by an extratropical cyclone passing over New Zealand (Liefting et al., 2018). The storm tide level reached by this event was less than a 0.5% annual exceedance probability (AEP) for tide levels, corresponding to a recurrence interval greater than 1 in 200 years.

The water level reached in that event were of the order of 2.8 to 2.9 m above mean sea level (Liefting, Personal Communication). Inspection of the time series output at Miranda (Figure 3.12) show peak tsunami water levels of ~0.6 and ~1.0 m for sources A1 and D2 respectively. This corresponds to absolute water levels of 2.4 and 2.8 m above MSL. Yet, the tsunami model does not show the same degree of inundation observes during the January 2018 storm.

This can be explained by the fact that during the simulated tsunami, the duration of these high-water levels is very short relative to the storm event. In the case of a coastal storm, high water levels can be sustained for up to an hour during the peak of the tide cycle. This allows for a gradual filling in of flood prone areas as well as the erosive effects of the storm waves which can lead to breaching of high standing areas and allowing more inundation.

During a tsunami event however, the peak water levels last only on the order of minutes and are assumed to be interacting with a dry coastline. Furthermore, the shallow water of the southern Firth of Thames acts to reduce tsunami energy contributing to the tsunami surge's inability to overtop the coastal berm and flood inland low-lying areas.

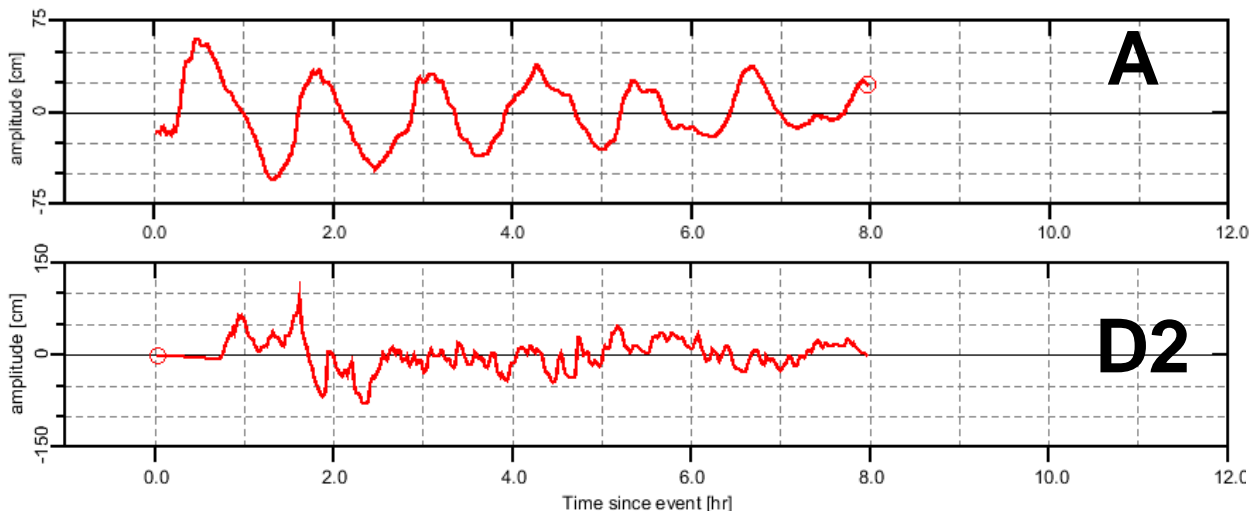


Figure 3.12 Time series of tsunami water level at Miranda for the A1 (top) and D2 sources (bottom).

4 MODEL RESULTS: TONGA-KERMADEC TRENCH SOURCES

4.1 *Arrival Times, Maximum Amplitudes and Tsunami Induced Currents*

An important consideration for the near source tsunami hazard is a clear understanding of the tsunami arrival time. 'Tsunami arrival' however can be defined either as the time of the first water motion (rise or drop) or the time of the maximum wave height. This is somewhat complicated in the Firth because the shallow water significantly slows the arrival of the tsunami waves while its semi enclosed nature results in water levels steadily rising rather than rising and falling evenly.

In Figure 4.1 we plot time series of modelled water level from the TK 8 scenario at MSL in each of the 8 C level grids. We see that the first arrival to the northernmost site of Colville is approximately 1.5 hours with the largest waves occurring between 3 and 4 hours after the earthquake. The arrival times steadily increases as we move further south and is a maximum of 3 hours for Thames.

In Figure 4.2 and Figure 4.3 we present the maximum modelled tsunami amplitudes in the A and B level grids. In these plots we can clearly see the focussing of the tsunami energy on to the eastern shore of Great Barrier island and the Coromandel peninsula. Also evident is the degree to which the Firth of Thames is sheltered from the direct impact of the tsunami energy.

Finally, in Figure 4.4 through Figure 4.11 we present the inundation extents predicted in each of the sites for the MSL and MHWS cases. Only in the Colville grid do we see an appreciable inundation with the predicted tsunami surges causing some localised inundation.

Strong tsunami induced currents are predicted at several sites as a result of the TK8 scenario. Results from select sites are presented in Figure 4.12. It is interesting to note that the current speeds in Coromandel Harbour are relatively small compared to other nearby sites such as Colville and Manaia. We also note that modelled current speeds are larger for the MHWS water levels (see Appendix 6 for a direct comparison).

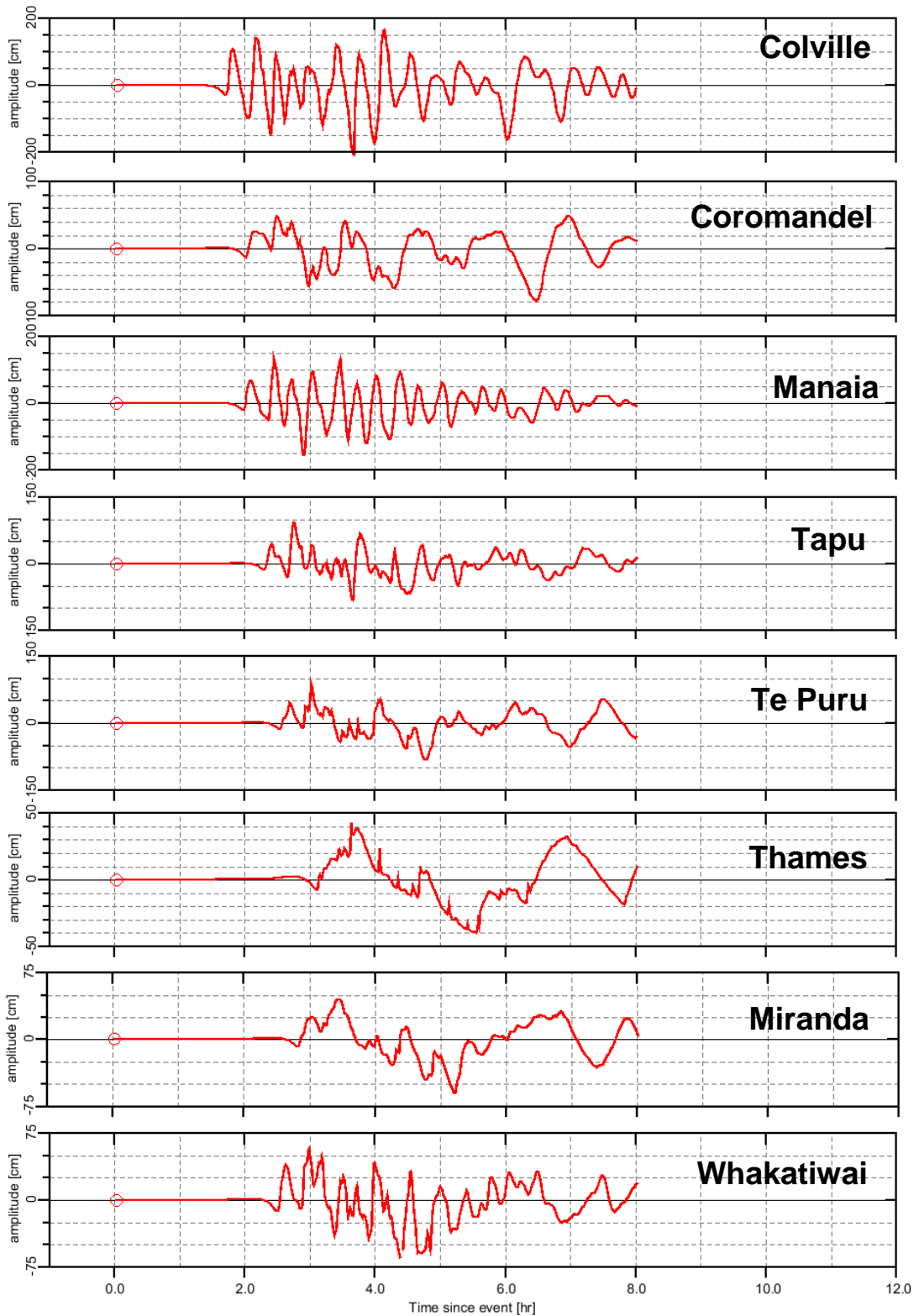


Figure 4.1 Water level time series plots for the TK 8 sources affecting the 8 study sites.

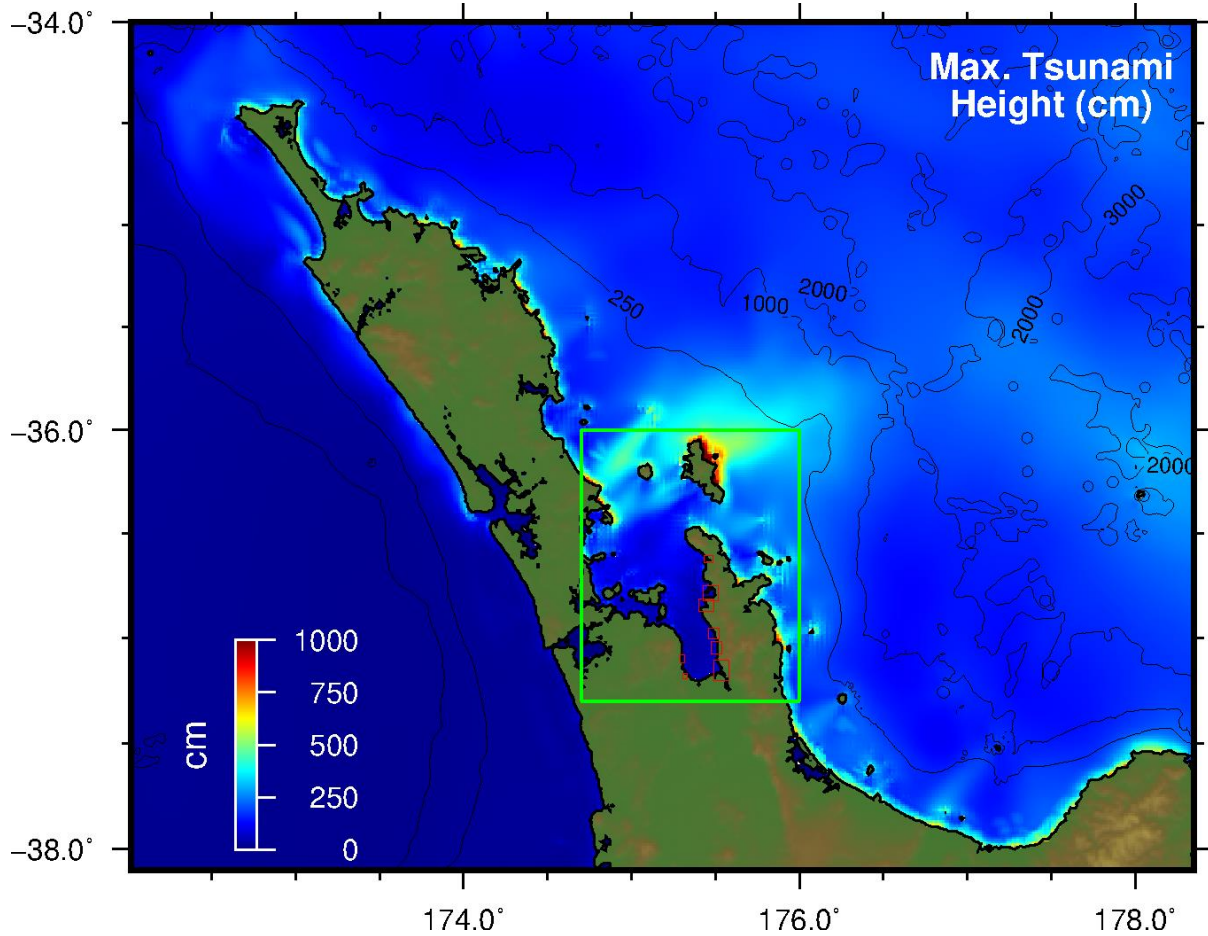


Figure 4.2 Maximum predicted tsunami amplitudes in the A grid for the TK 8 source.

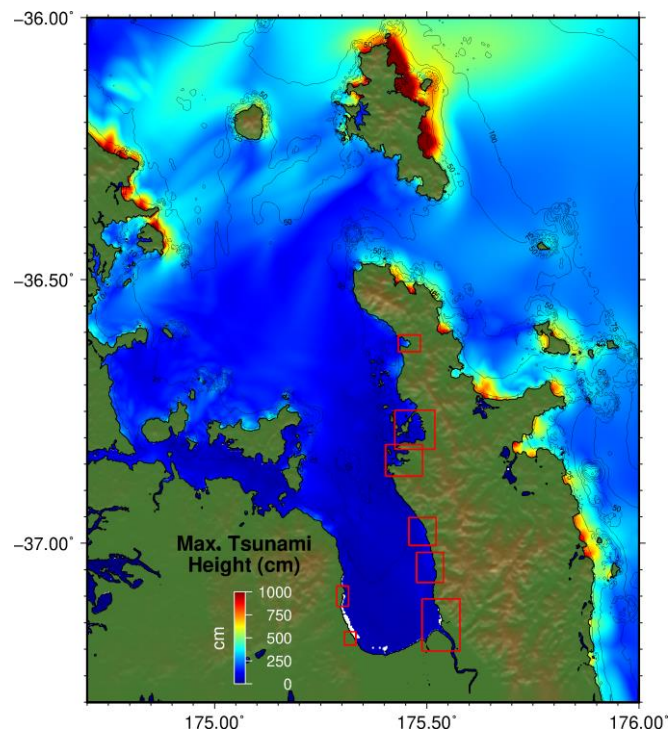


Figure 4.3 Maximum predicted tsunami amplitudes in the B grid for the TK 8 source

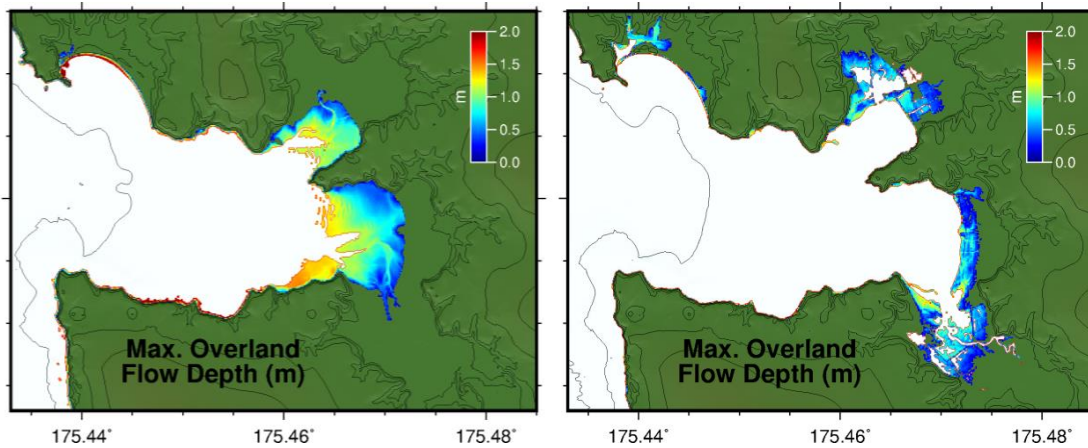


Figure 4.4 TK 8 scenario maximum overland inundation at Colville for MSL (left) and MHWS (right).

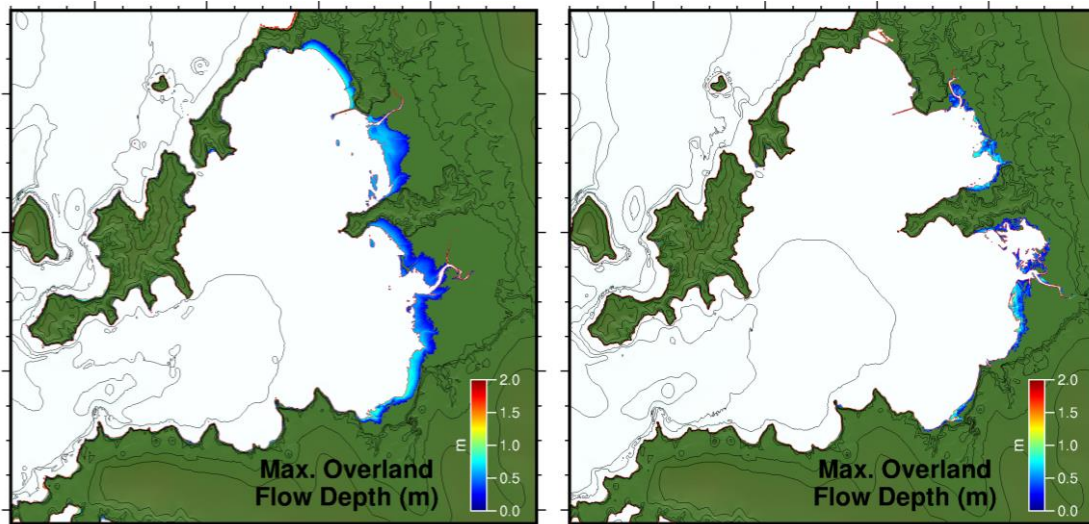


Figure 4.5 TK 8 scenario maximum overland inundation at Coromandel for MSL (left) and MHWS (right).

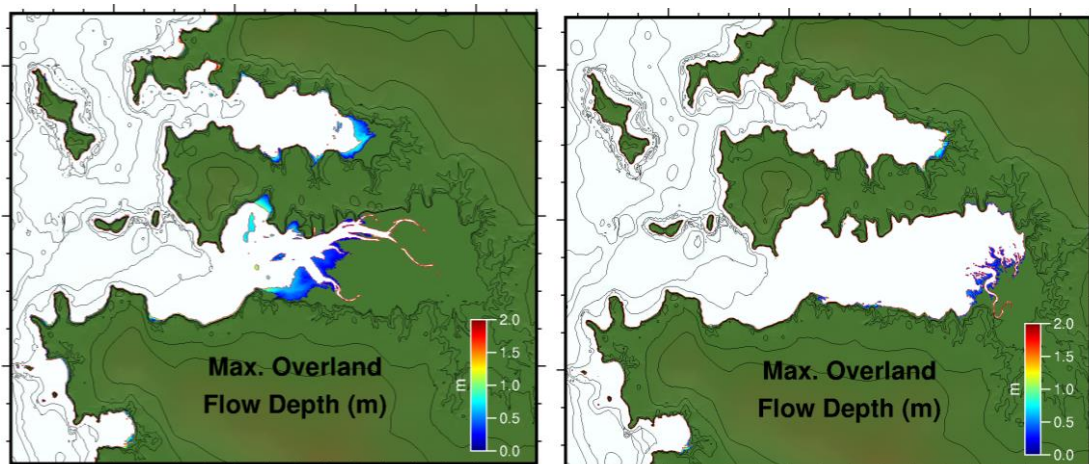


Figure 4.6 TK 8 scenario maximum overland inundation at Manaia for MSL (left) and MHWS (right).

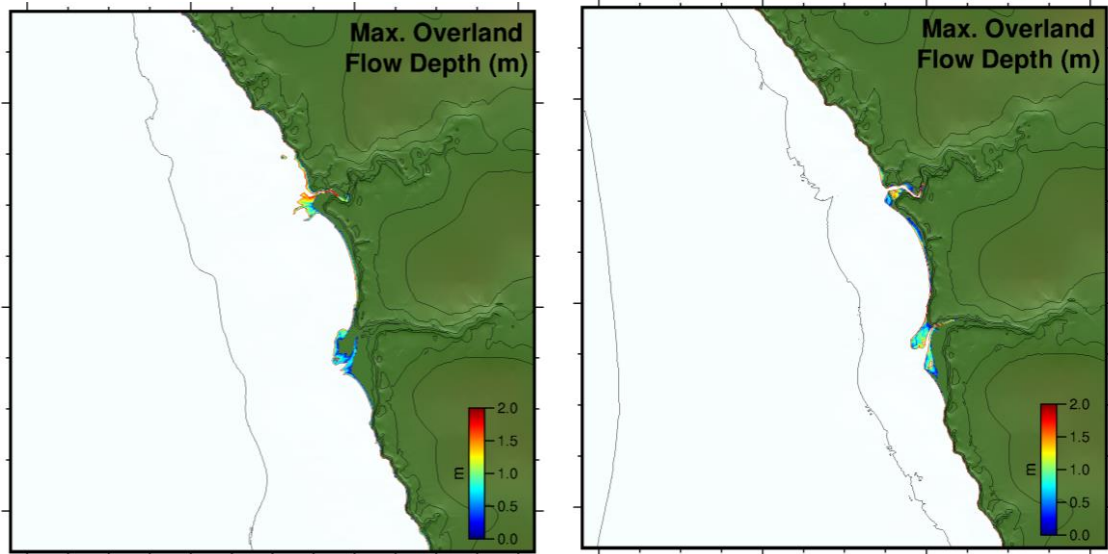


Figure 4.7 TK 8 scenario maximum overland inundation at Tapu for MSL (left) and MHWS (right).

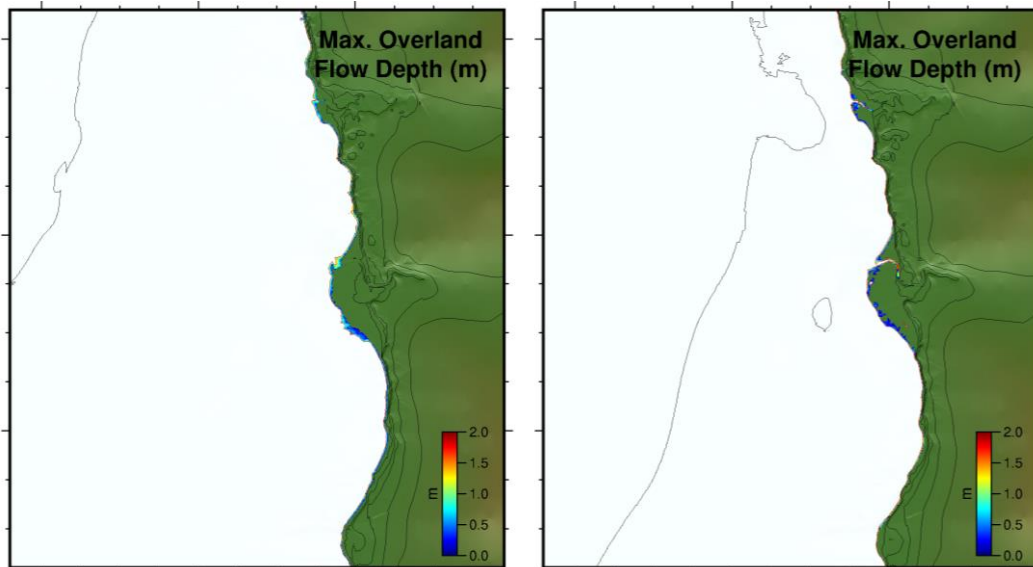


Figure 4.8 TK 8 scenario maximum overland inundation at Te Puru for MSL (left) and MHWS (right).

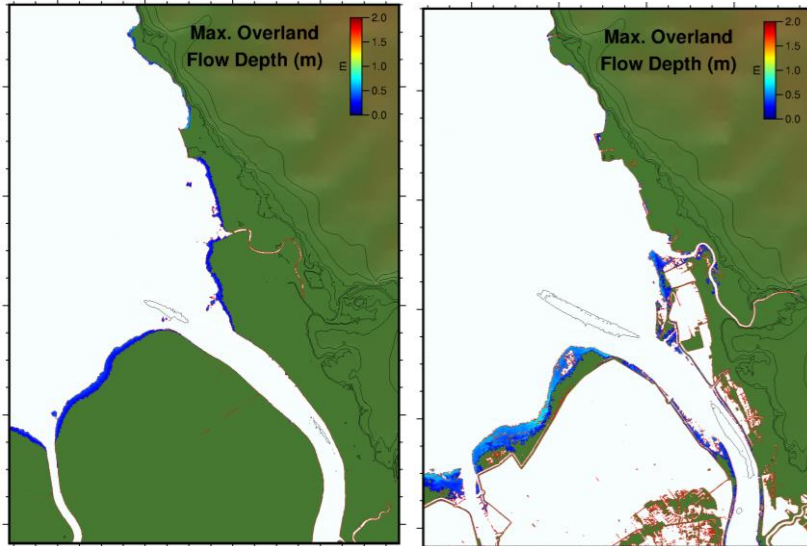


Figure 4.9 TK 8 scenario maximum overland inundation at Thames for MSL (left) and MHWS (right).

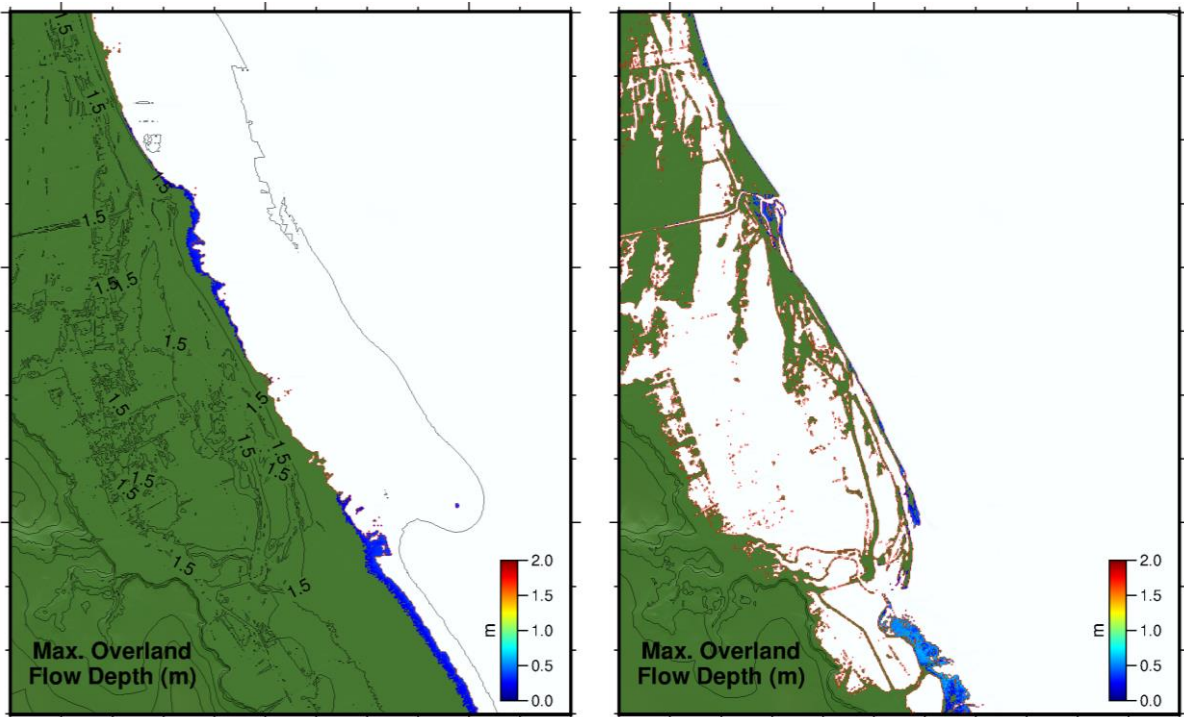


Figure 4.10 TK 8 scenario maximum overland inundation at Miranda for MSL (left) and MHWS (right).

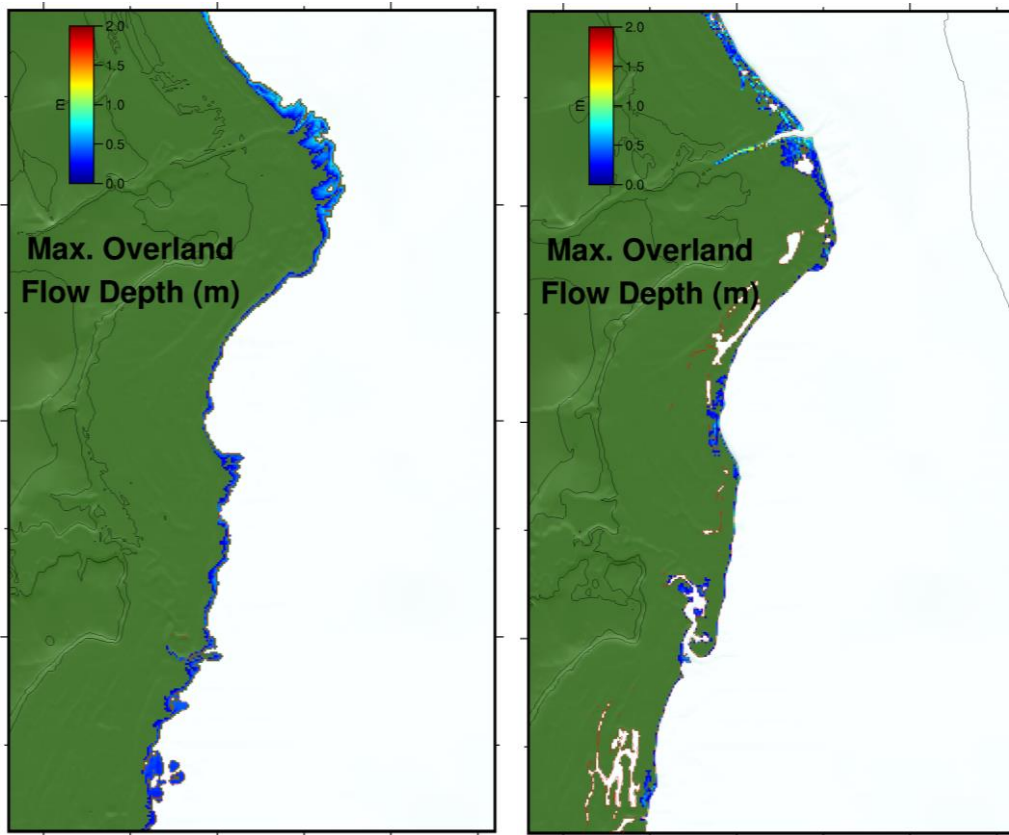


Figure 4.11 TK 8 scenario maximum overland inundation at Whakatiwai for MSL (left) and MHWS (right).

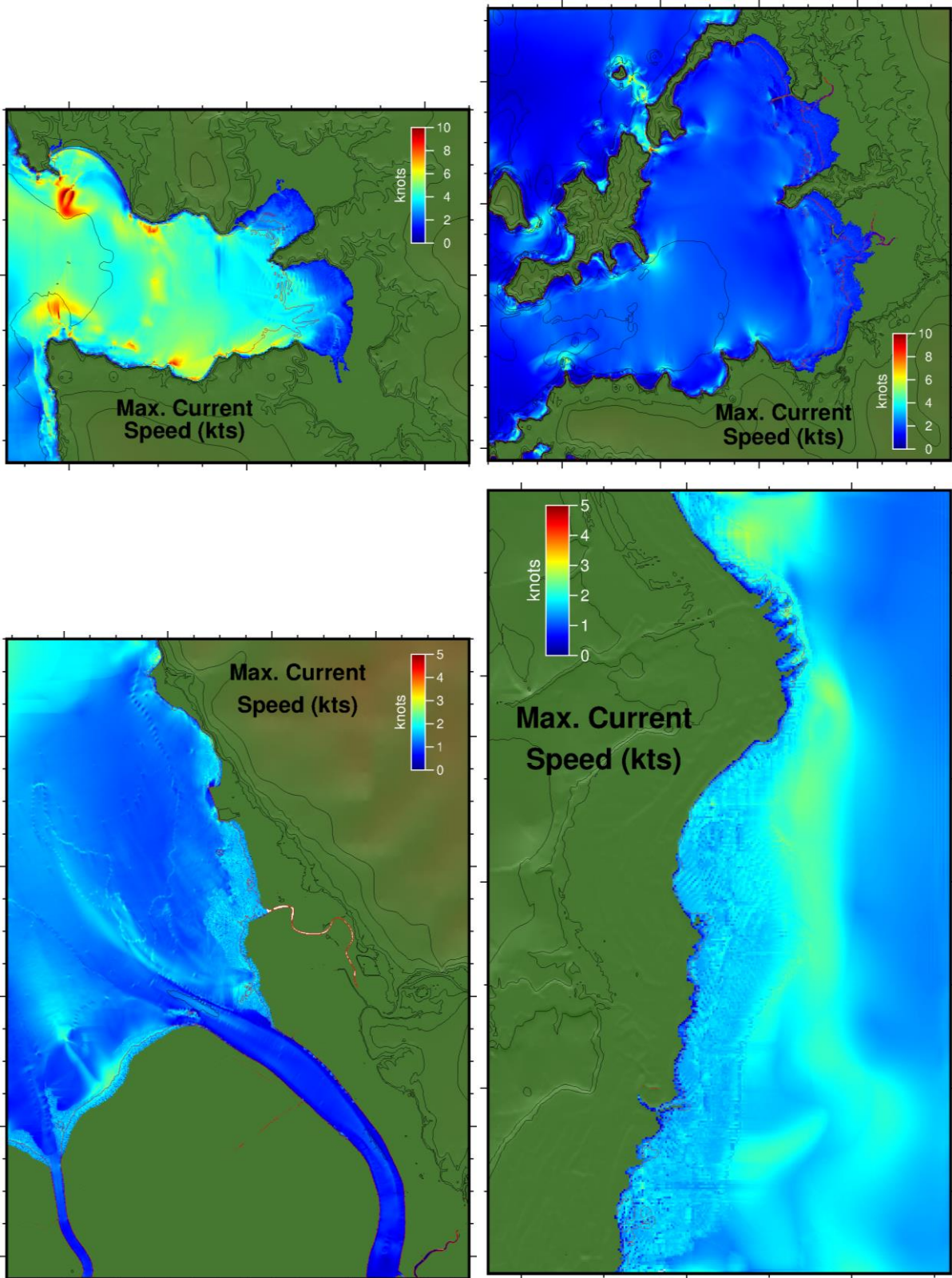


Figure 4.12 Modelled current speeds at select sites (Colville, Coromandel, Thames and Whakatiwai) caused by the TK8 scenario at MSL.

5 MODEL RESULTS: DISTANT SOURCE TSUNAMIS

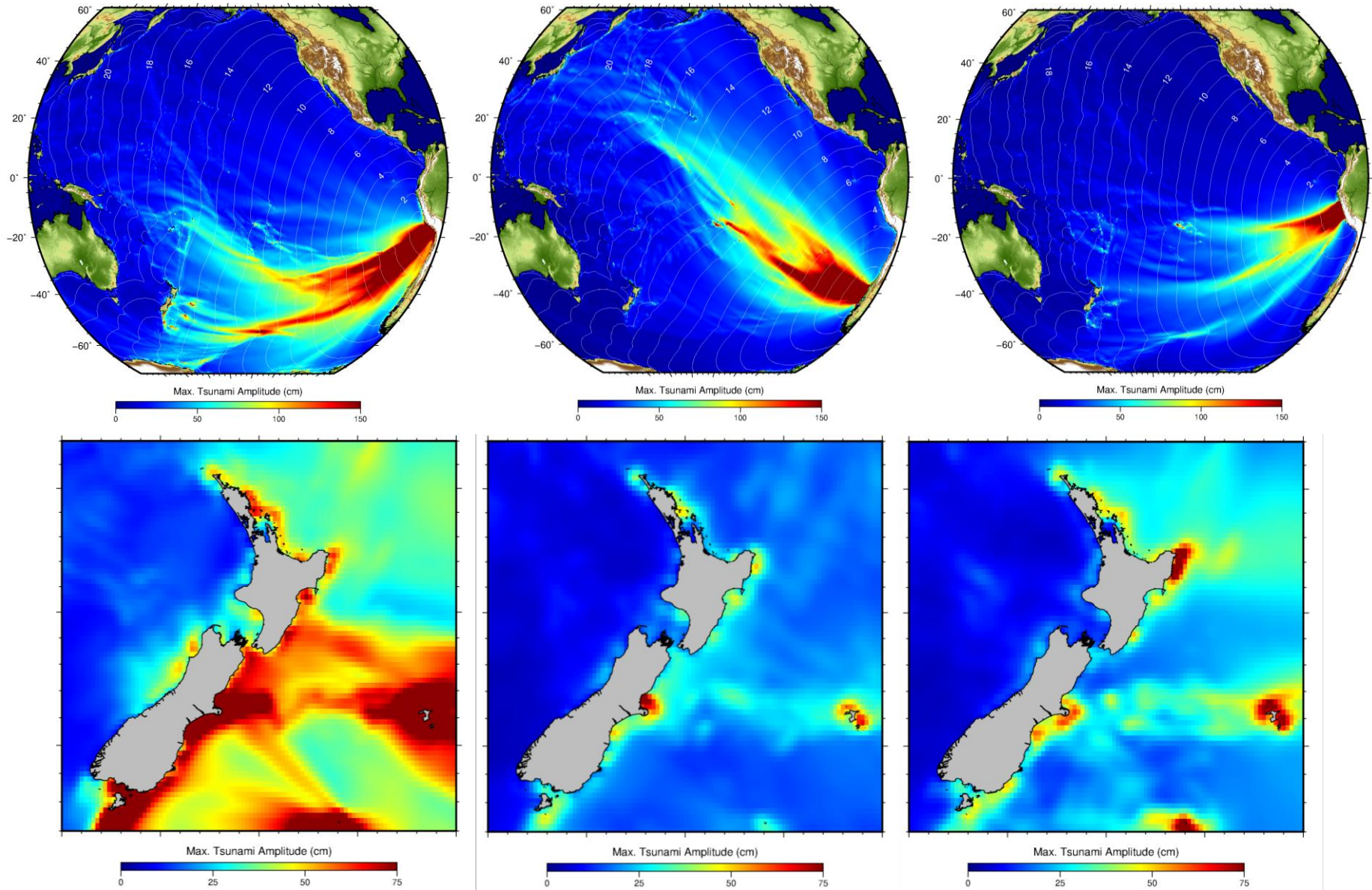
The model results for the distant source tsunami cases are presented below/

5.1 Propagation Models

In Figure 5.1 we present the trans-pacific propagation patterns for the 1868, 1960 and the FF 7 scenarios. From these plots we see that the coasts of northern Chile and Peru seem to be better positioned to project tsunami energy towards New Zealand as compared to the 1960 event from southern Chile. Recall that the FF 7 and 1960 scenarios are identical in terms of the total energy released. They differ only in their location along the coast of South America and the distribution of the co-seismic slip. The 1868 scenario is slightly larger in terms of energy release.

Inspection of Figure 5.2 shows the sheltering effect of the Coromandel Peninsula and Great Barrier Island have on the Firth of Thames with much larger tsunami amplitudes seen on the east coast of the Coromandel and the northern section of the Hauraki Gulf. It is interesting to note that despite the seemingly more favourable source location of the FF 7 scenario for projecting energy towards New Zealand, the 1960 scenario from Southern Chile produces larger tsunami heights inside the Firth of Thames. This result is also reflected in the time series plots presented in Figure 5.3 through Figure 5.5.

Figure 5.1 (following page) Comparison between trans-Pacific propagation patterns for the 1868 Arica (top left) 1960 Valdivia (top mid) and the FF 7 scenarios (top right). (bottom row) Close up on New Zealand for the trans-Pacific propagation.



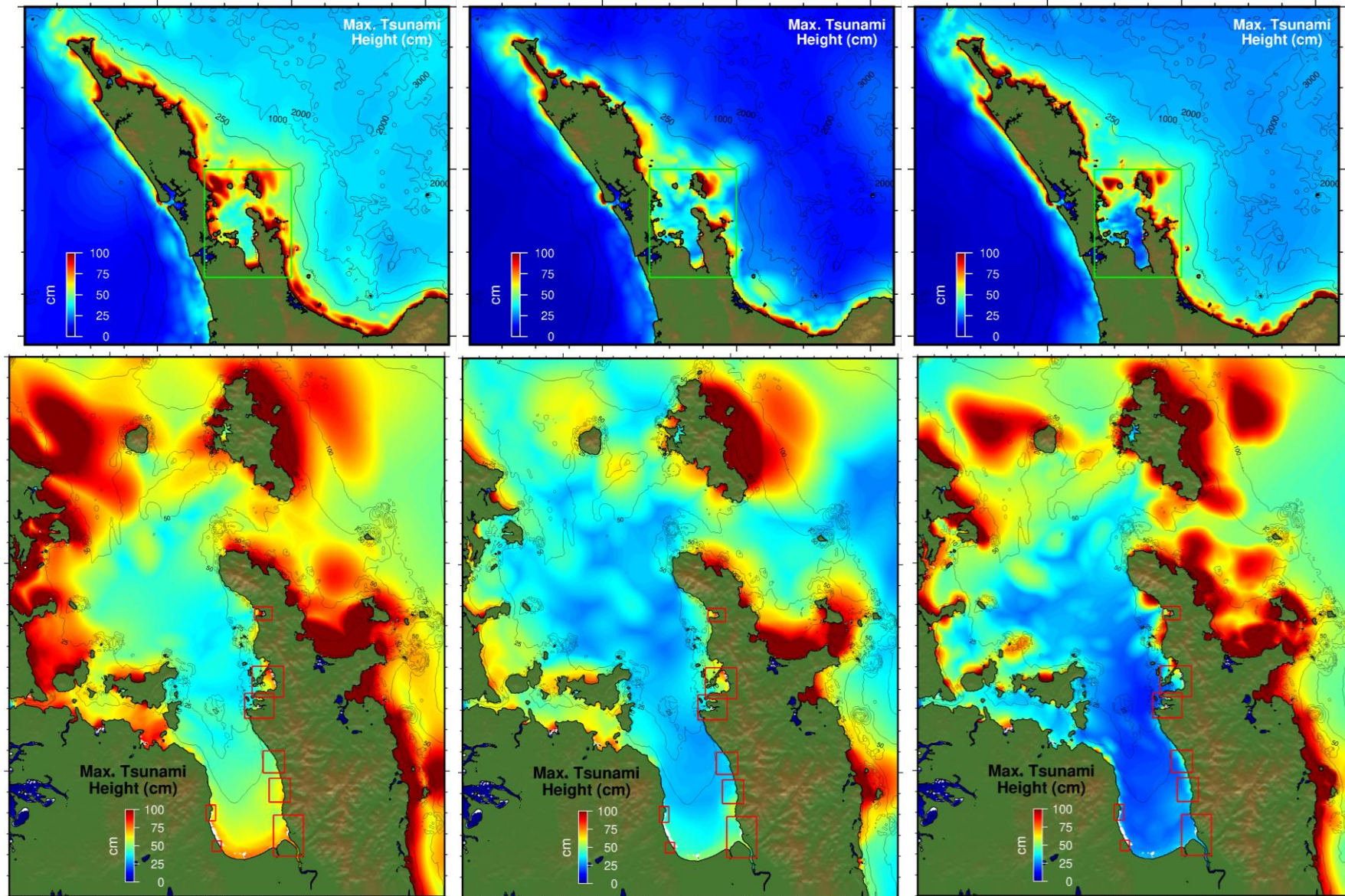


Figure 5.2 Maximum tsunami height in the A and B grids for the 1868 (left) 1960 (mid) and FF 7 scenarios.

5.2 Arrival Times

Time series of modelled water levels from a nearshore point in the Colville and Thames grids for the 1868, 1960 and FF 7 scenarios are presented in Figure 5.3 through Figure 5.5 (The full set of modelled time series results are presented in Appendix 3). These sites are compared as they show the earliest (Colville) and latest (Thames) arrival times for sites in the Firth of Thames with more than 1 hr of delay in arrival between the two sites.

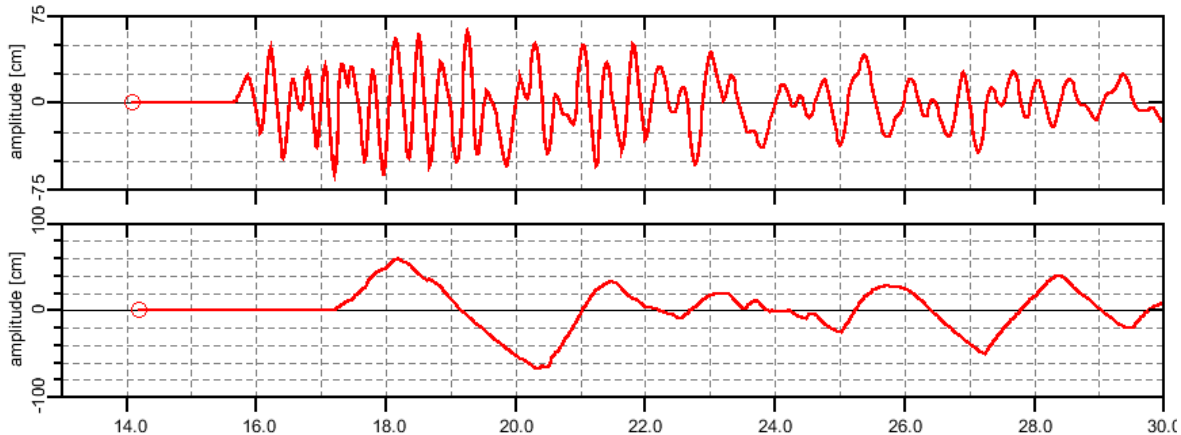


Figure 5.3 Modelled tsunami water levels at Colville (top) and Thames (bottom) for the 1868 scenario at MSL.

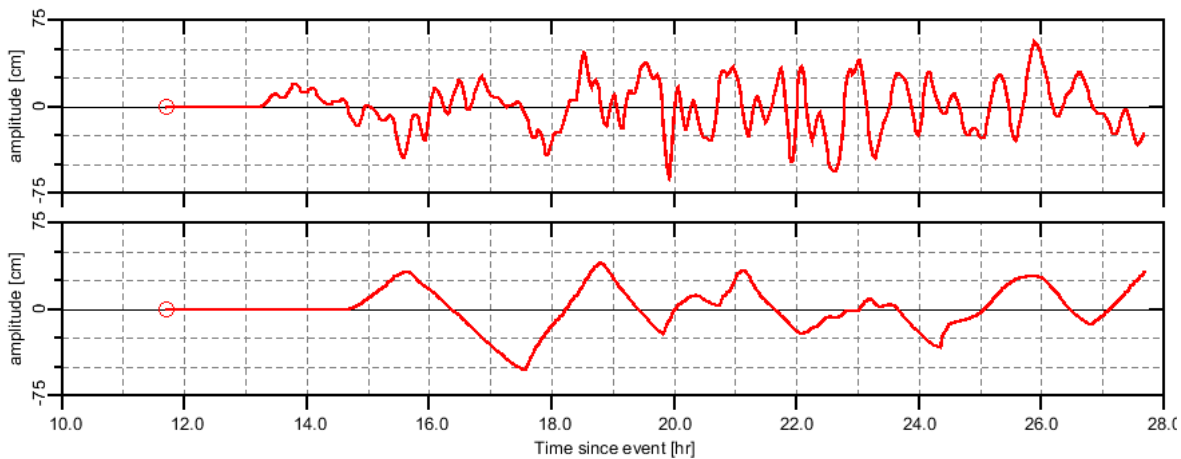


Figure 5.4 Modelled tsunami water levels at Colville (top) and Thames (bottom) for the 1960 scenario at MSL.

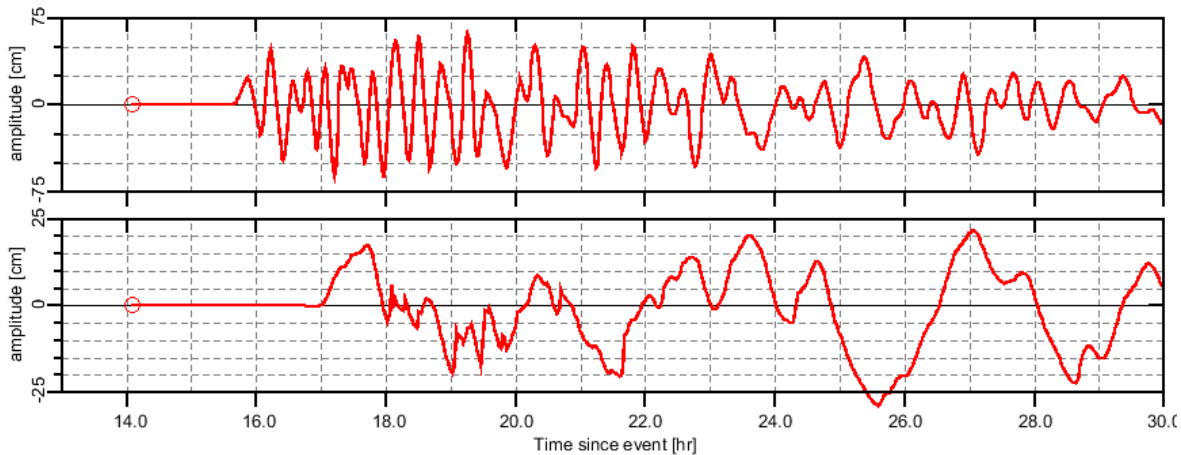


Figure 5.5 Modelled tsunami water levels at Colville (top) and Thames (bottom) for the FF 7 scenario at MSL.

Table 5.1 Modelled tsunami arrival times (in hours after the earthquake) at Coromandel and Thames for the three distant source scenarios.

Scenario	Coromandel (hrs)	Thames (hrs)
1868	16.0	17.2
1960	13.6	14.4
FF 7	16.0	17.0

5.3 Tsunami Heights, Inundation Extents and Current Speeds

In terms of inundation, the distant source scenarios also do not cause significant overland inundation. In Figure 5.6 and Figure 5.7 we present the maximum inundation extents at Colville and Thames for the three distant source scenarios during MSL and MHWS. There is some small-scale inundation predicted for the 1868 scenario at Colville, with comparatively less inundation for both the 1960 and FF 7 cases. At Thames we see that the predicted tsunami heights from these scenarios are not great enough to overtop the flood protection stop banks, even at MHWS water levels.

The maximum tsunami induced current speeds predicted by the model are presented in Figure 5.8 through Figure 5.10 for the Colville, Coromandel, Manaia and Thames grids. These sites are chosen as they are the sites where commercial or recreational maritime interests are most exposed to tsunami effects. The results suggest that shallow areas, particularly around headlands, passes between islets and inshore areas are most susceptible to strong currents and eddies with maximum current speeds approaching 4 knots.

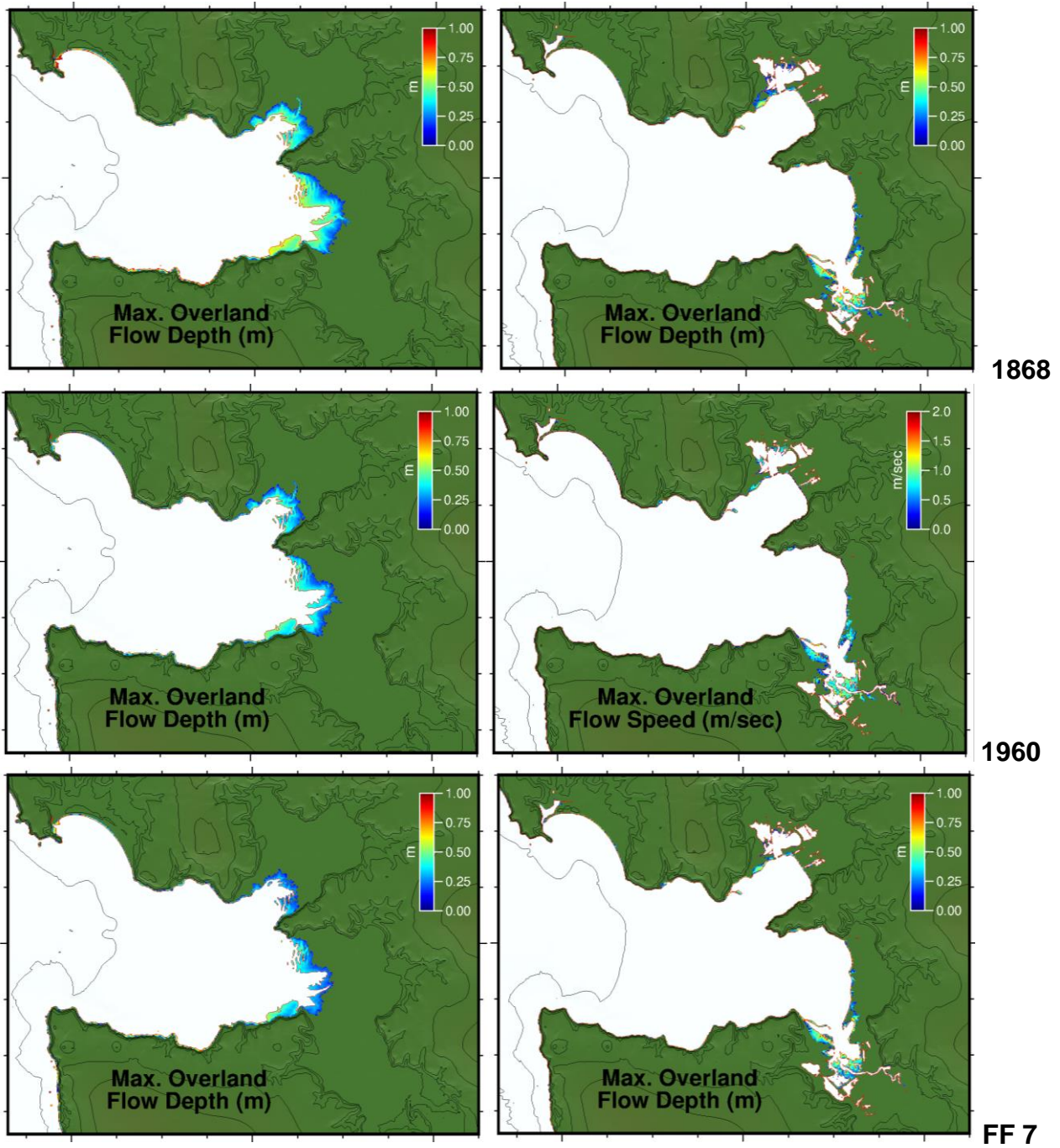


Figure 5.6 Predicted inundation extents at Colville for the 1868 (top) FF 7 (mid) and 1960 (bottom) scenarios. MSL on the left and MHWS on the right.

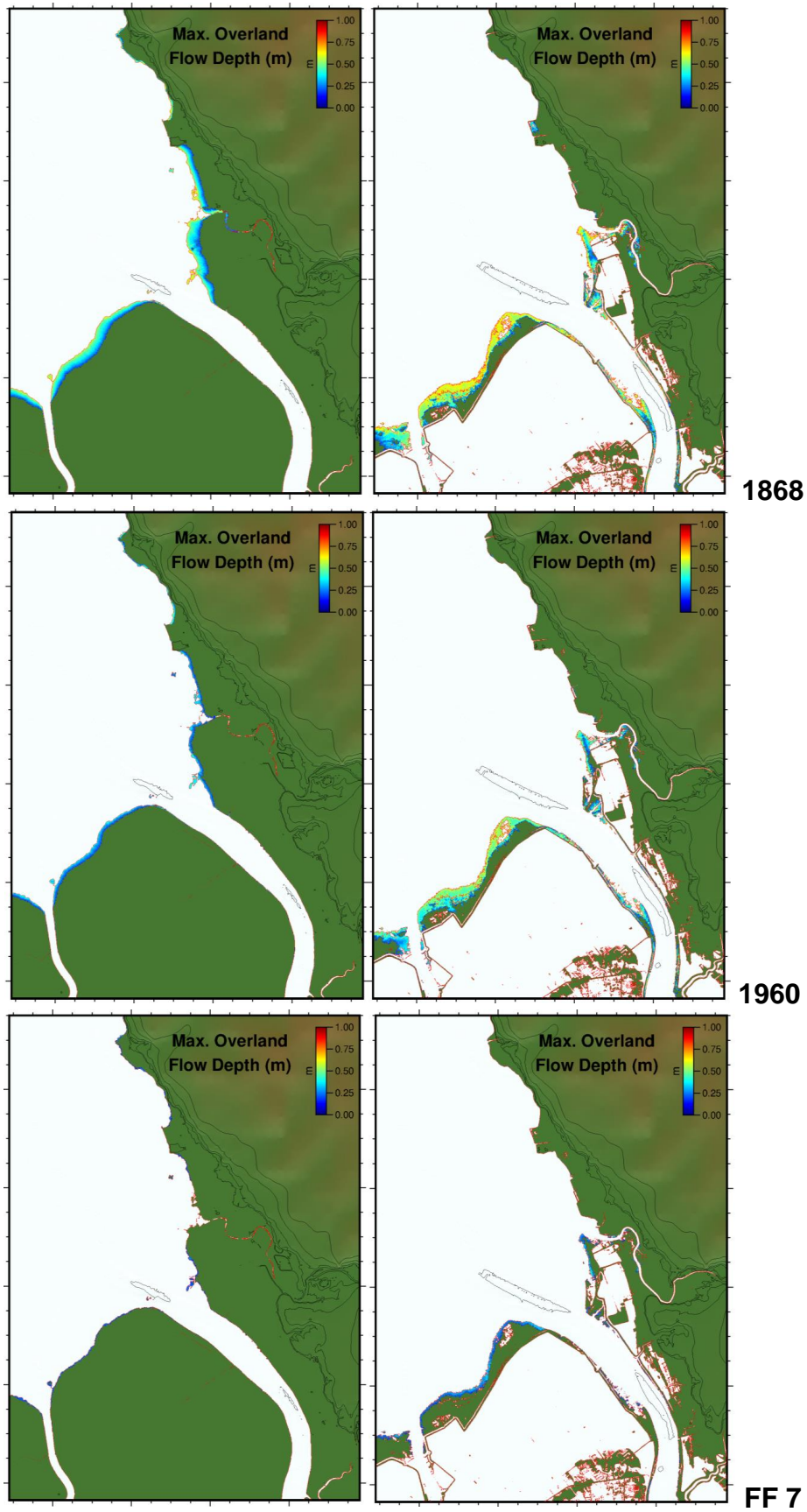


Figure 5.7 Predicted inundation extents at Thames for the 1868 (top) FF 7 (mid) and 1960 (bottom) scenarios. MSL on the left and MHWS on the right.

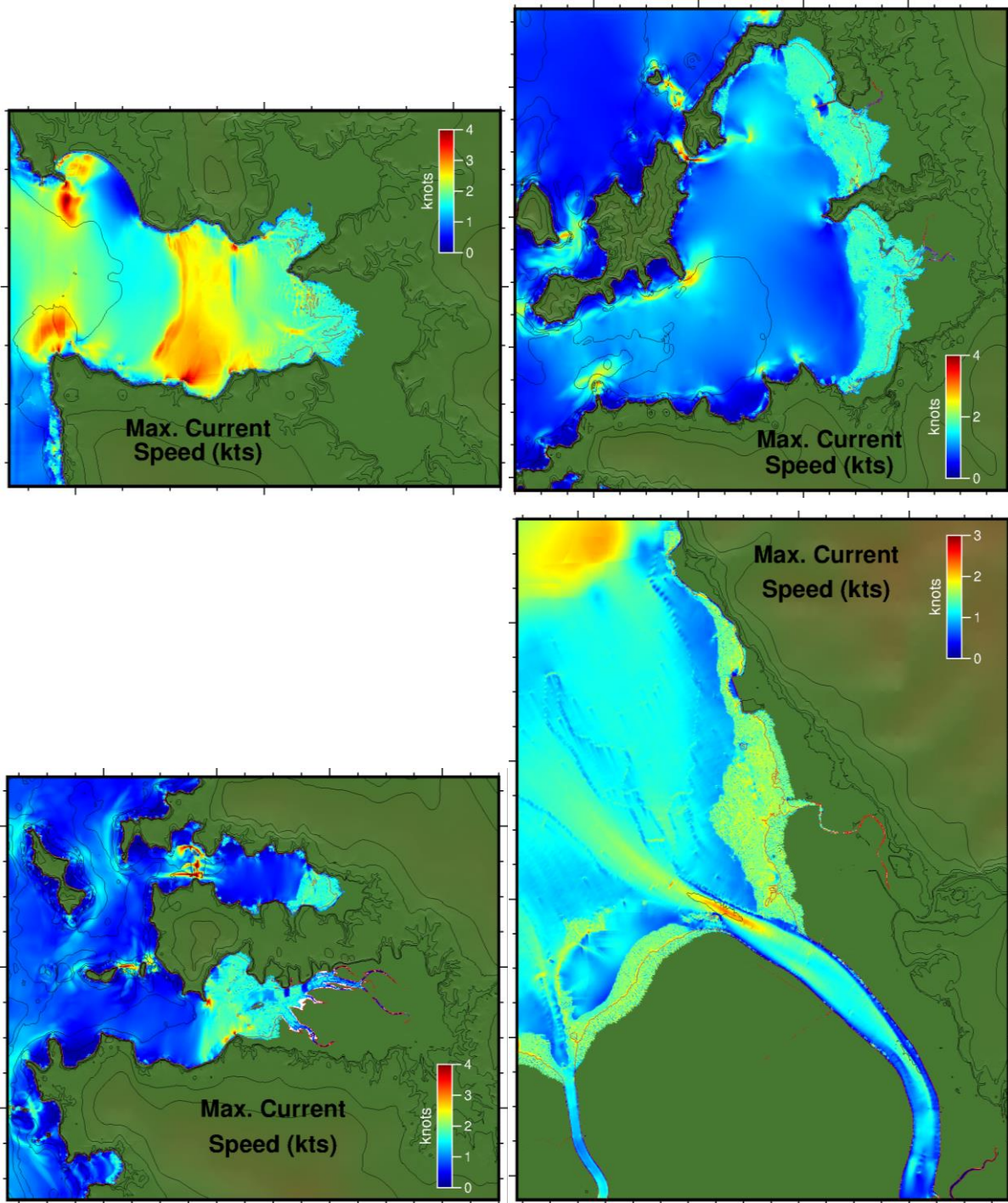


Figure 5.8 Maximum current speeds at Colville, Coromandel, Manaia and Thames for the 1868 scenario at MSL.

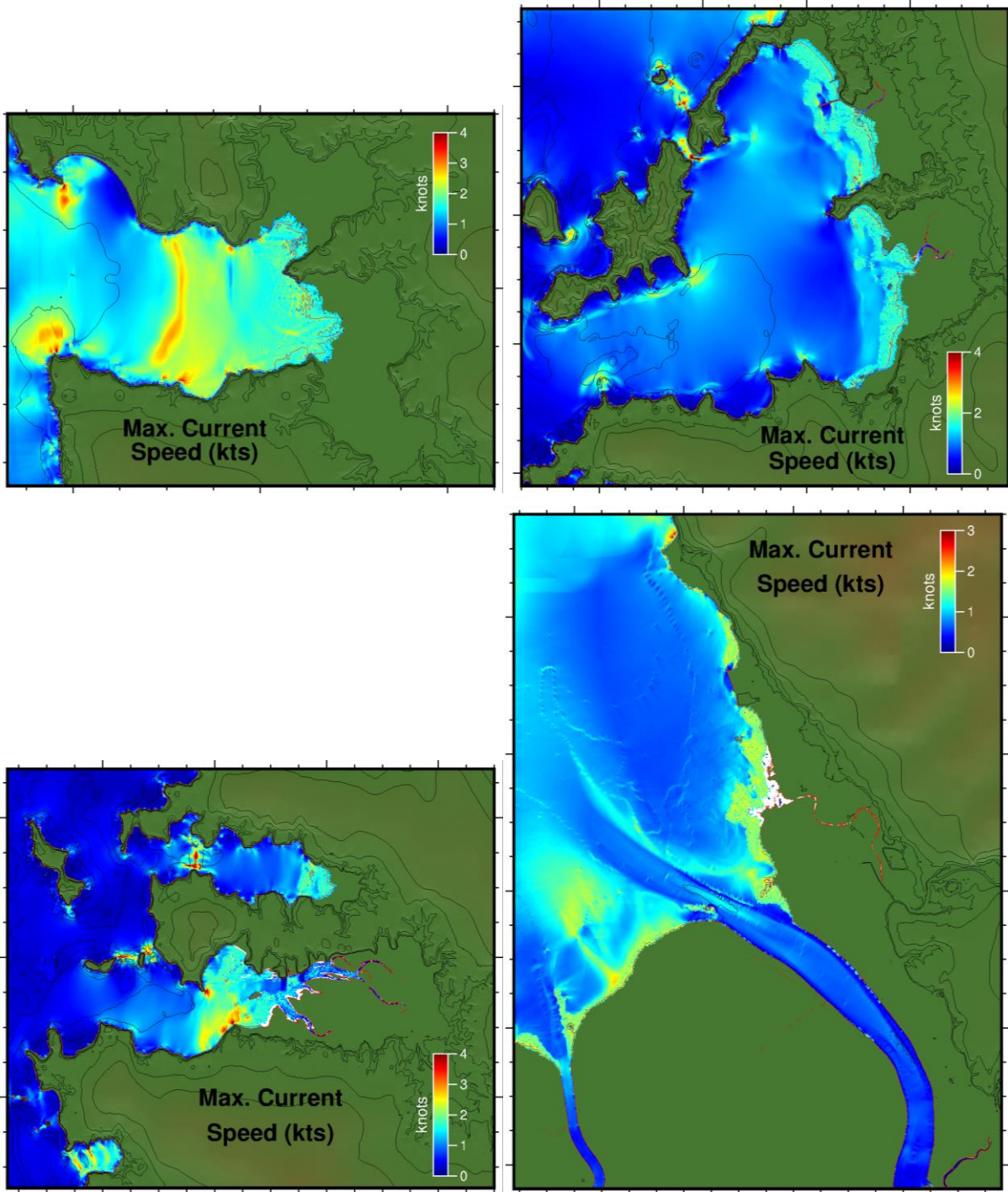


Figure 5.9 Maximum current speeds at Colville, Coromandel, Manaia and Thames for the FF 7 scenario at MSL.

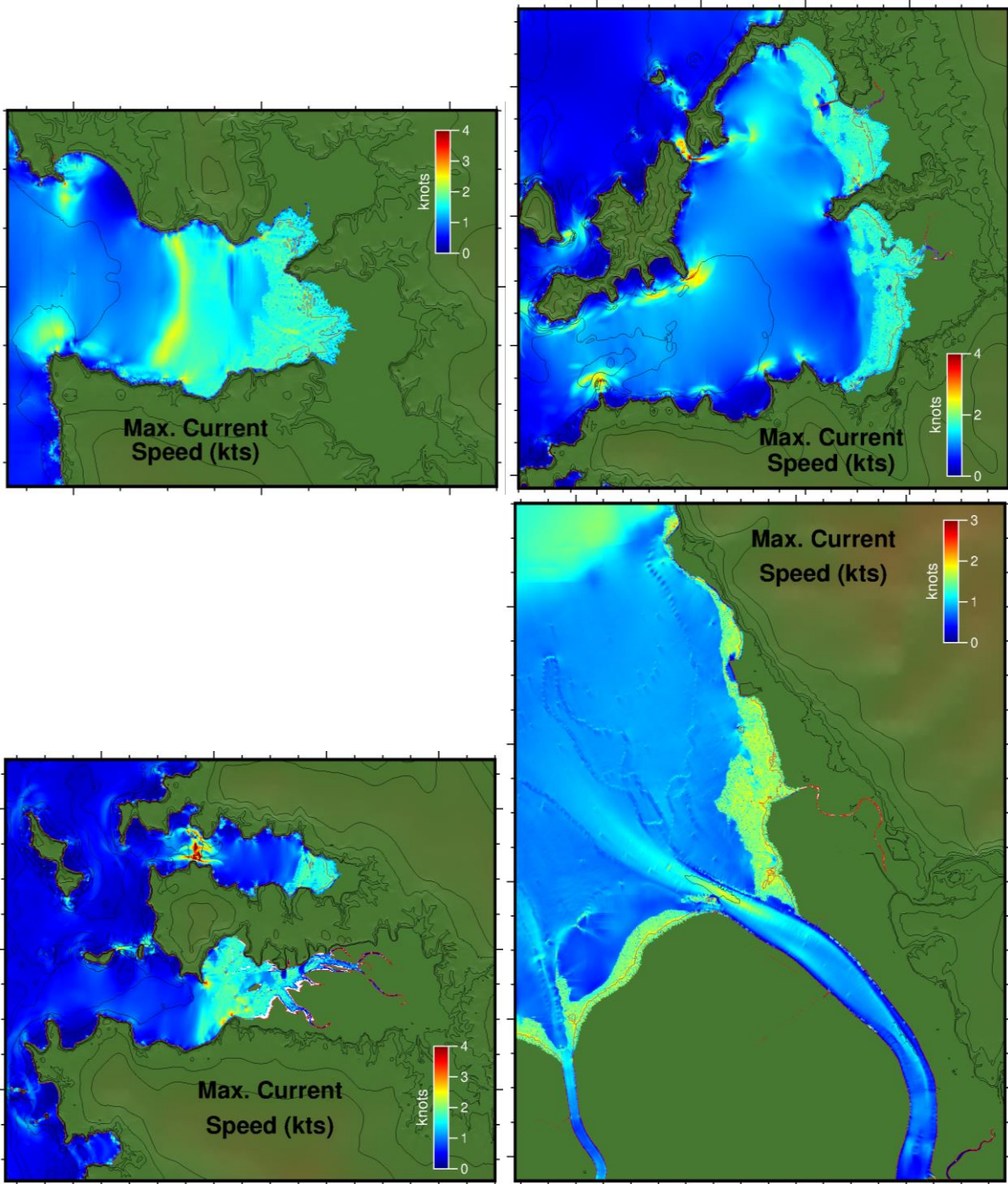
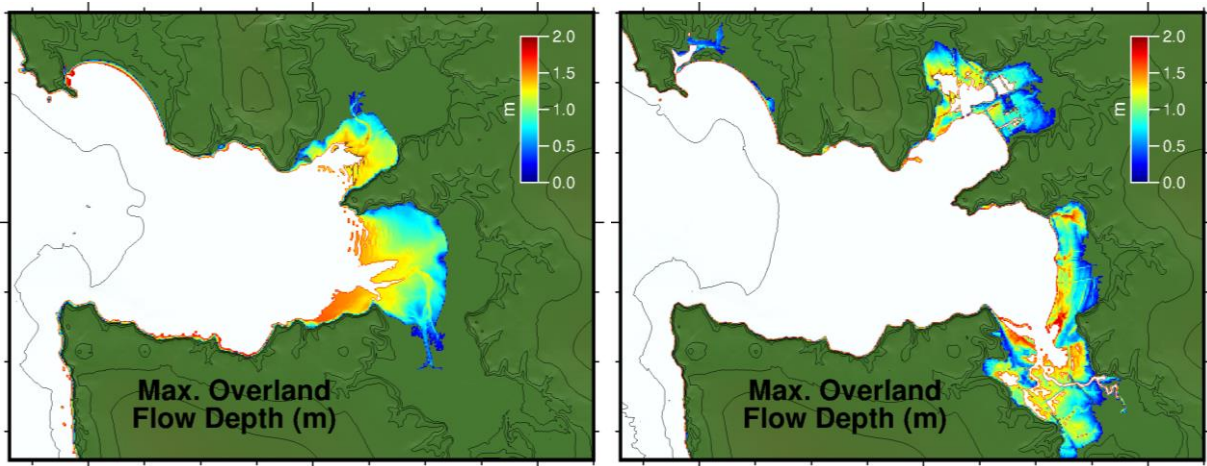


Figure 5.10 Maximum current speeds at Colville, Coromandel, Manaia and Thames for the 1960 scenario at MSL.

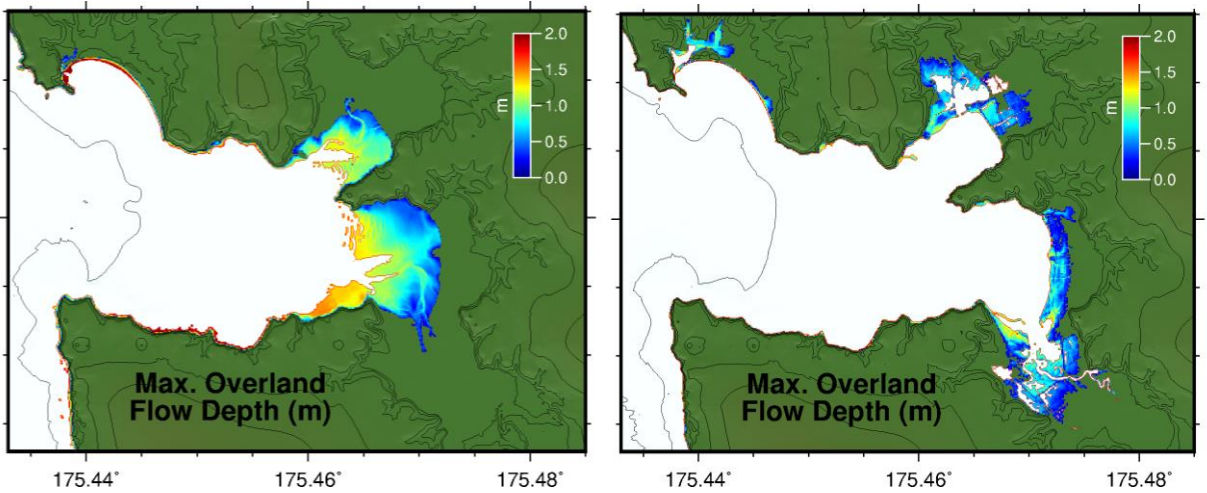
6 RESULTS SUMMARY

6.1 *Direct Comparison of Inundation extents*

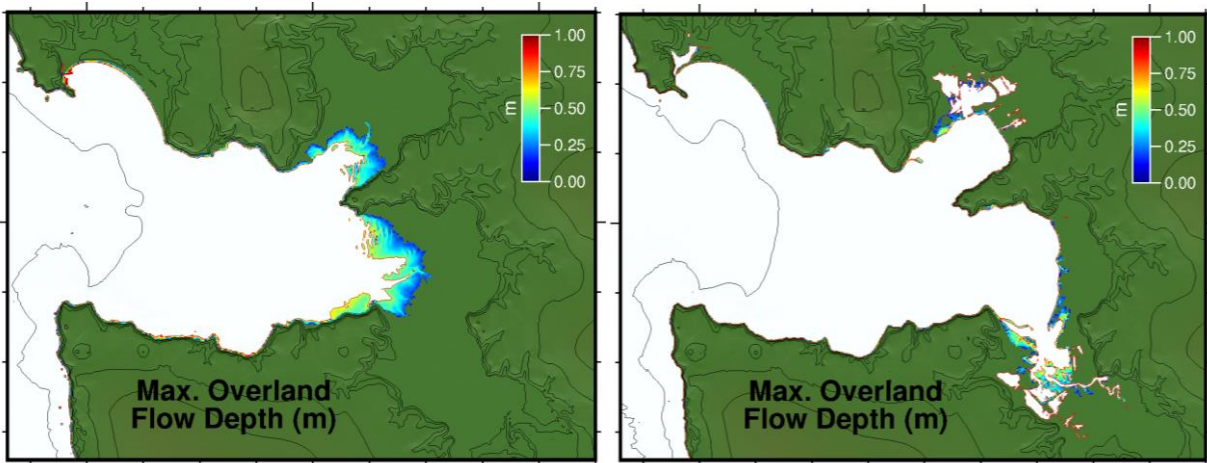
In Figure 6.1 and Figure 6.2 we present a direct comparison between the modelled inundation extents for the three dominant sources within each source category (local, regional or distant). The results show that of these sources, the D2, local source scenario generally produces the greatest inundation extents. Particularly in the northern Colville model grid. At Thames in the southern end of the Firth none of these scenarios produces significant inundation or tsunami height able to overtop the existing stop banks.



D2 Local



TK8 Regional



1868 Distant

Figure 6.1 Direct comparison between the D2 local, TK8 regional and 1868 distant source scenarios at Colville

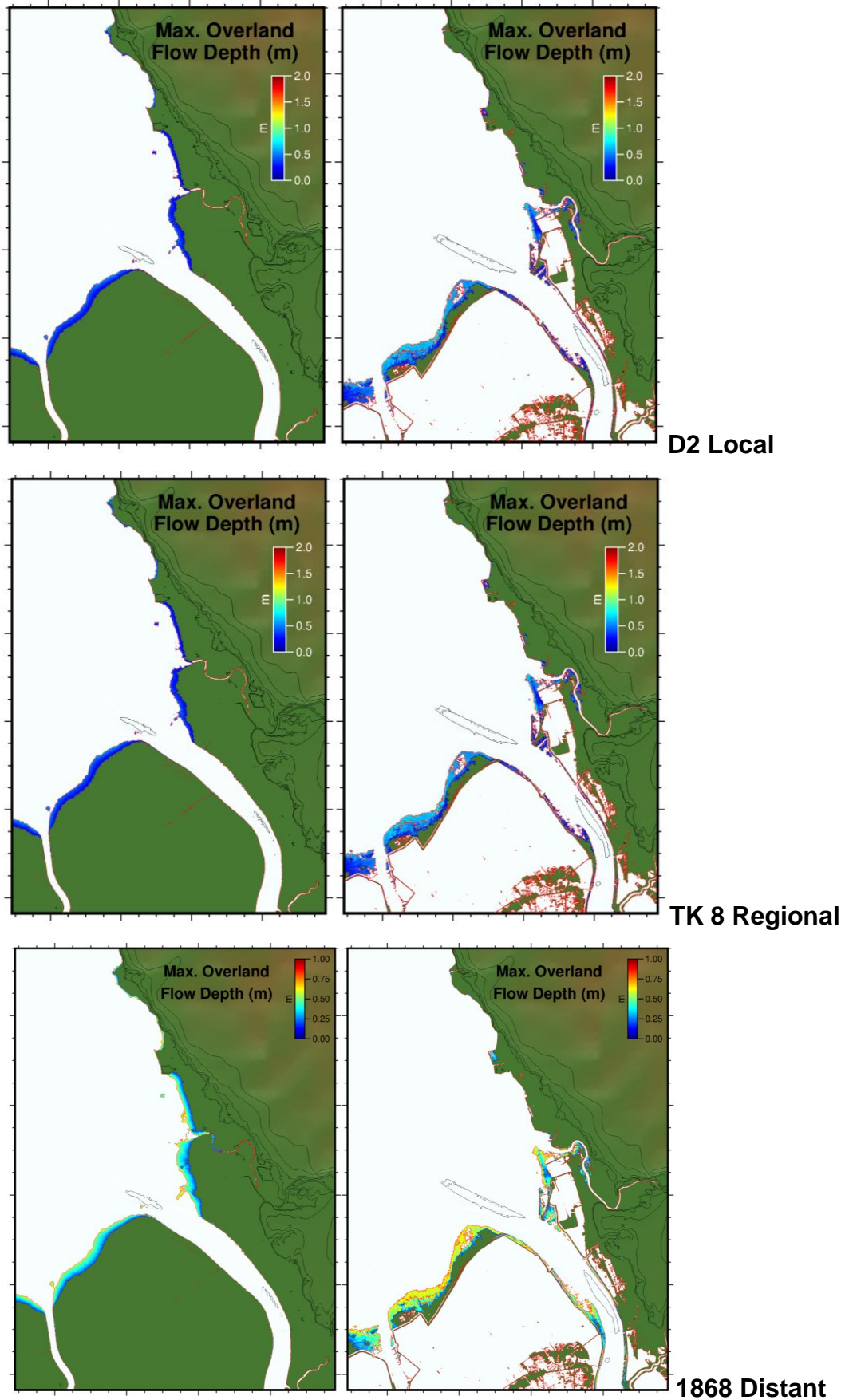


Figure 6.2 Direct comparison between the D2 local, TK8 regional and 1868 distant source scenarios at Thames. Note the different colour scale for the 1868 scenario.

6.2 Comparison to Modelling of Chick (1999)

The model results here differ significantly from the results presented in Chick (1999) for several reasons. Firstly, in her thesis, Chick (1999) employed three separate models to model tsunami propagation and inundation; a finite element model TSUNAMI, and two different depth averaged, finite difference hydrodynamic models ('3DD' a general-purpose hydrodynamic model and the more tsunami-specific TUNAMI-N2).

The only modelling presented in Chick (1999) that deals with fault ruptures on the Karepehi Fault is that which uses the finite difference model TSUNAMI. In her thesis, Chick (1999) does not provide any details on the model other than a reference to another MSc thesis (Prasetya, 1998) which presumably describes the origins and development of the model.

It is not clear what method Chick (1999) used to determine the initial sea-floor displacement based on the earthquake parameters. Judging by the results described in the thesis, we assume that some sort of elastic dislocation model was used in the TSUNAMI model. For example, in Case D2, the 7.35 m of slip on fault segment D2 resulted in 2.8 m of sea surface displacement. However, this differs significantly from the results presented here where source D2 produces ~5.0 m of vertical uplift. It should be noted that the elastic deformation model used in this study is based on the theory of Okada (1985) and has been validated numerous times.

In the modelling using 3DD and TUNAMI-N2, Chick does not model the tsunami from source, but rather she develops a modelling grid area then forces a sinusoidal wave boundary condition across one or more of the open boundaries.

In this regard, the 3DD model was used to simulate a far-field tsunami by applying a sinusoidal boundary condition with a height of 1.0 m (peak to trough) and a period of 10, 15, 20, 25 and 30 minutes. While this approach may have been appropriate at the time, we now have much better techniques for simulating the effects of trans-Pacific tsunami affecting the Firth of Thames. Specifically, the modelling presented in Section 1.5 and Chapter 5 of this report where we model the entire evolution of the tsunami from its source in South America, its transformation across the Pacific and ultimately its effects in our local study area.

For tsunami inundation, Chick (1999) again uses the forced boundary approach with the TUNAMI N2 model. In this case a model grid was constructed covering the area of the Thames township. She then forced a time series of water levels with a 3 m amplitude and 10-minute period over the open western boundary of the grid. This resulted in significant inundation affecting Thames. A second simulation was run using the same input wave, however the topography grid was modified to include 3.5 m high stop banks. Unsurprisingly the presence of the stop banks reduced the degree of inundation.

While this is a robust result – that the presence of elevated topography reduces modelled inundation – the way it was achieved is somewhat questionable. We argue that the 3.0 m water level time series is unrealistically large based on the model results from our study.

Given the good fit between the measured and modelled tsunami wave trains presented in Figure 1.10, Figure 1.12 and Figure 1.15, we have very strong confidence in the modelling

presented here and we caution against using any of the Chick (1999) results for hazard assessment purposes.

7 SUMMARY AND CONCLUSIONS

This study analysed tsunami induced inundation at several sites in the Firth of Thames, New Zealand. The study considered inundation caused by local, regional and distant tsunami sources generated by earthquakes. In general, the results suggest that the tsunami hazard at sites within the Firth of Thames is relatively low compared to other sites in New Zealand, particularly those on the east coast of the North Island. This is due mostly to the fact that the Firth of Thames is relatively shallow which dissipates incident wave energy and because the Firth is sheltered from direct tsunami impact of regional and distant source tsunamis by the Coromandel Peninsula and Great Barrier Island.

While some studies (i.e. Chick 1999) suggest the possibility of tsunamigenesis from ruptures of the Kerepehi Fault which lies within the Firth of Thames itself, the earthquakes proposed as the potential tsunami sources are relatively small and generally do not produce significant tsunami inundation. Of the five rupture scenarios proposed by Chick (1999), four have magnitudes (M_w) of 6.8 or less with coseismic displacements of just 2.4 m. This results in a net sea floor deformation of the order of 1 m producing generally inconsequential tsunami effects. The exception to this is source 'D2' which is located at the northern end of the Firth of Thames and is believed to be capable of producing a magnitude 7.1 earthquake with up to 8.5 m of coseismic slip. This source produces initial sea floor deformation of ~4 m and results in significant inundation at all the sites considered. At Thames, the tsunami generated by this source does not lead to overtopping of the existing flood protection stop banks.

We stress however, that the results presented here are for tsunamis generated by purely tectonic source mechanisms and we do not consider the possibility of secondary or alternate tsunami sources such as submarine or subaerial landslides or slumps or tsunami caused by volcanic eruptions. As with the results of Chick et al. (2001) we also do not consider the effect of tsunami amplification due to slow seismic ruptures in areas of soft sediments (i.e. *'tsunami earthquakes'*). However, these types of earthquakes are generally associated with shallow ruptures in subduction zones and not with high-angle crustal faults such as the Kerepehi Fault. However, we attempted to mitigate this concern by using slightly larger fault displacements at shallower depths than modelled by Chick (1999).

We also point out that the modelling presented here does not consider other factors that could affect inundation, particularly fine scale ground movements such as liquefaction induced subsidence or the possible failure of flood protection structures due the earthquake shaking. It is possible that ground shaking from earthquakes on either the local (Kerepehi) or regional (Tonga-Kermadec Trench) faults could cause these earthen structures to fail and under certain circumstances this could lead to greater tsunami inundation than is predicted here. Earthquake intensity (MMI) values of VII-VIII in Thames are reported by Persaud et al. (2015) for ruptures of the offshore segments of the Kerepehi Fault as described by Chick et al. (2001).

Although the modelling here does not predict significant inundation for any of the sources trailed, it is the local source 'D2' scenario that produces the largest overall tsunami heights and inundation extents. While the inundation from source D2 is relatively small for the sites considered in this study, we note that sites in the Auckland Region, particularly around

Orere Point and on the eastern shores of Waiheke and Pakihi Islands, are much more susceptible to tsunami effects from this source with projected tsunami heights on the order of 4 m.

As with the findings of Chick et al. (2001) we note that the tsunami hazard from the Kerepehi Fault is relatively minor given the long recurrence interval for maximum credible events of 2,500 – 9,000 years. Persaud et al. (2015) however state that major earthquakes could occur on the Kerepehi Fault (including the offshore segments) once every 1000 years or have a 1% probability of occurrence in 10 years.

8 REFERENCES

- Borrero, J.C. (2013). *Numerical modelling of tsunami effects at two sites on the Coromandel Peninsula, New Zealand: Whitianga and Tairua-Pauanui*, (Waikato Regional Council Technical Report No. 2013/24, (Vol. 4355, pp. 1–96).
- Borrero, J.C. (2014). *Numerical modelling of tsunami effects at Whangamata, Whiritoa and Onemana, Coromandel Peninsula New Zealand*, Report prepared for the Waikato Regional Council, September 2014.
- Borrero, J.C. (2015) Observations and Modeling of Tsunami Inundation at Port Charles, Coromandel Peninsula, New Zealand, Prepared for Waikato Regional Council, January 2015.
- Borrero, J.C. and Greer, S.D. (2012) Comparison of the 2010 Chile and 2010 Japan tsunamis in the Far-field, *Pure and Applied Geophysics*, 170, 1249-1274, DOI 10.1007/s00024-012-0559-4.
- Borrero J.C. and Goring D.G (2015) South American Tsunamis in Lyttelton Harbor, New Zealand, *Pure and Applied Geophysics*, Volume 172, Issue 3, pp 757-772.
- Chick, Louise Mae (1999) Potential Tsunami Hazard Associated with the Kerepehi Fault, Hauraki Gulf, New Zealand. MSc. Thesis, University of Waikato.
- De Lange, W.P., & Healy, T.R. (1986). New Zealand tsunamis 1840–1982. *New Zealand Journal of Geology and Geophysics*, 29(1), 115–134. doi:10.1080/00288306.1986.10427527
- De Lange, W. P., & Healy, T. R. (2001). Tsunami hazard for the Auckland region and Hauraki Gulf, New Zealand. *Natural Hazards*, 24(3), 267–284. <http://doi.org/10.1023/A:1012051113852>
- Dorbath, L., A. Cisternas, and C. Dorbath (1990). Assessment of the size of large and great historical earthquakes in Peru, *Bull. Seismol. Soc. Am.* 80, 551–576.
- Downes, G., A. Barberopoulou, U. Cochran, K. Clark, and F. Scheele (2017), The New Zealand Tsunami Database: Historical and Modern Records. *Seismological Research Letters*, 88 (2), 342-353, doi: 10.1785/0220160135.
- Fujii, Y., & Satake, K. (2012). Slip Distribution and Seismic Moment of the 2010 and 1960 Chilean Earthquakes Inferred from Tsunami Waveforms and Coastal Geodetic Data. *Pure and Applied Geophysics*, 170 (9-10), 1493–1509. doi:10.1007/s00024-012-0524-2
- Gibson, F. (1868). On the Wave Phenomena observed in Lyttelton Harbor, August 15, 1868. *Transactions and Proceedings of the New Zealand Institute*, 1, 195:196.
- Liefting, R. Craig, H., Hunt, S. and Stephens, S. (2018) Firth of Thames Storm Surge Event, January 2018. Proceedings of the New Zealand Coastal Society Annual Conference, Gisborne (abstract).

- Morris, B. and Borrero, J.C. (2014) Inundation of Whitianga town during the 1960 Chilean Tsunami, Waikato Regional Council Technical Report 2014/65, June 2014, ISSN 2230-4363 (Online)
- Persaud, M., Villamor, P., Berryman, K., Ries, W., Cousins, J., Alloway, B. (2015) The Kerepehi Fault, Hauraki Rift, New Zealand: active fault characterisation and hazard. *New Zealand Journal of Geology and Geophysics*, V 59, No. 1.
- Power, W.L., & Gale, N. (2010). Tsunami Forecasting and Monitoring in New Zealand. *Pure and Applied Geophysics*, 168(6-7), 1125–1136. doi:10.1007/s00024-010-0223-9
- Power, W.L., Downes, G., & Stirling, M. (2007). Estimation of Tsunami Hazard in New Zealand due to South American Earthquakes. *Pure and Applied Geophysics*, 164(2-3), 547–564. doi:10.1007/s00024-006-0166-3
- Power, W.L., Wallace, L., Wang, X., & Reyners, M. (2011). Tsunami Hazard Posed to New Zealand by the Kermadec and Southern New Hebrides Subduction Margins: An Assessment Based on Plate Boundary Kinematics, Interseismic Coupling, and Historical Seismicity. *Pure and Applied Geophysics*, 169(1-2), 1–36. doi:10.1007/s00024-011-0299-x
- Prasetya, G. S., & Wang, X. (2011). *Tsunami frequency analysis for Eastern Coromandel and Waikato Region from Kermadec Trench and local sources within the Bay of Plenty* (No. 2011/135) (p. 65).
- Titov, V. V., & González, Frank, I. (1997). *Implementation and testing of the Method of Splitting Tsunami (MOST) model* (No. ERL PMEL-112) (p. 14). Retrieved from <http://www.pmel.noaa.gov/pubs/PDF/tito1927/tito1927.pdf>
- Titov, V. V., Moore, C. W., Greenslade, D. J. M., Pattiaratchi, C., Badal, R., Synolakis, C. E., & Kânoğlu, U. (2011). A New Tool for Inundation Modeling: Community Modeling Interface for Tsunamis (ComMIT). *Pure and Applied Geophysics*, 168(11), 2121–2131. doi:10.1007/s00024-011-0292-4
- Titov, V.V., and C.E. Synolakis (1995): Modelling of breaking and nonbreaking long wave evolution and runup using VTCS-2. *J. Waterways, Ports, Coastal and Ocean Engineering*, 121(6), 308–316.
- Titov, V.V., and C.E. Synolakis (1997): Extreme inundation flows during the Hokkaido-Nansei-Oki tsunami. *Geophys. Res. Lett.*, 24(11), 1315–1318.
- Titov, V.V. and Synolakis, C.E. (1998) Numerical modeling of tidal wave runup, *Journal of Waterways, Port, Coastal and Ocean Engineering*, ASCE, 124 (4), 157-171.
- Wei, Y., Chamberlin, C., Titov, V. V., Tang, L., & Bernard, E. N. (2013). Modeling of the 2011 Japan Tsunami: Lessons for Near-Field Forecast. *Pure and Applied Geophysics*, 170(6–8), 1309–1331. <http://doi.org/10.1007/s00024-012-0519-z>
- Wei, Y, Newman, A, Hayes, G, Titov, V, Tang, L (2014). Tsunami Forecast by Joint Inversion of Real-Time Tsunami Waveforms and Seismic or GPS Data: Application to the Tohoku 2011 Tsunami. *Pure Appl. Geophys.* doi:10.1007/s00024-014-0777-z

Waikato Regional Council, (2018) "Firth of Thames Levels":

<https://www.waikatoregion.govt.nz/services/regional-services/regional-hazards-and-emergency-management/coastal-hazards/coastal-flooding/coastal-inundation-tool/pre-defined-water-level-scenarios/fot-levels/>.

9 APPENDIX 1 – TIME SERIES FOR LOCAL SOURCE SCENARIOS

Table 9.1 Locations where time series data in the following plots were extracted.

Region	Name	Longitude	Latitude	Depth MSL (m)	Depth MHWS (m)
01	Coleville	175.549	-36.621	0.5	2.0
02	Coromandel	175.47774	-36.78314	3.8	5.4
03	Manaia	175.43657	-36.84710	3.7	5.3
04	Tapu	175.49729	-36.98187	0.8	2.5
05	Te Puru	175.51465	-37.04208	2.4	4.1
06	Thames	175.51773	-37.14527	1.7	3.5
07	Miranda	175.33915	-37.16693	1.4	3.2
08	Whakatiwai	175.30937	-37.09694	1.4	3.1

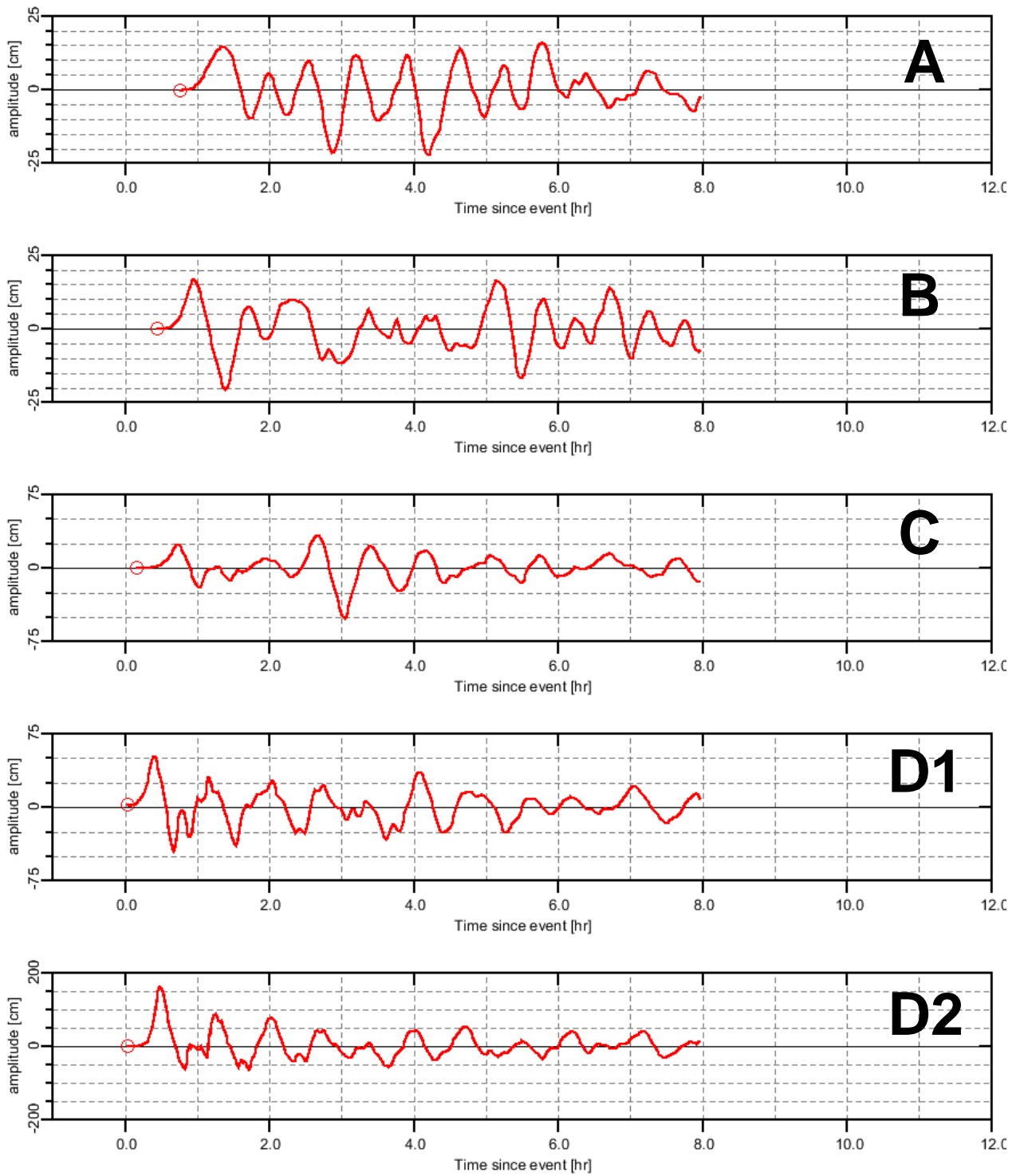


Figure 9.1 Time series of modelled tsunami water levels at Colville (MHWS). Note the varying y-scale-for each scenario.

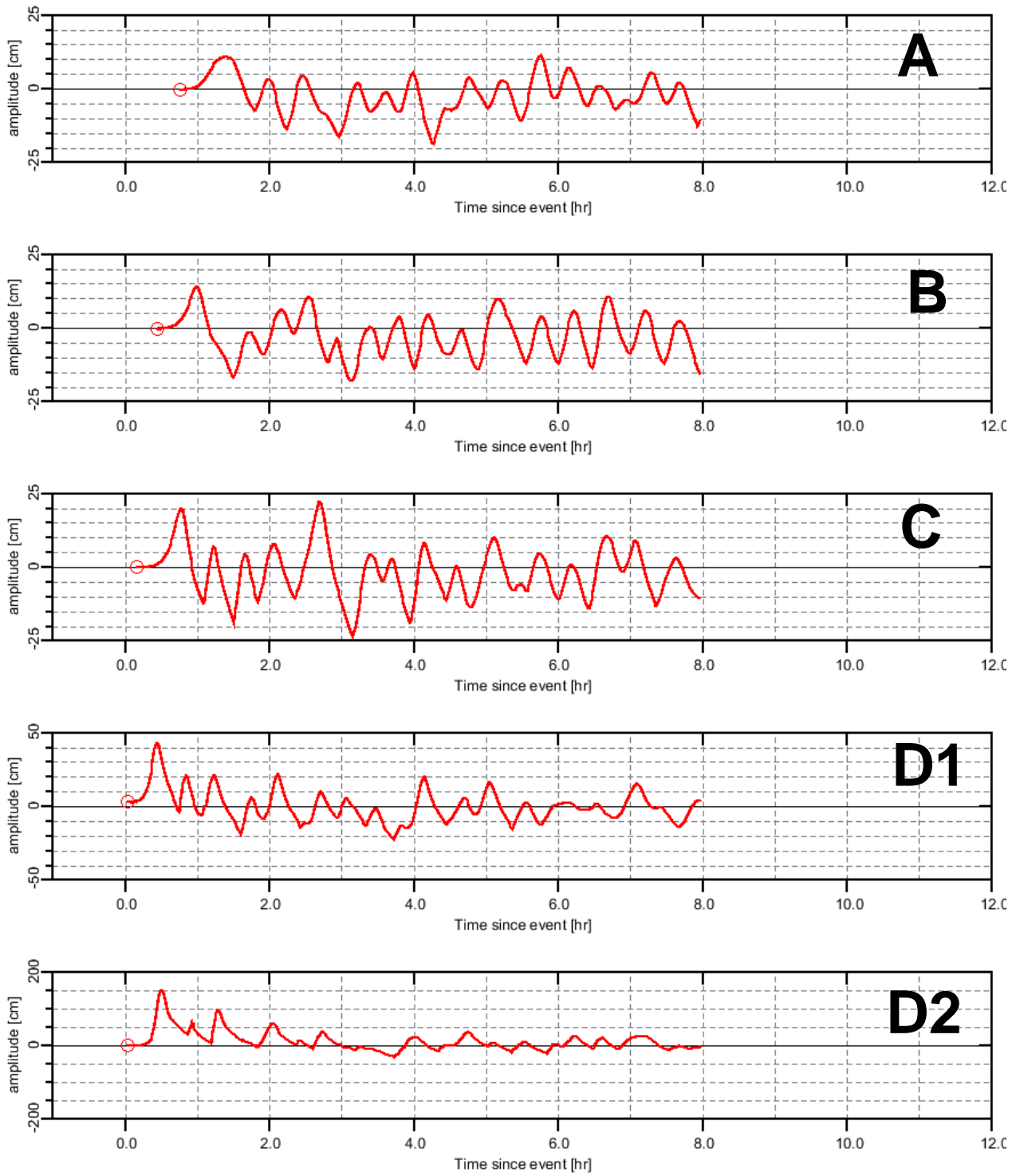


Figure 9.2 Time series of modelled tsunami water levels at Colville (MSL). Note the varying y-scale-for each scenario.

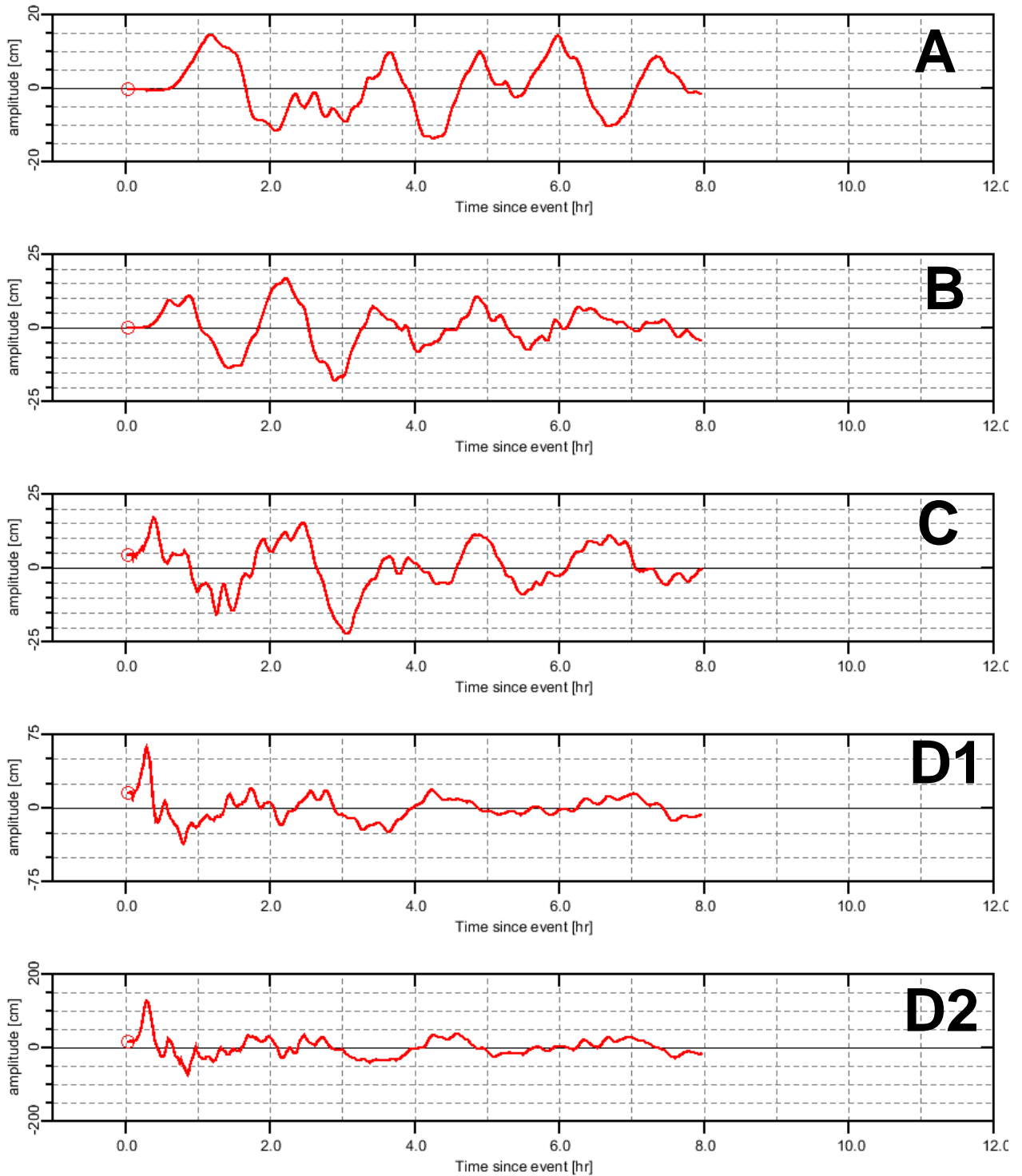


Figure 9.3 Time series of modelled tsunami water levels at Coromandel (MHWS). Note the varying y-scale for each scenario.

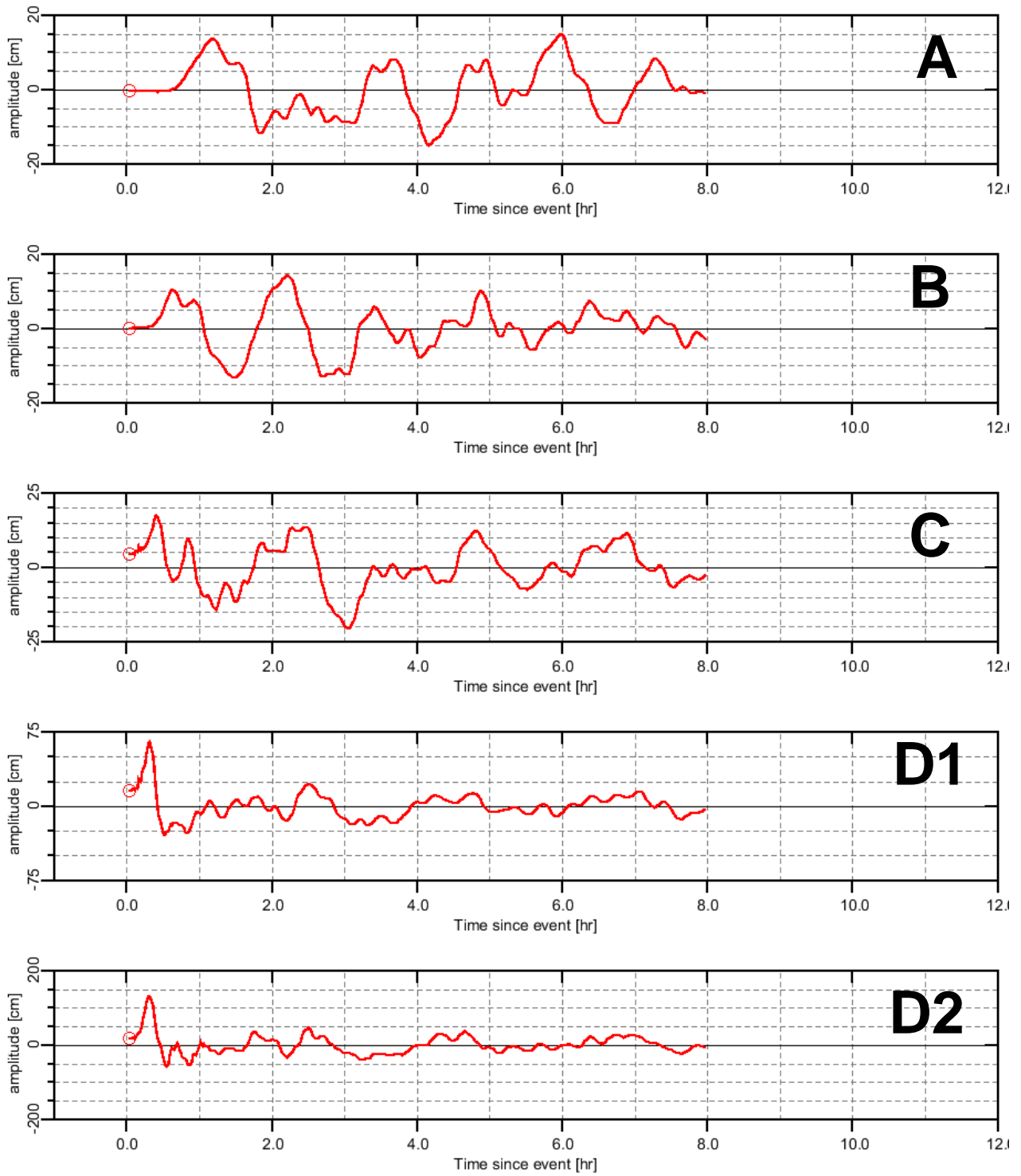


Figure 9.4 Time series of modelled tsunami water levels at Coromandel (MSL). Note the varying y-scale for each scenario.

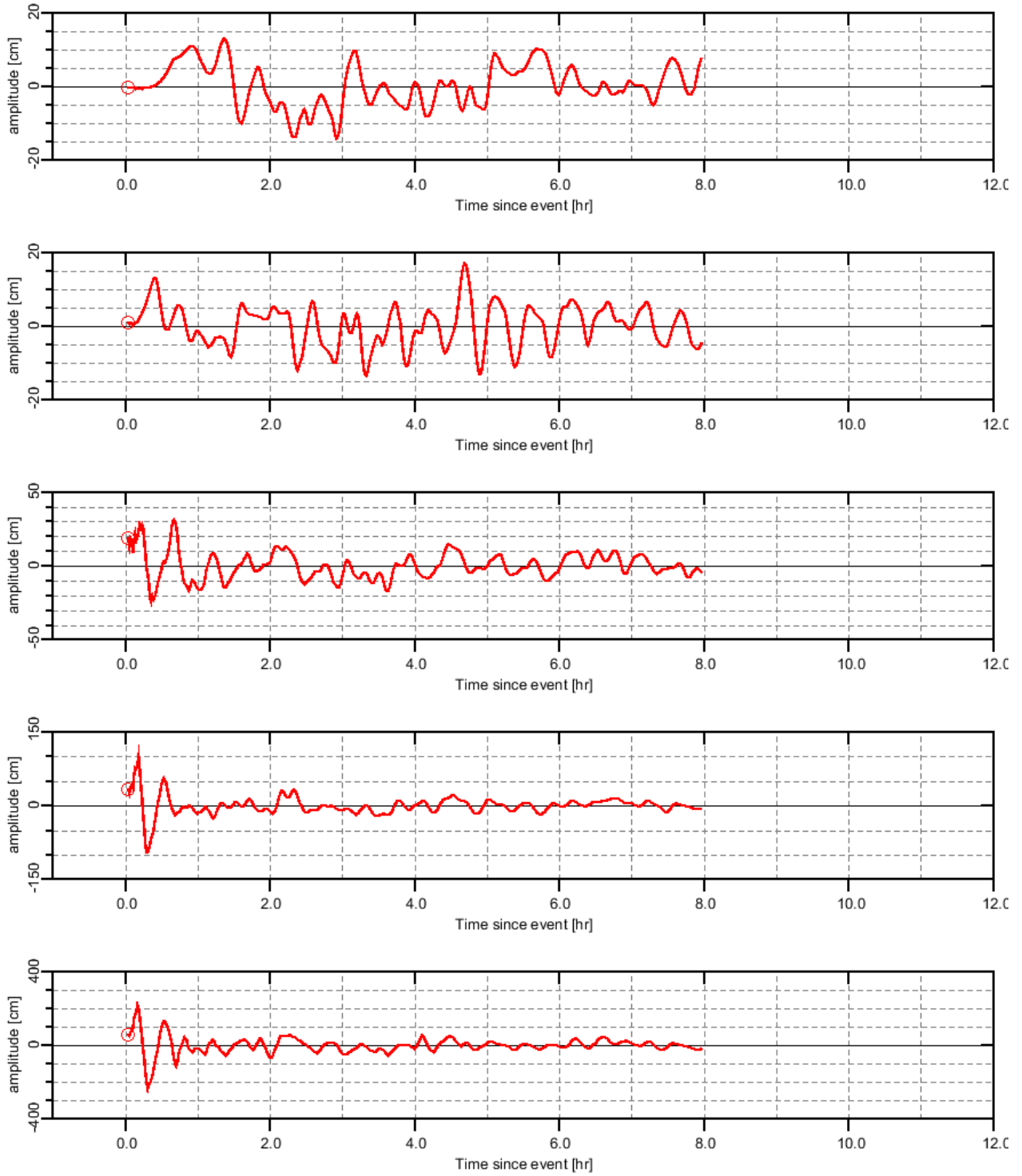


Figure 9.5 Time series of modelled tsunami water levels at Manaia (MHWS). Note the varying y-scale for each scenario.

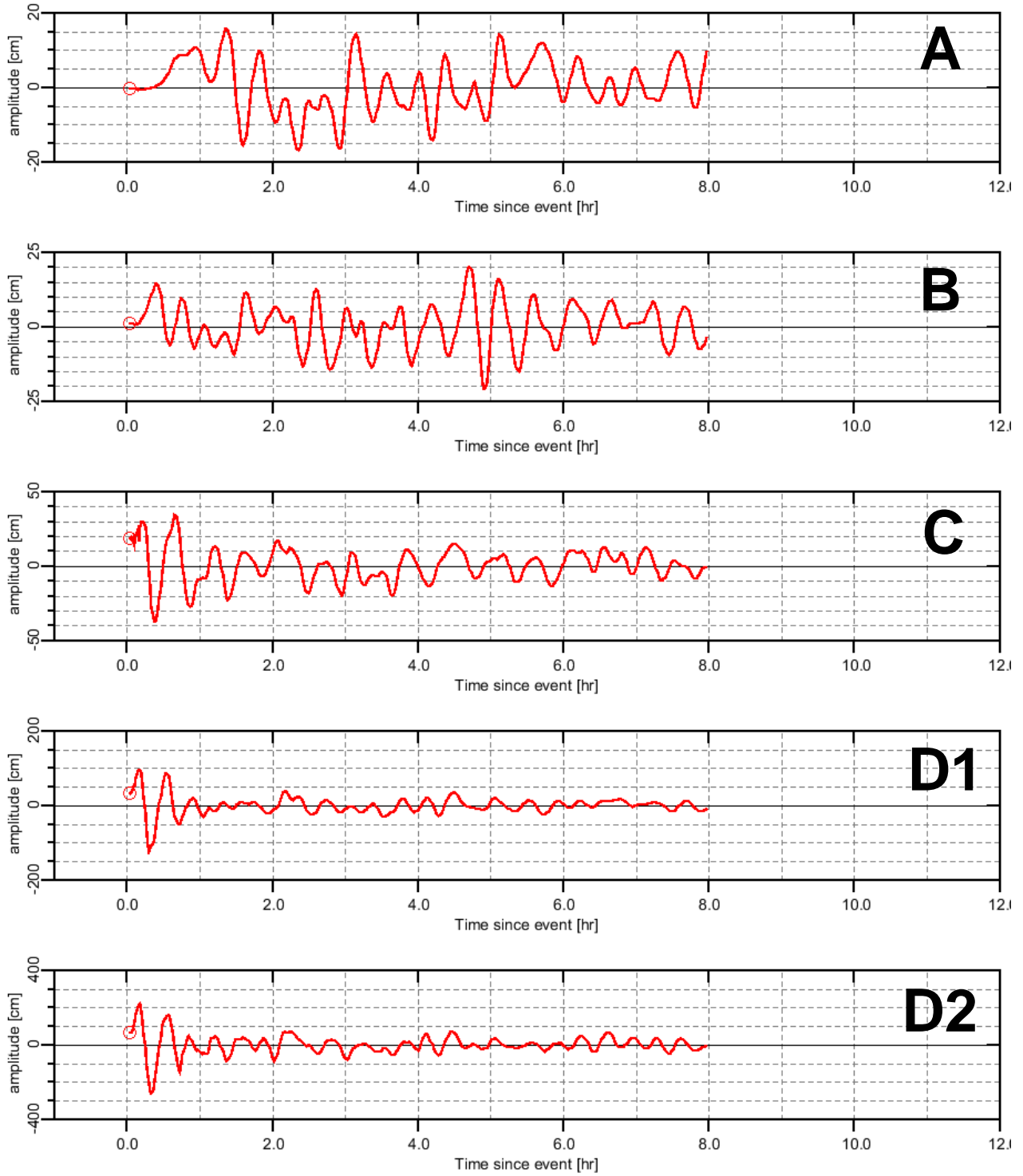


Figure 9.6 Time series of modelled tsunami water levels at Manaia (MSL). Note the varying y-scale for each scenario.

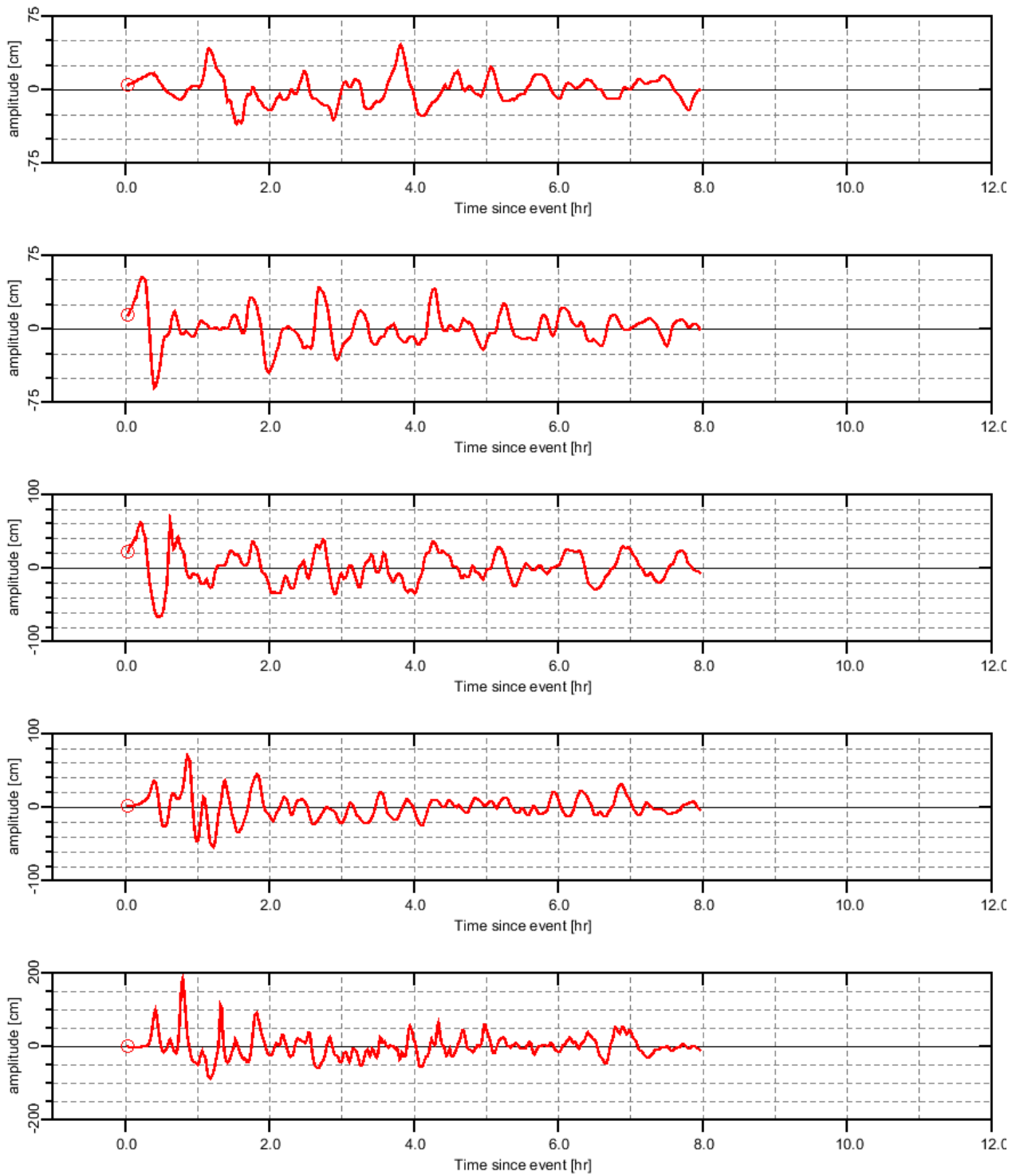


Figure 9.7 Time series of modelled tsunami water levels at Tapu (MHWS). Note the varying y-scale for each scenario.

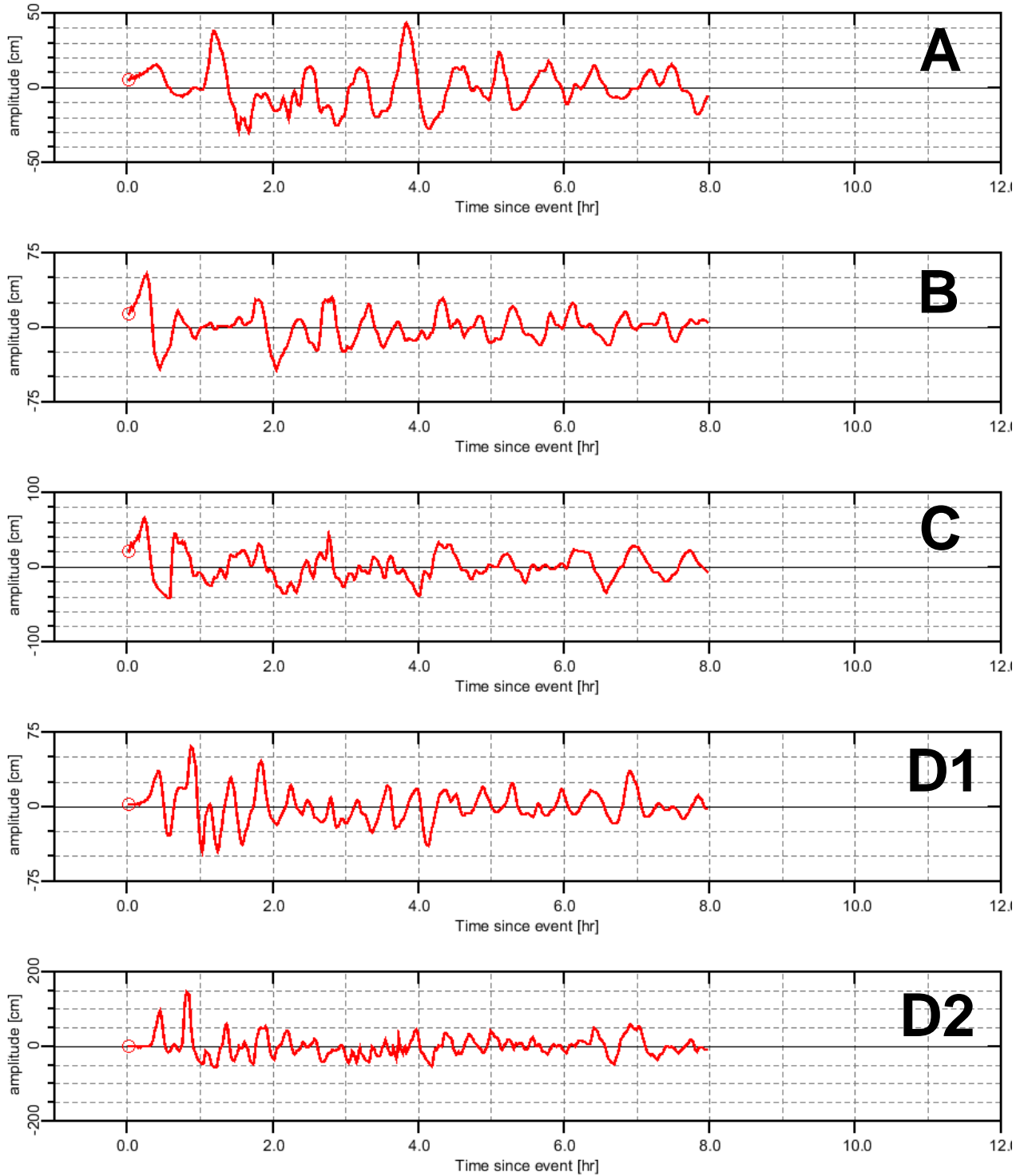


Figure 9.8 Time series of modelled tsunami water levels at Tapu (MSL). Note the varying y-scale for each scenario.

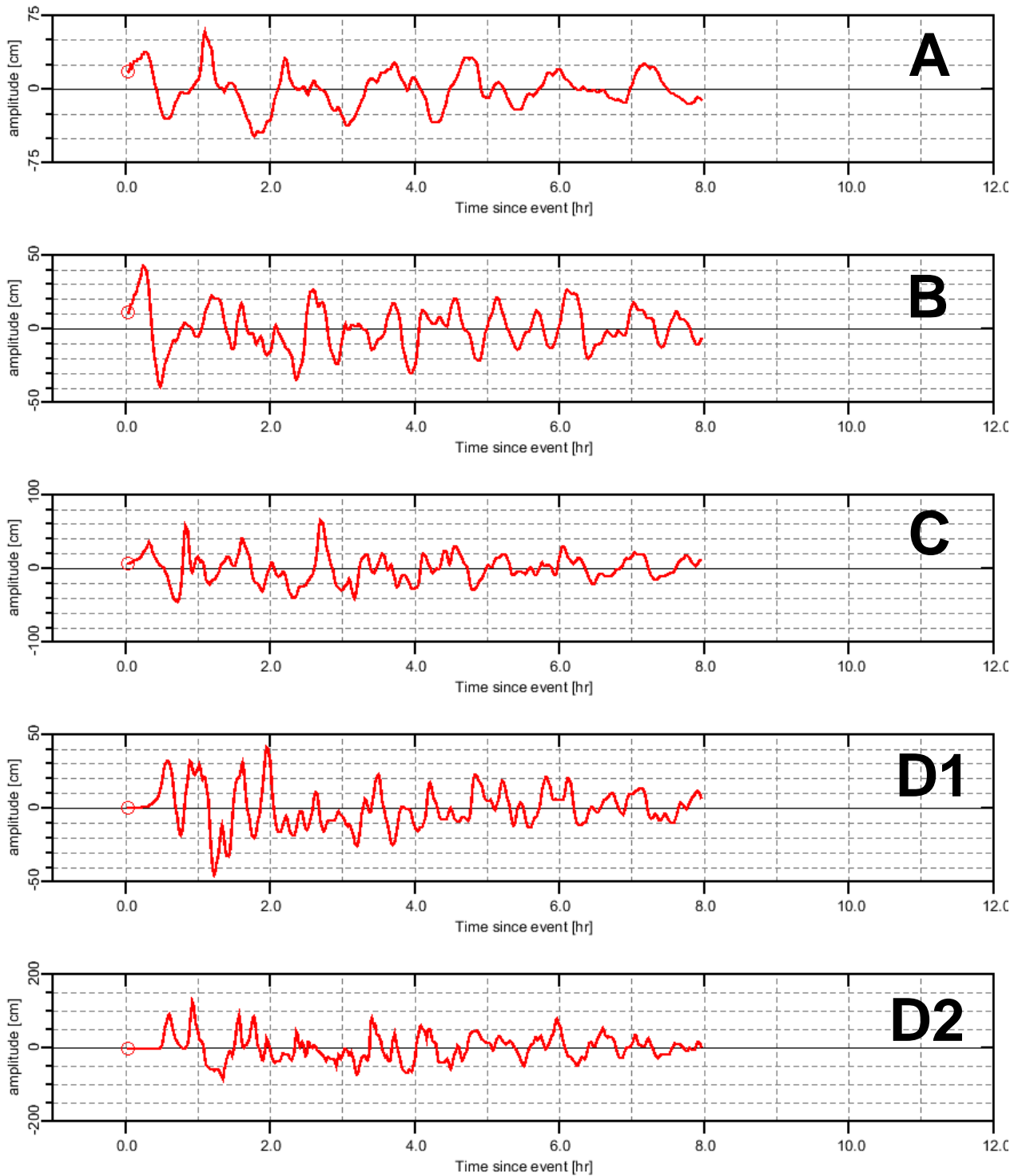


Figure 9.9 Time series of modelled tsunami water levels at Te Puru (MHWS). Note the varying y-scale for each scenario.

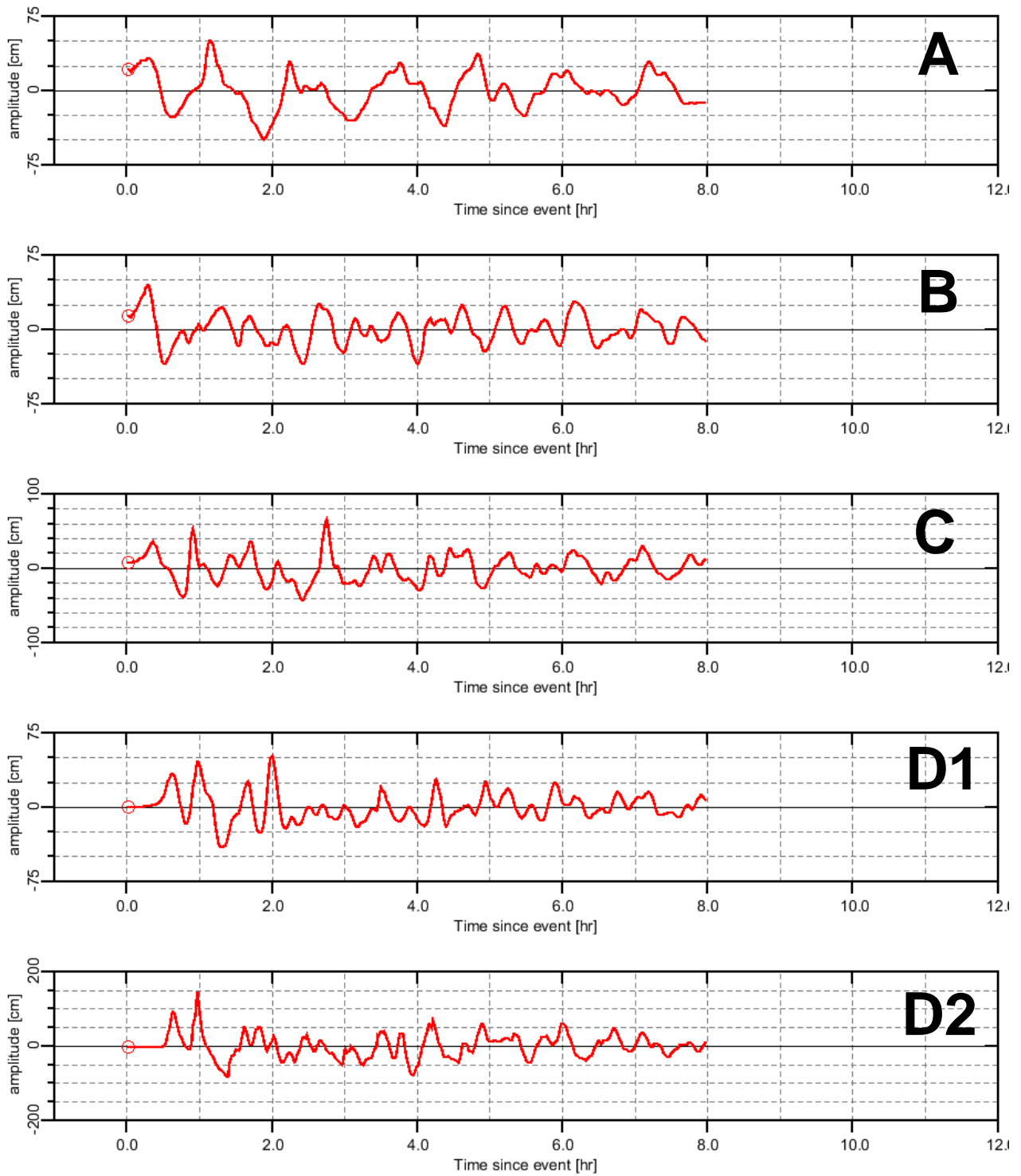


Figure 9.10 Time series of modelled tsunami water levels at Te Puru (MSL). Note the varying y-scale for each scenario.

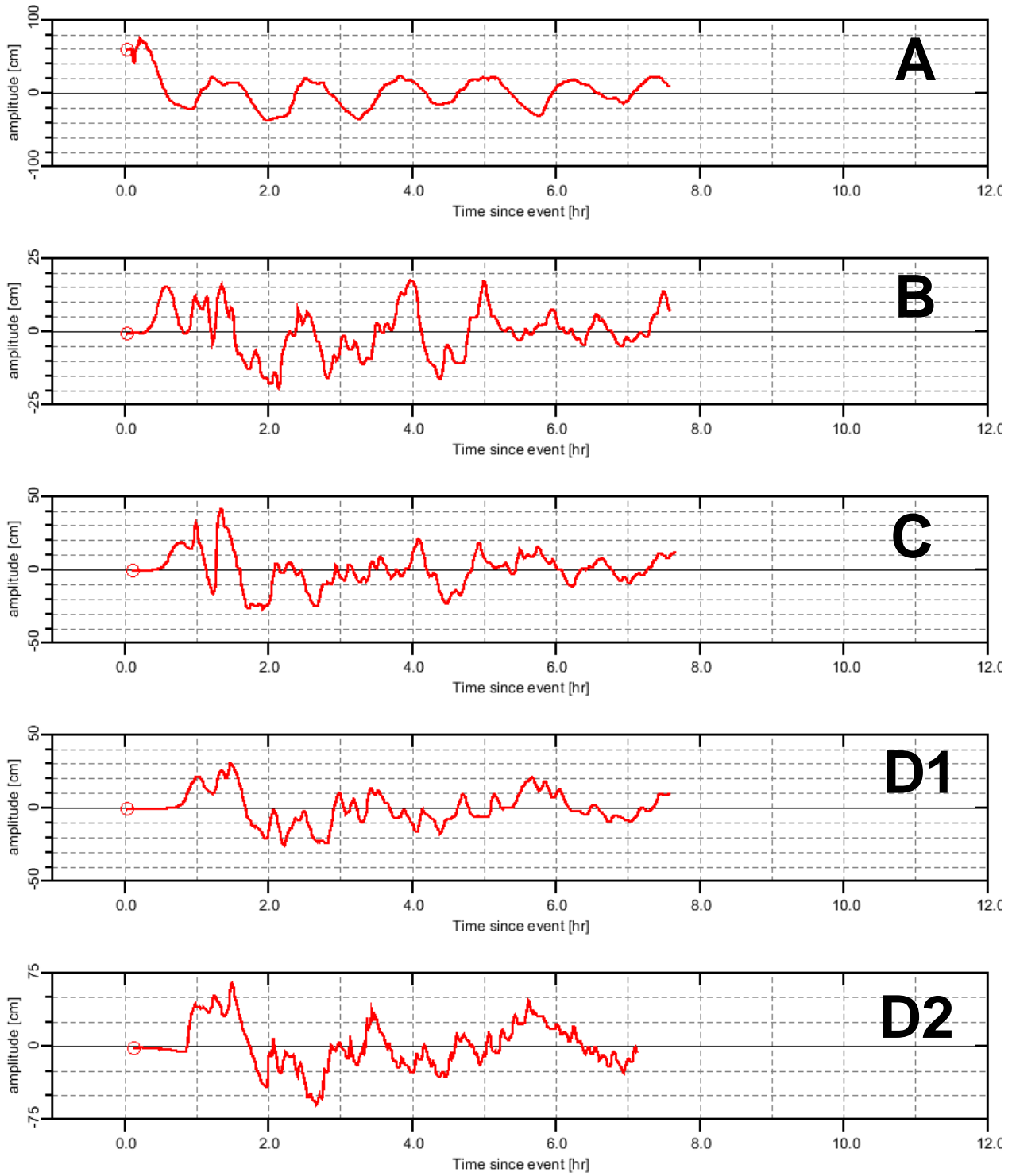


Figure 9.11 Time series of modelled tsunami water levels at Thames (MHS). Note the varying y-scale for each scenario.

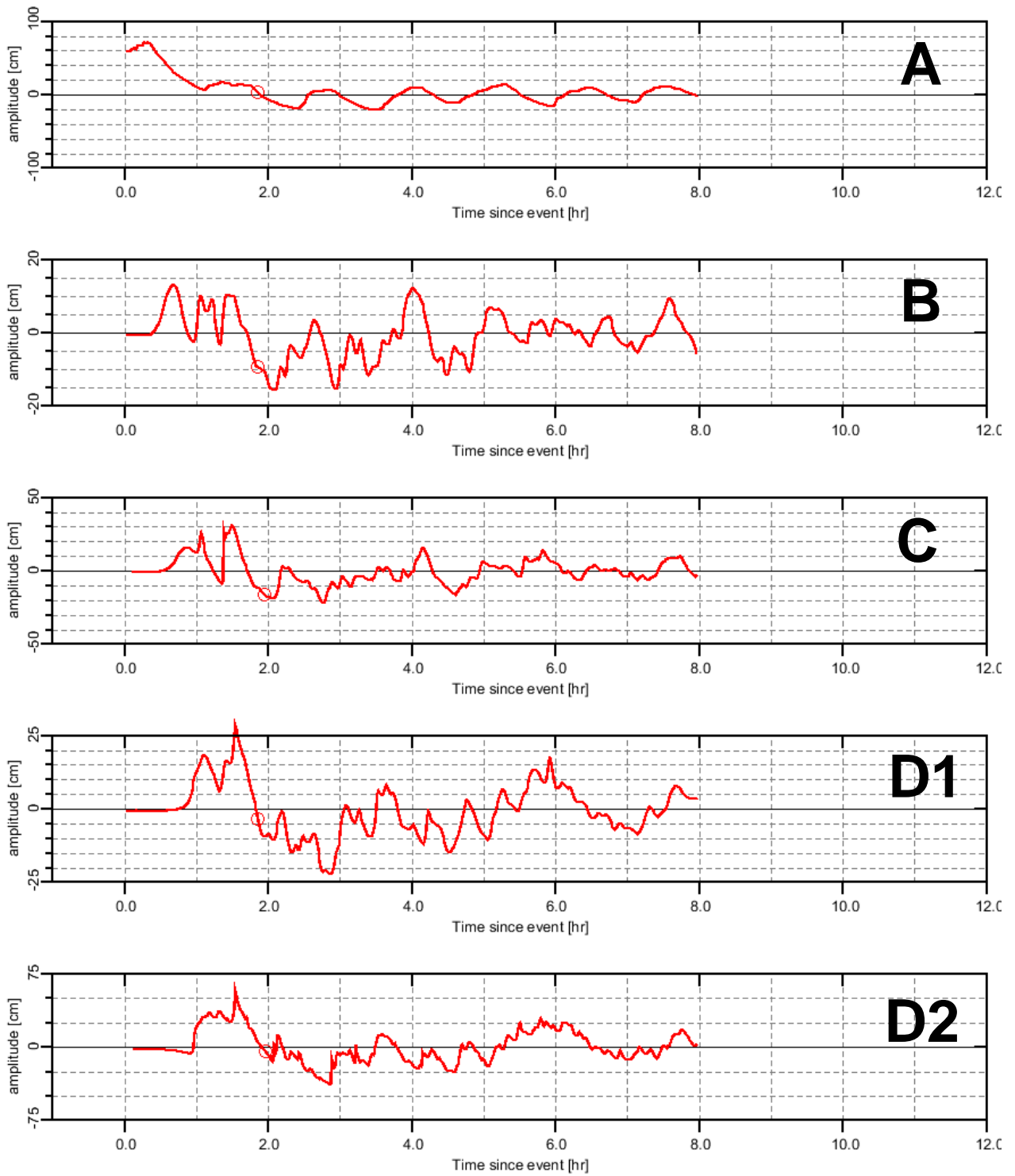


Figure 9.12 Time series of modelled tsunami water levels at Thames (MSL). Note the varying y-scale for each scenario.

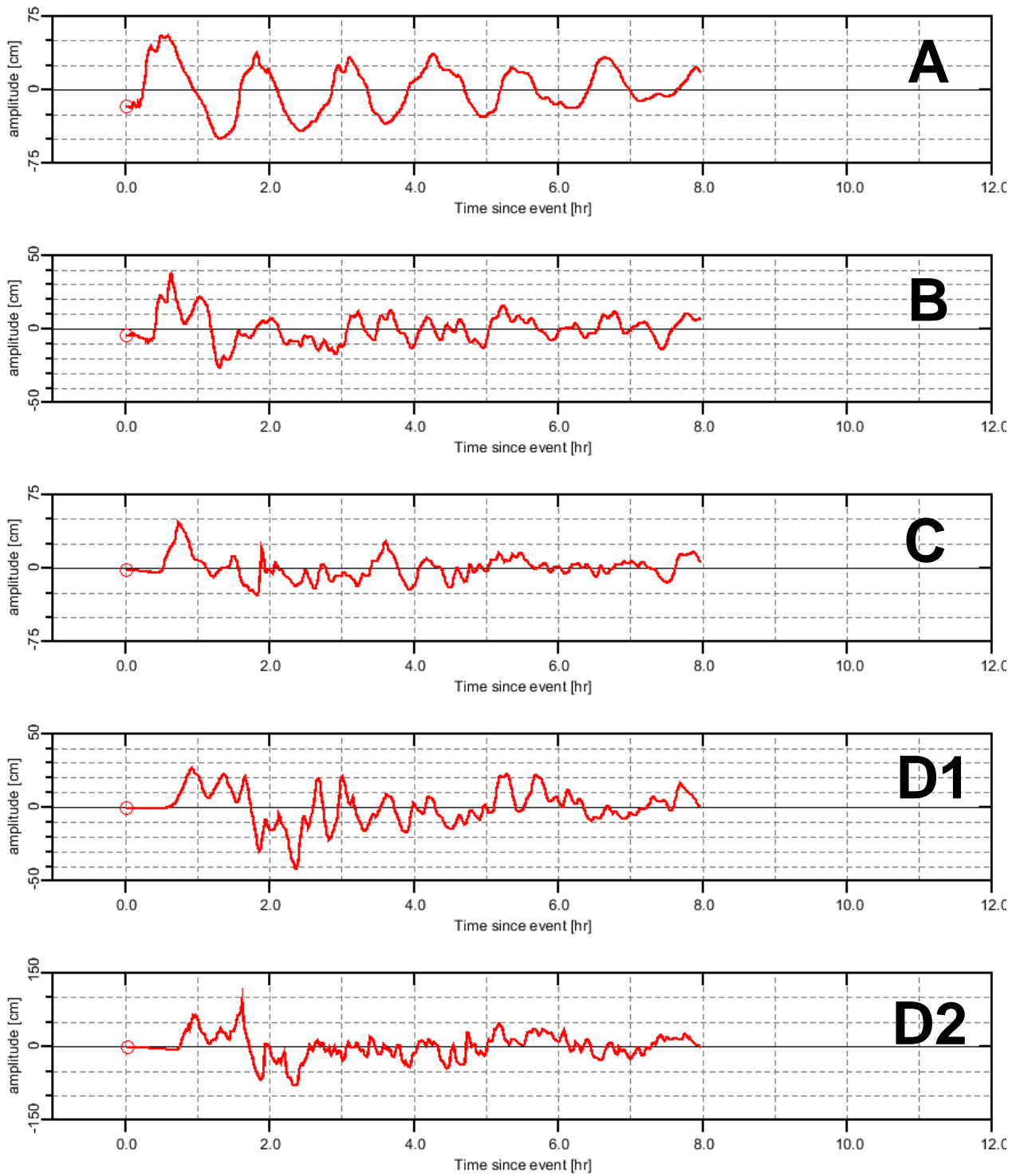


Figure 9.13 Time series of modelled tsunami water levels at Miranda (MHWS). Note the varying y-scale for each scenario.

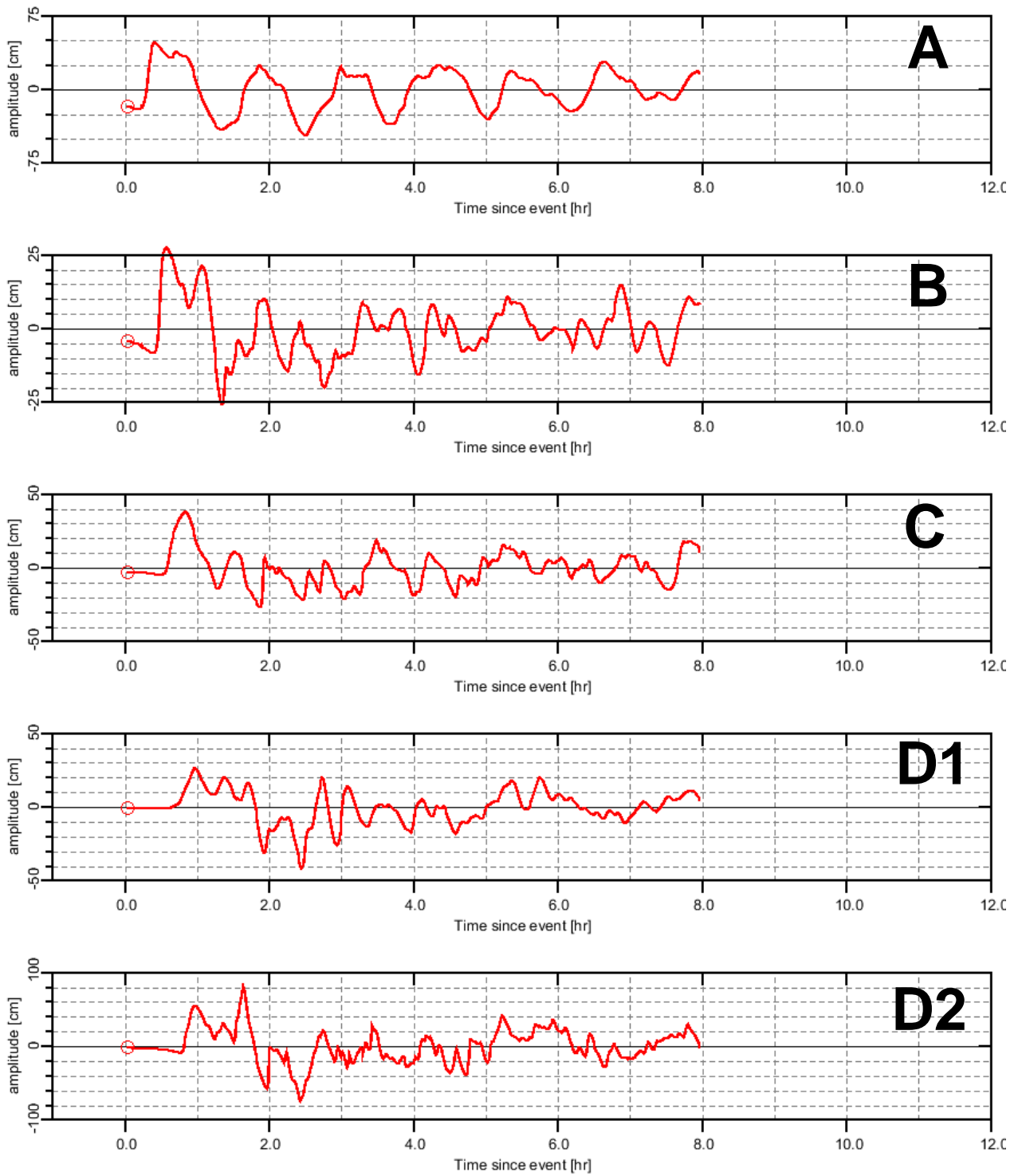


Figure 9.14 Time series of modelled tsunami water levels at Miranda (MSL). Note the varying y-scale for each scenario.

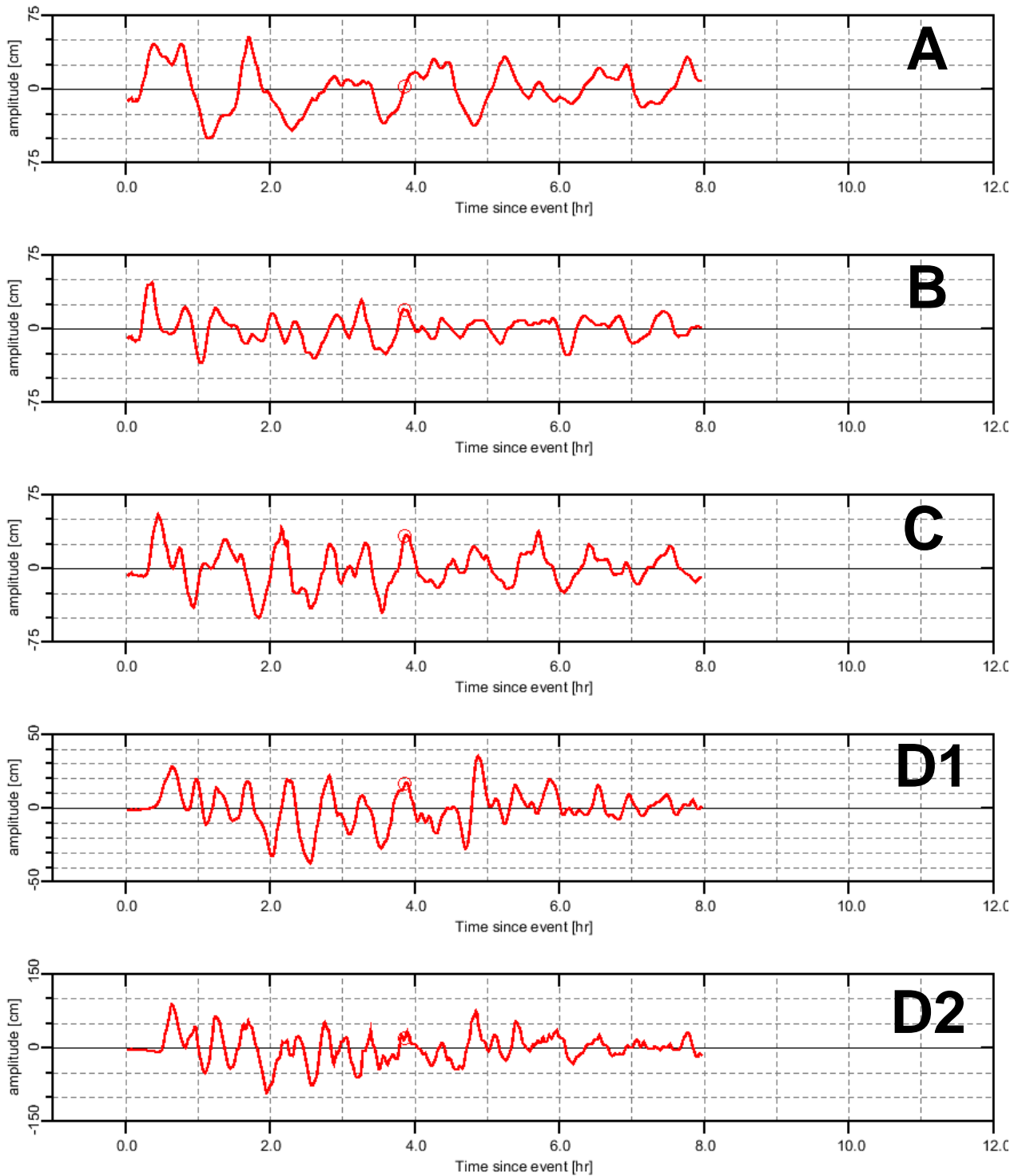


Figure 9.15 Time series of modelled tsunami water levels at Whakatiwai (MHWS). Note the varying y-scale. For each scenario.

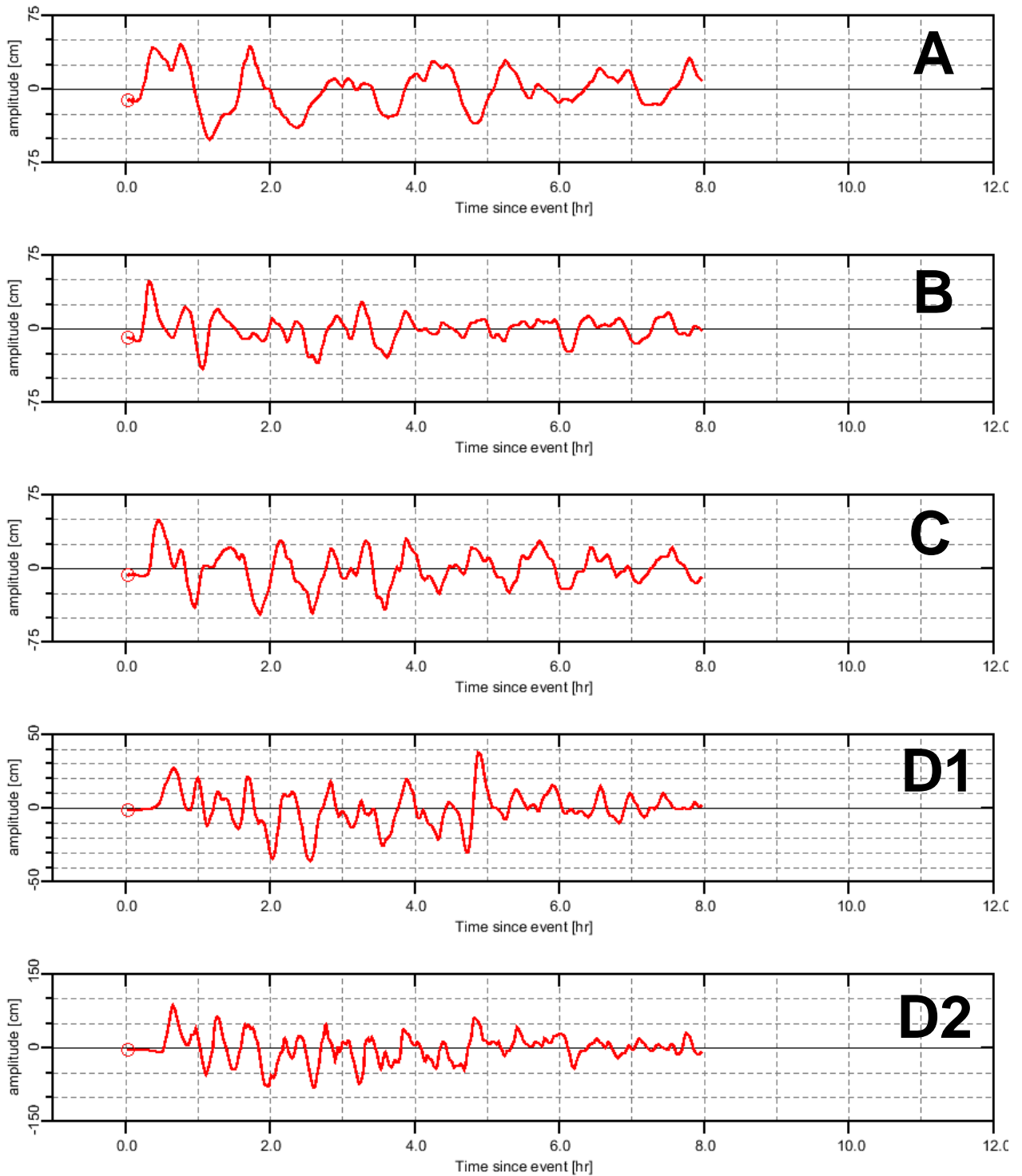


Figure 9.16 Time series of modelled tsunami water levels at Whakatiwai (MSL). Note the varying y-scale. For each scenario.

10 APPENDIX 2 – TIME SERIES FOR TK TRENCH SCENARIO

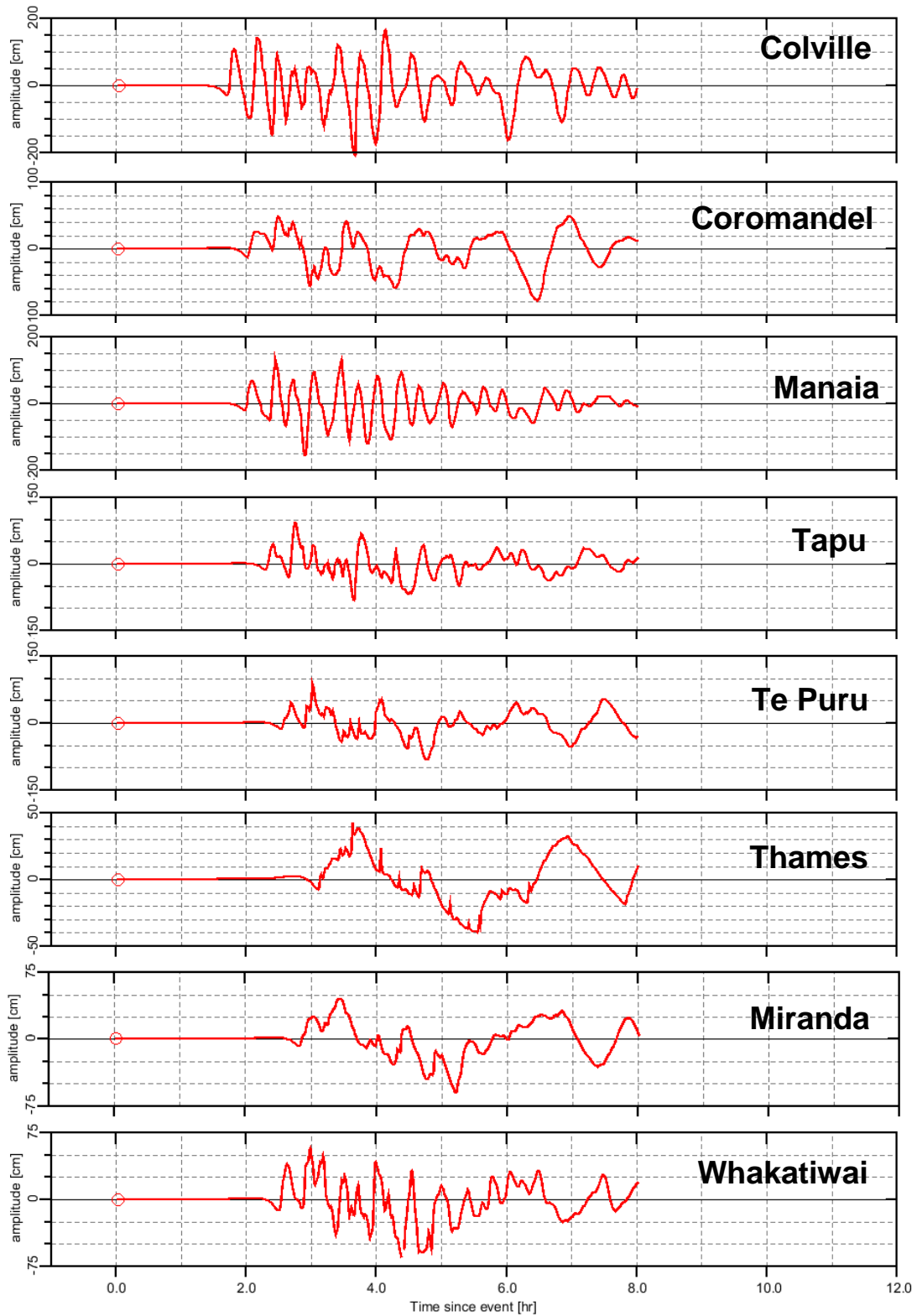


Figure 10.1 Water level time series plots for the TK 8 at MSL sources affecting the 8 study sites.

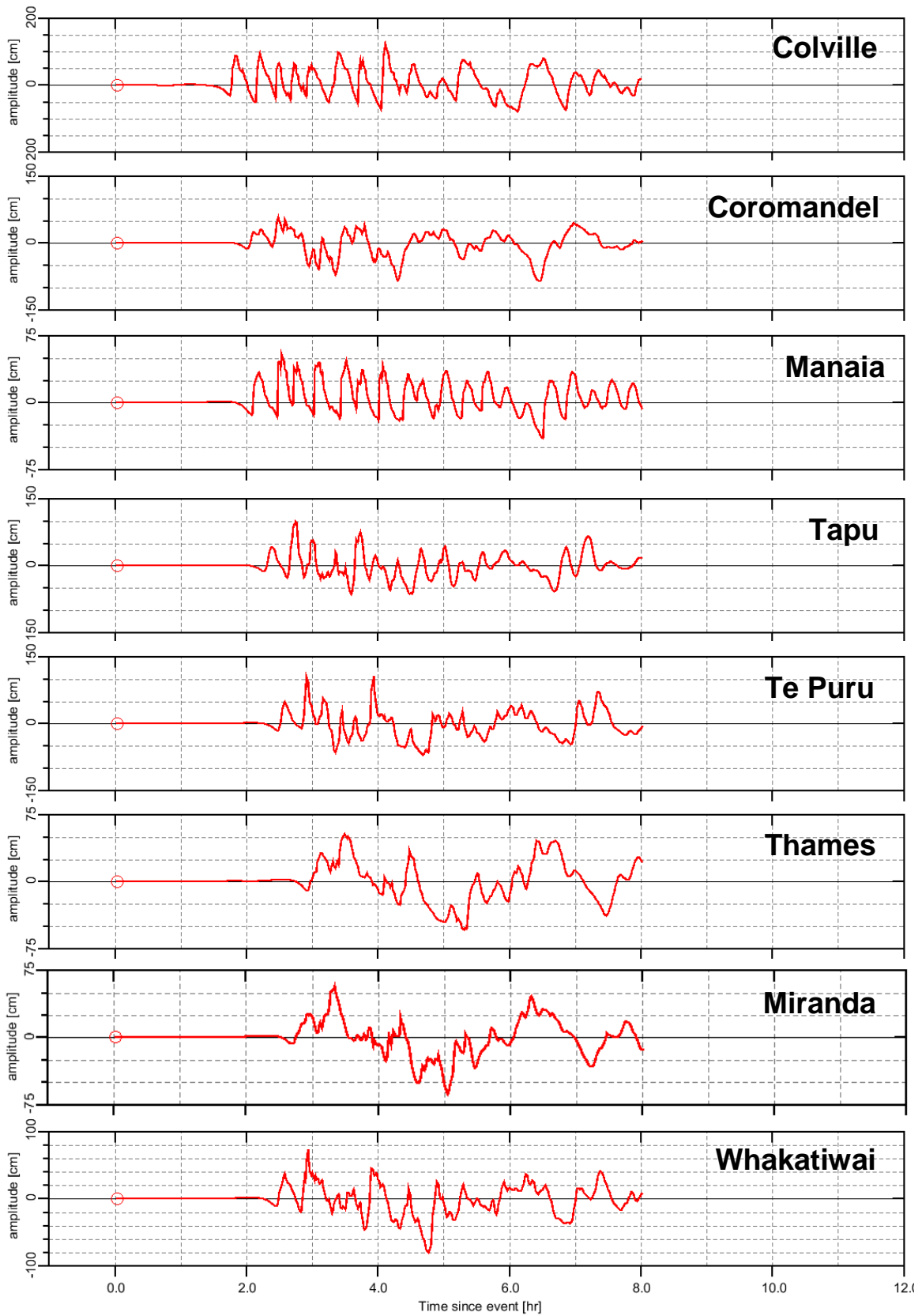


Figure 10.2 Water level time series plots for the TK 8 at MHWS sources affecting the 8 study sites.

11 APPENDIX 3 – TIME SERIES FOR DISTANT SOURCE SCENARIOS

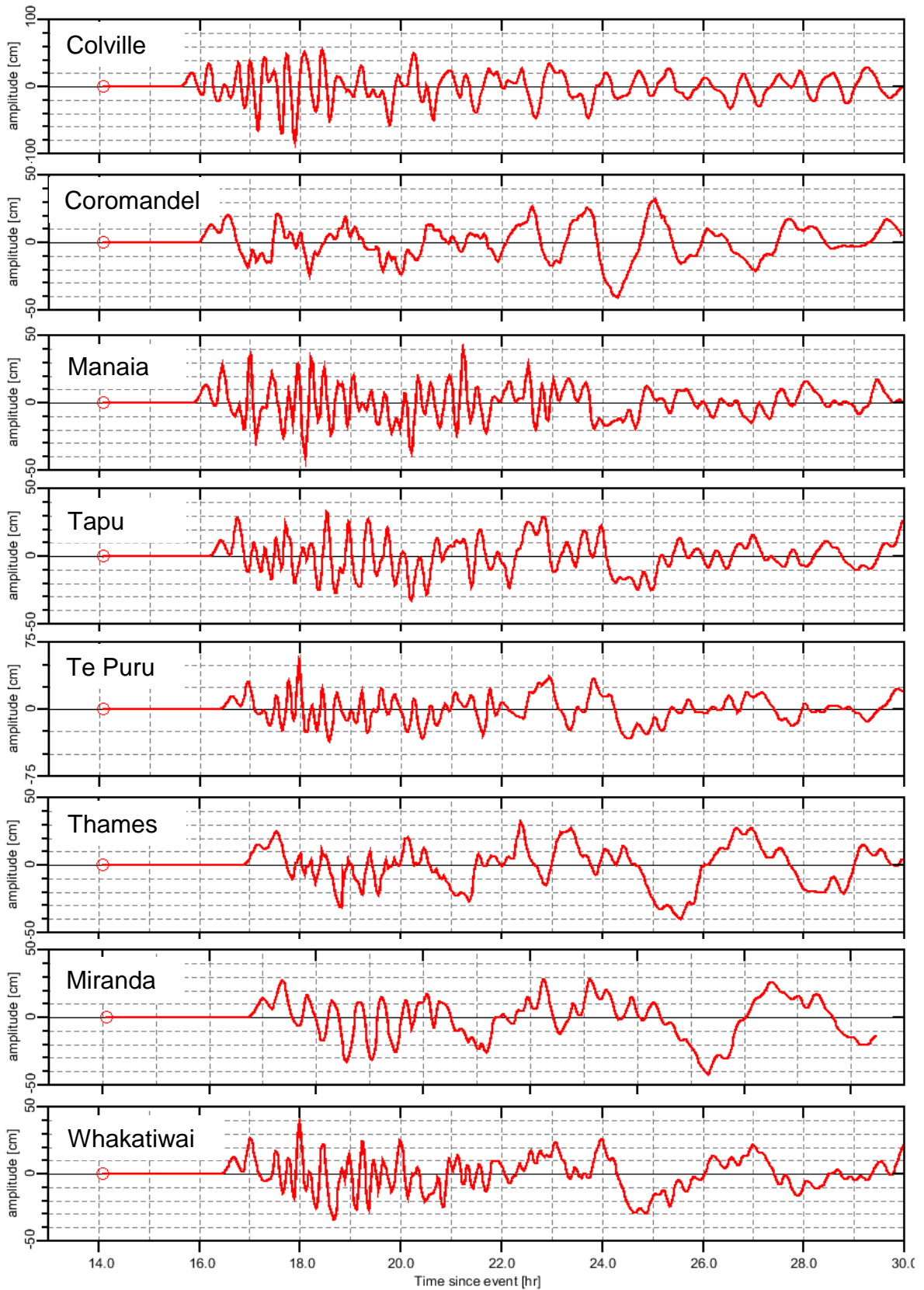


Figure 11.1 FF7 MHWS

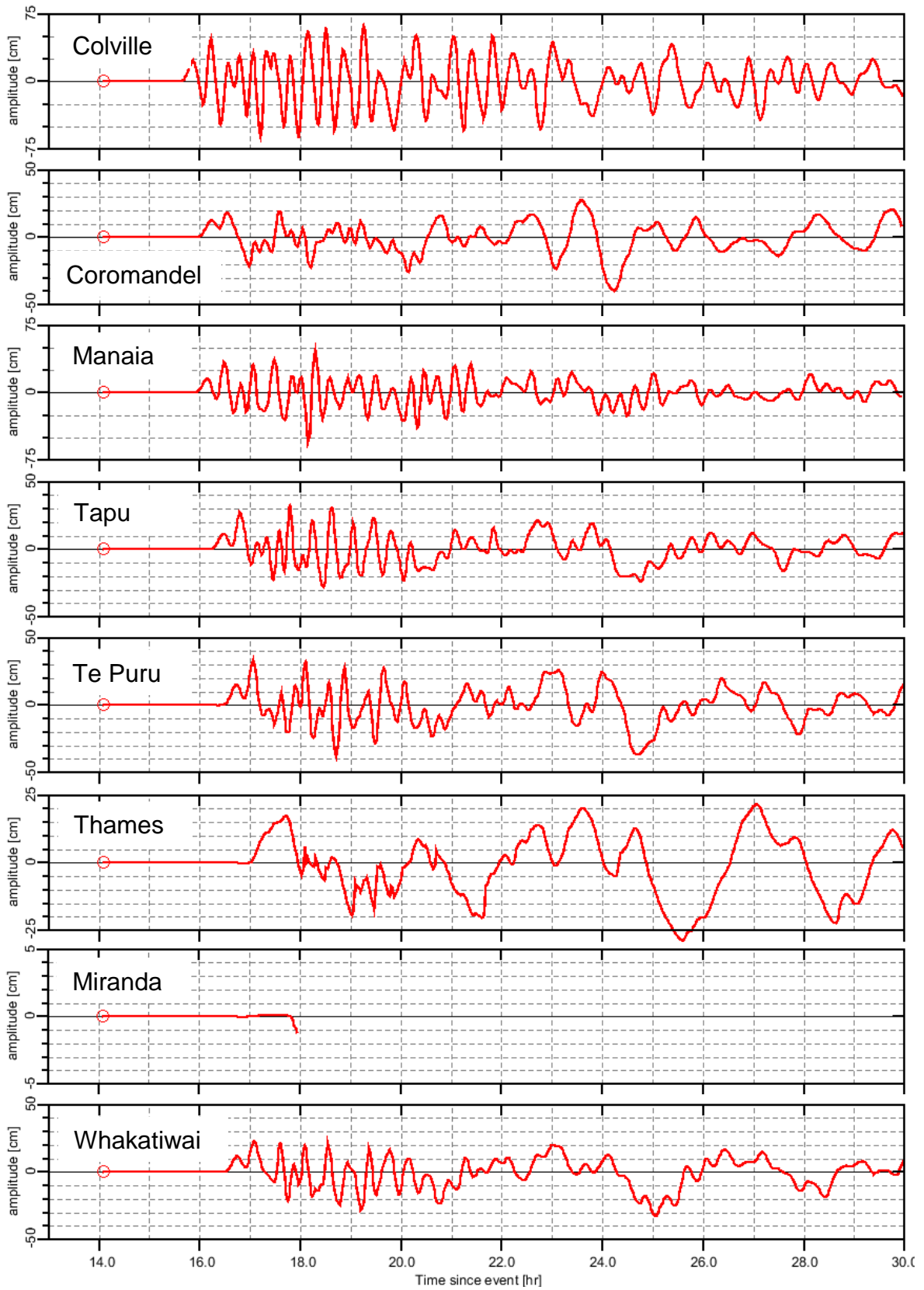


Figure 11.2 FF7 MSL

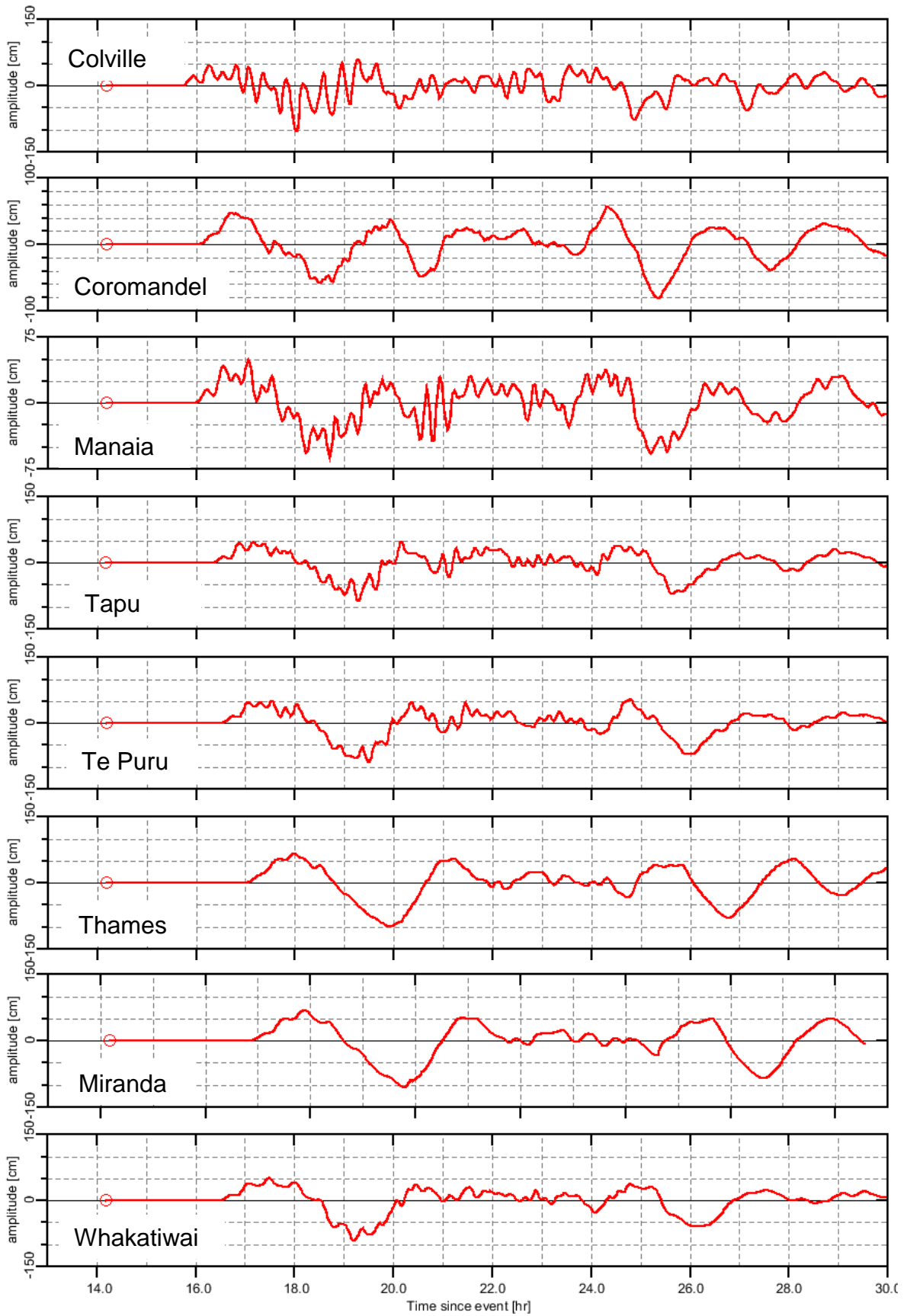


Figure 11.3 FF 1868 MHWS

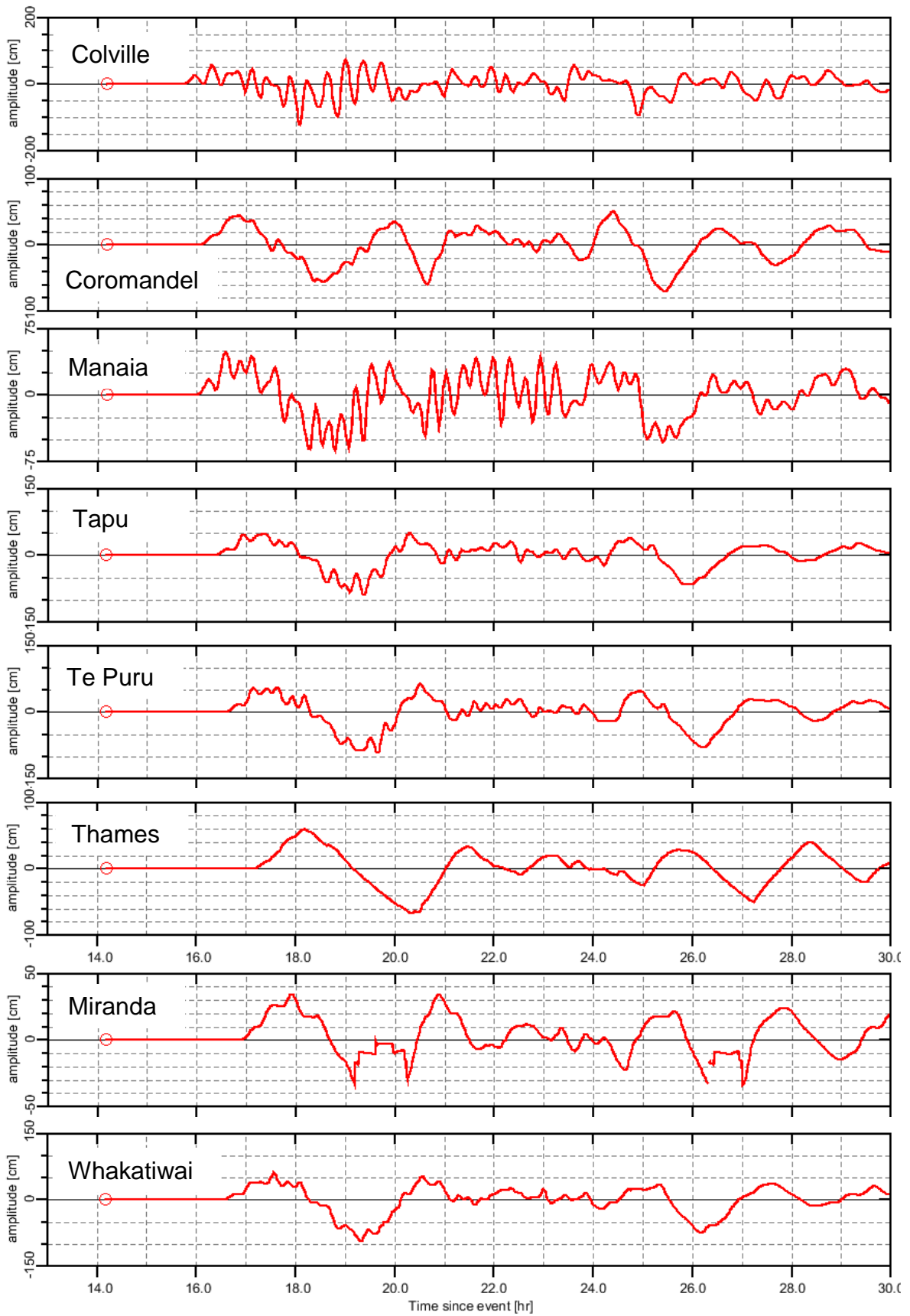


Figure 11.4 FF 1868 MSL

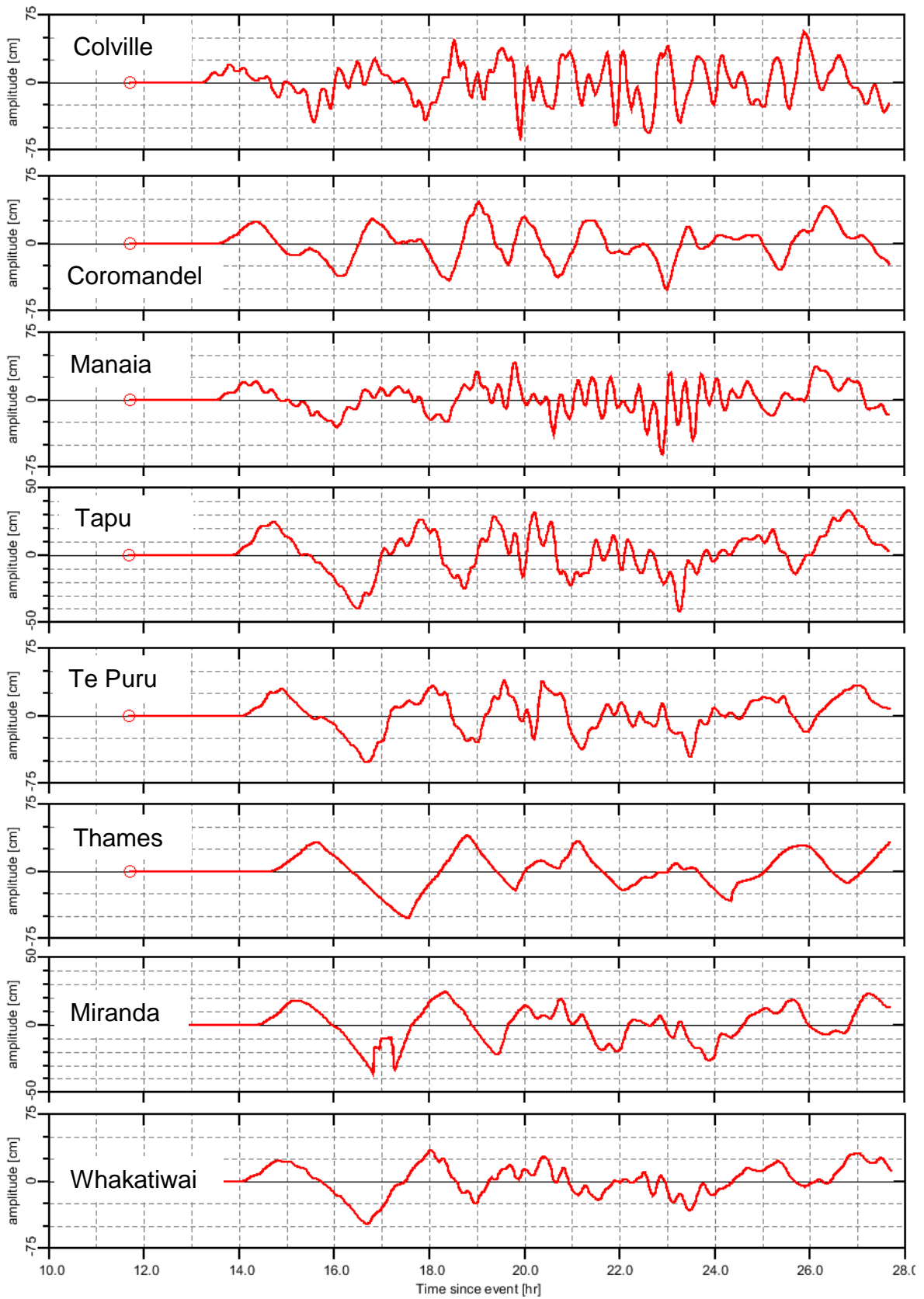
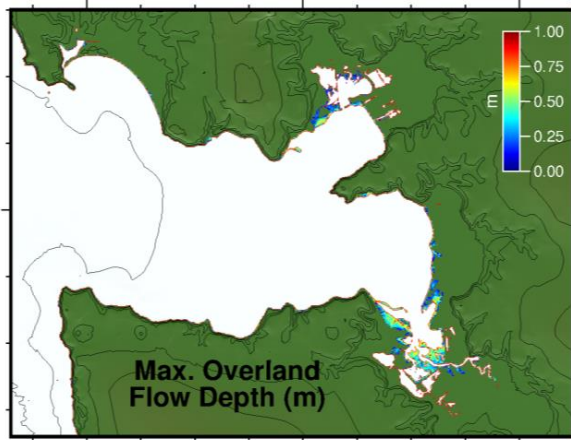
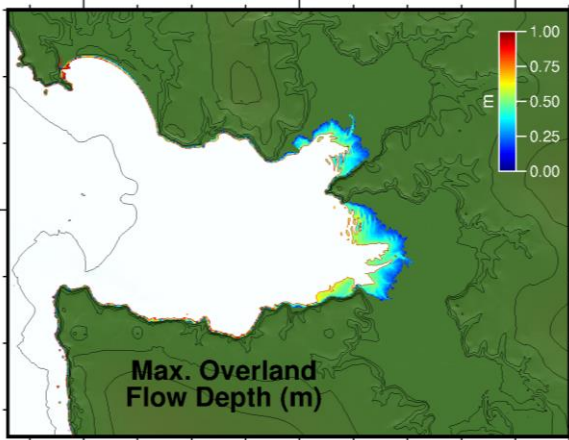
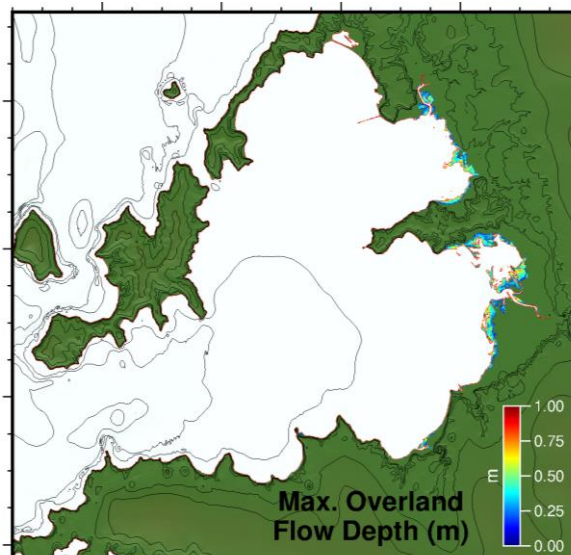
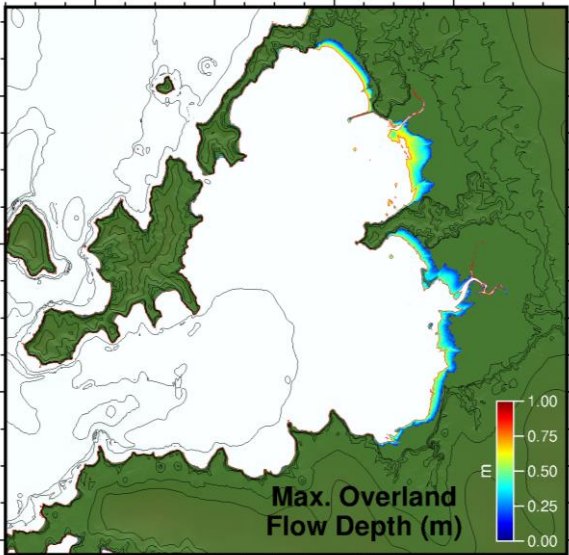


Figure 11.5 FF 1960 MSL

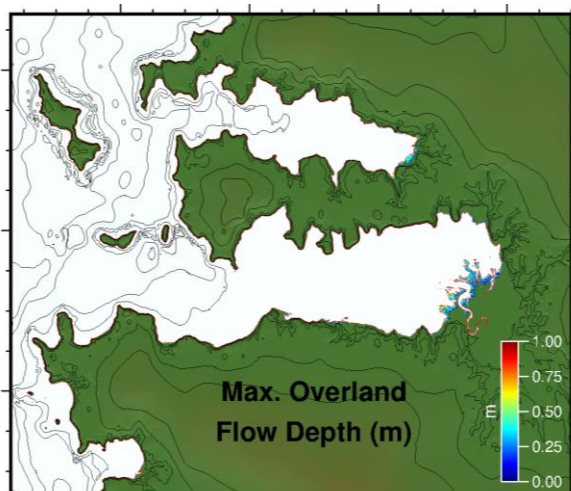
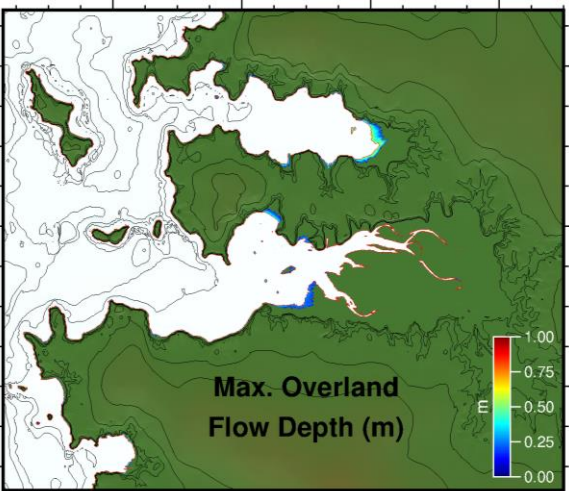
12 APPENDIX 4 – INUNDATION PLOTS FOR DISTANT SOURCE SCENARIOS



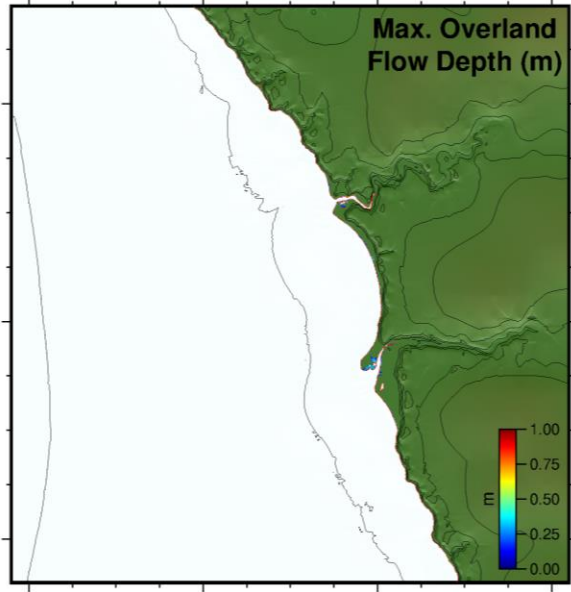
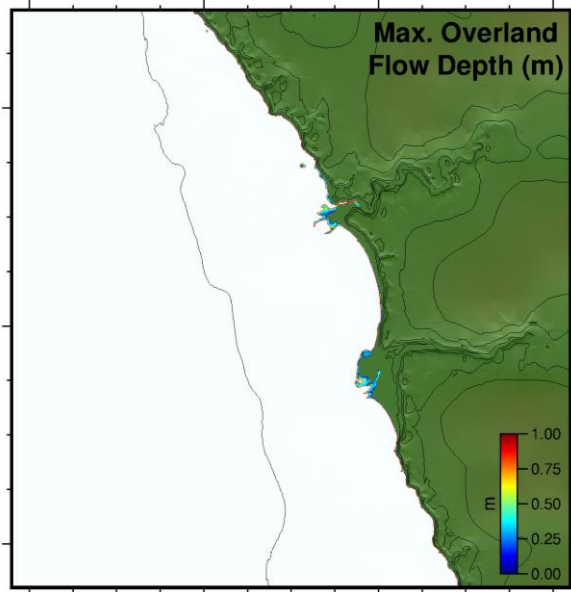
Colville



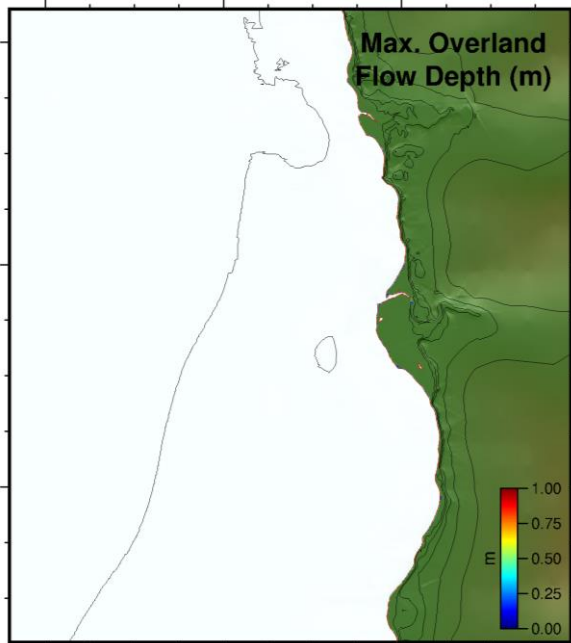
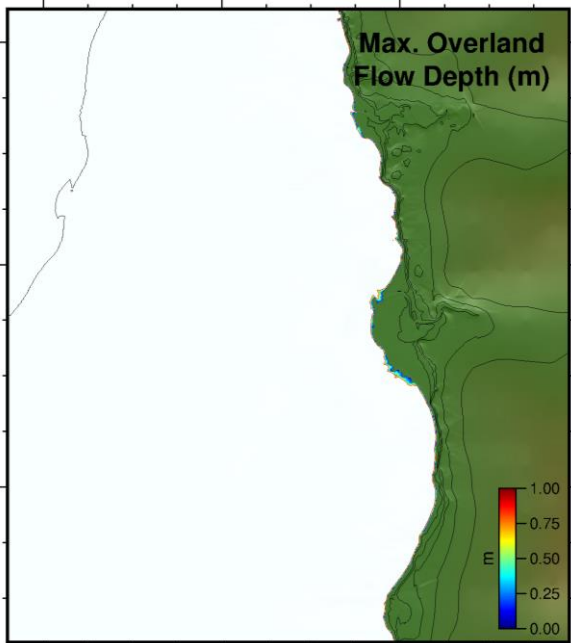
Coromandel



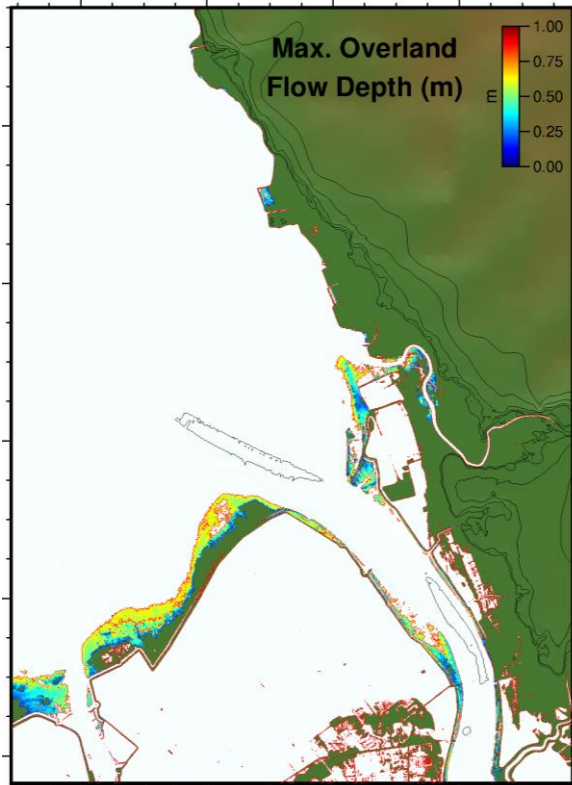
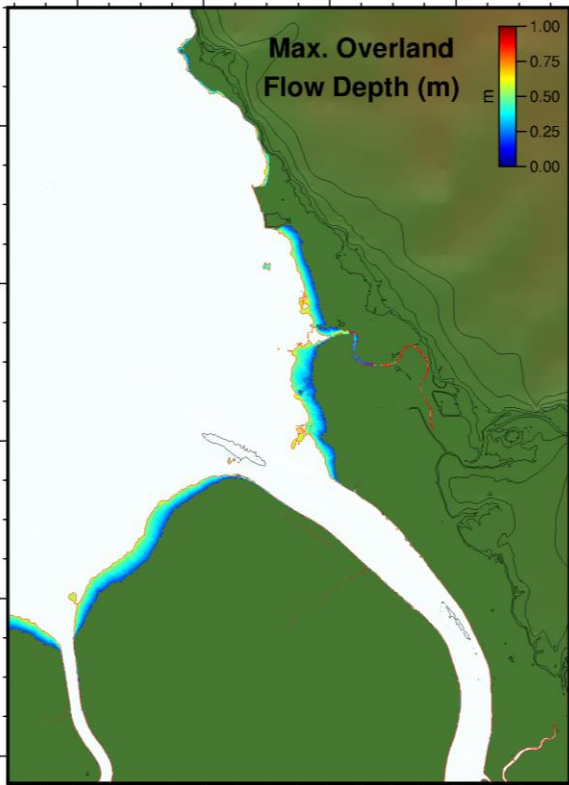
Manaia



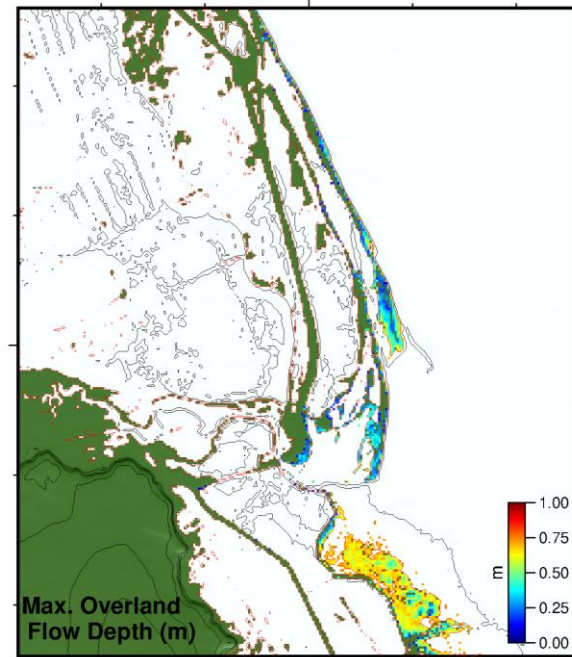
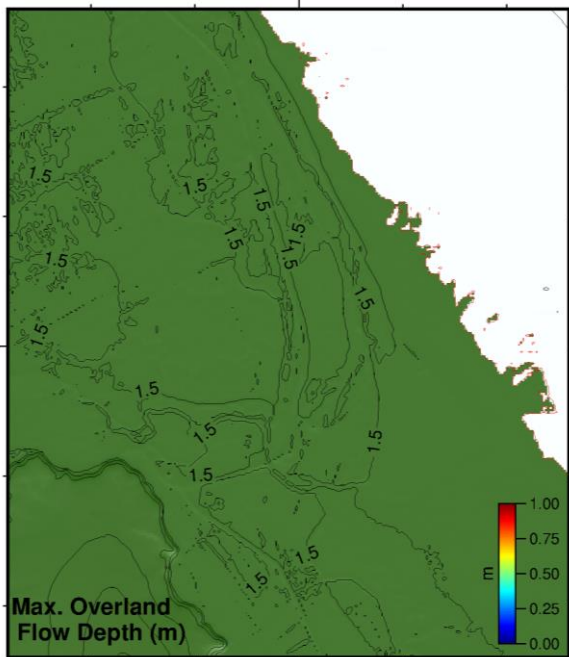
Tapu



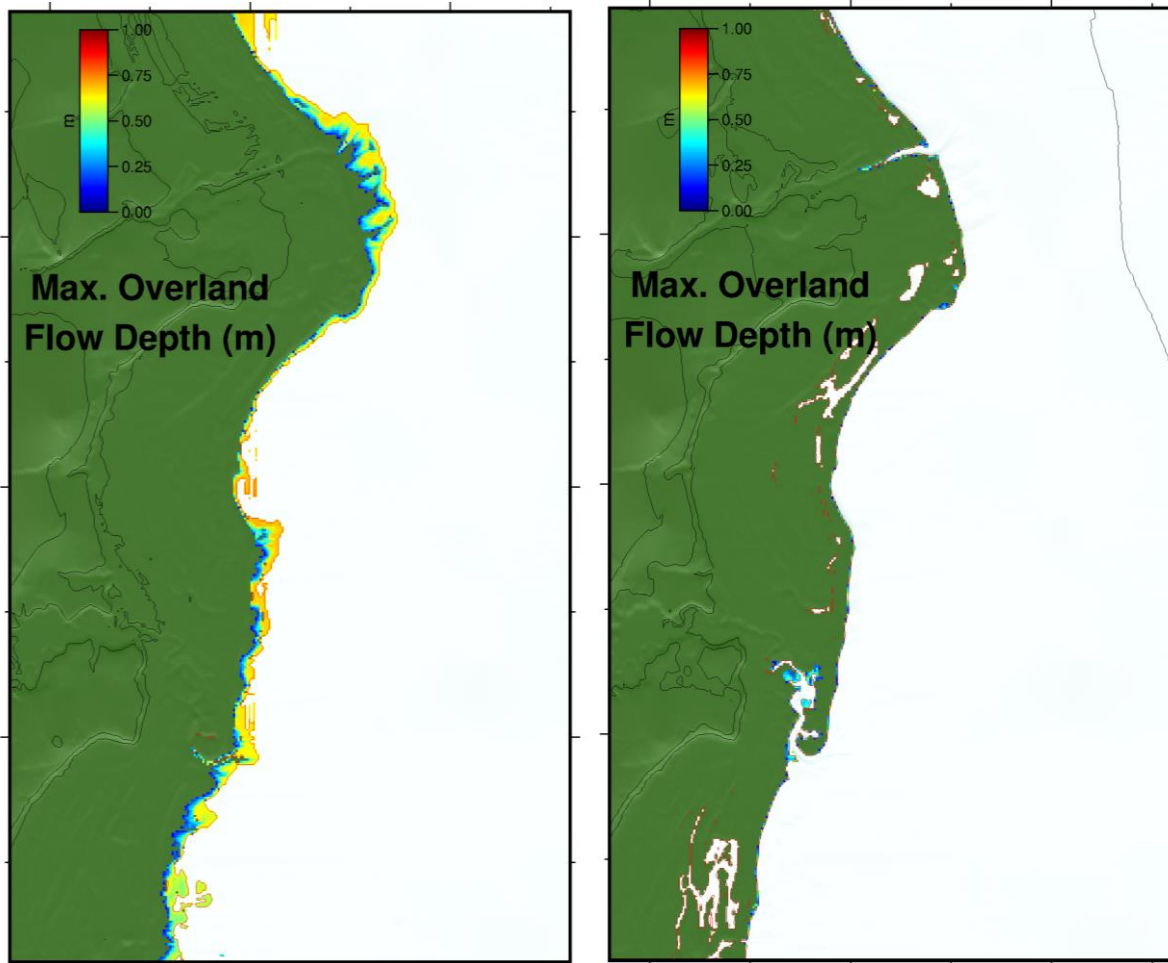
Te Puru



Thames

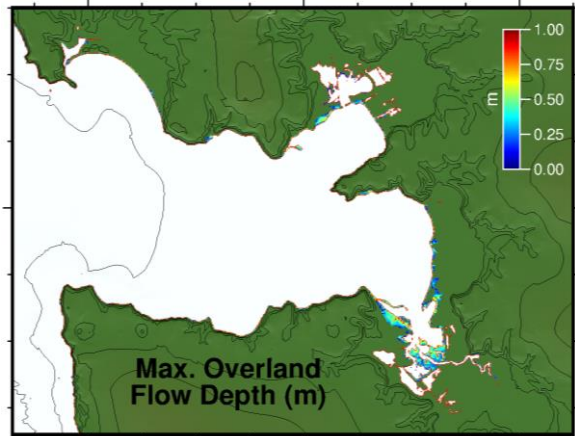
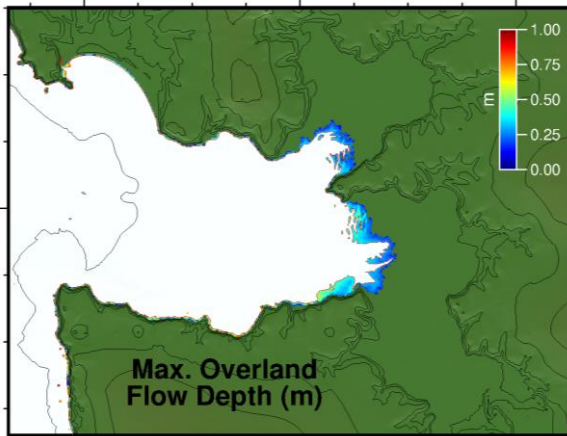


Miranda

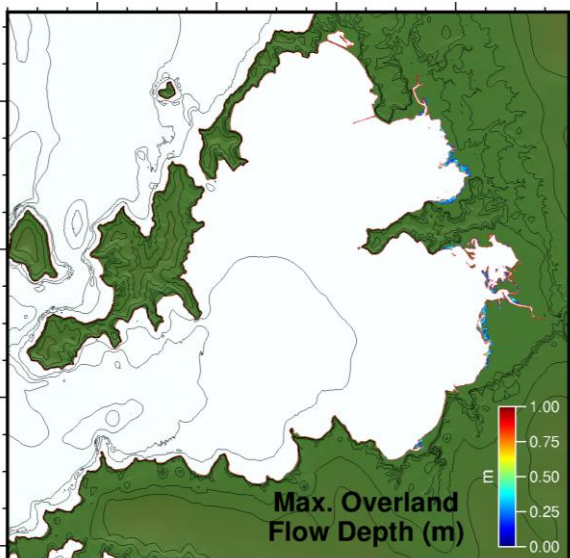
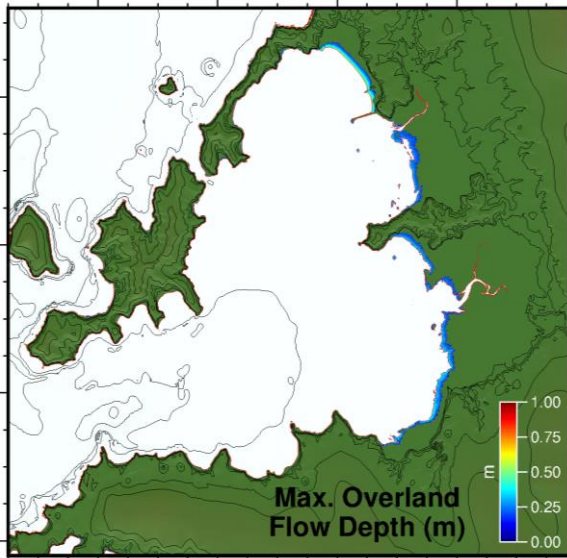


Whakatiwai

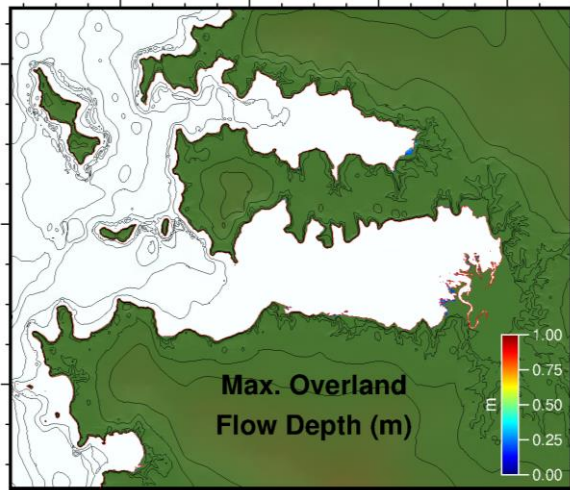
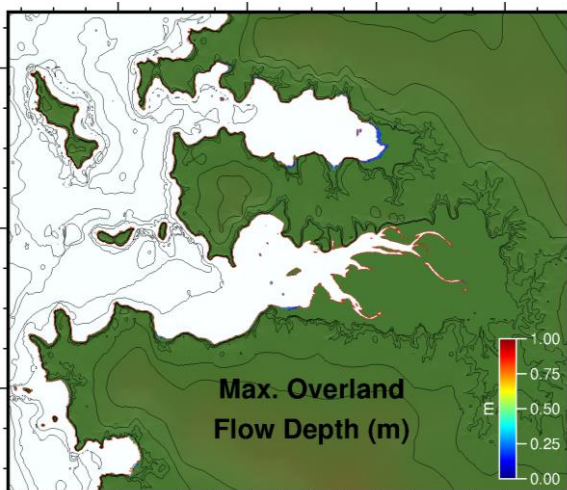
Figure 12.1 Inundation extents for the 1868 scenario at MSL (left column) and MHWS (right column).



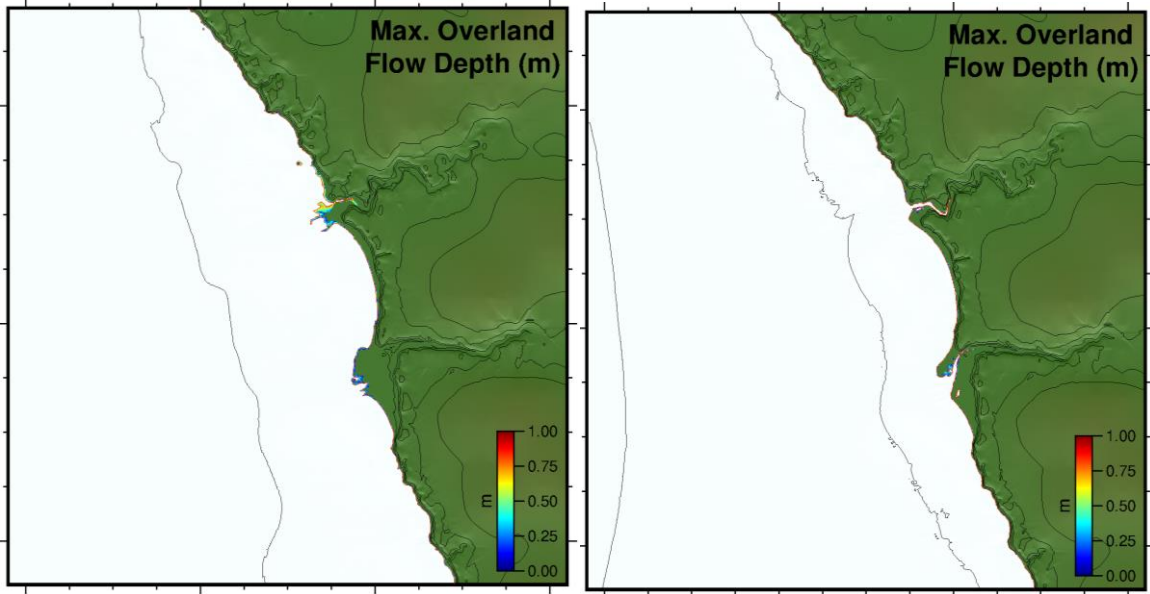
Colville



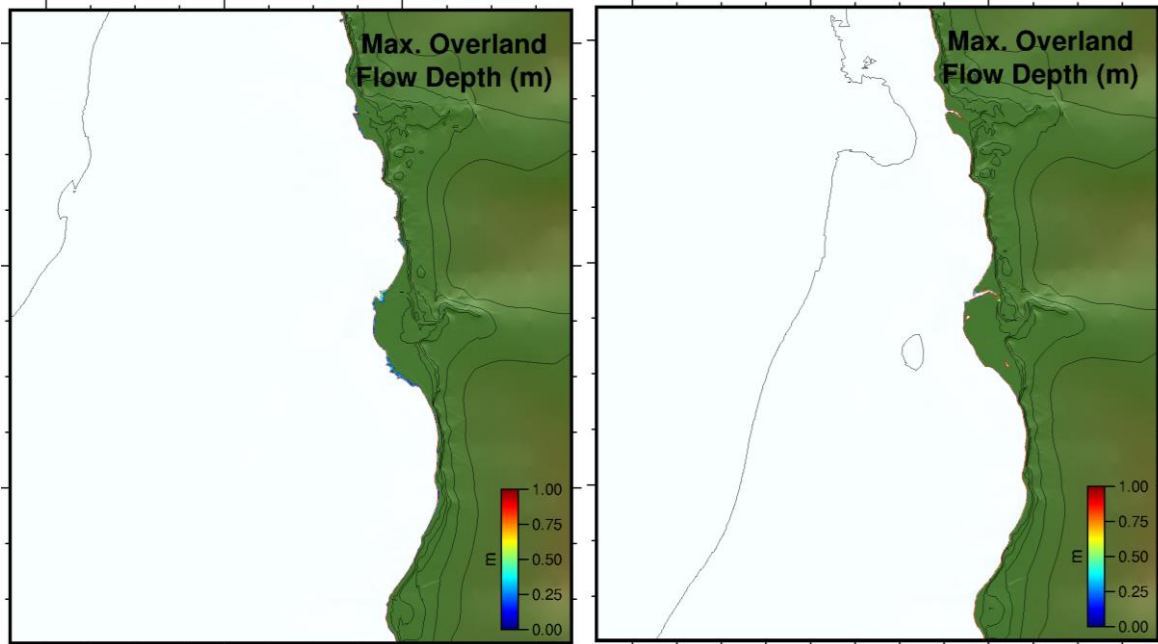
Coromandel



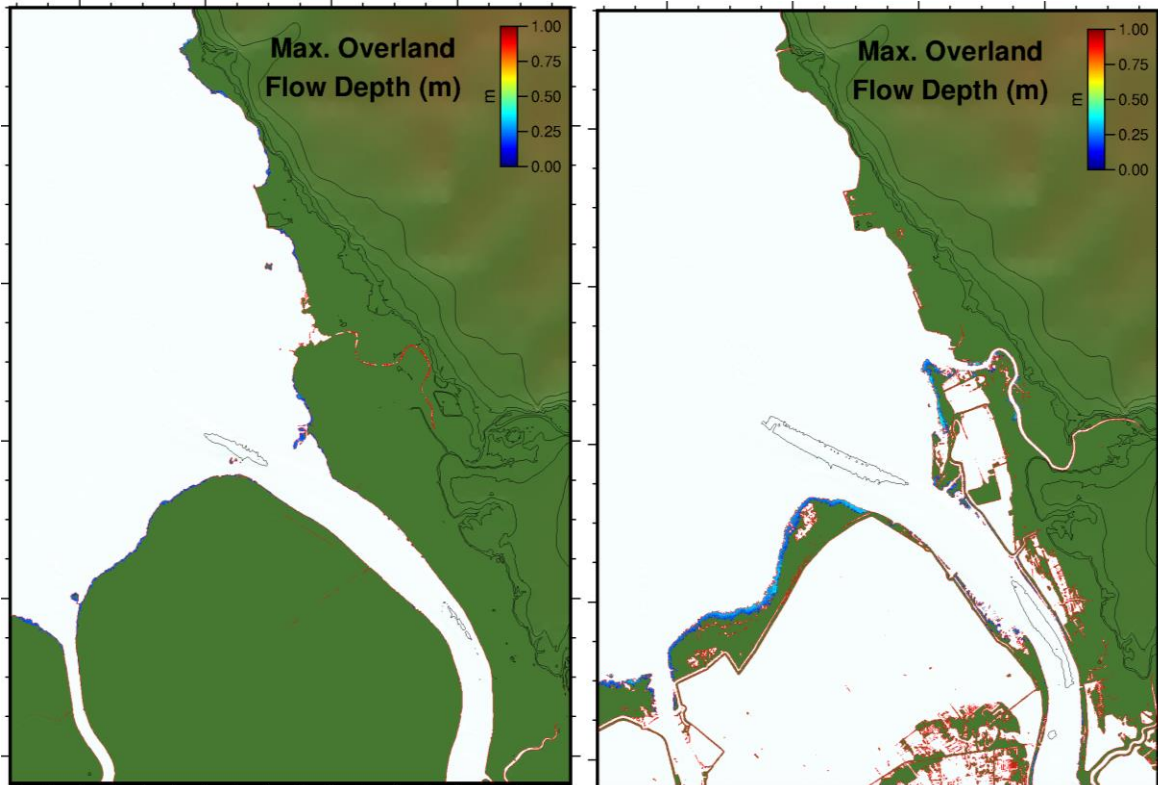
Manaia



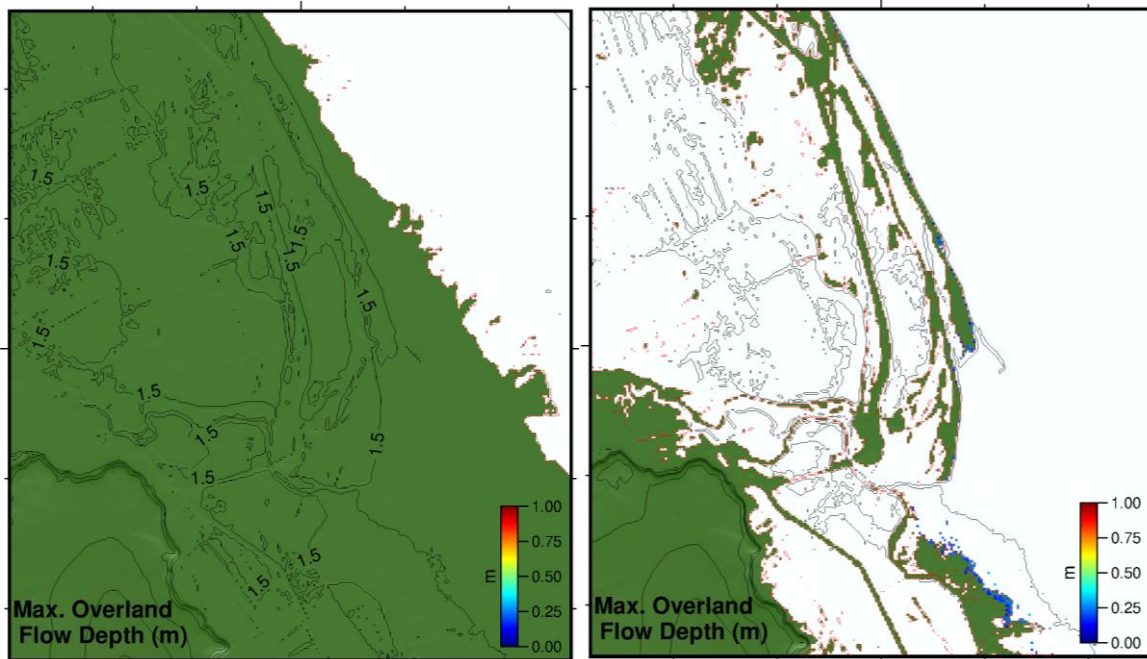
Tapu



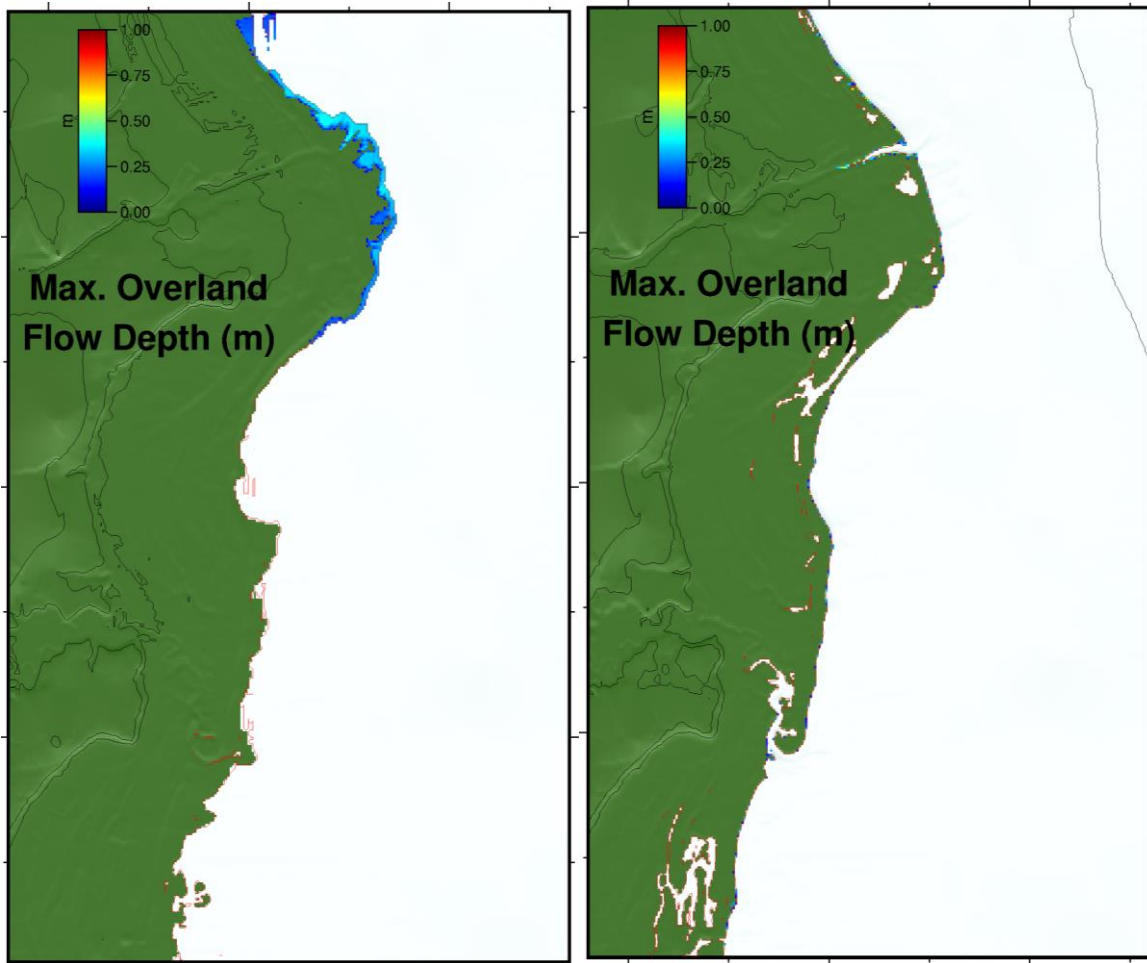
Te Puru



Thames

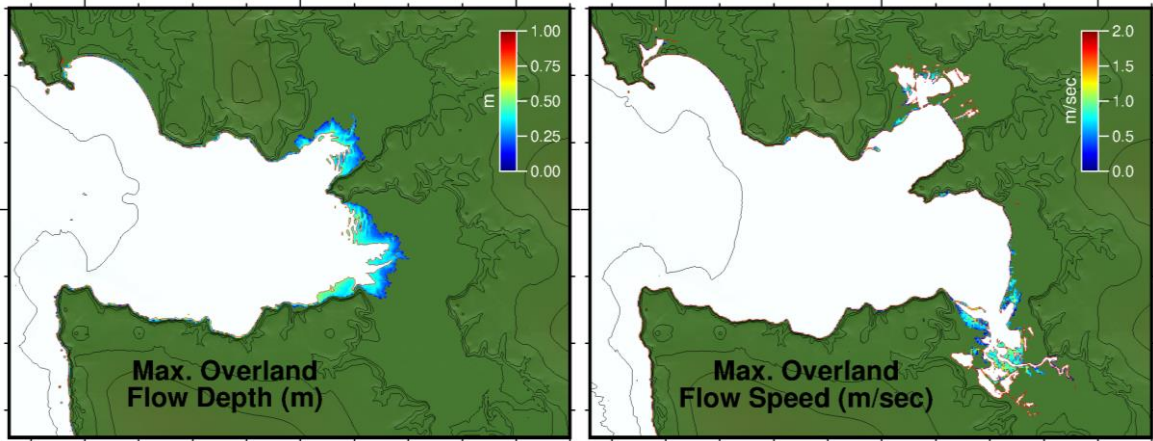


Miranda

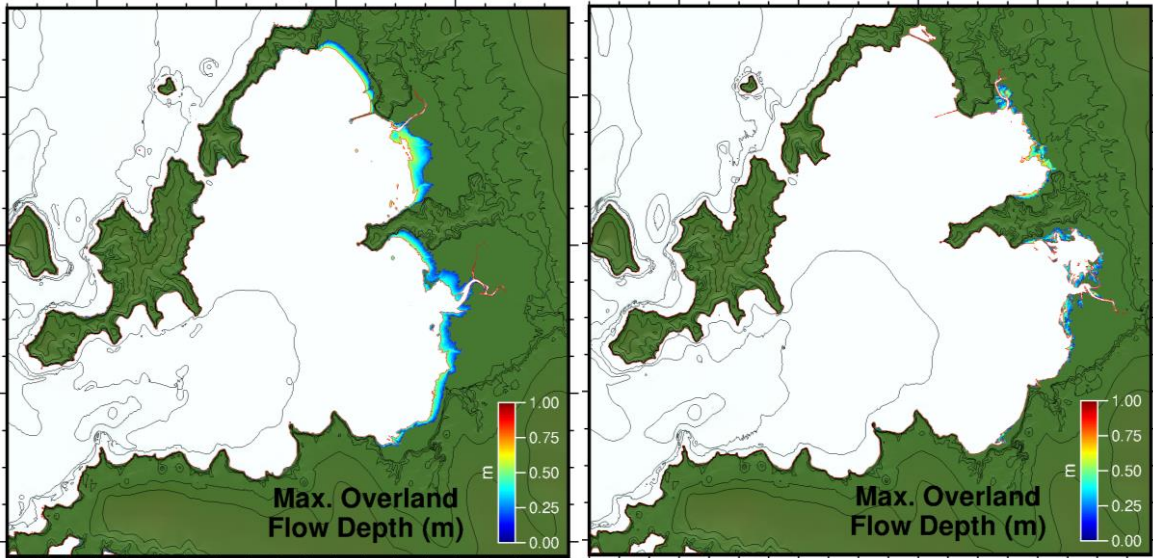


Whakatiwai

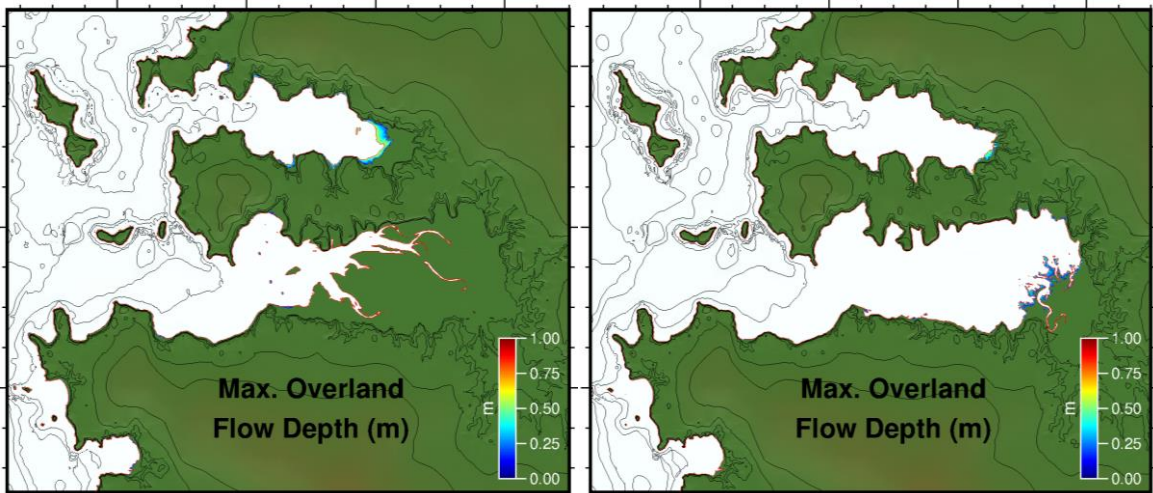
Figure 12.2 Inundation extents for the FF 7 scenario at MSL (left column) and MHWS (right column).



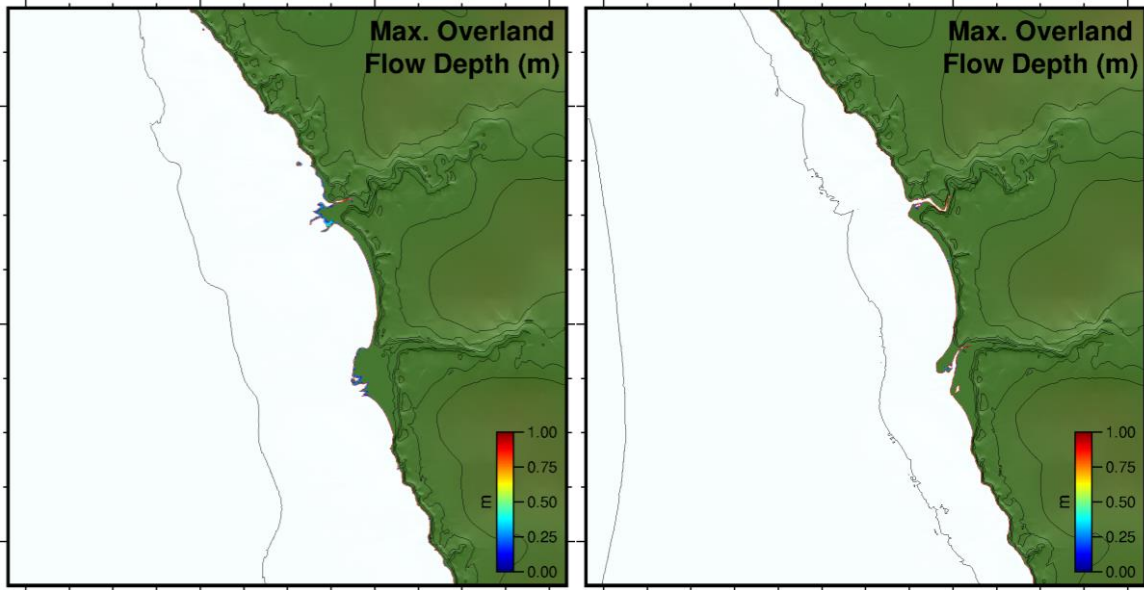
Colville



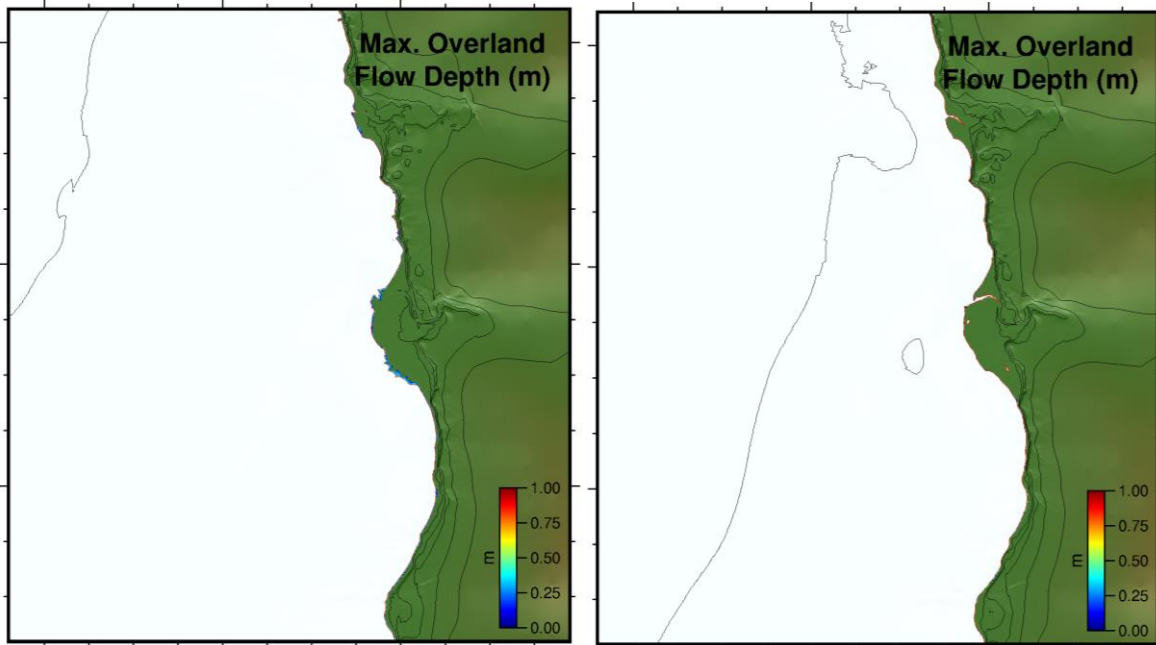
Coromandel



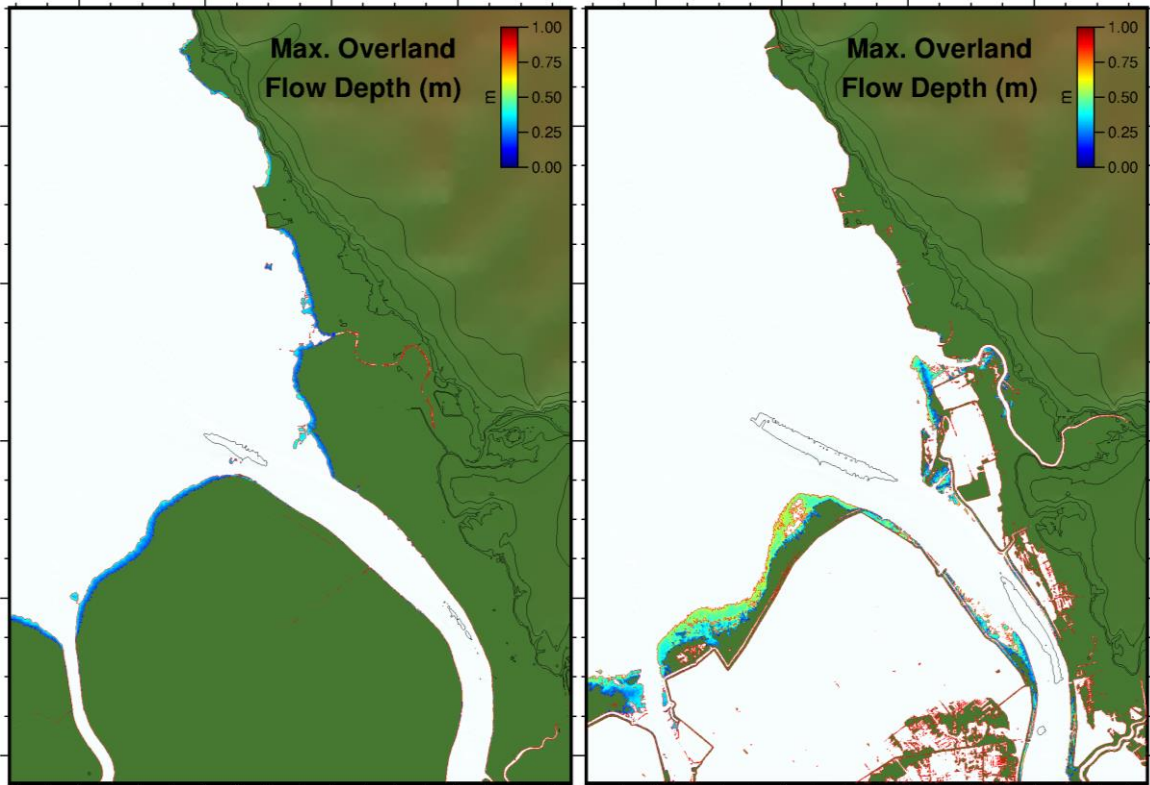
Manaia



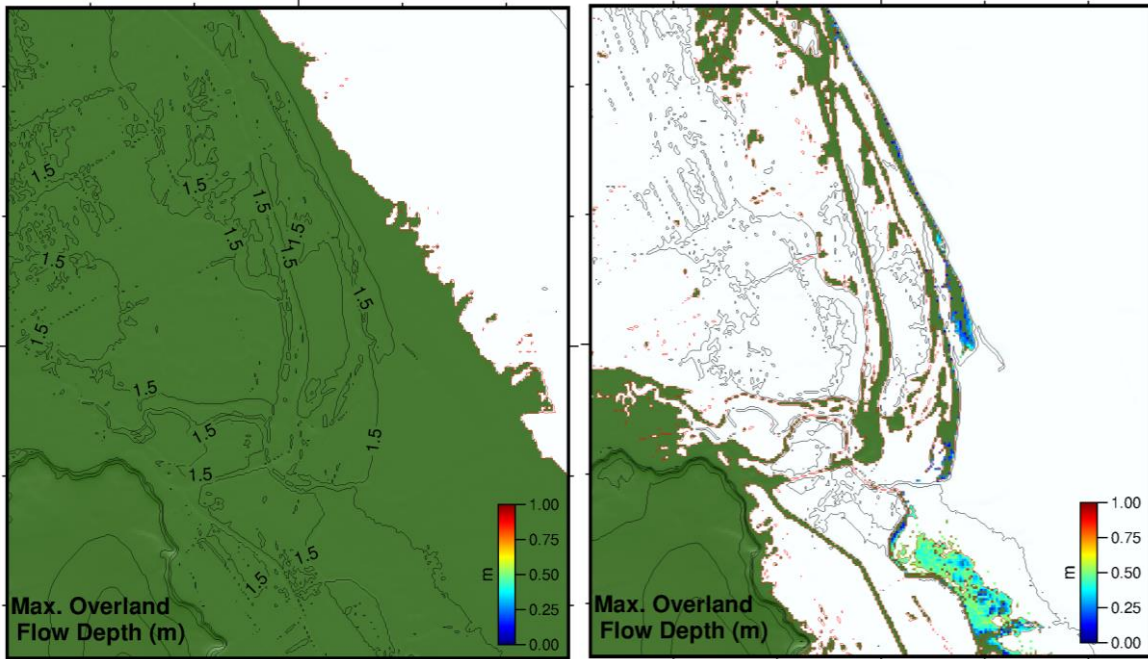
Tapu



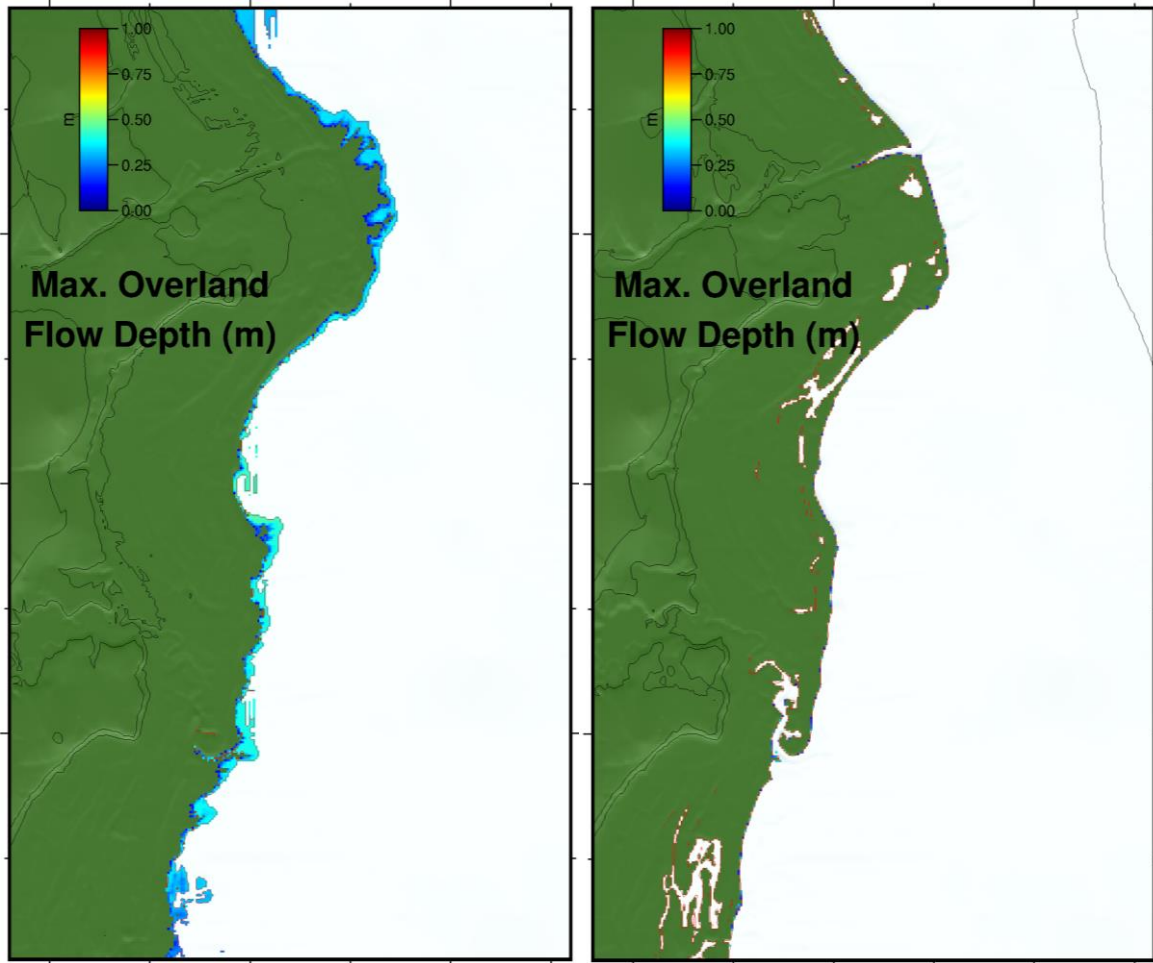
Te Puru



Thames



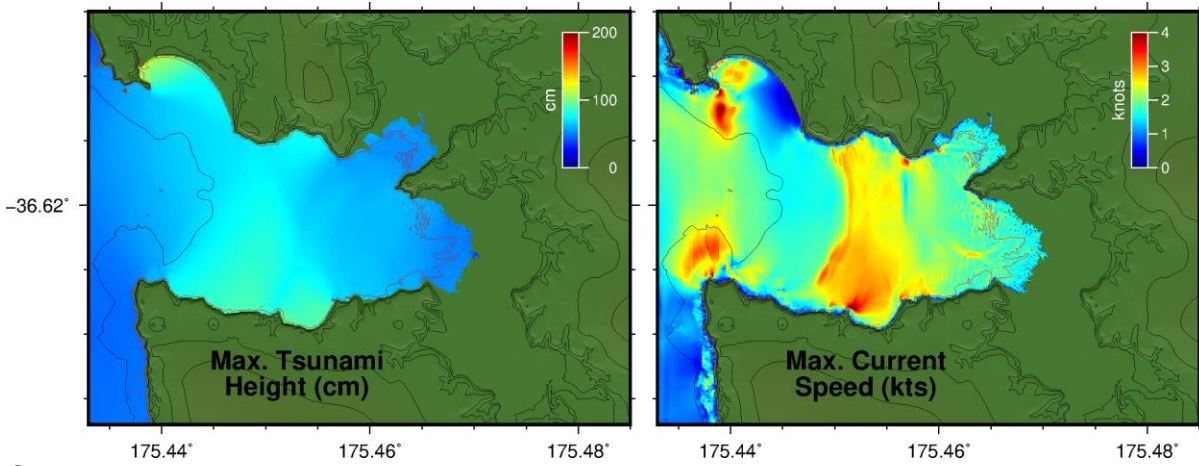
Miranda



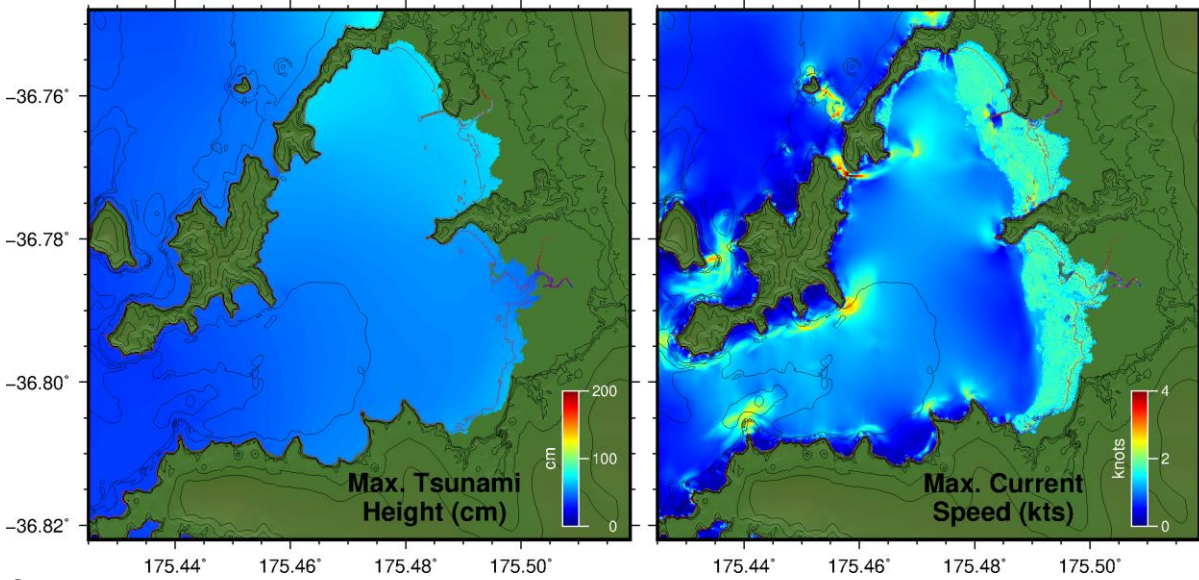
Whakatiwai

Figure 12.3 Inundation extents for the 1960 scenario at MSL (left column) and MHWS (right column).

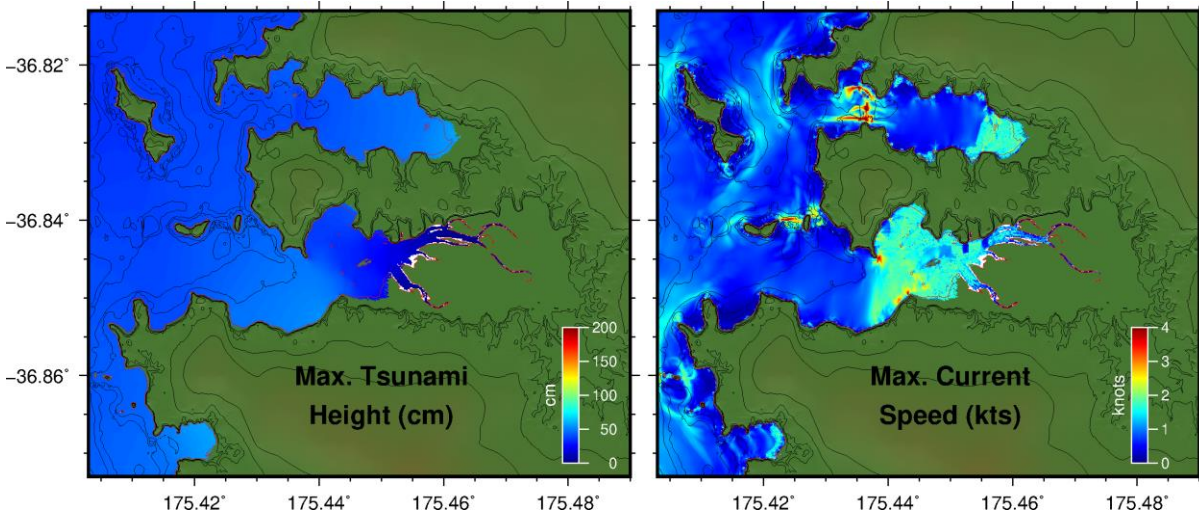
13 APPENDIX 5 – MAX TSUNAMI HEIGHT AND CURRENT SPEED FOR DISTANT SOURCE SCENARIOS



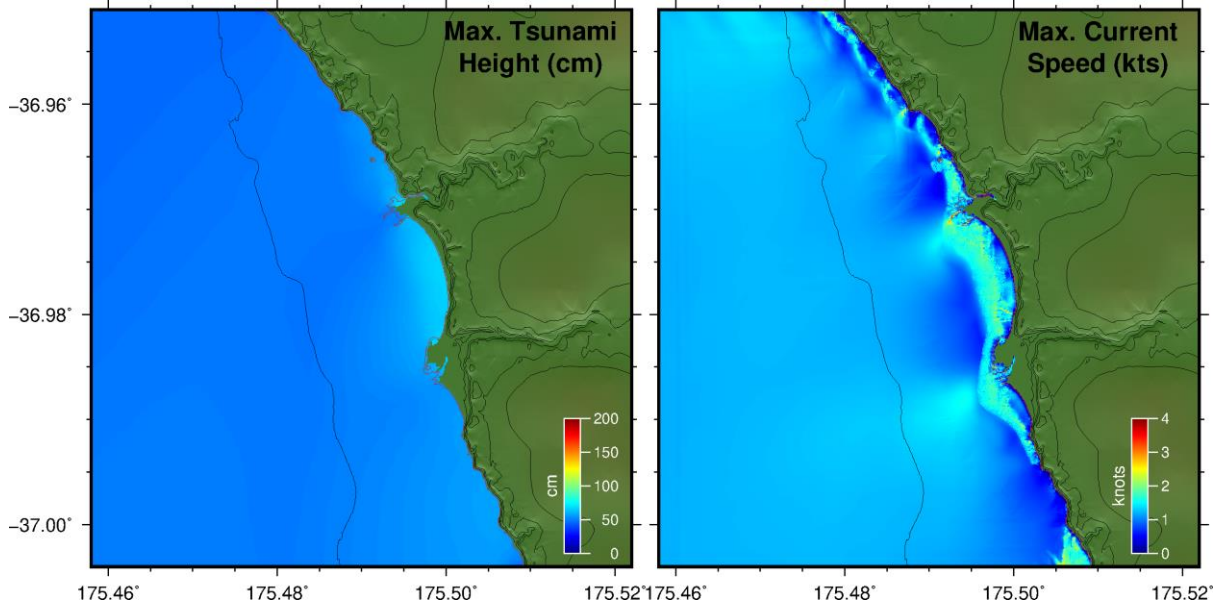
Colville



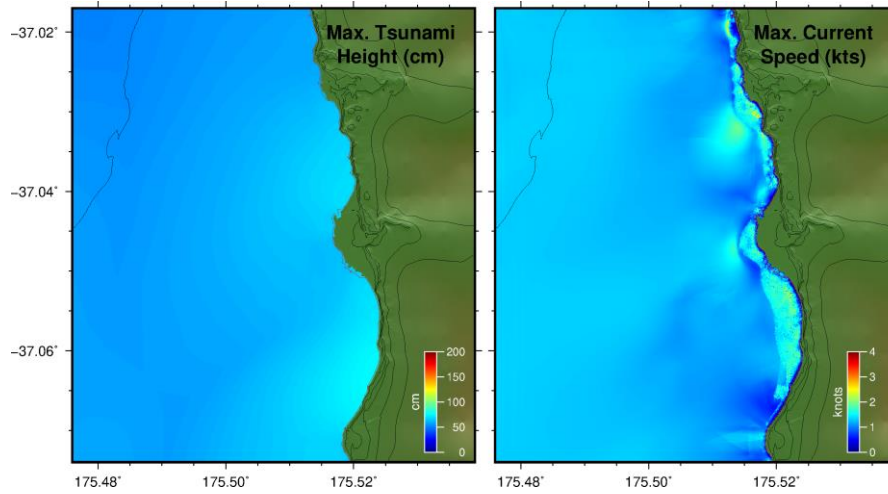
Coromandel



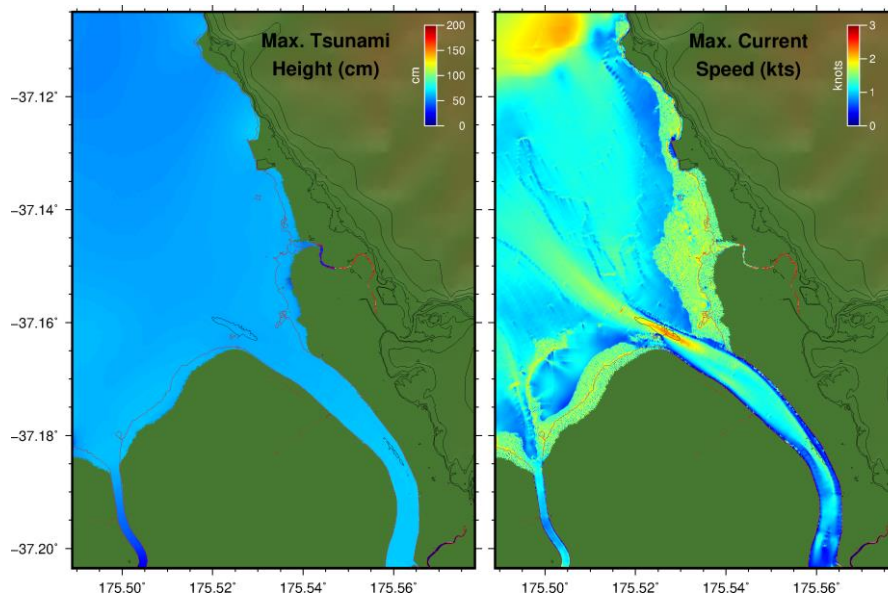
Manaia



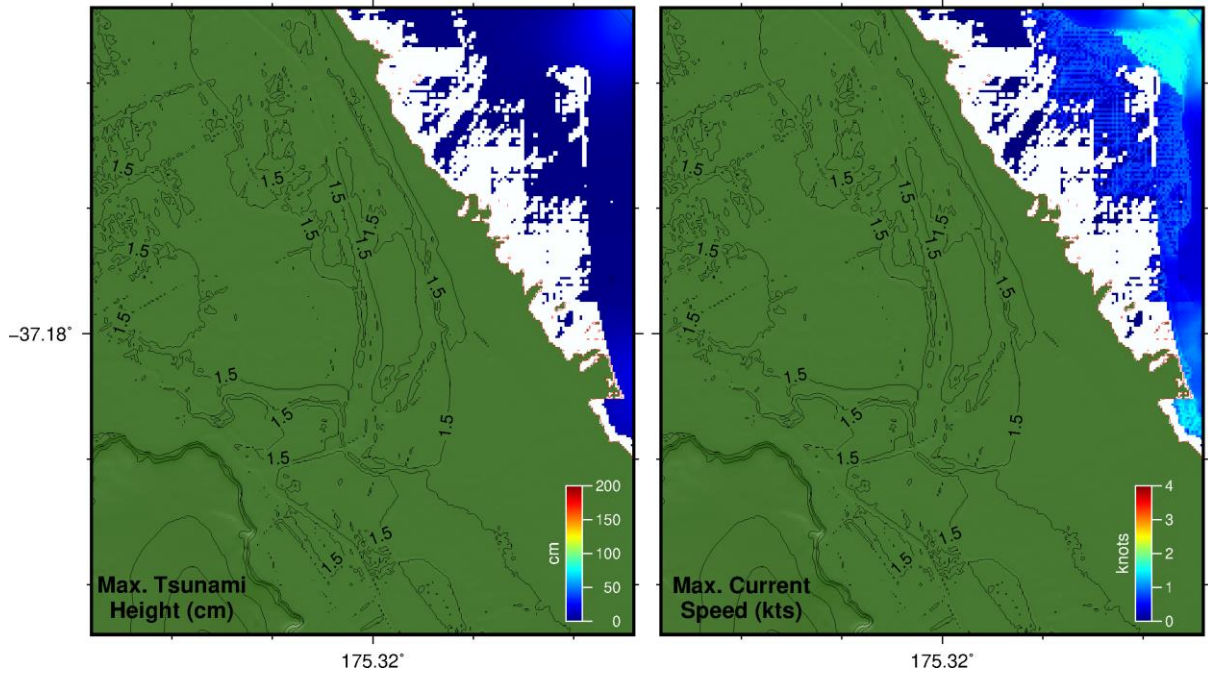
Tapu



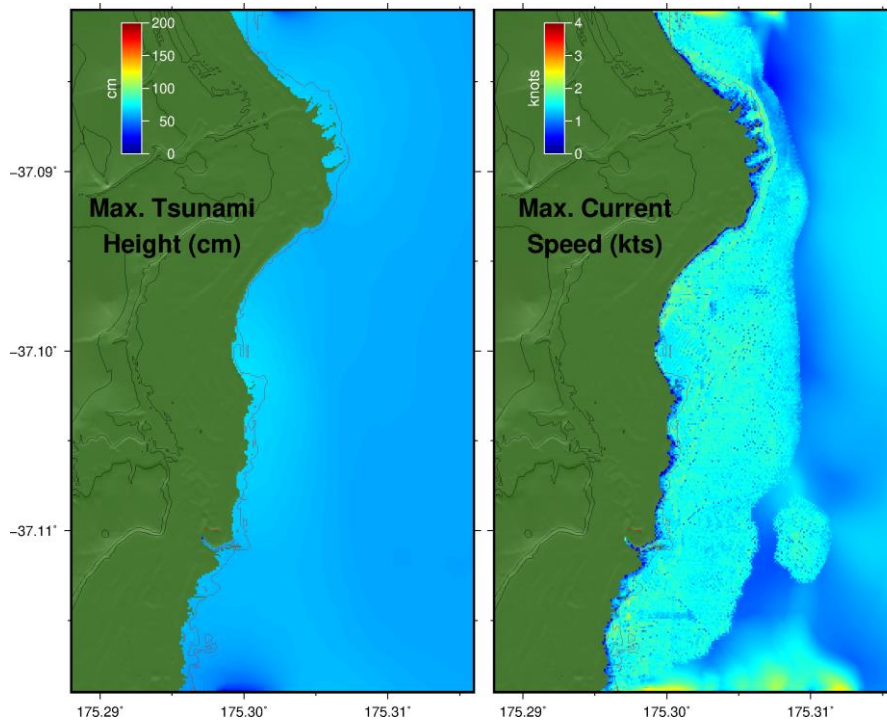
Te Puru



Thames

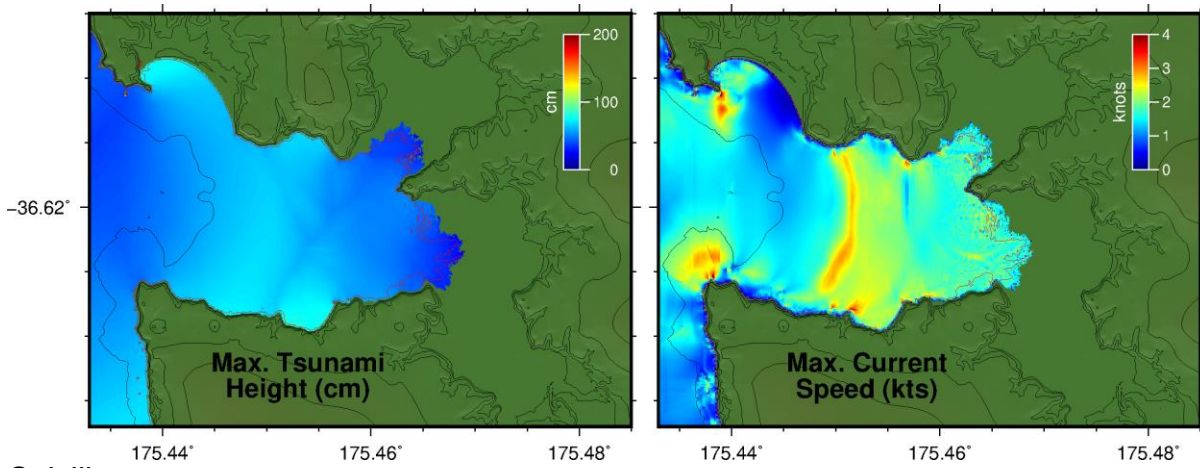


Miranda

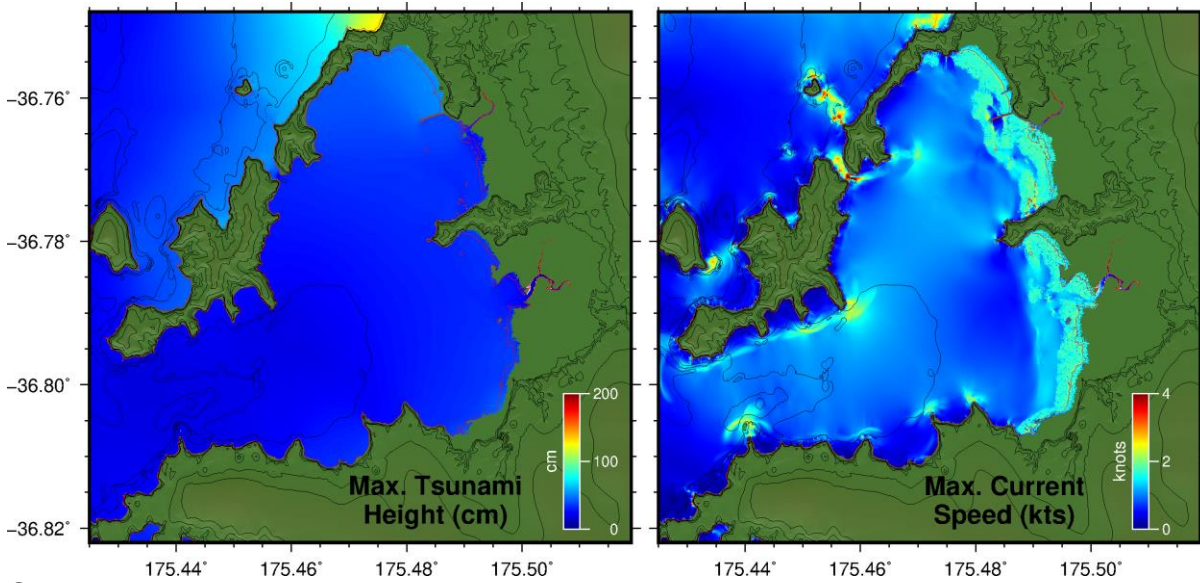


Whakatiwai

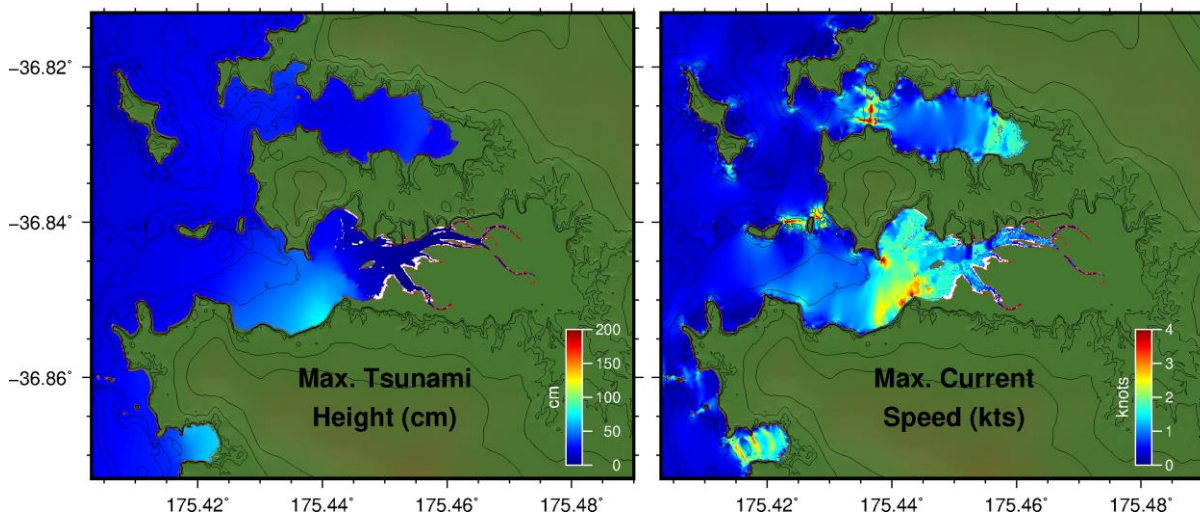
Figure 13.1 Maximum modelled tsunami heights and current speeds for the 1868 scenario at MSL.



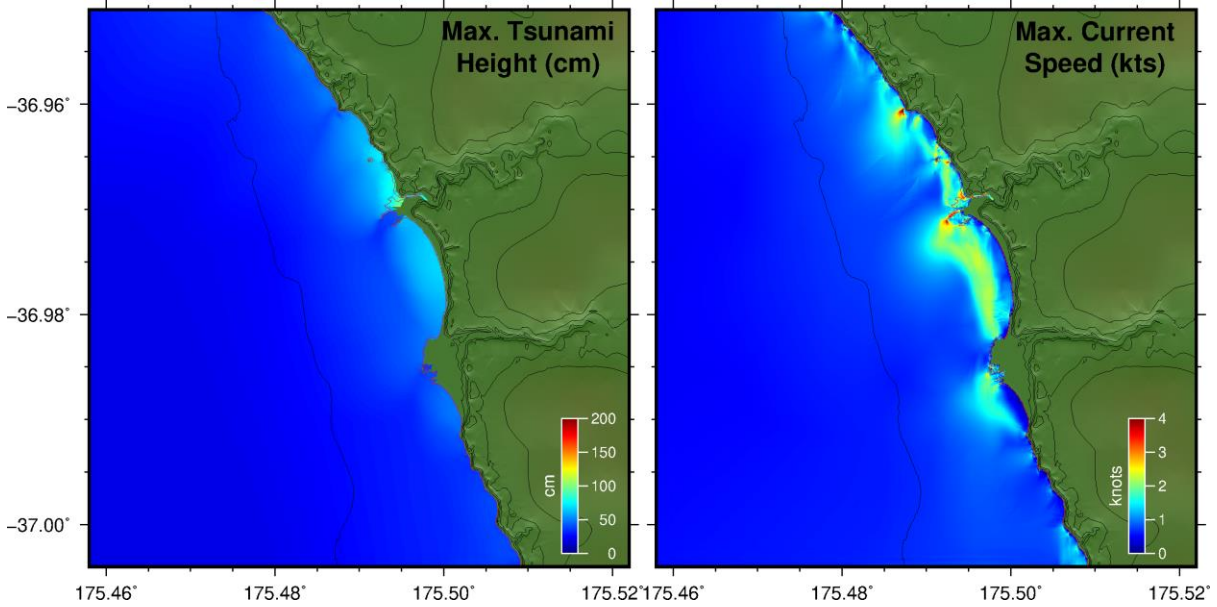
Colville



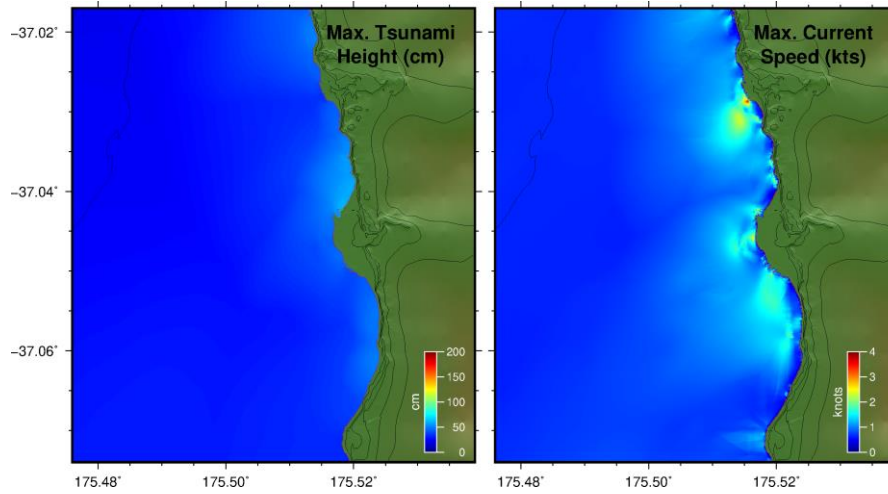
Coromandel



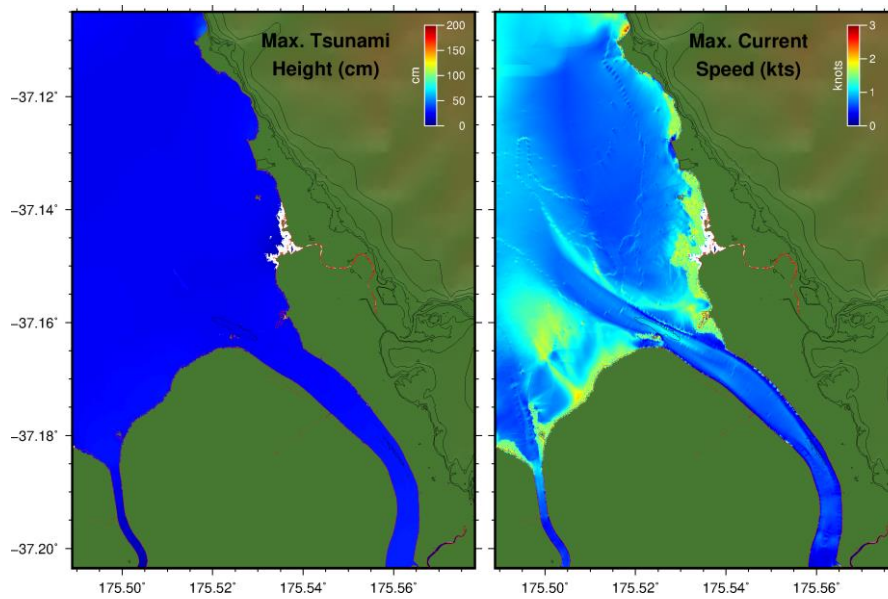
Manaia



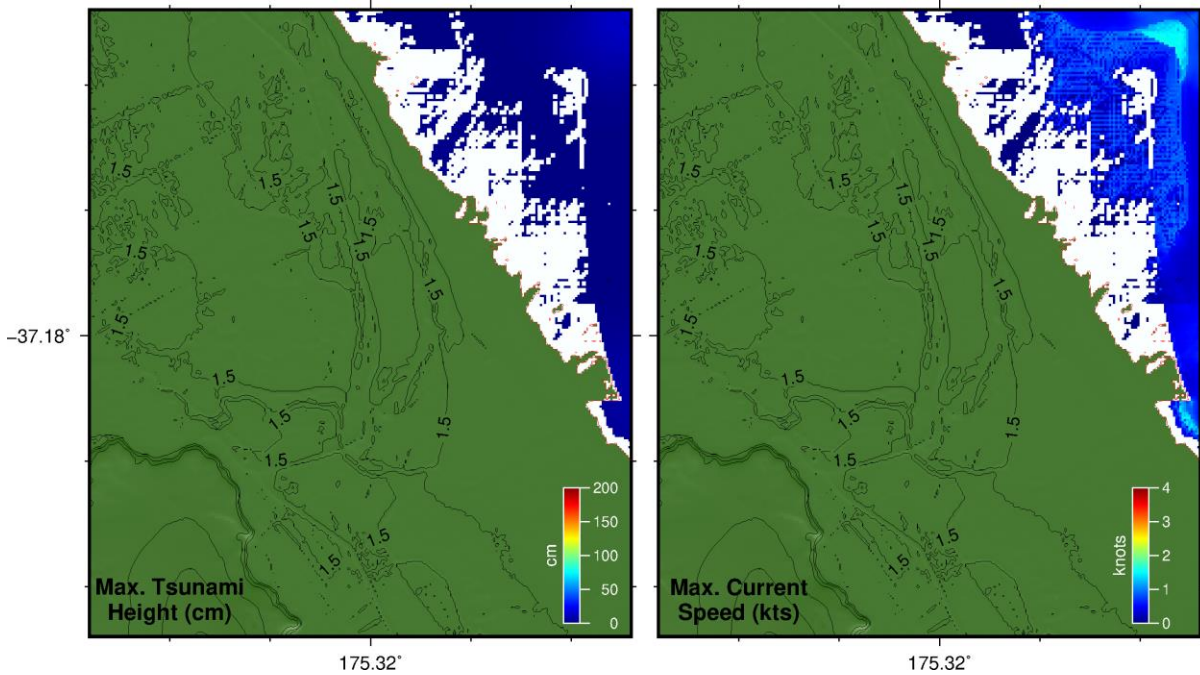
Tapu



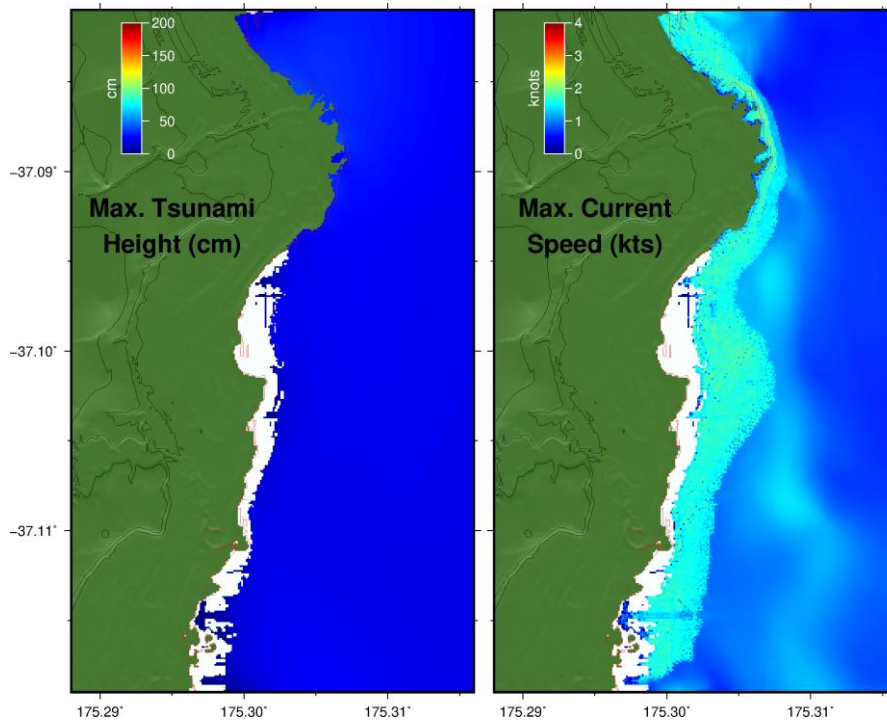
Te Puru



Thames

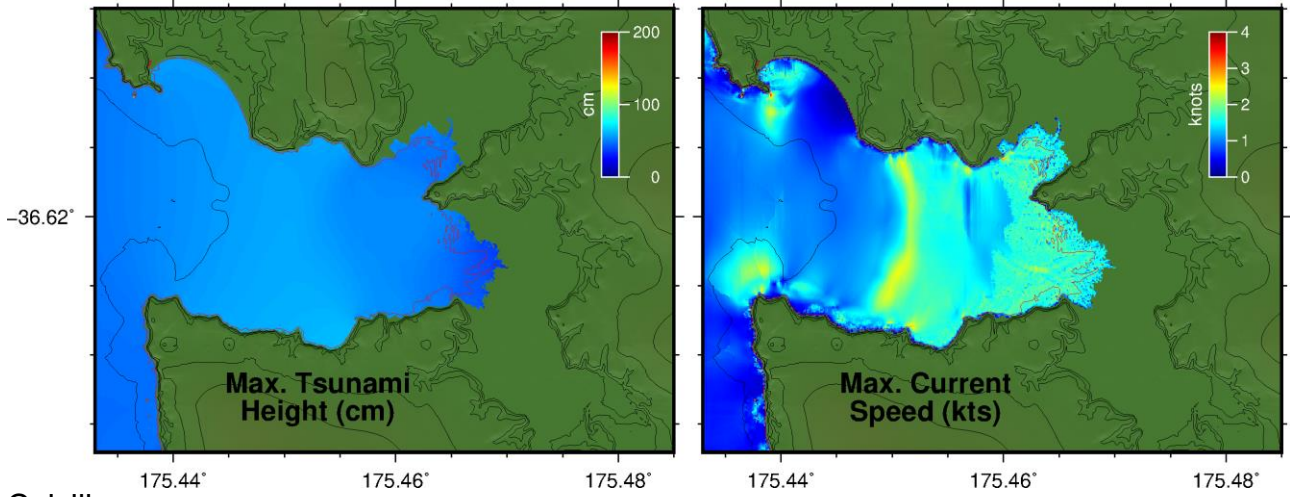


Miranda

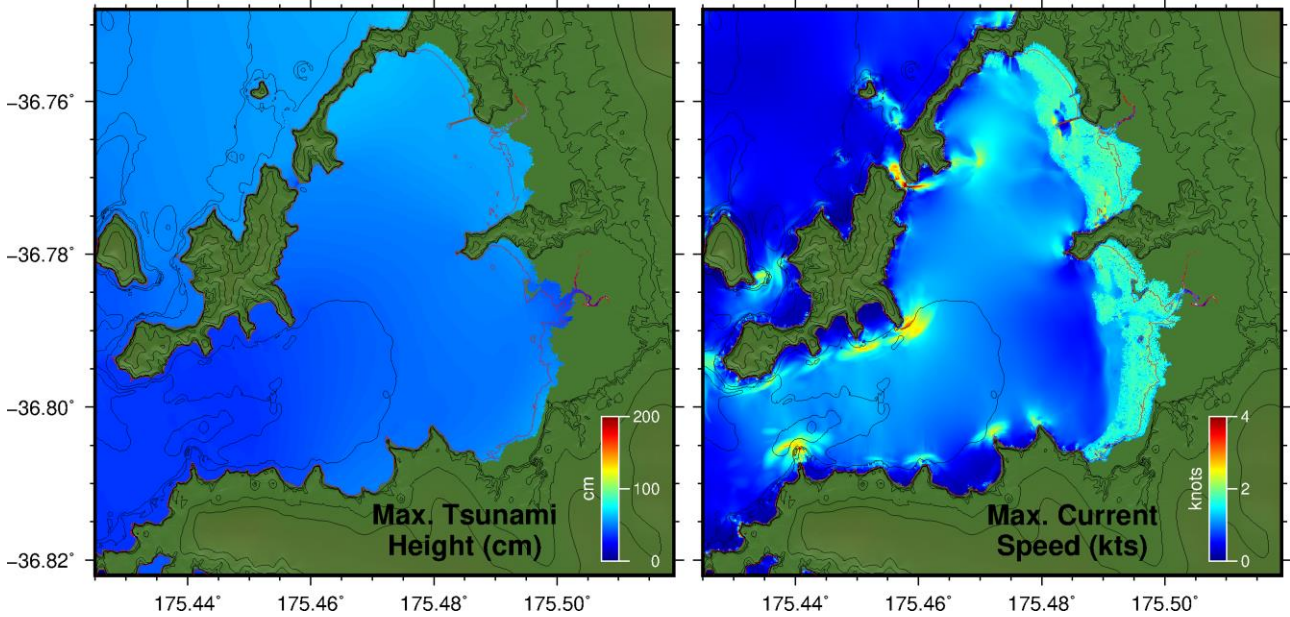


Whakatiwai

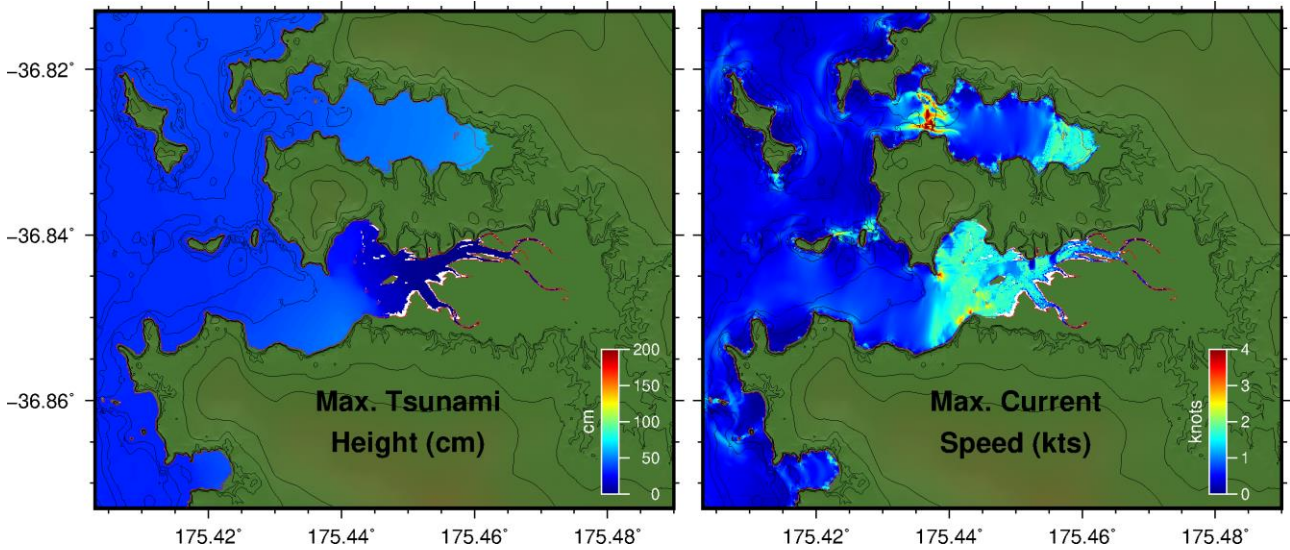
Figure 13.2 Maximum modelled tsunami heights and current speeds for the FF 7 scenario at MSL.



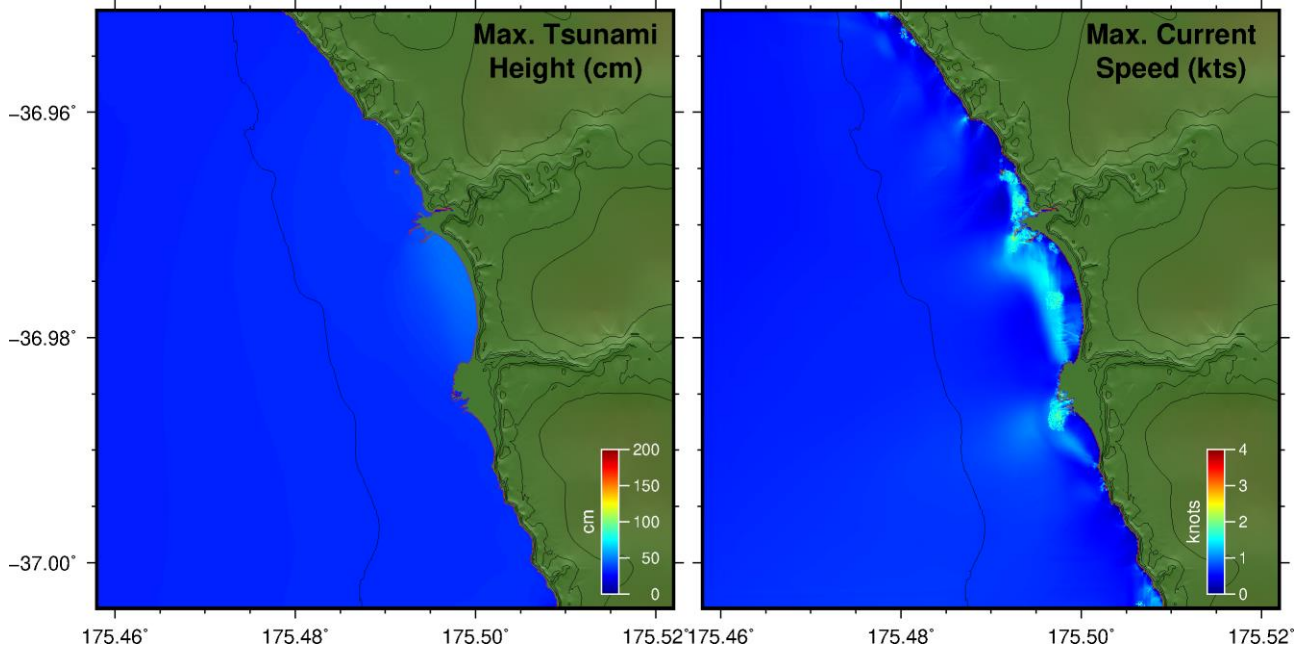
Colville



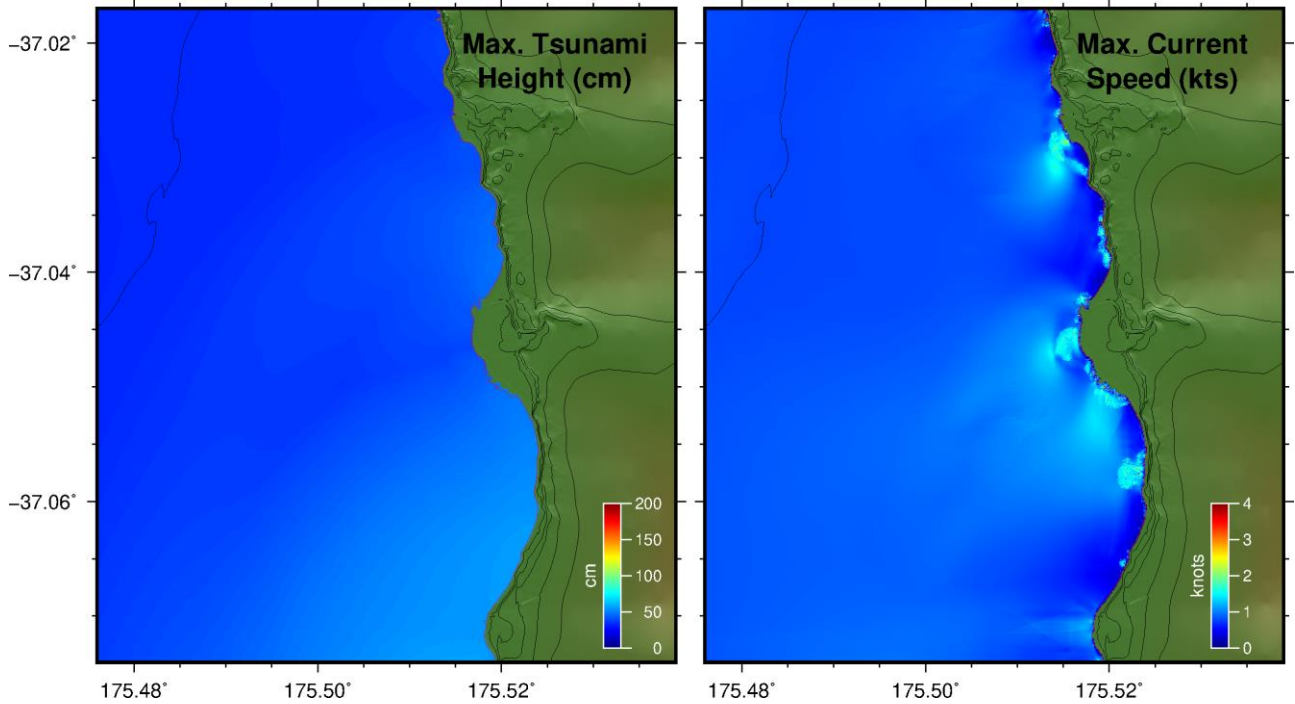
Coromandel



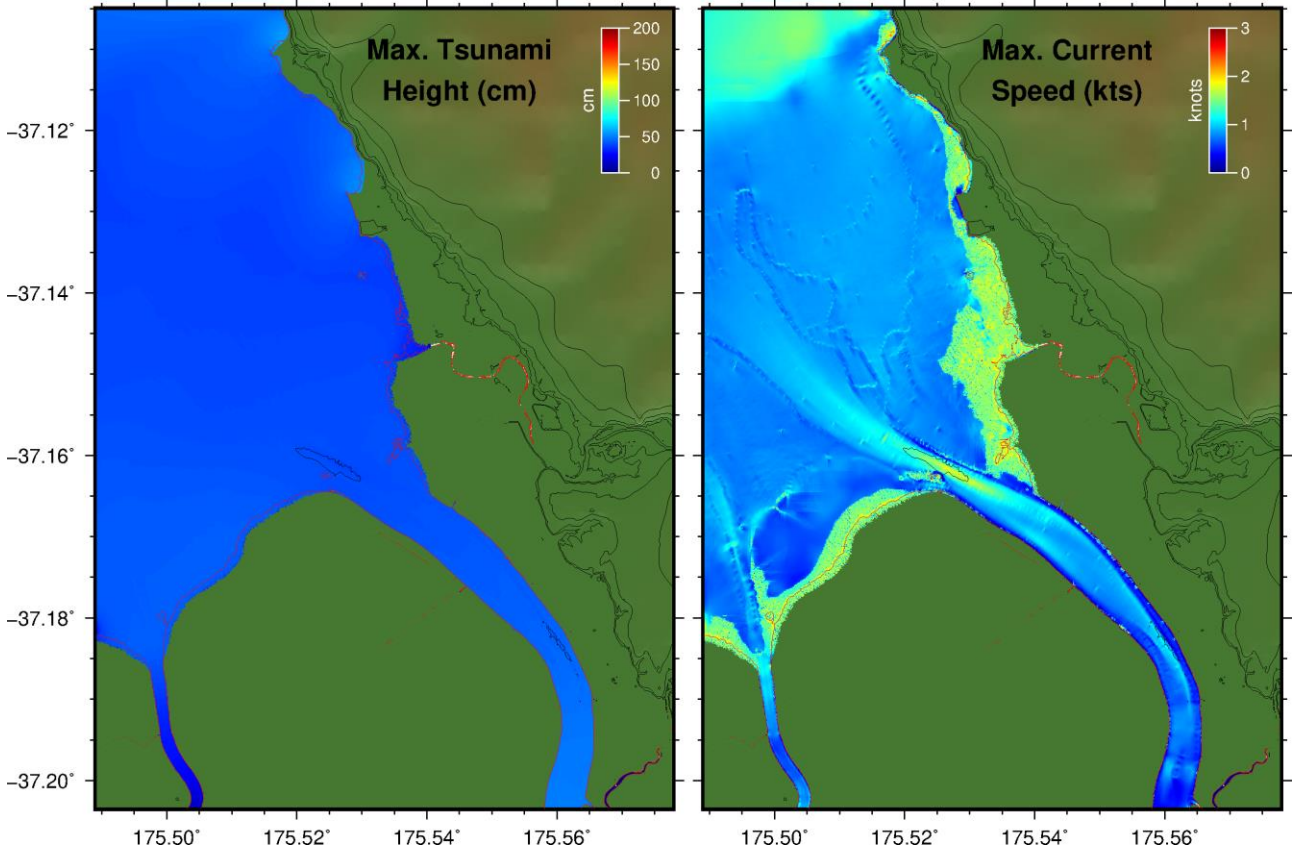
Manaia



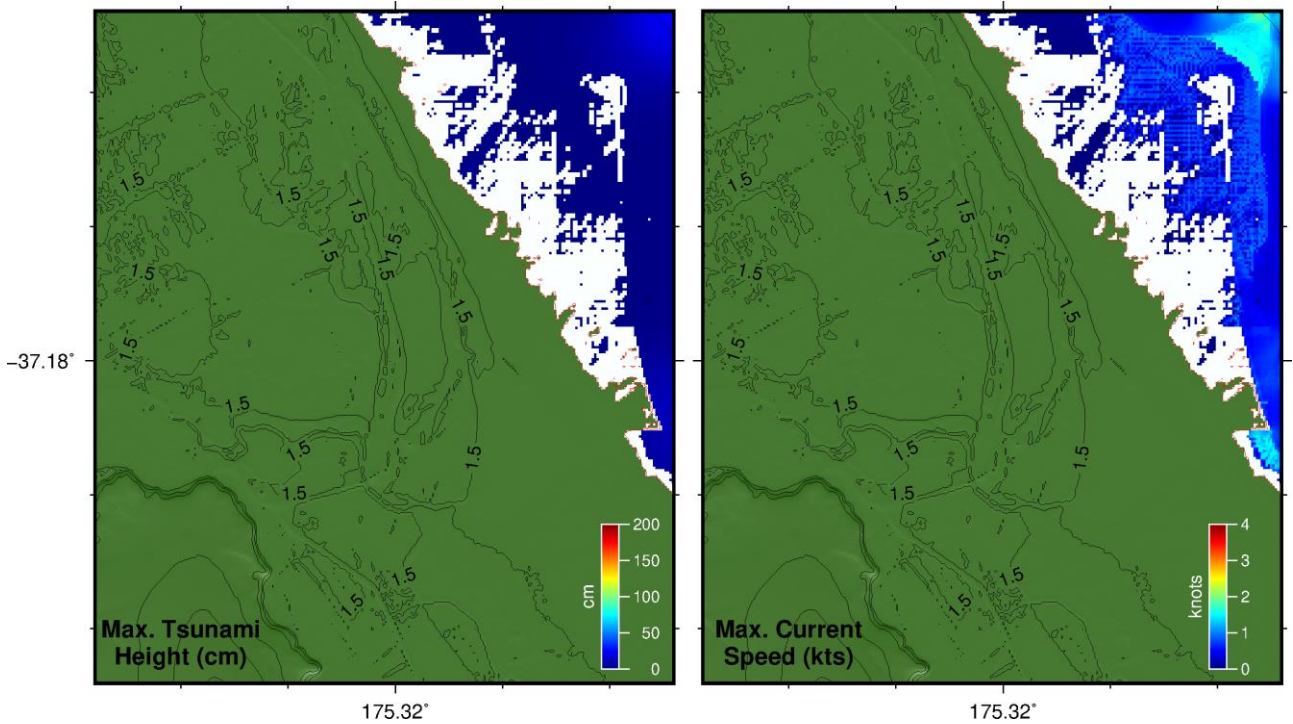
Tapu



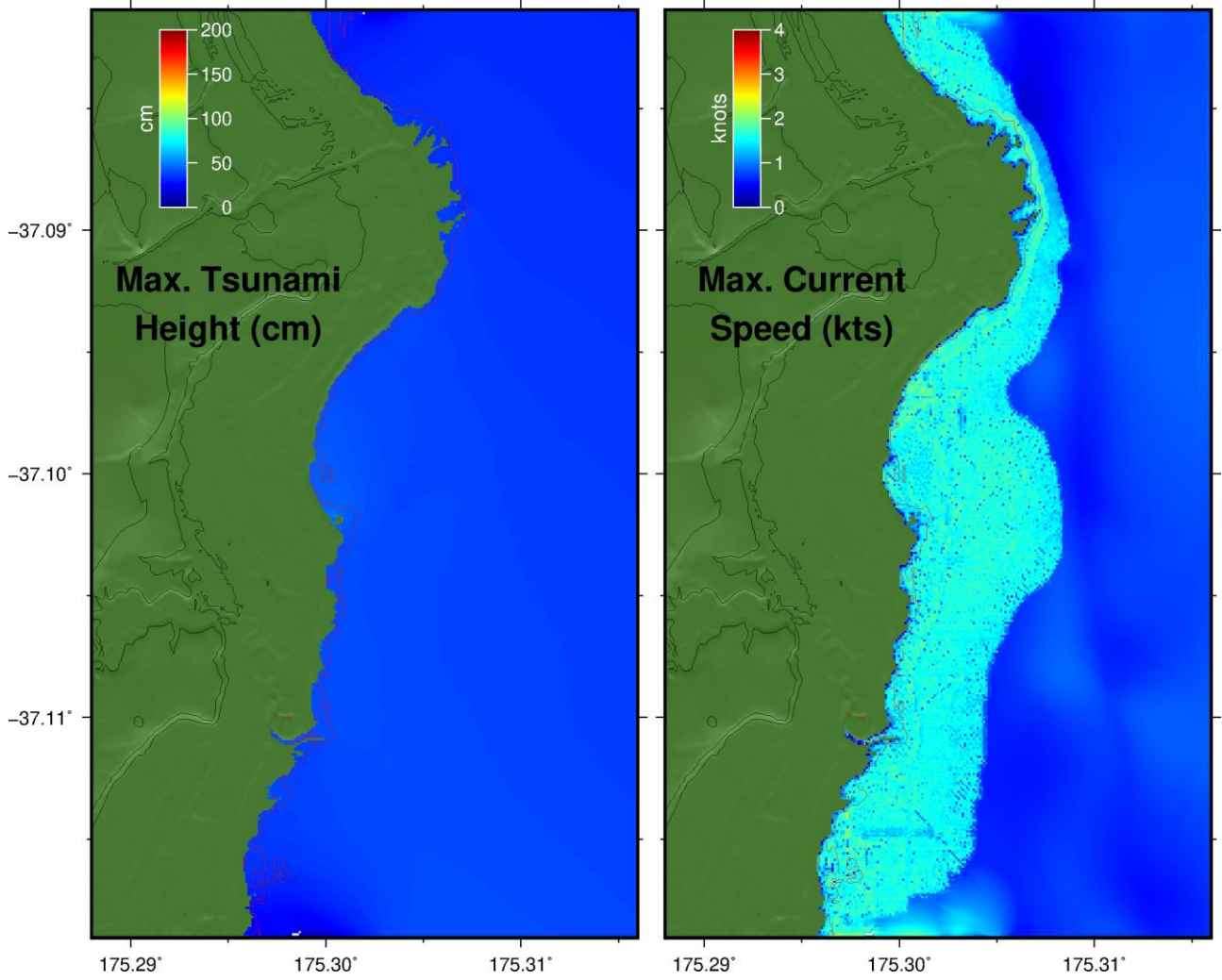
Te Puru



Thames



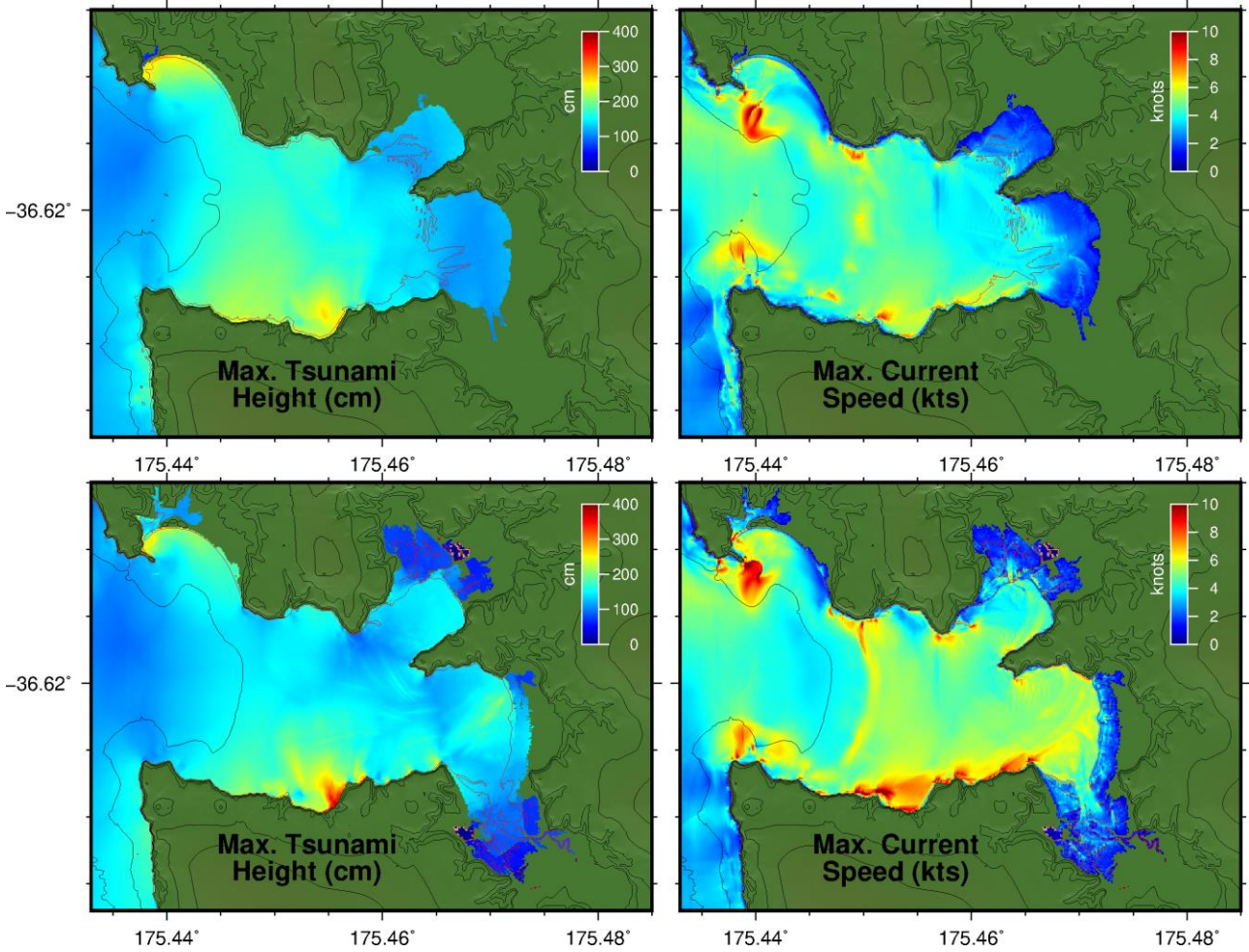
Miranda



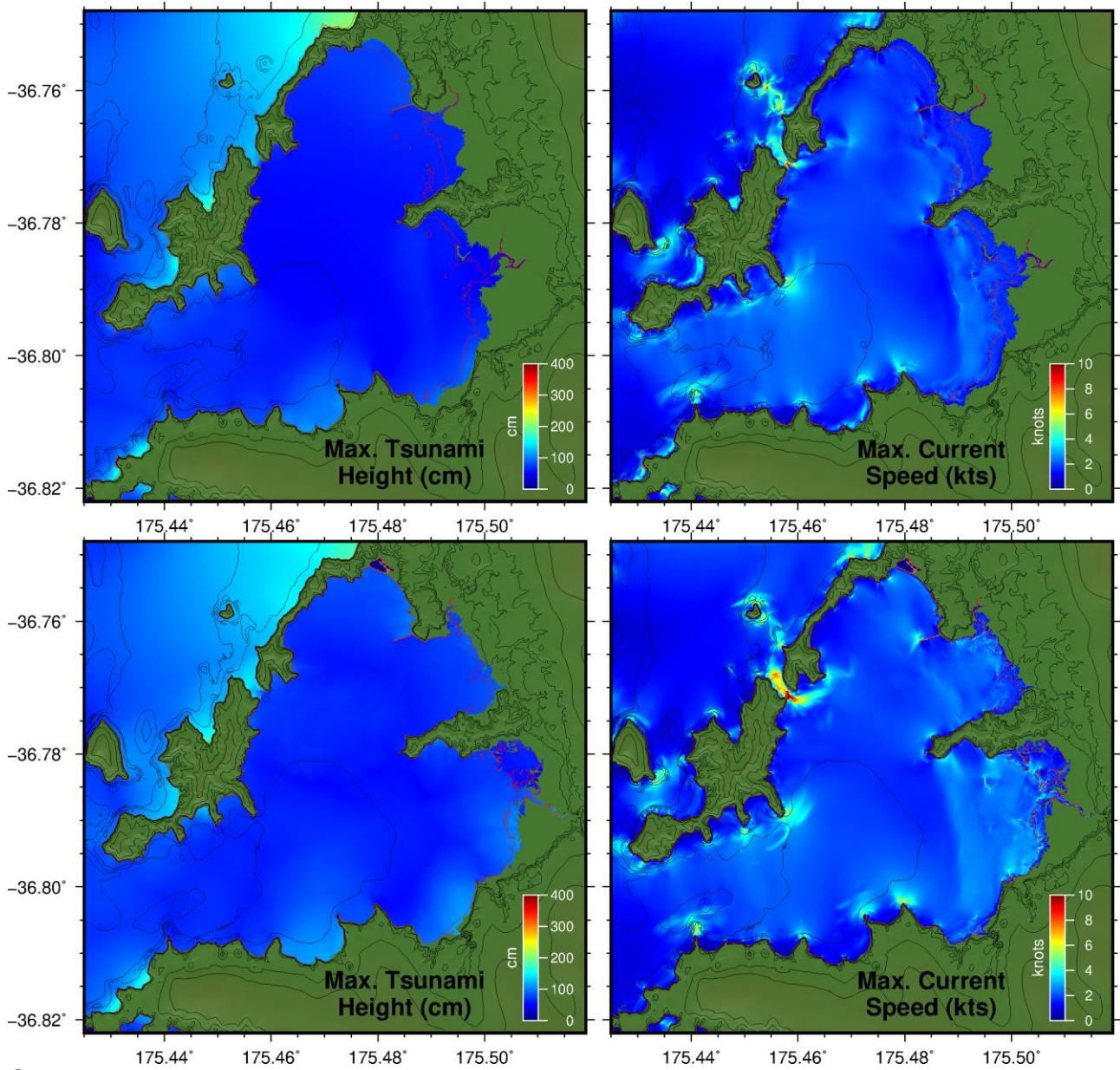
Whakatiwai

Figure 13.3 Maximum modelled tsunami heights and current speeds for the 1960 scenario at MSL.

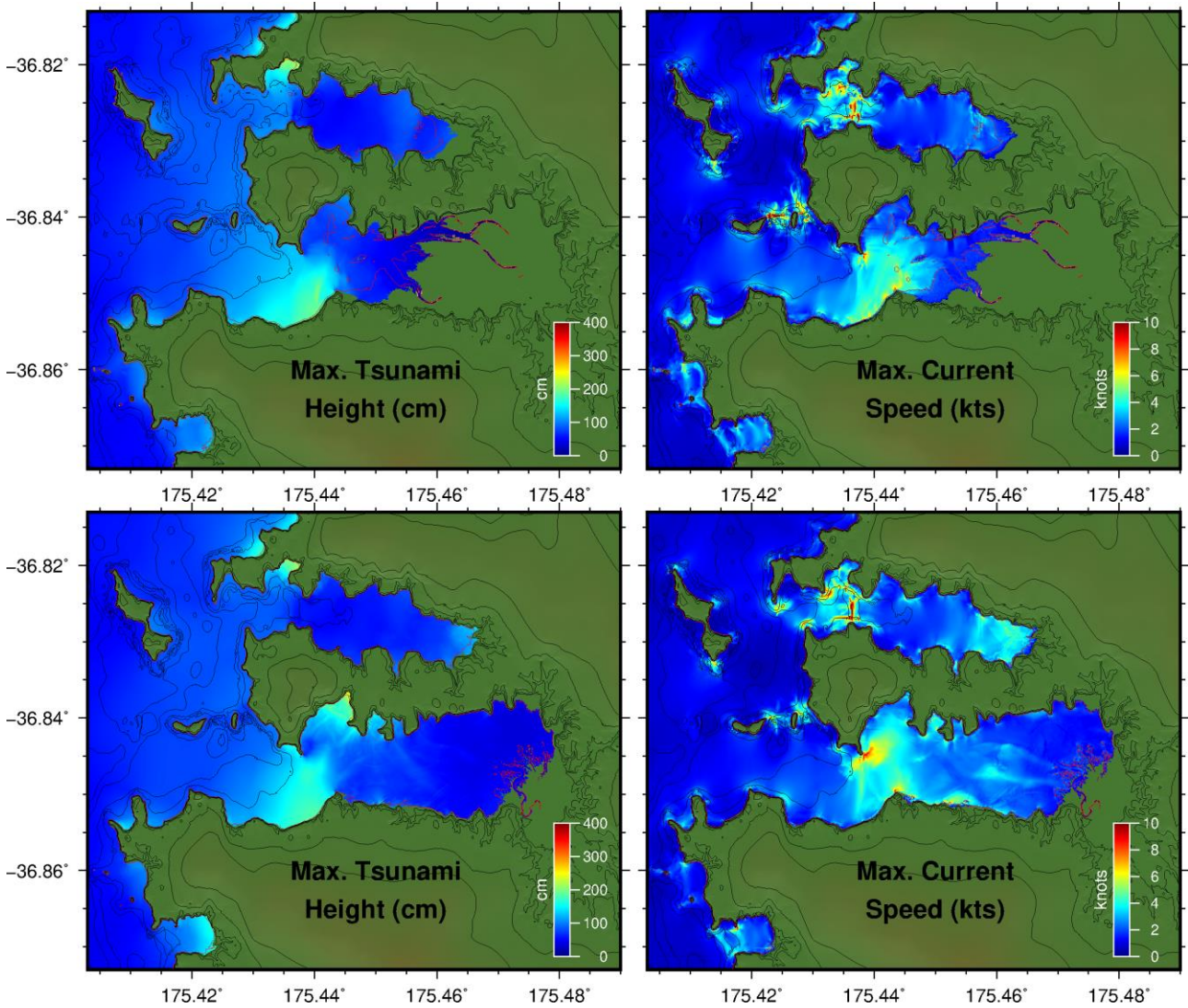
14 APPENDIX 6 – MAX TSUNAMI HEIGHTS AND CURRENT SPEEDS TK8 SCENARIO.



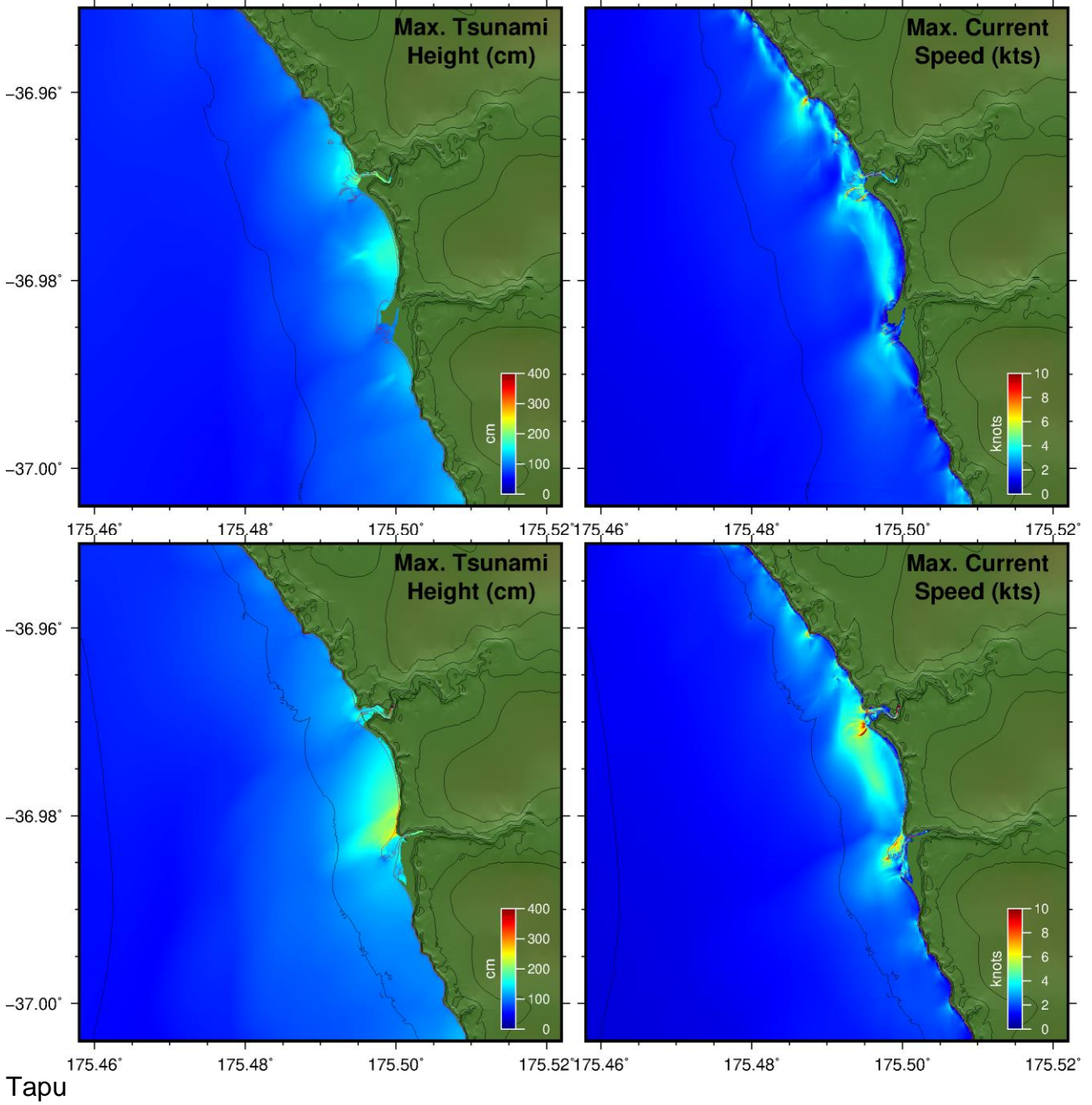
Colville

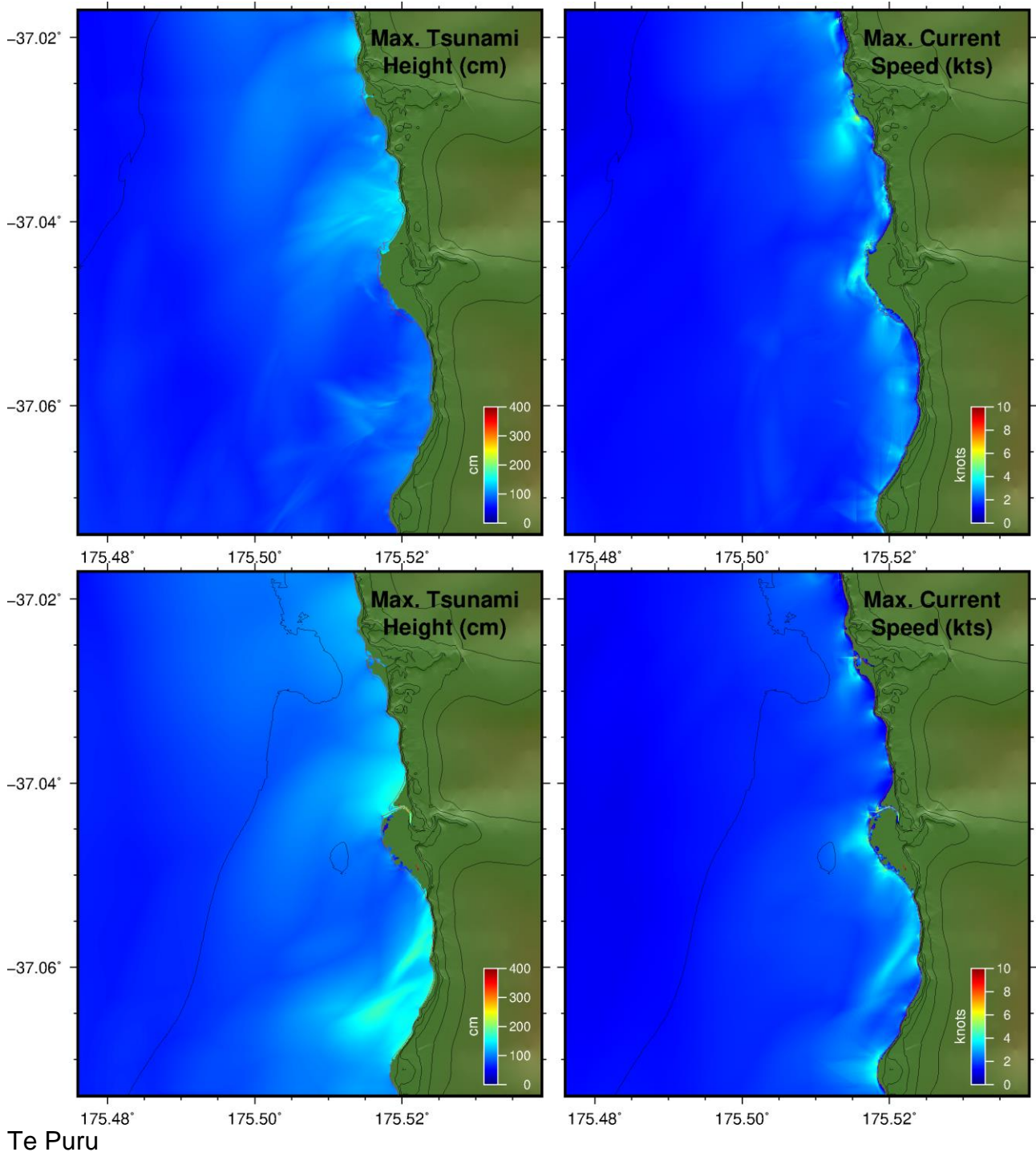


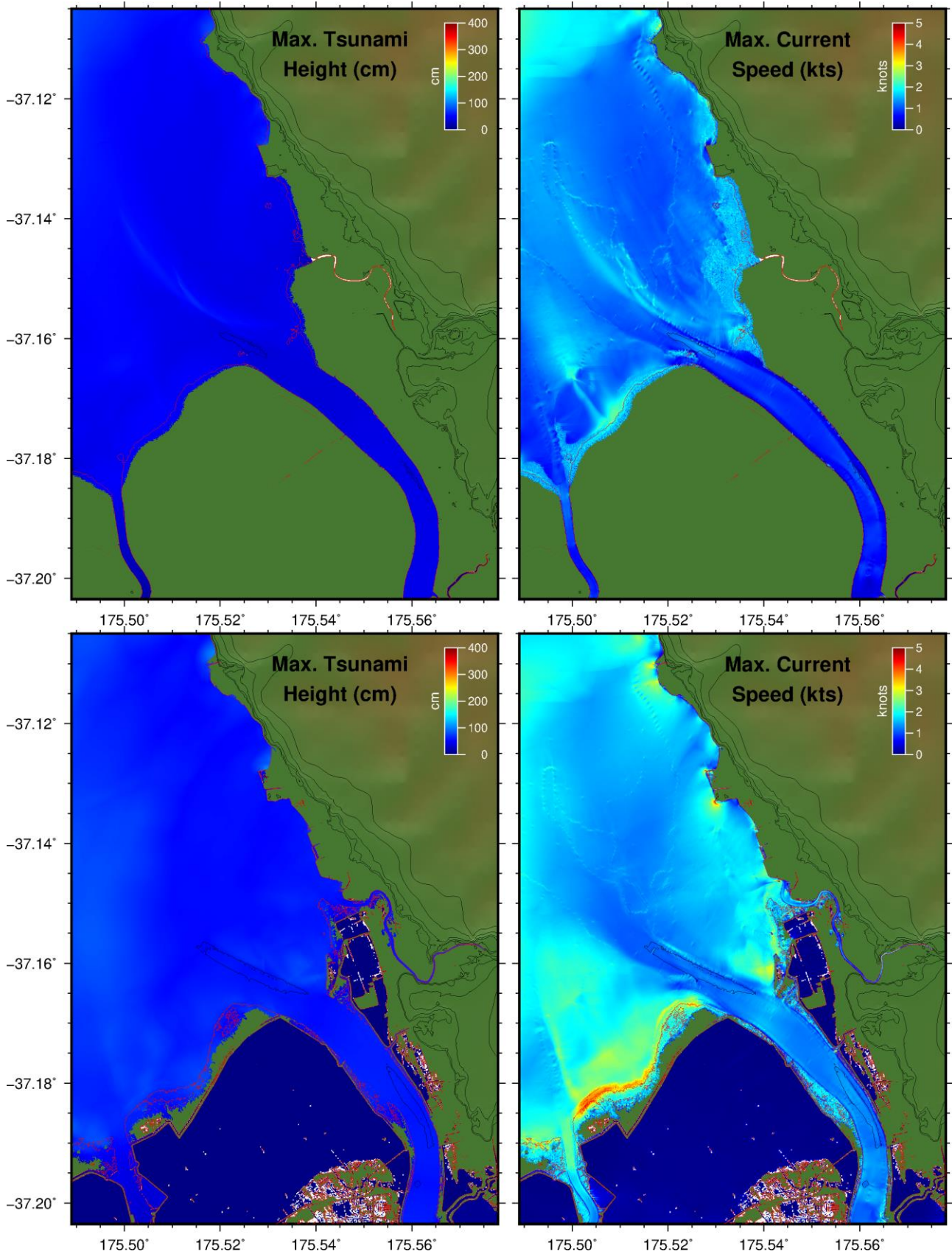
Coromandel



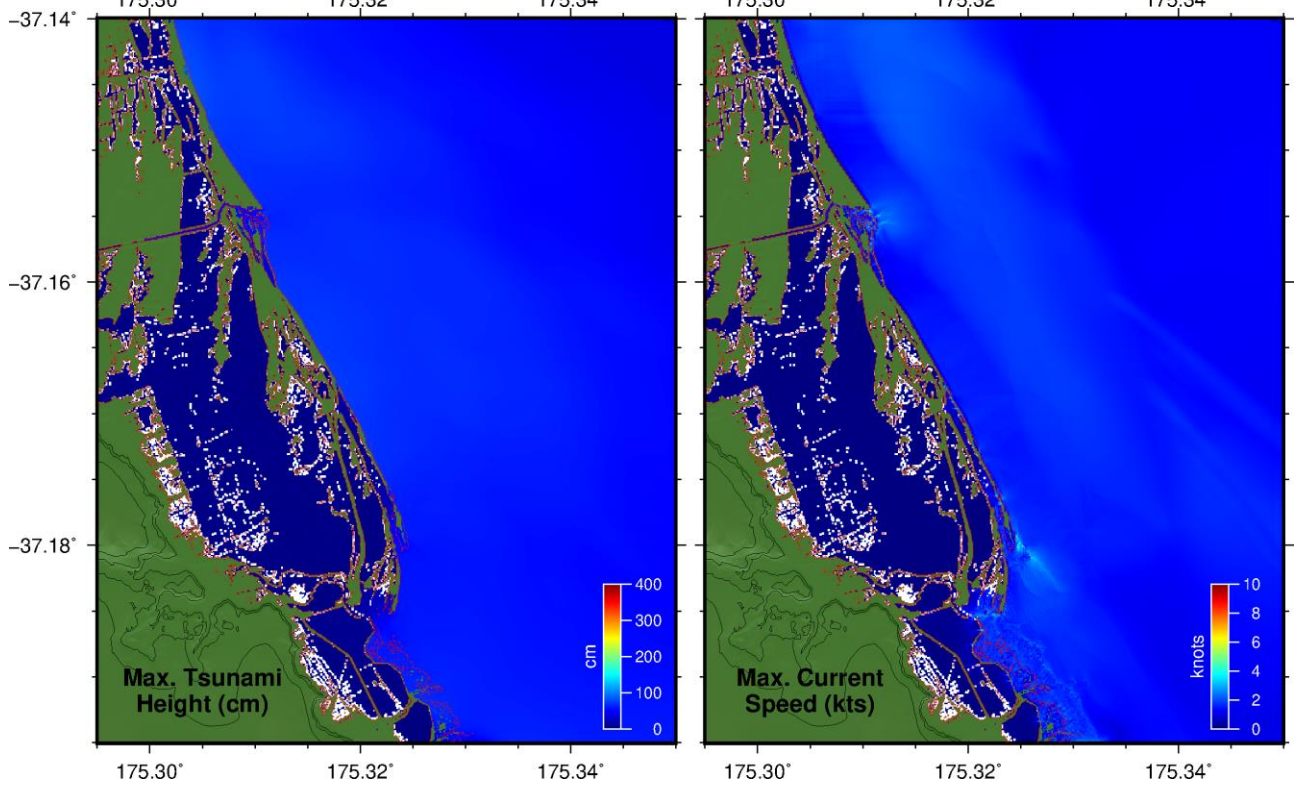
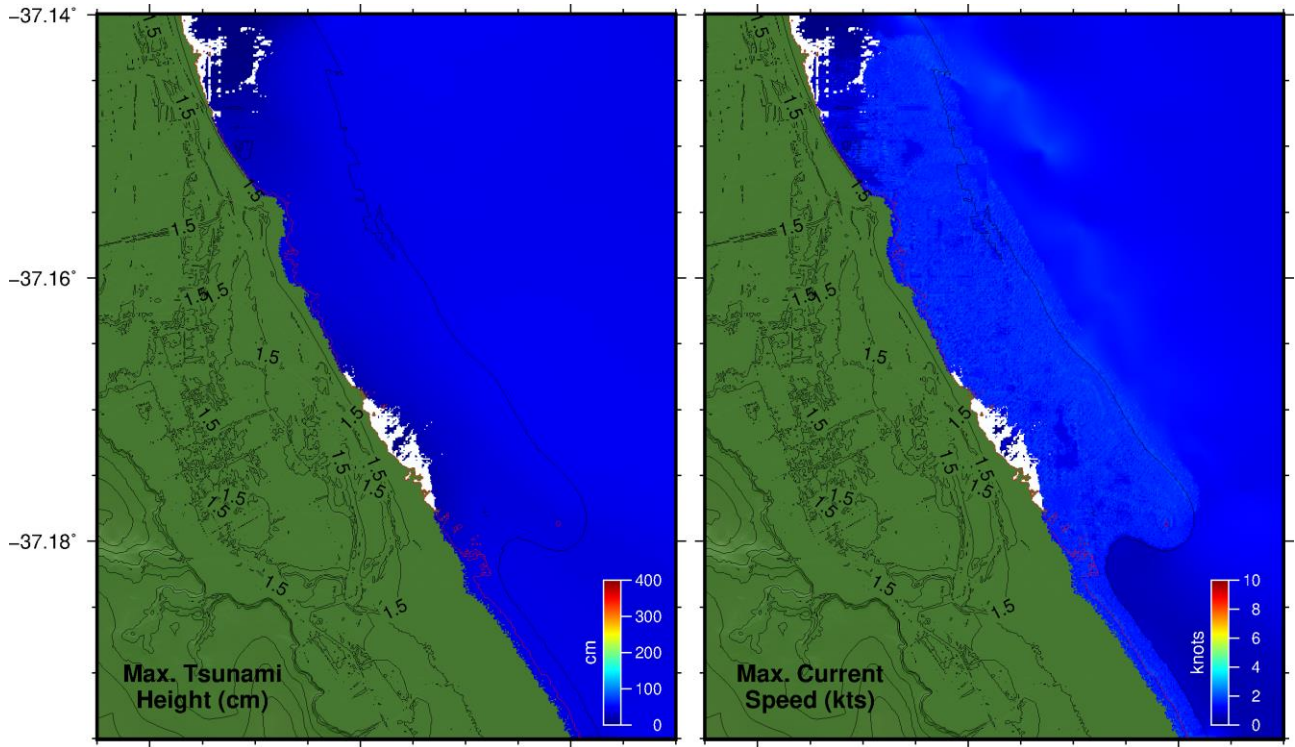
Manaia



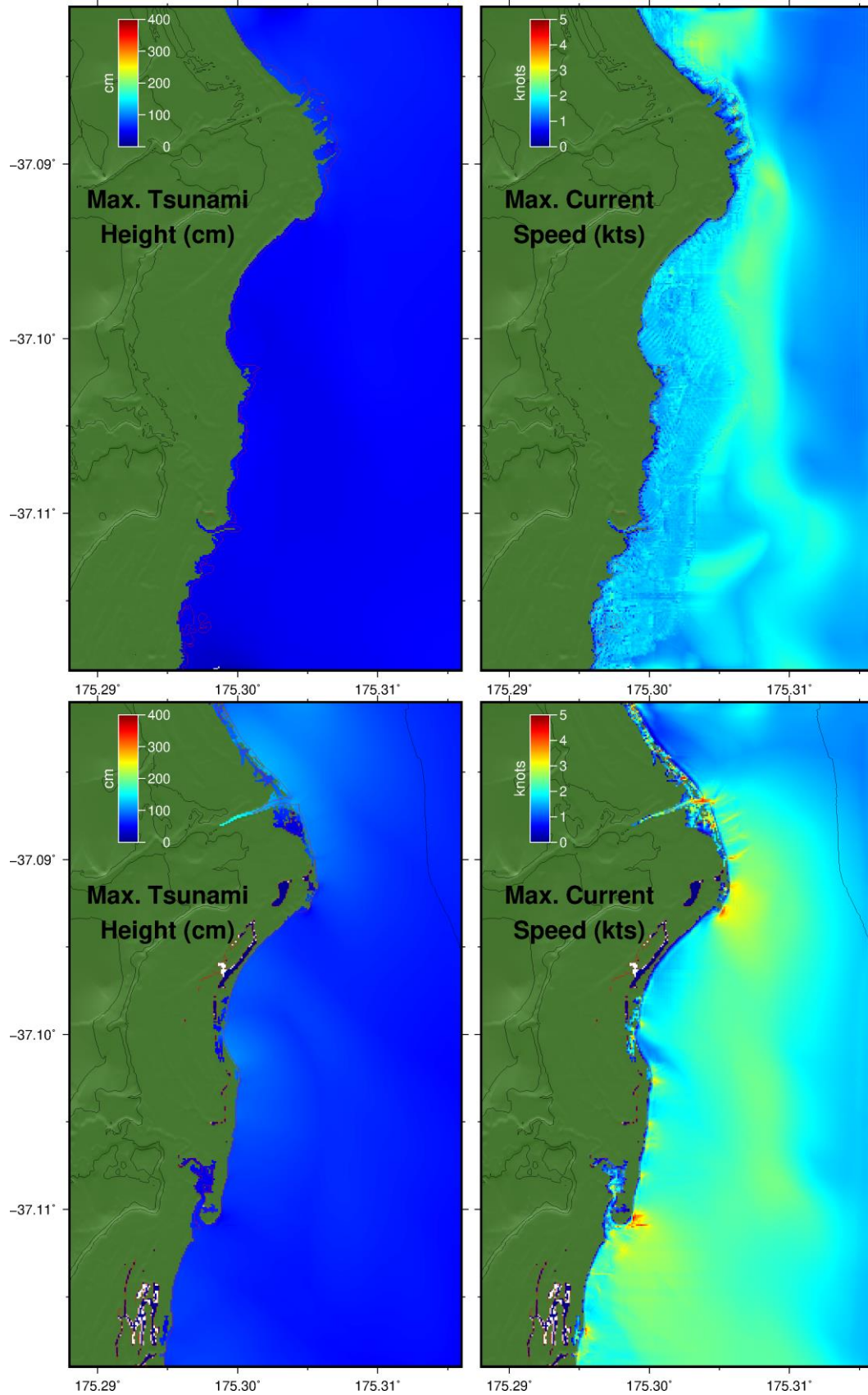




Thames



Miranda



Whakatiwai

Figure 14.1 Maximum modelled tsunami heights and current speeds for the TK8 scenario at MSL (upper panels) and MHWS (lower panels).